Department of Naval Architecture, Ocean and Marine Engineering

Predicting the Effects of Fouling Control Coatings and Heterogeneous Hull Roughness on Ship Resistance

Roberto Ravenna

A thesis presented in fulfilment of the
requirements for the degree of Doctor of Philosophy

2023

This thesis is the result of the author's original research. It has been composed by the author and has not been previously submitted for examination which has led to the award of a degree.

The copyright belongs to the author under the terms of the United Kingdom Copyright Acts as qualified by University of Strathclyde Regulation 3.50. Due acknowledgement must always be made of the use of any material contained in, or derived from, this thesis.

Signed: *Roberto Ravenna*

Date: 27 January 2023

Acknowledgements

Contents

List of Figures

List of Tables

Abstract

This research builds on one of the spotlights of fluid-hull interaction theories: the effects of hull surface conditions on ship hydrodynamics.

Several factors, such as biofouling accumulation, coatings failure, and corrosion, deteriorate the hull surfaces (i.e., increasing the hull roughness). Although the consequences of poor hull surface conditions on fuel consumption and emissions are well-known, the rationales behind the hull roughness effects on ship performance are yet to be thoroughly understood. Furthermore, there is epistemic uncertainty associated with biofouling management strategies (e.g., the choice of fouling control coatings and drydocking operations). Last but not least, although hull roughness is typically spatially heterogeneous, most research has only dealt with homogeneously distributed hull roughness. Therefore, given the importance of hull roughness on ship performance from economic and environmental perspectives, this thesis aims to investigate the effects of fouling control coatings, mimicked biofouling and heterogeneous hull roughness on ship hydrodynamics using experimental and numerical methods.

Part I (Chapters 4 and 5) of the thesis presents experimental roughness function data for different surfaces, including a hard foul-release coating developed from the fully turbulent flow channel (FTFC) facility of the University of Strathclyde. Furthermore, the results of the FTFC tests were compared against flat plate towing tank tests showing excellent agreement. Afterwards, Part II (Chapter 6 and 7) employed the experimental results in similarity law scaling and Computational Fluid Dynamics (CFD) analysis for full-scale predictions at different speeds. Notably, more than one of the paints tested showed a reduction in the estimated effective power requirements (i.e., up to 5.7%). Finally, Part III (Chapter 8) extended the CFD analysis to the effects of the heterogeneous distribution of hull roughness on ship resistance by simulating heterogeneous scenarios with various hull forms, and speeds. Eventually, the results were correlated by defining a *Roughness Impact Factor* (*RIF*) which could have practical implications for biofouling management decisions.

Nomenclature

V	Velocity (ship)
R_T	Total resistance (ship)
S	Wetted surface area (ship)
P_E	Effective power (ship)
C_T	Total resistance coefficient (ship)
C_F	Frictional resistance coefficient (ship)
C_R	Residuary resistance coefficient (ship)
Fr	Froude number
Re	Reynolds number
Re_L	Reynolds number (based on ship length at water level)
R_a	Mean arithmetic roughness height (based on probability density)
R_{t50}	Roughness height (over a length of 50 mm)
k	Roughness length scale
k^+	Roughness Reynolds number
ΔU^+	Roughness function
Re_M	Reynolds number (based over panel length and bulk flow velocity)
c_f	Skin friction coefficient (panel)
R^2	Coefficient of determination
τ_w	Wall shear stress
U_τ	Friction velocity based on wall shear stress
D_h	Hydraulic diameter
Δp	Pressure drops value
Δx	Streamwise pressure gauges distance
U_M	Mean bulk velocity of the flow in the test section
h	Channel height
b	Channel beam
κ	von-Karman constant
υ	Kinematic viscosity
ρ	Density
U_A	Total uncertainty
P_A	Precision uncertainty limit
B_A	Bias uncertainty limit

Superscript

$+$	Inner variable (normalized with U_τ)

Subscript

smooth (s)	Smooth surface
rough (r)	Rough surface

Acronym

FTFC   Fully Turbulent Flow Channel
CFD   Computational Fluid Dynamics
FCC   Fouling Control Coating
KRISO   Korea Research Institute of Ships & Ocean engineering
KCS   KRISO Container Ship
KVLCC2   KRISO Very Large Crude Carrier 2
UoS   University of Strathclyde
NAOME   Naval Architecture, Ocean and Marine Engineering
KHL   Kelvin Hydrodynamics Laboratory
DU   Dalhousie University
GIT   Graphite Innovation and Technology
AF01   Anti-Fouling 01 (Self-Polishing antifouling coating)
BL01   Boundary-Layer 01 (Gelcoat barrier coating)
FR01   Foul-Release 01 (Soft foul-release coating)
FR02   Foul-Release 02 (Hard foul-release coating)
Sand 220 Aluminium oxide sand grit 220 (Medium light slime surface)
Sand 60-80 Aluminium oxide sand grit 60-80 (Medium slime surface)

1. Introduction

1.1. Introduction

This chapter introduces the general perspectives, motivations, aim and objectives, and structure of the present PhD thesis.

Section 2 presents a brief overview of the general perspectives on the latest requirements for energy-efficient shipping, including the effects of hull roughness on ship performances and, therefore, the importance of this study. Section 3 summarises the motivations behind this PhD thesis in bullet points, from which it can be seen that there is a real necessity for this research effort. Section 4 outlines this PhD work's aim and objectives, along with the Chapters in which the objectives are addressed. Finally, Section 5 gives an outlook of the thesis structure to help the reader navigate the multiple chapters.

1.2. General Perspectives

1.2.1. Economic and Environmental Needs: Energy Efficient Shipping

Ships are considered the most environmentally friendly means of transportation. In fact, despite transporting over 90% of the world's cargo, shipping is responsible for only 11% of the global CO_2 emissions from transport. Nevertheless, the shipping industry must do its part towards the *Net Zero by 2050* scenario pledged by the United Nations (IEA, 2021). Making ships more energy efficient is also crucial for preserving marine ecosystems and, last but not least, from an economic point of view. Hence, new mandatory measures are periodically issued by regulators such as the International Maritime Organisation (IMO) to implement the energy efficiency of ships. For example, the operating expense index (OPEX), Energy Efficiency Existing Ship Index (EEXI) and the Carbon Intensity Indicator (CII) are enforced on all ships (IMO, 2021).

Shipping is a contributor to global emissions, responsible for approximately 2-3% of total greenhouse gas emissions. Some examples of emissions from shipping include:

- Carbon dioxide (CO_2): the most significant contributor to shipping emissions. It is produced by the combustion of fuel oil in ship engines.

- Nitrogen oxides (NO_x): a product of high-temperature combustion and is a major contributor to air pollution and acid rain.

- Sulphur oxides (SO_x): produced by the combustion of sulphur-containing fuels and contributes to air pollution and acid rain.

- Particulate Matter (PM): a mixture of solid particles and liquid droplets suspended in the air, which can have negative impacts on human health and the environment.

In response to the urgent need to reduce emissions from shipping, the world leaders are contributing to the global effort to tackle climate change. For example, the United Kingdom has pledged to achieve net zero emissions by 2050, meaning that the country will take actions to reduce its emissions to the lowest possible level and balance any remaining emissions with removal of CO_2 from the atmosphere. In line with this goal, the UK has been working towards establishing "zero port zero" and "green shipping corridors." Zero port zero refers to the concept of creating ports that are powered by renewable energy sources and produce zero emissions. This would help reduce the emissions produced by ships while they are at port. Green shipping corridors refer to routes that are designated as environmentally friendly, with ships using clean technologies, optimized routes, and reduced speeds to minimize their emissions. By implementing these initiatives, the UK government hopes to reduce shipping emissions, improve air quality, and contribute to the global effort to tackle climate change.

1.2.2. Ship Resistance and Hull Roughness

The total resistance of a ship is made up of several components caused by various factors that interact with one another in a highly complicated way. Furthermore, ship

resistance is the most relevant "energy consumer" for conventional displacement ships like containerships and tankers. In fact, most of the total fuel input energy is purely used to match the hydrodynamics losses and navigate at the desired speed. Moreover, frictional resistance is the largest single component of the total resistance for these so-called displacement vessels at some speeds. Experiments have shown that for new ships, frictional resistance accounts for 80 to 85 per cent of the total resistance (van Manen and van Oossanen, 1988). According to (Lackenby, 1962), when the hull is considered hydrodynamically smooth, the frictional resistance goes up to 90% of the total resistance for a low-speed ship, *Figure 1-1*.

Figure 1-1: Hull cleaning operations. Photo credit: IMO - Lee Adamson.

On the other hand, the increased hull roughness of in-service ships increases the wall shear stress. This leads to a reduction of the flow velocity, hence, increased resistance. In other words, the hull surface conditions directly affect their speed, power requirements and fuel consumption. Naval architects, shipowners, and operators are fully aware of the economic and environmental penalties linked to a poorly maintained hull. In fact, it is well established that hull roughness is foremost responsible for the decay of ship performance over time.

1.2.3. Importance of this Study

A ship's hull surface condition is crucial to its hydrodynamic performance. Biofouling accumulation, antifouling coating failure, and corrosion are the leading causes of the increase in roughness on the hull surfaces (Townsin, 2003). For example, from a purely economic point of view – a newly painted midsize container ship at design speed experiences about a 10% increase in fuel consumption after only one month at sea due to added hull roughness. This leads to an extra 150,000 USD of fuel consumed per month. Extrapolating to an entire fleet of, e.g., 500 vessels, over one year, ship owners lose 1.5-2 billion USD a year due to hull roughness alone (Hydrex, 2010). It is of note that in 2021 the world merchant fleet accounted for 53,973 vessels, and it is safe to assume that all the vessels suffered from increased hull roughness *Figure 1-2*.
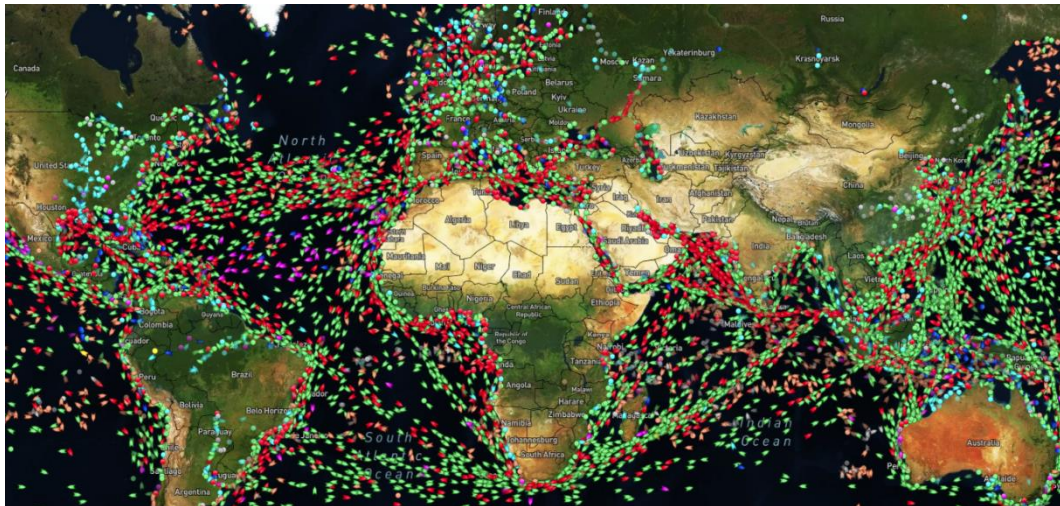
Figure 1-2: Representative screenshot of the world marine traffic (https://www.marinetraffic.com/ Accessed on 15 December 2022).

Nevertheless, our understanding of the hull roughness effect on ship resistance is limited. Dry-dock and fouling control coating (FCC) strategies to mitigate the roughness effect on ship resistance are arguably incomplete. The typical approach of ignoring the vessel's underwater hull conditions for long dry-dock intervals is a significant cause of considerable losses to a fleet's economy.

Moreover, vessels can act as a means of transportation for bio-organisms accumulated on their hull surfaces. Once in the new ecosystem, the alien species released can out-compete the native species and harm biodiversity. Hence, choosing suitable fouling control coating (FCC) and drydock strategies for a vessel can offer more than the obvious economic and environmental advantages. Furthermore, improving hull performances associated with surface conditions enables the vessels to comply with the IMO regulations (IMO, 2021). Hence, the International Towing Tank Conference (ITTC) recommends that researchers develop new methods and experimental data to improve the efficiency of ship resistance (ITTC, 2017a).

Furthermore, roughness accumulates in a complicated and typically heterogeneous way on ship hulls resulting in more difficult predictions of its effects on ship resistance. Therefore, extending the knowledge on hull roughness effects on ship resistance is necessary, especially from a biofouling management perspective. Hence, it is essential to conduct further study into the correlation between roughness and drag to develop CFD prediction methods and hull maintenance strategies.

Numerical methods can be used to predict the hull roughness effect on ship resistance. Specifically, the Granville method (Granville, 1978, 1958), based on the turbulent boundary layer similarity law scaling technique and Computational Fluid Dynamics (CFD)-based simulations, are commonly used for ship resistance predictions. However, the effect of hull roughness on ship resistance can be predicted only if the experimental roughness function models of the surface in question are known. In fact, the specific roughness function models can effectively represent fouling control coatings as applied or biofouled. Hereafter, for roughness function is intended the difference between the velocities in the boundary layer between a rough surface and a hydraulically smooth reference surface. However, no universal roughness function can represent all surfaces. Therefore, the roughness functions – hydrodynamic fingerprints of any given surface – must be developed experimentally.

Finally, combining experimental and numerical methods is the most rational approach to tackling the effect of ship hull roughness, including biofouling. This would require determining the roughness functions using experimental methods. Consequently, several experimental methods have been developed for determining the roughness

function of rough surfaces. A successful alternative to determine the roughness functions of given surfaces is the fully turbulent flow channel (FTFC). In fact, FTFCs can provide reliable results combined with a quick turn-around of experimental plates and significant financial savings. However, little research has been done using the state-of-the-art FTFC of the University of Strathclyde.

1.3.   Structure of this Thesis

The structure of this PhD thesis is organised as follows:

Chapter 2 presents a comprehensive literature review on relevant topics including, a brief background of biofouling and fouling control coatings on in-service vessels, a theoretical overview of the roughness effect in the turbulent boundary layer, and a review of the state-of-the-art literature in the field of predicting the effects of hull roughness on ship hydrodynamics. The literature gaps, along with motivation and research aim and objectives are also identified and detailed at the end of Chapter 2.

Chapter 3 explains the general methodology used in this PhD thesis and gives an insight of the methodology adopted in each chapter.

Chapter 4 presents an experimental determination of the roughness functions of different fouling control coatings including the newly developed GIT hard-foul release (*FR02*) paint and mimicked biofouled surfaces. The fully turbulent flow channel (FTFC) experiments to obtain the roughness functions data are detailed along with the experimental uncertainty analysis.

Chapter 5 briefly describes the towing tank resistance tests conducted on a flat plate conveniently with aluminium-oxide sand (*Sand 220*). The roughness functions data obtained from the towing tank tests are compared with the FTFC tests performed on a surface coated with the same sand. Further comparison with similar studies in the literature is presented at the end of Chapter 5.

Chapter 6 presents the effects of the FCCs and mimicked biofouled surfaces on ship resistance and power requirements of the full-scale KCS hull at design and low speed. The

predictions are carried out using Granville's similarity law scaling procedure (Granville, 1958). It is of note that different hull roughness conditions at both design and low speed are detailed in Chapter 6.

Chapter 7 describes CFD-based predictions of the effect of the surfaces tested on the KCS full-scale hydrodynamics. To characterise rough surfaces in CFD, the modified wall-function approach is used. Therefore, the roughness function models developed in Chapter 4 and Chapter 5 are embedded in the CFD solver (StarCCM+). Comparison across similarity law based, CFD-based and similar predictions in the literature is presented at the end of Chapter 7.

Chapter 8 details the investigations on the effects of heterogeneous hull roughness on ship hydrodynamics to the KCS and KVLCC2 hulls in model scale. A coefficient, the roughness impact factor (RIF) is proposed to quantify the impact of increased hull roughness of specific areas on the ship hydrodynamics performances. The added resistance coefficients and effective power values are calculated for different smooth/rough scenarios along with the roughness impact factors. Comparison across the CFD results for the KCS and KVLCC2 models and similar predictions in the literature is presented at the end of Chapter 8.

Chapter 9 extends the CFD-based simulations conducted on the full-scale KCS hull with heterogeneous distributions of hull roughness at design and low speed. Extensive figures depict and compare the in-house CFD full-scale predictions at the end of Chapter 8.

Finally, Chapter 10 provides a comprehensive summary of this PhD thesis, including the achievement of the research aim and objectives, main conclusions and discussions, novelties and contributions to the field, and recommendations for future work.

1.4. Chapter Summary

The general perspectives, motivations behind the PhD study, aim and objectives, and structure of the thesis have been presented in this chapter.

2. Literature Review

2.1. Introduction

An extensive literature survey was conducted in the relevant field to understand the previous research into the dedicated subject and to be aware of the current state-of-the-art. This chapter outlines the theoretical information, including the turbulent boundary layer, the roughness effect on the velocity profile, the definition of the roughness functions, and the experimental techniques for the roughness function determinations. The important cornerstones of this survey are provided in this chapter from a critical point of view to determine the literature gaps and justify the aim and objectives of this PhD thesis. Similar PhD theses have recently carried out similar literature reviews (Song, 2020; Demirel, 2015; Candries, 2001). Therefore, notable credit must be given to these authors. The present chapter is structured as follows:

Section 2.2 gives an insight into ship resistance and summarises the typical approach of naval architects to decompose it. Furthermore, the different ship resistance components and their basic equations are presented. Section 2.3 introduces the reader to the biofouling accumulation mechanisms. Moreover, some backgrounds on the categories of marine biofoulers are given in this section. Section 2.4 presents an outlook of the fouling-control coatings (FCCs), essential systems to minimise the impacts of marine biofouling on ship resistance and powering. Section 2.5 summarises the historical cornerstones of the investigations into the effect of hull roughness on ship hydrodynamics. Section 2.6 reviews the roughness function determination theory. Specifically, it details the experimental methods used in the present thesis to determine the roughness functions of the fouling control coatings and mimicked biofouling tested. Section 2.7 gives a brief description of the ship resistance prediction methods adopted in this thesis. Finally, Section 2.8 identifies the main research gaps to the best of this author's knowledge.

2.2. Ship Resistance

Ship resistance can be decomposed into different components, such as in *Figure 2-1* (Larsson and Baba, 1996).
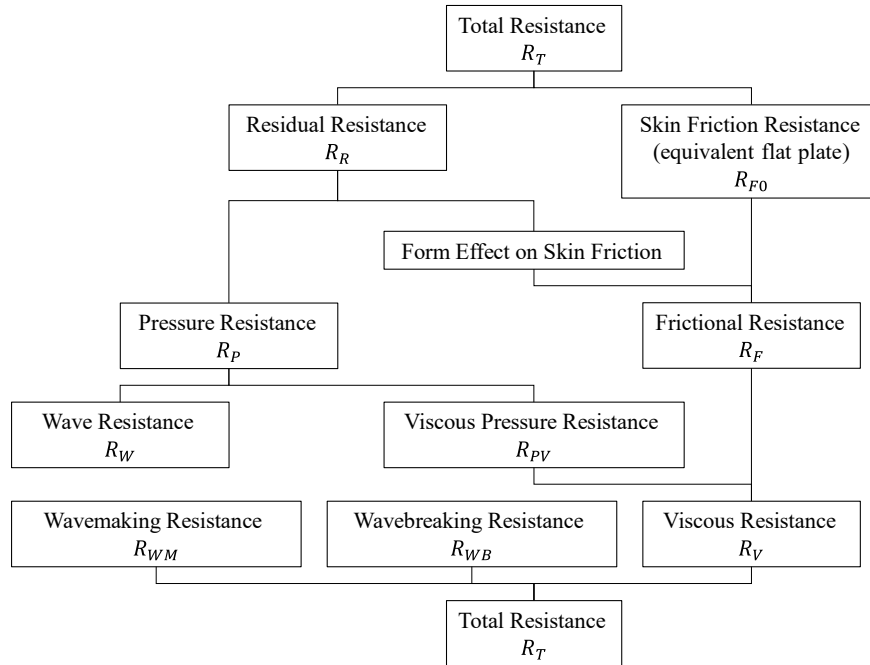
Figure 2-1 Resistance decomposition (Larsson and Baba, 1996).

Typically, naval architects deal with ship resistance through its dimensionless components. Showing similarity to the resistance decomposition, the total ship resistance coefficient, C_T, can be defined as a function of the total drag, R_T, the dynamic pressure, $1/2\,\rho V^2$, and the hull wetted surface area, S, equation (2-1):

$$C_T = \frac{R_T}{1/2\,\rho\,S\,V^2} \tag{2-1}$$

where V is the ship speed, ρ is the water density, and S is the wetted surface. Below are presented the basic equations widely adopted for ship resistance investigations, adapted from the well-known book *Principles of Naval Architecture* (van Manen and van Oossanen, 1988). Among all the possible ways of decomposing ship resistance (Larsson and Baba, 1996), a straightforward approach is believed to be the most effective for the present scope. Therefore, the total ship resistance coefficient, C_T, is

decomposed into two main components: the frictional, C_F, and the residuary, C_R resistance coefficients, as given by equation (2-2), (Schultz and Flack, 2007; van Manen and van Oossanen, 1988):

$$C_T = C_F(Re) + C_R(Fr) \qquad (2\text{-}2)$$

When energy efficiency is concerned, predicting ships' in-service resistance is essential. It is because ships' resistance can vary with several factors in operation, such as loading conditions, weather, and hull surface conditions. In particular, the effect of hull roughness is known to increase different components of ship resistance (Song et al., 2019). Specifically, hull roughness can cause a significant increase in frictional resistance. The surface roughness of a ship's hull increases over time due to various factors, including mechanical causes (e.g. mechanical damage, sand-blasting, plate waviness, welds, mechanical damage to the marine coatings), chemical and electrochemical processes (i.e. corrosion), and last but not least, the accumulation of biofouling, which is often the most critical (Tezdogan and Demirel, 2014; Townsin, 2003).

Since frictional resistance often takes the most significant portion of the total resistance (up to 95% for displacement ships at slow speed), hull roughens can be responsible for significant efficiency loss (Schultz, 2007). The importance of frictional resistance for displacement vessels is graphically explained in *Figure 2-2* from (Molland, 2008), where it can be seen that the wave resistance coefficient, C_W, represents a small part of the total resistance at low Re. In other words, hull roughness mainly affects frictional resistance, while wave resistance is the dominant component at higher speeds.

Furthermore, the key parameters affecting the frictional resistance of a vessel, hence the total resistance, are the wetted surface area of the hull, the water viscosity, and the surface roughness. Obviously, the viscosity of water cannot be changed, and it does not alternate significantly around the globe. The wetted surface area cannot undertake many improvements once the deadweight tonnage requirements of a vessel design are fixed. Consequently, the hull surface roughness is the parameter that requires further attention. Finally, considering that biofouling is the primary cause of increased hull

roughness and therefore has the most damaging effects from both environmental and economic perspectives, it is imperative to have appropriate biofouling management strategies on slow-speed ships.
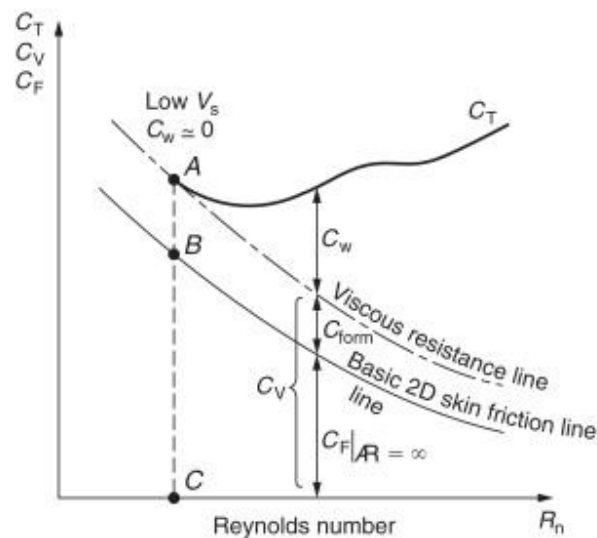
Figure 2-2: Hughes model of ship resistance (Molland, 2008).

2.3. Marine Biofouling

Marine biofouling, or simply *biofouling,* is the accumulation of living and non-living material on any submerged or semi-submerged surface in freshwater or seawater. Marine environments' biodiversity presents thousands of organisms causing marine biofouling (Lewis, 1998). The detrimental effects of fouling on ships' hydrodynamics have been well-known since humanity started going at sea (Candries, 2001). Fouling causes surface roughness, increasing a ship's frictional resistance and fuel consumption (Kempf, 1937). Furthermore, marine biofouling is also responsible for transporting dangerous alien species (Demirel, 2015). *Figure 2-3* (Atlar, 2008) and *Figure 2-4* (Taylan, 2010) demonstrate different classifications of marine foulers.

According to (Little and Depalma, 2013), there are four stages in the formation of the biofilm; (i) *conditioning*, (ii) *attachment*, (iii) *colonisation*, and (iv) *growth*. *Figure 2-6* illustrates the four stages of forming the biofilm (Chambers et al., 2006b). As seen in *Figure 2-5* (Davis and Williamson, 2002), the biofouling process begins with the

accumulation of microorganisms. Where the conditions are met, bacteria and/or other microorganisms colonise any surface placed in seawater within minutes (Gehrke and Sand, 2003). They form sticky coatings commonly referred to as 'biofilms'. The accumulation of biofilms (microfouling) is often a precursor to subsequent fouling by macrofoulers (Chambers et al., 2006a).

```
                          ┌───────┐
                          │ Plant │
                          └───┬───┘
              ┌───────────────┴─────────────┐
        ┌───────────┐                 ┌────────────┐
        │ Microalgae│                 │ Macroalgae │
        │  (slime)  │                 │   (weeds)  │
        └───────────┘                 └─────┬──────┘
                              ┌─────────────┼─────────────┐
                          ┌───────┐    ┌────────┐    ┌────────┐
                          │  Red  │    │ Brown  │    │ Green  │
                          └───────┘    └────────┘    └────────┘


                          ┌────────┐
                          │ Animal │
                          └───┬────┘
              ┌───────────────┴────────────────┐
        ┌──────────┐                      ┌──────────┐
        │   Soft   │                      │   Hard   │
        │  Bodied  │                      │  Shelled │
        └────┬─────┘                      └────┬─────┘
        ┌────┴─────┐            ┌──────────────┼──────────────┐
   ┌───────────┐ ┌─────────┐ ┌──────────┐ ┌────────────┐ ┌─────────┐
   │ Unlimited │ │ Limited │ │ Barnacles│ │ Tube Worms │ │ Mussels │
   └───────────┘ └─────────┘ └──────────┘ └────────────┘ └─────────┘
```
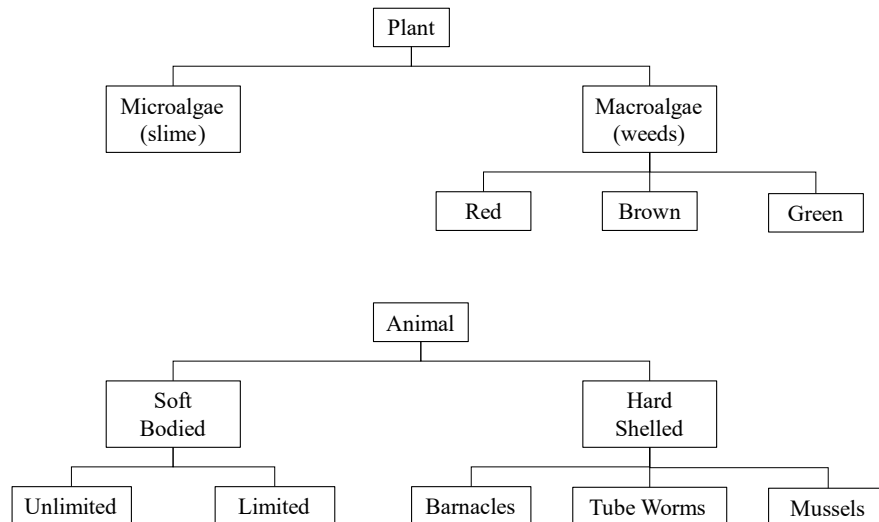
Figure 2-3: Classification of marine biofouling types, adapted from (Atlar, 2008).

```
                          ┌─────────┐
                          │ Fouling │
                          └────┬────┘
              ┌────────────────┴──────────────────┐
         ┌───────┐                            ┌───────┐
         │ Macro │                            │ Micro │
         └───┬───┘                            └───┬───┘
       ┌─────┴────────┐                           │
  ┌──────────┐   ┌──────────┐               ┌──────────┐
  │  Animal  │   │   Weed   │               │  Slime   │
  │  Fouling │   │  Fouling │               │  Fouling │
  └──────────┘   └──────────┘               └──────────┘
```
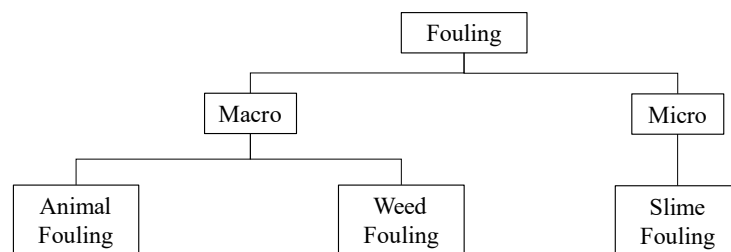
Figure 2-4: Fouling organisms, adapted from (Taylan, 2010).

A film of organic and inorganic matter adsorbed from the aquatic phase is formed within seconds of a surface being immersed at sea, Figure *2-6*. This is the first stage of biofouling accumulation (*conditioning*). Consequently, the primary colonisers (often rod-shaped bacteria) attach to the surface within several hours (*attachment*). It is of note that this second stage is reversible until the bacteria secure non-reversible

attachment by secreting extracellular adhesive polysaccharides. Within 24 hours, the microfouling bacteria start to assimilate nutrients.

Consequently, polymeric substances synthesised by the colonisers accumulate on the surface (*colonisation*). Finally, the colonisers grow, reproduce, and continue synthesising polymeric substances creating fully developed biofilms within two weeks (*growth*). The gel matrix created provides enzymatic interaction, exchange of nutrients in the biofilms, protection against environmental stress and increased resistance to biocides (Morton et al., 1998; Videla, 1996). In other words, biofilms provide both a food source and a convenient interface to which the larger organisms can adhere (Titah-Benbouzid and Benbouzid, 2015).
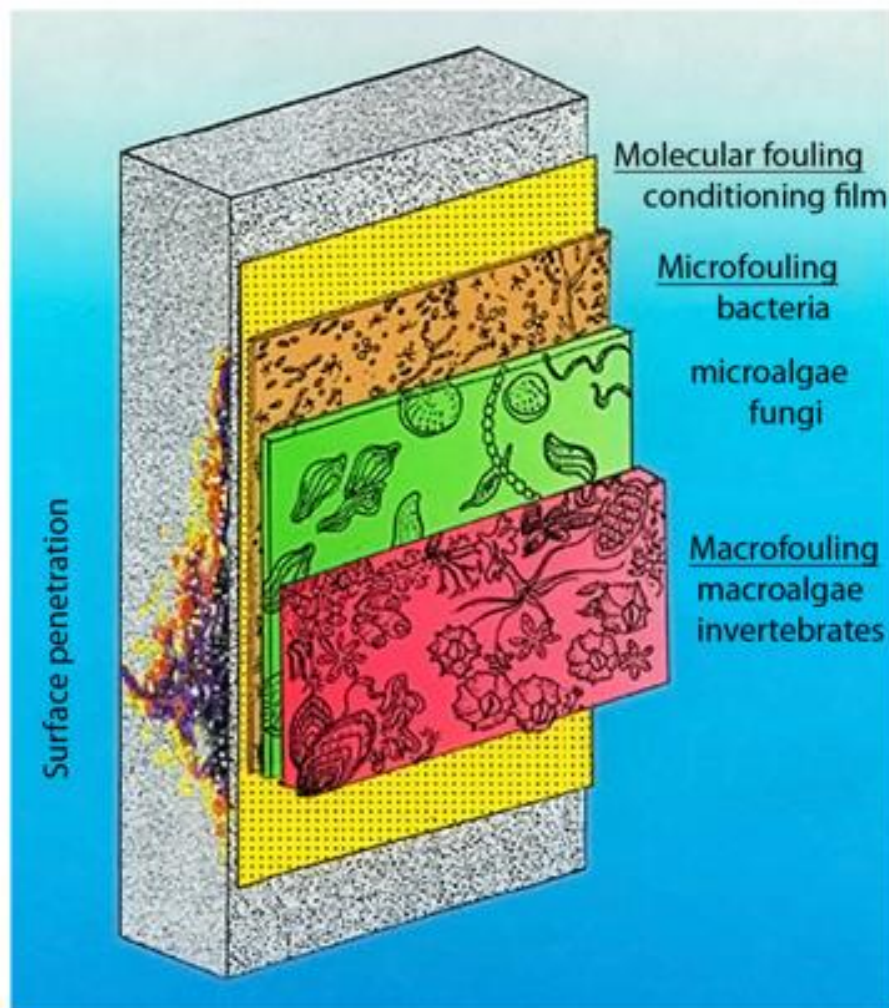
Figure 2-5: Build-up of marine biofouling, source: (Davis and Williamson, 2002).

CONDITIONING	ATTACHMENT	COLONISATION	GROWTH
O_2 Fe^{2+}		WATER CHANNELS	
STEEL SUBSTRATE			
1 minute to 1 hour	1 hour to 24 hours	24 hours to 1 week	2 weeks to 1 month

Microorganism · Spore · Adsorbed organics
Larvae · Extracellular polymeric substances (EPS) · Seawater
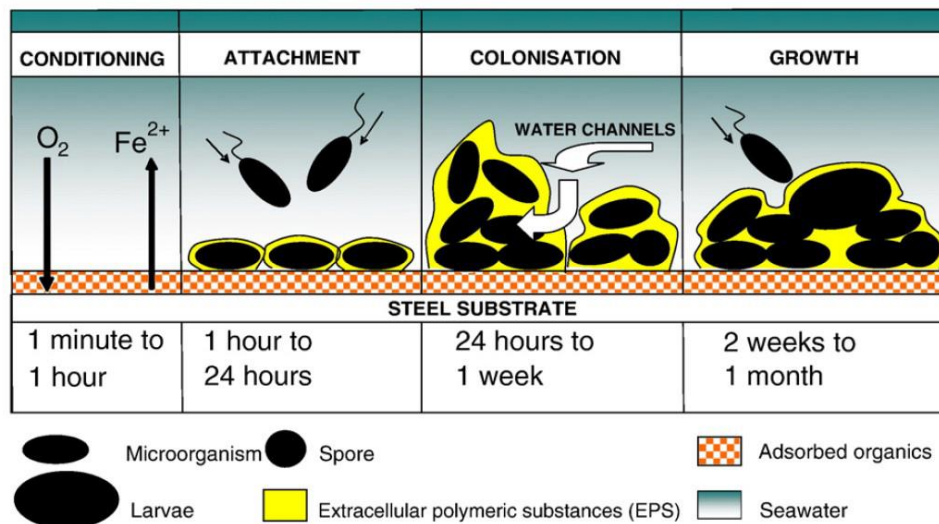
Figure 2-6: Four stages of forming the biofilm, source: (Chambers et al., 2006b).

A macrofouling community *Figure 2-5*, consisting of animal and weed fouling, develops, and grows above the microfouling community. Multicellular organisms, characterised as soft and hard fouling organisms, attach, settle and grow within several days to weeks after the first surface exposure to water (Lewis, 1998). Soft fouling includes algae and invertebrates such as soft corals, sponges, anemones, tunicates and hydroids, while hard fouling includes barnacles, mussels, and tubeworms (Doble and Kumar, 2014). These macrofoulers have diverse attaching techniques, e.g., some species produce an adhesive to attach to the immersed surface. Furthermore, often the attaching processes consist of temporary and permanent adhesions. It is notable that adhesion and settlement stages are critical in the life cycle of marine organisms and are also essential aspects in the perspective of antifouling. In other words, biofouling could be controlled if the attachment and settlement processes could be prevented (Chambers et al., 2006a).

It is important to note that biofouling is particularly likely to occur when a ship is stationary, such as at port. Furthermore, fouling builds up more quickly in tropical waters and varies depending on a ship's operational geographical area. Several factors affect the biofouling accumulation, including the length of time spent at sea, the water temperature, the geographical location of the ship, surface conditions and the salinity of the sea. In general, the longer the ship's immersion time, the greater the level of fouling. Eventually, the more biofouling, the more significant increase in a ship's

resistance. Above all, biofouling accumulates immediately after a ship is immersed in water and will continue to occur throughout a ship's life at sea until a cleaning process is performed (Demirel, 2015).

Biofouling causes an increase in surface roughness, leading to detrimental ship resistance and fuel consumption (Kempf, 1937). (Schultz, 2007) investigated the effect of fouling on the required shaft power for a frigate at a speed of 15 knots. He found that slime (microfouling) caused a 21% increase in shaft power compared to an otherwise identical slime-free frigate, whereas heavy calcareous fouling (macrofouling) led to an 86% increase in shaft power requirements. Biofouling mitigation is, therefore, very desirable from both an economic and environmental point of view (Townsin, 2003).

The impact of biofouling on ship performance is critical and depends on the type of fouling present and the amount of coverage. Furthermore, biofouling is one of the major vectors for spreading non-indigenous species. This spread has been recognised as a great threat to the planet's ecological well-being, human, animal and plant life, the aquatic environment, and cultural and economic activities (IMO, 2019). Vessels can act as a transportation mean, for those forms of life, assisting them to migrate and invade other ecosystems, out-competing them and eventually forcing them into extinction while harming biodiversity.

2.4. Fouling-Control Coatings

The increase in hull roughness due to hull fouling results in an increased ship resistance, fuel consumption and cost associated with drydocking. From an environmental perspective, the increased drag results in increased greenhouse gas (GHG) emissions and the transport of invasive alien species. The optimum method identified to reduce the adverse effects of biofouling on ship performance and marine life sustainability is to prevent biofouling accumulation through fouling control coatings (FCCs). In this context, FCC systems are essential to minimise the fore-mentioned impacts of marine biofouling. The historical development of antifouling

strategies is detailed in (Dafforn et al., 2011). The study highlights how antifouling strategies have changed over time due to new technologies and legislation.

Tributyltin (TBT) based antifouling paints, widely used from the 1960s until the 2000s, can be considered the most successful coatings against marine biofouling. However, TBT compounds persist in water, showing toxic effects on marine organisms even with a low concentration, and they may accumulate in marine organisms and hence enter the food chain (Okay, 2004). Consequently, IMO banned the application of antifouling coatings containing TBT in 2003 and banned the operation of ships coated with TBT paints in 2008 (Champ, 2003; IMO, 2001). Today, several types of coatings are used to mitigate biofouling, but they are not as effective as TBT (Demirel, 2015).
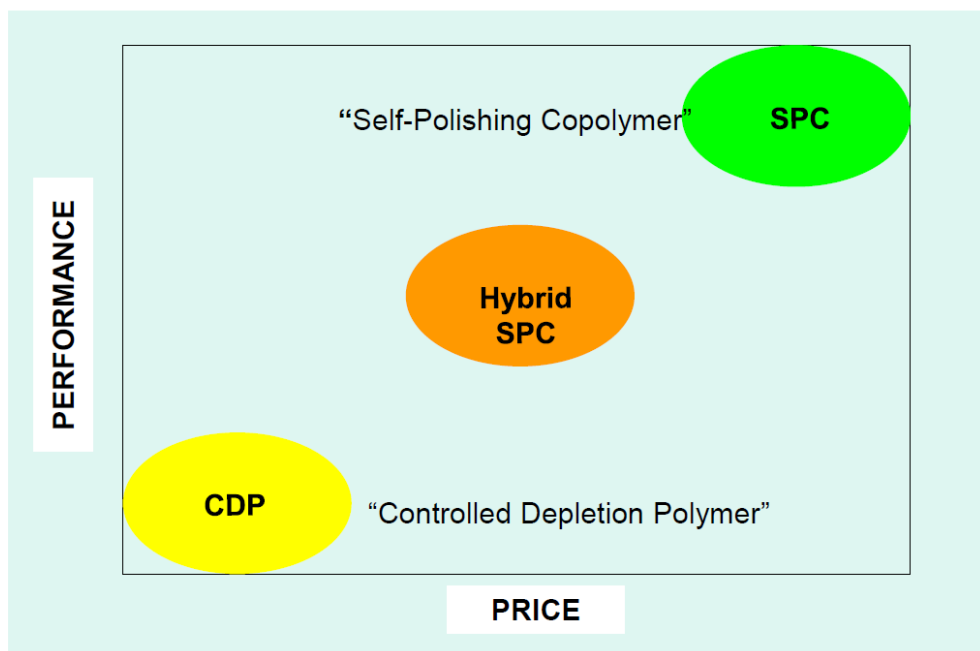
Figure 2-7: Comparison of the performance and price of the key biocidal antifouling coatings, adapted from (Atlar, 2008).

The conventional antifouling method involves the application of antifouling paints (fouling control coatings, FCCs). Furthermore, FCCs can be classified into two main categories based on their compositions: biocidal and non-biocidal coatings. Although many non-chemical methods, including ultrasonics, electric currents, magnetic fields,

16

and optical methods, have been proposed, biocidal FCCs have been the most popular antifouling method due to their unbeatable antifouling performance and low cost. The advantages of biocidal FCCs include ease of manufacture, high-speed and low-cost application, durability, and applicability to various structural forms and compositions (Little and Depalma, 2013), *Figure 2-7*.

Biocidal coatings (or toxic antifouling) can be listed as Controlled Depletion Polymer (CDP), Self-Polishing Copolymer (SPC) and Hybrid SPC. Biocide in the paint surface is gradually released into seawater, forming a toxic layer around the hull. This layer prevents fouling species from attaching to the hull, either by killing the fouling organisms or deterring their settlement (Song, 2020). CDPs use a hydration process and release biocides into the marine environment. They are used for vessels with short drydock intervals and are preferred for ships operating in low-fouling regions (Atlar, 2008). Their effectiveness is said to be up to 3 years (Van Rompay, 2012).

On the other hand, Self-Polishing Copolymers (SPC) have good initial hydrodynamic performance owing to their smooth surfaces and have better antifouling abilities due to a controlled release of the biocide via hydrolysis. They are preferred for vessels which have longer drydock intervals. In fact, SPCs can remain effective for up to 5 years (Van Rompay, 2012). Hybrid SPCs' biocide release method may be regarded as a hybrid of hydrolysis and hydration. The life span of Hybrid SPCs is between 3 and 5 years (Taylan, 2010). However, all biocidal antifouling coatings are under scrutiny regarding their toxic effects; hence, they are all affected by legislative issues and may still be banned soon (Demirel, 2015).

Non-biocidal coatings are foul-release coatings (FR), also called non-stick coatings. Foul release (FR) coatings prevent the attachment of marine species on hulls owing to their physical surface properties (Wahl, 1989), which act like a non-stick coating and prevent the build-up of fouling organisms. However, FR coatings cannot release all the slime from the hull. Additionally, they are only effective above a certain speed since the release mechanism to detach the marine organisms works due to the shear force. Therefore, FR coatings are inappropriate for slow ships and ships that spend a long time in ports (Candries et al., 2003). Also, they are costly compared to other coatings and may be damaged easily by hard-shelled fouling organisms or any

mechanical effects such as cleaning. Due to these limitations, a great deal of effort is being devoted towards developing an environmentally friendly antifouling solution that can eliminate all the drawbacks of the current antifouling coatings. Some of the critical properties of typical SPCs and FR coatings are shown in

Table 2-1 (Van Rompay, 2012). A comprehensive review of the modern approaches to environmentally friendly antifouling systems can be found in (Demirel, 2015; Chambers et al., 2006a).

Table 2-1: Properties of existing hull coatings, adapted from (Demirel, 2015; Van Rompay, 2012).

	Protection and longevity	**Fuel saving properties and conditions**	**Need to drydock for repainting**	**Environmental concerns**
Typical antifouling coatings (SPC)	Soft coating. Fairly easy damaged 3-5 years before AF coating needs to be replaced. Full recoating down to bare steel 2 or 3 times in 25 years. Not suitable for aluminium hulls.	Unfouled hull roughness from AF coating gives 2-4% fuel penalty. Usually, sails with slime up to 20% fuel penalties. Coating degradation increases fuel penalty over time.	5-8 drydockings required for paint alone during ship's service life including 1-3 full blasting and repainting. Multiple coats and length curing times can mean 2-3 weeks in drydock for a full repaint.	Contaminates marine environment with toxic biocides, harming marine life, the food chain, and humans. Pulse release of biocides if cleaned in water. High VOC content when applied. Limits fuel consumption and GHG emissions from effects of heavy fouling.
Typical FR coating system	Soft coating. Easily damaged. 3-5 year before FR coat needs repair/reapplication. Full recoating required 1-3 times in 25 years.	Smoothest tested surface when unfouled. Usually sails with slime = up to 20% fuel penalty. Can foul badly if vessel has long lay-ups. Coating degradation increases fuel penalty over time.	5-8 drydockings required for paint alone during ship's service life including 1-3 full blasting and repainting. Multiple coats and length curing times can mean 2-3 weeks in drydock for a full repaint.	Does not contain biocides but leaches potentially harmful oils, alters enzymes in barnacle glue; some silicones catalysed by highly toxic dibutyltin dilaurate.

The main difficulty in developing an antifouling system is finding a compromise among different and conflicting parameters. In fact, several considerations need to be made in designing a new FCC for optimal results. Details of the main aspects are given in *Figure 2-8* (Demirel, 2015; Chambers et al., 2006a). Furthermore, the requirements for an optimal fouling control coating are described in detail by (Demirel, 2015; Chambers et al., 2006a) in

Table 2-2.

In 2021, Graphite International Technologies (GIT) developed a new fouling control coating, specifically, a hard-foul release coating (also called *FR02* in the present thesis). This new FCC is a result of GIT's effort to develop environmentally friendly antifouling technology to optimise the energy efficiency of ships. As a collaborative effort between the University of Dalhousie and the University of Strathclyde, the hydrodynamic performance of GIT's new hard-foul release coating has been tested. Within this framework, further commercial FCCs and mimicked biofouled surfaces are tested in this thesis to assess the effect of hull roughness on ship hydrodynamics.
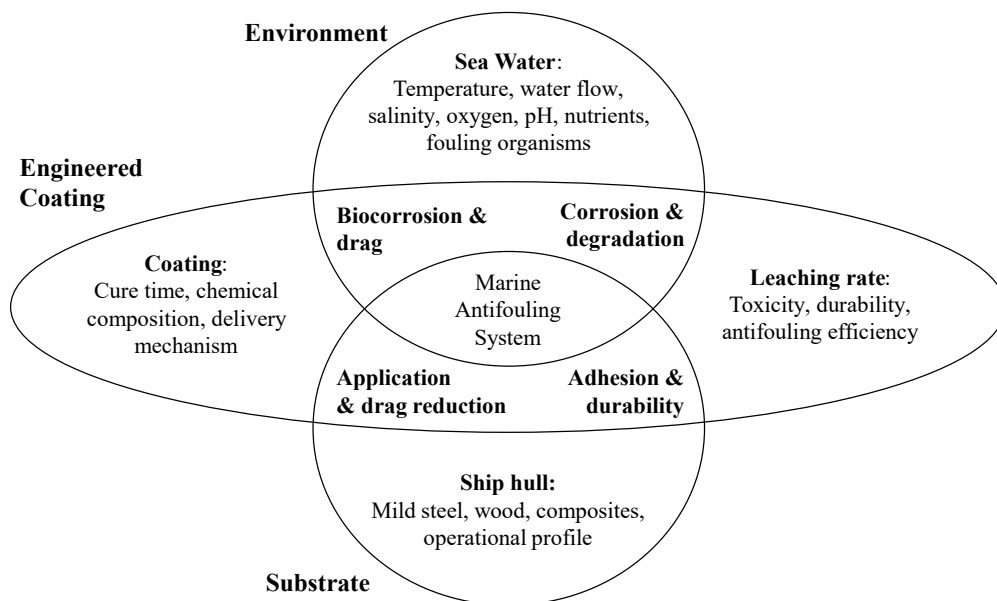
Figure 2-8: Key parameters for fouling control coatings, adapted from (Chambers et al., 2006a).

Table 2-2: Requirements for an optimal fouling control coating, adapted from (Chambers et al., 2006a).

Must be	Must not be
Anticorrosive	Toxic to the environment
Antifouling	Persistent in the environment
Environmentally acceptable	Expensive
Economically viable	Chemically unstable
Long life	A target for non-specific species
Compatible with underlying system	
Froude number	
Reynolds number	
Centre of gravity	
Metacentric height	

2.5. Effects of Hull Roughness on Ship Hydrodynamics

The total resistance for a ship in rough conditions, $C_{T_{rough}}$, can be determined by equation (2-3):

$$C_{T_{rough}} = C_{T_{smooth}} + \Delta C_T \qquad (2\text{-}3)$$

where the total roughness allowance, ΔC_T is the variation in the total resistance coefficient between the rough, $C_{T_{rough}}$, and smooth, $C_{T_{smooth}}$, conditions, and can be given by equation (2-4):

$$\Delta C_T = C_{T_{rough}} - C_{T_{smooth}} \qquad (2\text{-}4)$$

A ship's hull surface condition is crucial to its hydrodynamic performance, and biofouling is the foremost responsible for increased hull roughness which results in increased ΔC_T. In the hull-water interaction scenario, variance depends on two surface roughness parameters: the physical and the biological. The physical roughness is related to the form of the coating. Thus, a ship resistance reduction can be achieved by selecting a more delicate finishing material and further surface treatment.

Predicting the effects of hull roughness on ship hydrodynamics is an active area of research, and there have been several recent advancements in this field. Numerical simulations and experimental studies are commonly used to investigate the impact of hull roughness on ship hydrodynamics. An extensive critical review of the state-of-the-art techniques for monitoring and evaluating the biofouling state and its effects on the vessel's hull and propeller performance can be found in (Valchev et al., 2022). Here are some of the recent state-of-the-art developments in this area:

- Computational Fluid Dynamics (CFD) simulations are commonly used to study the effects of hull roughness on ship hydrodynamics. Recent advancements in CFD techniques have enabled researchers to model the roughness of hull surfaces more accurately. For example, researchers have used the modified wall-function technique to model the turbulent flow around rough surfaces, and they have found that the turbulence intensifies with increasing roughness (Demirel, 2015).

- Experimental studies are commonly used to validate numerical simulations and investigate the impact of hull roughness on ship hydrodynamics. Recent studies have conducted towing tanks model resistance tests in rough conditions (Song et al., 2021b)

- Machine learning and data-driven modeling techniques are also being used to predict the effects of hull roughness on ship hydrodynamics. These techniques use data from experiments or simulations to develop predictive models that can be used to estimate the impact of roughness on ship performance (Coraddu et al., 2019)

- Coating Technologies: Researchers are also investigating the use of advanced coating technologies to reduce hull roughness and improve ship hydrodynamics. For example, researchers have investigated hydrophobic coatings that can repel water and reduce frictional resistance (Ravenna et al., 2022a)

These developments are expected to lead to more accurate predictions of the performance of ships with rough hull surfaces and lead to more efficient and sustainable shipping practices.

Furthermore, extensive literature has been dedicated to assessing the economic and environmental problem of increased hull roughness in the last century (Schultz, 2007; Townsin, 2003). A detailed review can be found in studies such as (Song, 2020) or (Demirel, 2015). Nevertheless, below are reported the most relevant cornerstones of research on the effects of hull roughness on ship resistance.

The first experimental investigation of the effect of hull roughness on ship resistance was conducted by (Froude, 1872) on a destroyer, as reported by (van Manen and van Oossanen, 1988). However, only more than 40 years later, the first comprehensive tests of the effect of fouling on frictional drag were conducted (McEntee, 1916). In (McEntee, 1916), flat plates were coated with anticorrosive paints, exposed to seawater, and then towed periodically to determine the frictional resistance. The results after twelve months showed that the resistance of the plate increased up to four times due to the barnacle's growth on the surface. Later, in 1934, (Hiraga, 1934) reported a 20% increase in the total drag of coated brass plates after 24 days of immersion with grown slime and barnacles on the surface. In the same year, (Izubuchi, 1934) conducted a full-scale towing test to examine the effect of fouling on ship resistance using a destroyer. This vessel was docked, painted, and had the propeller removed and immediately subjected to a towing test. The towing tests were repeated at intervals to show the effect of hull fouling by time. For example, an increase of 100% was found at 16 knots after 375 days due to surface fouling, (Izubuchi, 1934).

Several observations indicate that the frictional resistance of a submerged surface may increase with time of immersion in the absence of macroscopic fouling. This effect is attributed to the slime film, which rapidly develops on surfaces exposed at sea. Therefore, several studies were devoted to investigating biofilms' effect on ship resistance – for example, (Benson et al., 1938) towed plates covered with slime. More than a decade later, (Denny, 1951) observed a 5% increase in skin friction on a vessel was moored for 40 days. The increase was attributed to the thin coat of slime and the deterioration of the bituminous aluminium paint on the hull. Denny also stated that

vessels lying in brackish water increased their frictional resistance by nearly ½ per cent per day for several months, even when there was no evident fouling. Similarly, a ship resistance increase of 9-10% due to slime fouling was measured on a slime-coated ship model (Watanabe et al., 1969).

The hypothesis that thin slime films on rough surfaces may reduce the frictional resistance by effectively smoothing it has been questioned and proved wrong. In fact, (Loeb et al., 1984) found that the slime on the rough surface increases the frictional resistance by 10% compared to the rough surface without slime. Similarly, (Lewkowicz and Das, 1986) found 18% higher frictional resistance for the model slime with a background roughness compared to the background roughness alone. (Haslbeck and Bohlander, 1992) conducted a full-scale trial on a frigate coated with an ablative antifouling paint. With a slime film and little macrofouling on the hull, an 18% increase in the delivered power was observed after 22 months of being moored at sea. Furthermore, (Schultz and Swain, 1999) conducted experiments to study the effect of biofilms and algae on skin friction. The experiment involves boundary layer measurements in a recirculating water tunnel using a Laser Doppler Velocimeter (LDV). An average increase in the skin friction coefficient of 33 to 187% was measured on the fouled specimen. Similarly, (Andrewartha et al., 2010) conducted an experimental study to investigate the effect of biofilm on skin friction using a recirculating water tunnel. They measured up to a 99% increase in the drag of the test plates due to the biofilms on the plates.

Recently, the effect of biofouling has been investigated by replicating fouler geometries (mimicked biofouling). For example, (Demirel et al., 2017b) conducted an extensive series of towing tests of flat plates covered with artificial barnacle patches to obtain the roughness functions of barnacles with varying sizes and coverages. Different sizes of real barnacles were 3D scanned and printed into artificial barnacle patches. The result showed a 119% increase in skin friction with the most severe fouling condition (i.e., big barnacles, 20% coverage). (Uzun et al., 2020) extended the study of (Demirel et al., 2017b) to investigate the effect of the settlement pattern of barnacles. A chaotic settlement, which is called 'natural settlement', was designed to

represent real barnacle settlement in nature. The result showed that changes in settlement patterns alone could cause up to 10.5% additional frictional resistance.

Further realistic 'in-service' conditions were tested by (Li et al., 2019), who investigated the effect of marine biofilm on surfaces coated with different-sized cuprous oxide (Cu2O) particles. They installed conveniently coated panels on a detachable twin strut system to develop biofilms on the panels. The strut system was deployed under the moon-pool plug of a catamaran research vessel and exposed to the sea for various periods. Eventually, the frictional drag of the test panels was measured using a turbulent flow channel after every 6-week deployment period. Finally, the result showed an 83% increase in frictional drag due to the biofilm developed for six months.

Finally, although extensive literature was dedicated to assessing the effect of hull roughness on ship resistance, as summarised in this section, understanding the hydrodynamics behind the problem is still limited. Therefore, investigating the interaction between hull roughness and the turbulent boundary layer is essential to find the rationale behind the effect of hull roughness on ship hydrodynamics.

2.5.1. The Turbulent Boundary Layer

Hull resistance is a crucial parameter on ships as it negatively affects their speed, powering requirements, and fuel consumption. Intuitively, a rough surface creates higher friction than a smoother surface. Though how does hull roughness influence ship resistance? Understanding the turbulent boundary layer concept is essential to find the rationale behind the roughness effect on ship hydrodynamics.

Turbulent boundary layers occur when fluid flows over a surface with high velocity, creating eddies and turbulence in the boundary layer next to the surface. In other words, the boundary layer is a thin region near the surface of an object in a fluid flow (Schlichting and Gersten, 2017). One of the most fundamental theories in turbulent boundary layer research is the "law of the wall." This law states that the mean velocity profile of a turbulent boundary layer near a smooth wall can be described by a power-

law relationship with the distance from the wall. Specifically, the velocity varies proportionally to the logarithm of the distance from the wall, and this relationship is characterized by a universal constant known as the von Kármán constant. However, when the surface of the boundary layer becomes rough, such as with sandpaper or a rough surface, the law of the wall is modified. Roughness effects can change the velocity profile, and the roughness length is introduced as an additional parameter to describe the velocity profile. The roughness length characterizes the height of the roughness elements and can significantly affect the turbulence structure.

Furthermore, the work of Prof Javier Jimenez, Prof Ivan Marusic, Prof Beverley McKeon, and Prof Bharathram Ganapathisubramani has significantly advanced our understanding of turbulent boundary layers and roughness effects. Significant contributions to understanding roughness effects on turbulent boundary layers have been made in (Jiménez, 2004). This research has shown that the roughness length plays a critical role in the modification of the velocity profile near rough surfaces. Additionally, it proposed a new power-law relationship for rough surfaces that involves a second parameter, the roughness Reynolds number, which characterizes the roughness intensity.

Similarly, (Marusic et al., 2012) have also contributed to the understanding of roughness effects on turbulent boundary layers. Their work has shown that the roughness length and roughness Reynolds number are essential parameters in describing the turbulent structure of the flow near a rough surface. Furthermore, their research has shown that the roughness Reynolds number can affect the behaviour of the turbulent eddies and their interactions with the roughness elements.

Additionally, (McKeon et al., 2004) have focused on the impact of streamwise-aligned roughness on turbulent boundary layers Their research has shown that the length and height of the roughness elements can affect the behaviour of the turbulence structure, including the amplification or attenuation of turbulent eddies. Additionally, they studied the impact of surface roughness on flow separation and has proposed methods to mitigate the adverse effects of roughness on flow control.

Finally, (Ganapathisubramani et al., 2012) have investigated the effects of roughness on turbulent boundary layers in both experimental and numerical studies Their research has shown that roughness length, Reynolds number, and the spacing of the roughness elements all play significant roles in modifying the velocity profile and turbulence structure near rough surfaces. Furthermore, their work has shown that roughness effects can be mitigated by controlling the spacing and orientation of the roughness elements.

Notably, Prandtl introduced the boundary layer concept in 1904 to describe the flow around an object. It is known that the velocity at the surface of an object is zero (i.e., no-slip condition), whereas the fluid flow velocity is the freestream value at some distance away from the object (i.e., free-stream velocity). According to Prandtl, the boundary layer is the velocity gradient occurring in the thin layer between the no-slip condition and the freestream velocity. *Figure 2-9* illustrates the velocity gradient in the boundary layer and the growth of the boundary layer thickness. This boundary layer thickness, δ, is usually described as the distance between the wall and the point where the velocity magnitude of the flow reaches 99% of the free-stream velocity, U_∞. Furthermore, δ, increases as the fluid moves downstream and other fluid particles are accelerated.
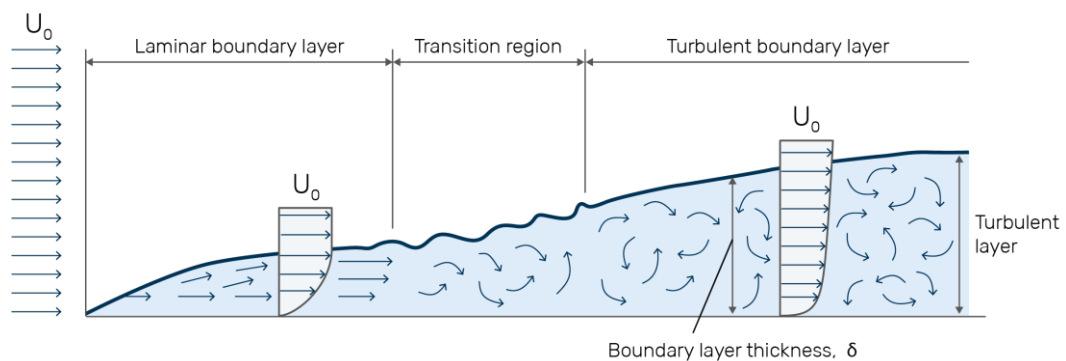
Figure 2-9: The development of a turbulent boundary layer over a flat surface in smooth conditions, adapted from: https://www.grasacoustics.com/.

As seen in *Figure 2-9*, the flow remains laminar for a distance downstream of the smooth flat plate. In this laminar region, the flow creates less skin friction than turbulent flow. It can be noted that the turbulent flow is reached after a certain distance from the leading edge of the plate and after the unstable transitional flow. The laminar

region takes a small portion of the flow around a ship, while the turbulent boundary layer covers most of the hull. For example, when the critical Reynolds number for a typical flat plate, $Re_{crit} = 5x10^5$ is used, the transition for a 230m-long container ship cruising at 24 knots occurs after 5cm from the leading edge (Song, 2020).

Moreover, the turbulent boundary layer can be divided into two main regions: inner and outer regions. The surface conditions, such as roughness, affect the inner region, whilst such conditions do not affect the outer region. Further assumptions made in this study are that the inner region is composed of a viscous sublayer and a log-law region, Figure 2-10. The mean average velocity in the inner region depends upon wall shear stress, the density of the fluid, kinematic viscosity, and the distance from the wall. Furthermore, In the inner region, consisting of the viscous sublayer and log-low region, about 70% of velocity variation occurs, although this layer is as thin as only 10-20% of the turbulent boundary layer thickness (Schultz and Swain, 1999).
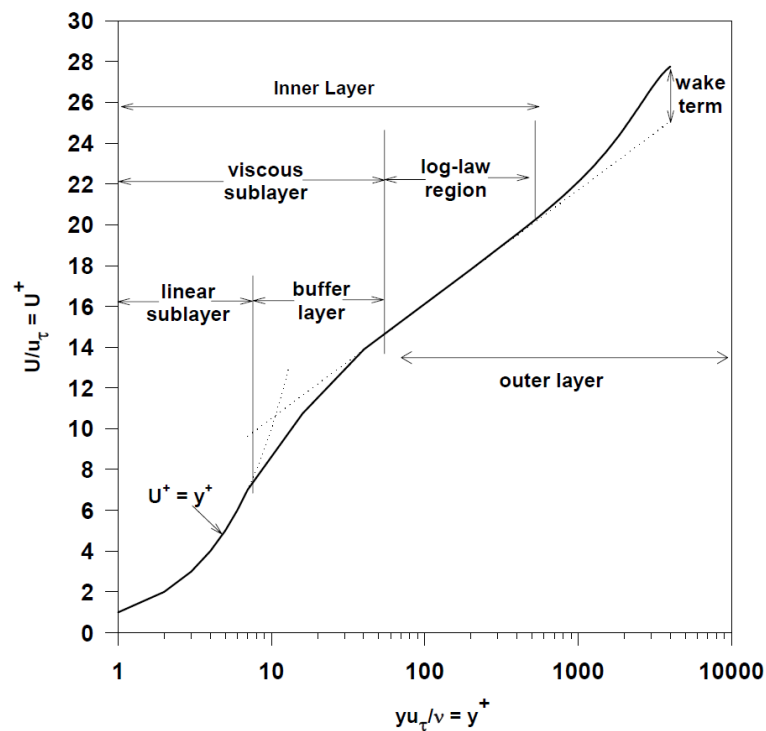
Figure 2-10: Velocity profile in a typical turbulent boundary layer, adapted from (Shapiro, 2004).

Figure 2-10 shows that the non-dimensional velocity profile in the inner region of the boundary layer, U^+, can be expressed as a function of the non-dimensional distance from the boundary, y^+, equation (2-5):

$$U^+ = f(y^+) \tag{2-5}$$

Where U^+ and y^+ can be further defined in equations (2-6) and (2-7), respectively.

$$U^+ = \frac{U}{U_\tau} \tag{2-6}$$

$$y^+ = \frac{y\,U_\tau}{\upsilon} \tag{2-7}$$

Where U_τ is the friction velocity defined as $\sqrt{\tau_w/\rho}$, τ_w is the wall shear stress, and υ is the kinematic viscosity defined as the ratio of dynamic viscosity and the fluid density, μ/ρ.

In the linear sublayer, $y^+ < 7$, the wall boundary conditions restrict the eddy motion. Therefore, no turbulence is expected; this layer is referred to as a linear sublayer, *Figure* 2-10. Hence, in the linear sublayer, the velocity profile can be expressed by equation (2-8):

$$U^+ = f(y^+) \tag{2-8}$$

On the other hand, in the buffer region of the viscous sublayer, $7 < y^+ < 30$, the velocity profile becomes unilinear. Finally, the velocity profile in the region outside the viscous sublayer, $30 < y^+ < 300$, follows the log-law. It is of note that for a smooth surface, the log-law velocity profile is given by equation (2-9):

$$U^+ = \frac{1}{\kappa}\ln y^+ + B \tag{2-9}$$

where, κ is the von Karman constant (0.42) and B is the log-law intercept constant that depends on the flow conditions.

It is of note that while the existence of a log-law region of the boundary layer has been proved by several studies such as (Clauser, 1956), the values of k and *B*, are still under debate (George, 2007). Furthermore, the remaining 80-90% of the turbulent boundary layer is called the outer region ($0.1 < \frac{y}{\delta} < 0.2$). Finally, the mean velocity and the turbulence intensity in this region are assumed not to be affected by the fluid viscosity and surface conditions, i.e., Townsend's hypothesis (Townsend, 1980). Therefore, the velocity defect law can be expressed by equation (2-10):

$$\frac{U_\infty - U}{U_\tau} = f\left(\frac{y}{\delta}\right) \qquad\qquad (2\text{-}10)$$

2.5.2. Roughness Effect in the Turbulent Boundary Layer

Surface roughness affects the boundary layer of water flowing over a rough surface by causing the flow to become more turbulent, which in turn increases the drag and frictional forces acting on the surface. When water flows over a hydraulically smooth surface, the boundary layer is thin and the flow generally tends to be laminar, with the water molecules moving in smooth layers parallel to the surface. However, when the surface is rough, the water molecules are disrupted by the surface irregularities, creating small vortices and eddies that mix the flow and cause it to become turbulent. This turbulence creates a thicker boundary layer, which increases the drag and frictional forces acting on the surface. As the surface roughness increases, the boundary layer becomes thicker and the turbulence more intense, resulting in even higher levels of drag and friction. This is why it is important to account for surface roughness when designing ships, pipelines, or other fluid systems, as it can have a significant impact on their performance and energy efficiency.

In the literature on turbulent flow, roughness is classified into two main categories: homogeneous and heterogeneous roughness. Homogeneous roughness refers to the surface where roughness elements are distributed uniformly in terms of size, shape, and spacing. For example, a surface covered with sandpaper of the same grit size would be considered a homogeneous rough surface. On the other hand, heterogeneous

roughness refers to a rough surface. that has variations in its roughness properties over its surface. For example, a surface with patches of different grit sizes of sandpaper would be considered a heterogeneous rough surface. Notably, in the current thesis, it is exploited a spatially heterogeneous hull roughness made by patches of homogeneous sandpaper like roughness.

Homogeneous roughness has a relatively predictable impact on ship resistance, as the regularity of the roughness allows for the use of mathematical models to estimate the increase in resistance. However, the impact of heterogeneous roughness is more difficult to predict, as the irregularity of the roughness can lead to a wide range of resistance values. To estimate the impact of heterogeneous roughness, empirical data obtained from model testing and full-scale trials are often necessary.

In terms of ship resistance in hull rough conditions, the literature on turbulent flow and roughness can be applied to understand how the hull surface affects the flow of water around the ship. A rough hull surface can lead to increased drag and resistance, which can result in higher fuel consumption and reduced speed. The degree of roughness and its distribution on the hull surface play a critical role in determining the resistance of a ship. By understanding the properties of roughness and how they affect turbulent flow, researchers can develop strategies to reduce hull roughness and improve the efficiency of ships.

In other words, surface roughness leads to increased turbulence manifesting itself as turbulent shear stress and wall shear stress increase. The increase in skin friction decreases the momentum of the flow, and this momentum loss due to the roughness effect can be observed in the velocity profile in the log-law region. In rough surface conditions, the velocity, U^+, in the turbulent boundary layer decreases, (Clauser, 1956), *Figure 2-11*. The mean log-law velocity profile decrease within the boundary layer is called the roughness function, ΔU^+, and it is a unique characteristic of a surface covered with a specific roughness. Schultz validated the assumption that roughness functions can represent given hull surface conditions by comparing his experimental results with others (Schultz, 2004). Therefore, the roughness effect can also be seen as a downward shift of the non-dimensional velocity profile in the turbulent boundary layer log-law region (i.e., variance in the local velocities).

The non-dimensional velocity profile (U^+) in the log-law region for a rough surface can be written as equation (2-11), (Hama, 1954):

$$U^+ = \frac{1}{\kappa}\ln y^+ + B - \Delta U^+ \qquad (2\text{-}11)$$

where κ is the von Karman constant, B is the log-law intercept constant. $y^+$is the dimensionless distance from the wall, defined as in equation (2-7). The roughness function, ΔU^+, which represents the difference between the actual velocity and the mean velocity of the flow, is a function of the roughness Reynolds number, k^+.

Equation (2-11) is used to describe the velocity profile of a turbulent boundary layer for a rough surface. The assumptions underlying this equation include: the flow is turbulent, fully developed, steady, incompressible, parallel to the boundary, isotropic (far away from the wall) and homogeneous; the boundary layer is thin compared to the characteristic length scale of the flow; the fluid properties are constant, and the effects of viscosity dominate over other forces, such as inertia or gravity.

These assumptions allow the equation to provide a reasonably accurate approximation of the velocity profile in many practical applications, such as in the prediction of surface roughness effects on flows, in the design of pipelines or the analysis of atmospheric flows. However, it should be noted that there are limitations to the law of the wall, and it may not be applicable in all situations, particularly in cases where the flow is highly non-uniform, or the boundary layer is not thin.

The roughness Reynolds number, k^+ is defined by equation (2-12), (Nikuradse, 1933):

$$k^+ = \frac{kU_\tau}{\nu} \qquad (2\text{-}12)$$

where, k is the roughness lengths scale of the surface, U_τ is the friction velocity defined as $\sqrt{\tau_w/\rho}$, τ_w is the wall shear stress, and ν is the kinematic viscosity defined as the ratio of dynamic viscosity and the fluid density, μ/ρ. Nikuradse equation is an empirical relation developed from experiments on pipe flow based on the assumption that the turbulence in the flow is fully developed and that the roughness of the wall is

the dominant factor affecting the fluid flow. The equation relates the roughness height to the friction velocity, which is a measure of the shear stress at the wall.

The model behind this equation assumes that the roughness of the pipe wall causes turbulent eddies to form in the fluid. The thinking behind Nikuradse model is that in turbulent flow, the velocity profile near a solid boundary is no longer linear, and the presence of roughness elements on the wall leads to additional turbulent mixing. In fact, the equation assumes that the friction velocity is proportional to the square root of the wall shear stress.

This assumption fails when the flow is not fully developed, such as in the case of a developing boundary layer or a transitional flow regime. In these cases, the velocity profile may not be fully developed, and the roughness of the wall may not be the dominant factor affecting the fluid flow. Additionally, the assumption may not hold for flows over very rough surfaces, where the roughness height is large compared to the boundary layer thickness, or for flows where the shape of the roughness elements deviates from the sand grain.

As mentioned, the law of the wall in the inner region changes in the presence of surface roughness. Therefore, the velocity in the inner region of the turbulent boundary layer over a rough surface becomes a function of y^+ and k^+, given by equation (2-13):

$$U^+ = f(y^+, k^+) \qquad (2\text{-}13)$$

It should be borne in mind that ΔU^+ is zero in the case of a smooth surface, Equation (2-11) becomes Equation (2-9). One can represent the change in the velocity profile due to roughness using ΔU^+, and the velocity profile can be defined by simply subtracting ΔU^+ from the smooth velocity profile given by equation (2-9). For this reason, (2-11) is used in this study to define the velocity profile.

The roughness of a surface refers to the irregularities, bumps, and texture that exist on the surface. When a fluid, such as air or water, flows over a rough surface, the flow behaviour can be greatly influenced by the type and degree of roughness present.

The different types of roughness can generate different flow regimes. For example, if the surface roughness is relatively small compared to the characteristic length of the flow (such as the diameter of a pipe), then the flow can be considered "smooth" and will exhibit laminar or turbulent flow depending on the Reynolds number. In this case, the roughness may not have a significant effect on the flow behaviour.

However, if the surface roughness is comparable or larger than the characteristic length of the flow, then the flow behaviour can change significantly. This is because the roughness can disrupt the flow, causing it to become more turbulent and unsteady. The flow can also separate from the surface, causing areas of recirculation or turbulence.

In general, there are four different flow regimes that can occur over rough surfaces:

- Smooth laminar flow: This occurs when the surface roughness is small and the flow is dominated by viscous forces.

- Transitional flow: This occurs when the surface roughness is comparable to the characteristic length of the flow and the flow is transitioning from laminar to turbulent.

- Turbulent flow: This occurs when the surface roughness is large and the flow is dominated by turbulent forces.

- Separated flow: This occurs when the flow separates from the surface due to the roughness, causing areas of recirculation and turbulence.

According to (Schlichting and Gersten, 2017), when the roughness height does not extend into the laminar sub-layer, the velocity profile in the boundary layer is not affected by the roughness. The flow regime, in this case, is called hydraulically smooth (smooth laminar flow). On the other hand, if the roughness is partly outside the laminar sublayer, the flow is then in the transitionally rough regime. In this case, the roughness generates an added resistance due to the form drag compared to an otherwise smooth surface. Finally, if all the roughness protrusions are outside the laminar sublayer, the flow is referred to as a fully rough regime, and the law of the resistance is quadratic. In other words, while the mean velocity of the outer region is always assumed not to

be affected by surface roughness and obeys the velocity defect law (Clauser, 1956; Hama, 1954), ΔU^+ is typically affected by the existence of surface roughness (Granville, 1987).

In other words, the type of roughness and the degree of roughness present can determine which flow regime occurs. For example, small-scale roughness such as sandpaper can generate transitional or turbulent flow, while large-scale roughness such as a brick wall can cause separated flow. The degree of roughness can also be quantified by the roughness height or the roughness length scale (the roughness height compared to the characteristic length of the flow), which can help predict the flow regime.

It should also be noted that different roughness types may generate different flow regimes on surfaces even if the same roughness Reynolds number is recorded (Schultz, 2007). For example, the flow on a uniform sand roughness can be classified as hydraulically smooth when $k^+ < 5$. The same flow would be classified as transitionally rough when $5 \leq k^+ \leq 70$, and it can be classified as fully rough when $k^+ > 70$. On the other hand, the flow on a three-dimensional rough surface representing real engineering surfaces, rather than a uniform sand roughened surface, can be classified as hydraulically smooth when $k^+ < 5$, and fully rough when $k^+ > 25$ (Schultz, 2007). Notably, the roughness regimes of this thesis fit into the fully rough when sandpaper like surfaces are tested. On the other hand, transitional flow regime is experienced by the fouling control coatings tested.

Another interesting point to note is that theoretical and numerical methods based on the turbulent boundary layer theory can predict the roughness effect on ship resistance, provided that the roughness function of the surface is known (Demirel, 2015). However, the ΔU^+ values are a unique characteristic of a rough surface and are typically obtained experimentally.
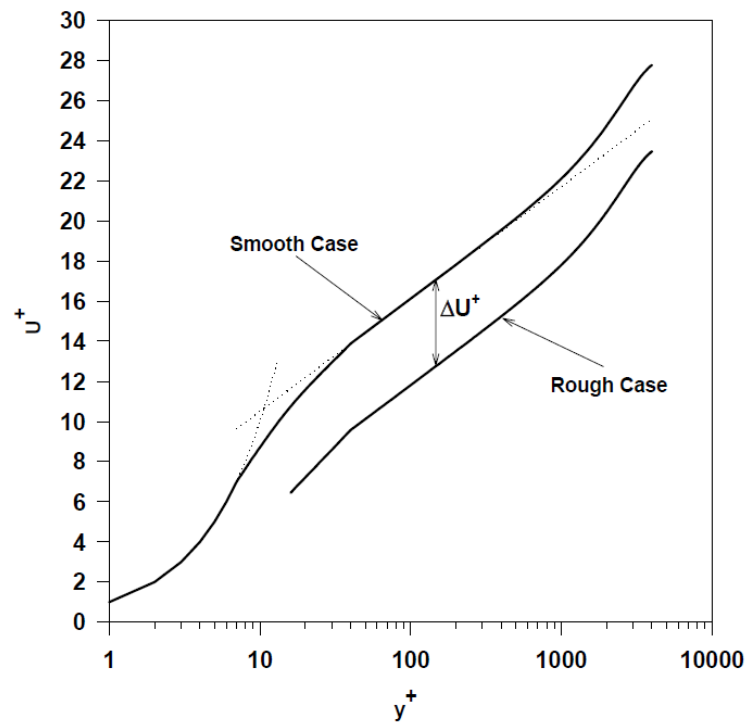
Figure 2-11: The roughness effect on a log-law velocity profile, adapted from (Schultz and Swain, 1999).

2.6. Roughness Functions Determination

It is to bear in mind that for the roughness function (or velocity loss function), ΔU^+, is intended further retardation of flow in the boundary layer over a rough surface due to the physical roughness of that surface, which manifests itself as additional drag relative to a smooth surface. The turbulent boundary layer similarity law analysis (Granville, 1978, 1958) can predict the drag of any structure covered with a specific roughness, provided that the roughness functions of the surface are known. Similarly, roughness function models can be embedded in CFD simulations using the modified wall-function approach to conduct ship resistance predictions. Furthermore, embedding the roughness function of the hull surface in CFD avoids the most challenging barrier of describing the actual hull surface numerically in CFD. However, different surfaces are characterised by different roughness functions, which can only be modelled experimentally (Schultz and Myers, 2003; Granville, 1958). (Lindholdt et al., 2015) gave a comprehensive overview of the experimental methods to obtain roughness functions and their advantages and disadvantages. Furthermore,

(Yeginbayeva et al., 2018) presented a historical overview of the experimental facilities used in hull coating hydrodynamic tests.

The roughness function types of Colebrook (Colebrook and White, 1937) and Nikuradse (Nikuradse, 1933) might be assumed to be the extreme cases (Demirel, 2015). Therefore, the roughness functions of realistic surfaces are expected to be between the monotonic Colebrook and inflectional Nikuradse type roughness functions, such as those presented by (Grigson, 1992) and (Schlichting and Gersten, 2017; Cebeci and Bradshaw, 1977). Equation (2-14) defines the Colebrook-type roughness function model, (Grigson, 1992):

$$\Delta U^+ = \frac{1}{\kappa} ln(1 + k^+) \qquad (2\text{-}14)$$

where the von Karman constant, κ is equal to 0.41.

Though how can roughness function be determined experimentally? Roughness functions can be determined through direct or indirect methods. The direct method requires the measurement of the boundary layer profiles, which requires more accessible channels and costly set-up systems (e.g., laser doppler anemometry). Furthermore, using direct methods, the determination of U_τ (non-dimensional velocity profile) for a rough-wall profile is more prone to error since the choice of the y-origin will directly affect the ΔU^+ values (Schultz and Myers, 2003). On the other hand, indirect methods are generally more straightforward and convenient as they are more readily attainable and require a less expensive investment to measure than direct methods (Granville, 1987). Therefore, in this thesis, two similar indirect methods have been used to determine the roughness functions of the test surfaces.

Granville derived several indirect methods, including the local method with displacement thickness (Granville, 1987) based on the work of (Hama, 1954), the overall method for towed plates (Granville, 1987, 1958), the indirect method for rotating disks (Granville, 1978), a local method without displacement thickness and finally the indirect method for pipes (Granville, 1987). There have been many experimental studies to determine the roughness functions, $\Delta U+$, and the corresponding roughness Reynolds number, $k+$, using these methods. However, only

the overall method for towed plates (Granville, 1987, 1958) and the indirect method for pipes will be used in this thesis and are described in detail below.

In particular, Granville's models for predicting the roughness functions of rough surfaces assume that the skin friction drag coefficient can be related to the boundary layer thickness and the momentum thickness. As mentioned earlier, the boundary layer is the layer of fluid that is adjacent to the surface of the plate, and the momentum thickness is a measure of the thickness of the boundary layer. Furthermore, Granville's models assume that the friction factor can be estimated by the Colebrook or Nikuradse equations and that the flow is fully developed. Notably, the models consider the effect of pipe diameter, roughness, and Reynolds number on the pressure drop. Additionally, the implementation of Granville's model involves the calculation of the Reynolds number based on the momentum thickness and the ratio of the displacement thickness to the boundary layer thickness, followed by the use of an explicit equation to calculate the skin friction drag coefficient. Despite being accurate for a wide range of Reynolds numbers, Granville model is limited to predicting the skin friction drag coefficient for flat surfaces.

At this point, it is also worth elaborating on the roughness models such as Colebrook (Colebrook and White, 1937) or Nikuradse (Nikuradse, 1933) since the first part of the thesis relies heavily on them and they form the backbone of the study. Notably, Colebrook or Nikuradse models were developed to estimate the friction factor (key parameter that affects the pressure drop and flow rate of a fluid in a given system) for fluid flow in rough pipes or channels.

Colebrook's model is used to predict the friction factor in turbulent pipe flow for both smooth and rough pipes. It assumes that the turbulent flow is fully developed which means that the velocity profile is logarithmic and does not change in the downstream direction. The roughness of the pipe wall is represented by the roughness height, and the Reynolds number is a measure of the flow regime. The Colebrook equation is used in engineering and is accurate for a wide range of Reynolds numbers and roughness heights. However, it requires an iterative solution and is not always easy to use.

Nikuradse's law is another roughness model that is used to predict the friction factor for turbulent flow in pipes. This model assumes that the roughness of the pipe wall is the dominant factor in determining the friction factor. The equation relates the friction factor to the relative roughness and the Reynolds number. The Nikuradse equation is less accurate than the Colebrook equation, and it is generally used only for small Reynolds numbers or very rough pipes. However, is simpler to use and requires fewer input parameters simpler to use and requires fewer input parameters.

One disadvantage of these methods is that they are based on certain assumptions that may not always hold true in real-world applications. As mentioned, the Colebrook equation assumes that the flow is fully developed and that the velocity profile is logarithmic, but these assumptions may not be valid for non-uniform flows or flows with high levels of turbulence. Similarly, the Nikuradse equation assumes that the roughness can be characterized by a single length scale, but this may not be accurate for surfaces with complex roughness patterns.

A graphic example of roughness functions is presented in *Figure 2-12* from (Schultz and Myers, 2003) showing the Nikuradse-type roughness function for uniform sand given by (Schlichting and Gersten, 2017; Cebeci and Bradshaw, 1977) and Colebrook-type roughness function of (Grigson, 1992). The roughness function values of different surfaces, such as the 60-grit sandpaper and 220-grit, are also presented in the figure. Furthermore, the figure shows the roughness functions values from three different methods, namely the velocity profile, towed plate, and rotating disk methods. It is seen from the results that there is an excellent agreement between the overall method and the velocity profile method. These results suggest that indirect methods can be used to evaluate the roughness functions. Additionally, the overall method is referred to as the best combination of accuracy and complexity by the (ITTC, 2011a).

Additionally, it is to be noted that the selection of the roughness length scale, k, is critical to define a roughness function model, though k does not affect the roughness function value - it only affects the abscissa of the profile of roughness functions against roughness Reynolds numbers (Demirel, 2015). For this reason, k, can be selected such that the ΔU^+ values fall on a pre-defined roughness function model, provided that the

observed behaviours are still deemed appropriate relative to each other. For example, in *Figure 2-12* the roughness functions against roughness Reynolds numbers for different surfaces are fitted to the Nikuradse or Colebrook models by changing the roughness length scale values.
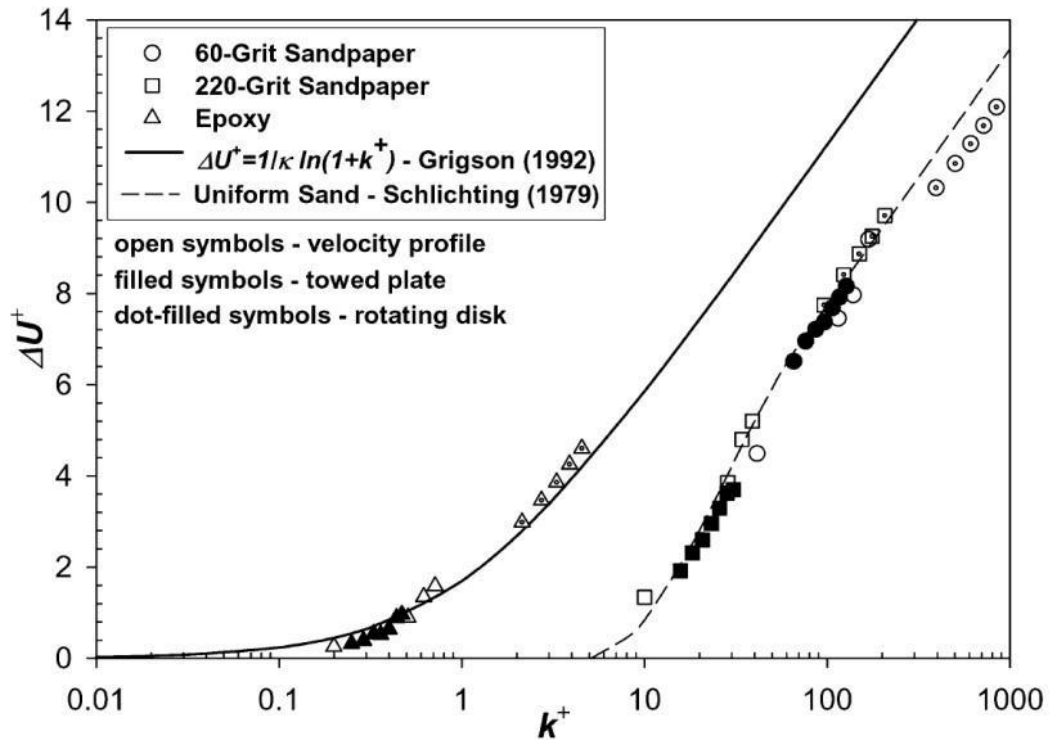
Figure 2-12: Roughness functions for the test surfaces obtained using the velocity profile, towed plate, and rotating disk methods (Schultz and Myers, 2003).

2.6.1. Overall Method: Towed Plate

The overall method to determine the roughness functions of a rough surface, *Figure 2-13*, was detailed by (Granville, 1987) following his earlier studies (Granville, 1958) and used in several studies such as (Demirel et al., 2017b; Demirel, 2015; Schultz, 2004; Schultz and Myers, 2003; Shapiro, 2004). This method can be used for flat plate towing tests, as in the present thesis; therefore, it is also called towed plate method. The procedure involves towing tests of flat plates covered with any roughness.
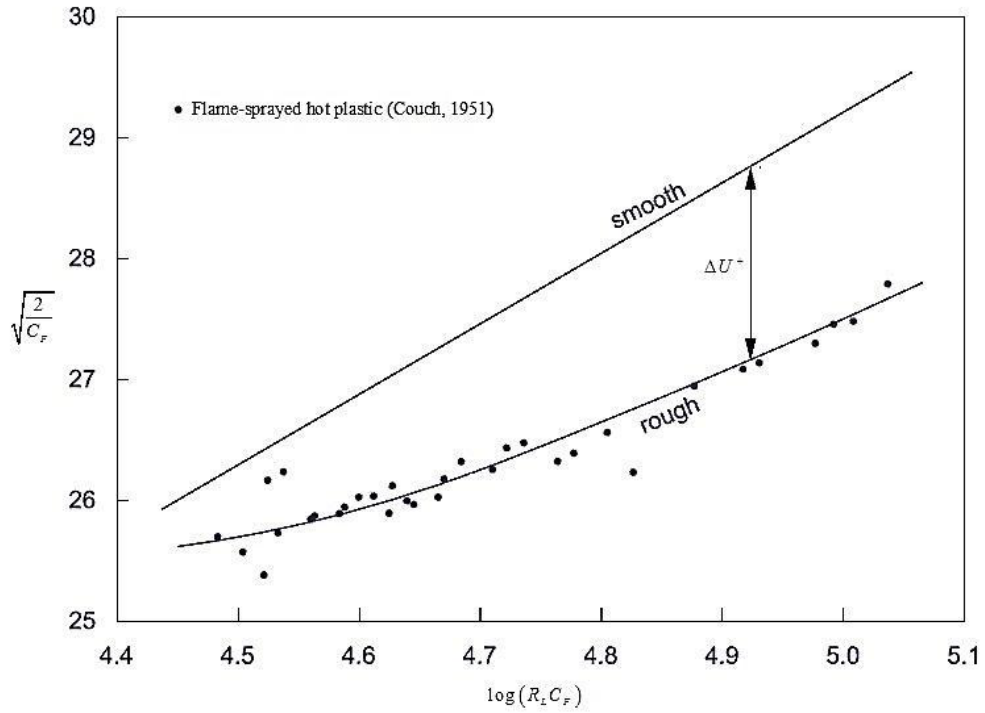
Figure 2-13: Overall method for towed plates to determine the roughness functions of a rough surface (Granville, 1987).

Once the global frictional resistance coefficients of the flat plate, $C_F = R_F / 0.5 \, \rho \, S \, V^2 = C_T - C_R$, are known from towing tests, the roughness functions, ΔU^+, and corresponding roughness Reynolds numbers, k^+, can be obtained as in equations (2-15) and (2-16), respectively:

$$\Delta U^+ = \left(\sqrt{\frac{2}{C_F}} \right)_s - \left(\sqrt{\frac{2}{C_F}} \right)_r - 19.7 \left[\left(\sqrt{\frac{C_F}{2}} \right)_s - \left(\sqrt{\frac{C_F}{2}} \right)_r \right]$$
$$- \frac{1}{\kappa} \Delta U^{+\prime} \left(\sqrt{\frac{C_F}{2}} \right)_r \tag{2-15}$$

$$k^+ = \left(\frac{k}{L}\right)\left(Re_L \frac{C_F}{2}\right)\left(\sqrt{\frac{2}{C_F}}\right)_r \left[1 - \frac{1}{\kappa}\left(\sqrt{\frac{C_F}{2}}\right)_r\right.$$
$$\left. + \frac{1}{\kappa}\left(\frac{3}{2\kappa} - \Delta U^{+\prime}\right)\left(\frac{C_F}{2}\right)_r\right]$$

(2-16)

where, L is the length of the towed plate, Re_L is the Reynolds number based on the plate length and the towing speed, $\Delta U^{+\prime}$ is the slope of the roughness function against $\ln k^+$. It is of note that the subscript s indicates a smooth condition, whereas the subscript r indicates a rough condition. Furthermore, the C_F values of smooth and rough conditions are the values at the exact value of $Re_L C_F$ (Granville, 1987). As the equations are implicit, they need to be solved iteratively.

2.6.2. Indirect Method for Pipes

The indirect method for characterizing the drag of an arbitrarily rough surface on a fully developed pipe flow was proposed by (Granville, 1987) (*Figure 2-14*). The procedure can be used to calculate the roughness function ΔU^+ and roughness Reynolds number k^+ as in equations (2-17) and (2-18):

$$\Delta U^+ = \sqrt{\frac{2}{c_{f,s}}} - \sqrt{\frac{2}{c_{f,r}}}$$

(2-17)

$$k^+ = \frac{1}{\sqrt{2}} Re_{M,r}\sqrt{c_{f,r}}\frac{k}{D_h}$$

(2-18)

where, $c_{f,s}$ and $c_{f,r}$ are the skin friction factors, or Fanning factors, measured in the smooth and rough pipes, respectively, at the same value of $Re_M\sqrt{c_f}$, and k is the roughness length scale. Re_M is the Reynolds number based on the mean bulk velocity and channel height. D_h is the hydraulic diameter of the pipe. It is important to note that these equations can also be used for the drag characterisation of rough surfaces with a

2D flow channel, as done in several studies (Li et al., 2019; Schultz et al., 2015), including the present thesis.
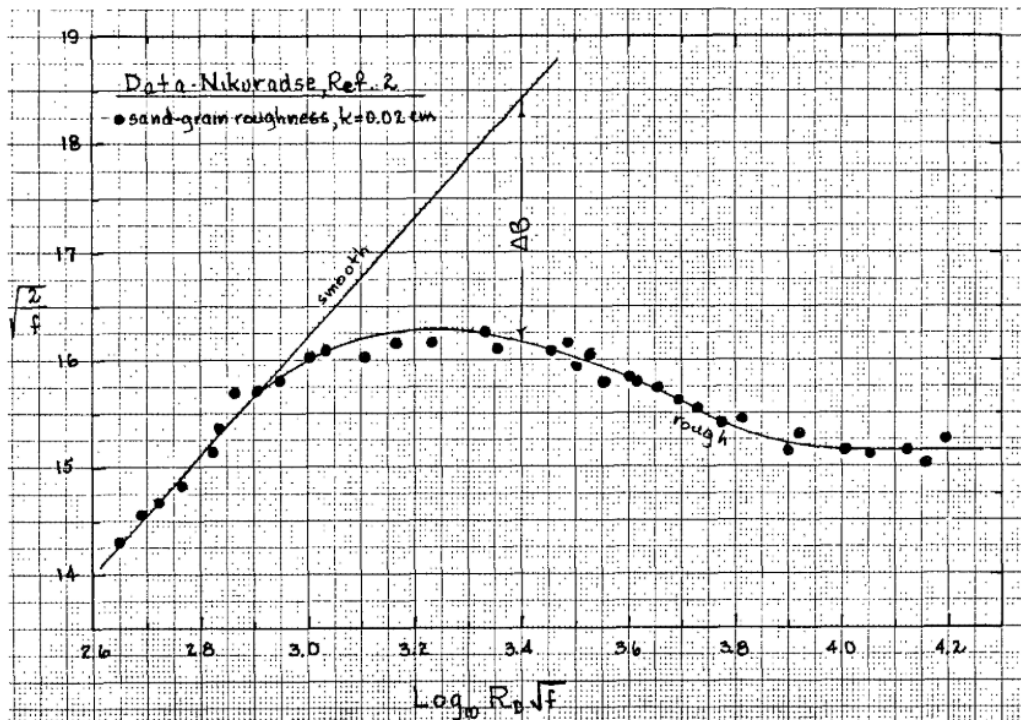
Figure 2-14: Indirect method for pipes method to determine the roughness functions of a rough surface (Granville, 1987).

2.7. Ship Resistance Prediction Methods

To study roughness effects on ship hulls, some assumptions that are commonly made include:

- The roughness is assumed to be isotropic, and a function of the surface roughness height and distribution.
- The roughness elements are assumed to be small compared to the length scale of the hull, and thus can be modelled as a perturbation to the smooth hull geometry.
- The hydrodynamic forces acting on the ship hull are assumed to be linear and time-independent, whereas in reality, these forces are complex and nonlinear.

Other assumptions made and models used in the study of roughness effects on ship hulls depend on the level of detail required and the intended use of the results. Researchers have obtained different methods to overcome the limitations and predict the effect of hull roughness on a vessel's performance (provided that the roughness functions of the surfaces are known), (Schultz, 2004). These models can be based on experimental data, empirical relations, or computational fluid dynamics (CFD) simulations. Analytical models are based on mathematical equations and can provide insight into the physics of the problem. These models are relatively simple and are often used for quick estimations of the added frictional resistance. Numerical models, on the other hand, use computational methods to simulate the flow around a rough hull. These models are more complex but can provide detailed information about the flow field and resistance of the ship. Both analytical and numerical methods can help to quantify the effects of roughness on the ship's performance, such as its resistance, speed, and fuel consumption.

In this thesis, the following approaches will be adopted:

• Extrapolation of the roughness effect on ship resistance applying the boundary layer similarity law scaling procedure proposed by (Granville, 1978, 1958).

• Model the roughness effect in Computational Fluid Dynamic (CFD) using the modified wall-function approach as done by several researchers such as (Song et al., 2020c; Demirel et al., 2017a).

2.7.1. Boundary Layer Similarity Law Scaling Procedure

The roughness of a ship's hull, often caused by marine coatings and biofouling, can dramatically increase a ship's frictional resistance, fuel consumption and greenhouse gas emissions. A well-known similarity law scaling procedure from (Granville, 1958) can be used to predict the effect of such roughness on the frictional resistance of flat plates of ship lengths, provided that the roughness function behaviour of such fouling is known (Schultz, 2007). As reported in (Demirel, 2015), some examples of this method are given by (Schultz et al., 2011; Flack and Schultz, 2010; Schultz, 2007,

2004, 2002; Shapiro, 2004). (Schultz, 2007) proposed a methodology to predict the effects of a range of coating and biofouling conditions on ship frictional resistance, using his experimental data using Granville's similarity law scaling procedure (Granville, 1958).

The similarity law scaling procedure is a method used in engineering for scaling fluid mechanics experiments to model real-world phenomena. The method assumes that geometrically similar systems will behave similarly if the relevant non-dimensional parameters are the same. These non-dimensional parameters include the Reynolds number (measure of the flow regime) and Froude number (measure of the importance of gravity). In other words, the procedure assumes that the flow in two different systems is similar if the ratio of the characteristic length scales and the ratio of the characteristic velocities are the same.

Additionally, many studies adopted Granville's method to predict a ship's frictional resistance with increased roughness due to hull fouling or marine coatings. For example, (Schultz, 2004) compared the frictional resistance of a 150 m flat plate with different antifouling surfaces in unfouled, fouled and cleaned conditions. The predicted increase in the frictional resistance of the surfaces in fouled conditions ranged from 50% to 217%. Consequently, the predicted increase in the required shaft power for a 144 m frigate at a constant speed (30 knots) due to the heavy calcareous fouling condition was 59%, while the speed loss at a fixed power was 10.7%. Similarly, (Shapiro, 2004) used Granville's method to estimate the roughness effect on the fuel consumption of a 150 m destroyer. The added annual fuel cost due to fouled ship bottom paint was estimated to be 3.0 million USD.

Furthermore, (Schultz et al., 2011) investigated the overall economic impact of hull fouling on a 142 m destroyer. The fuel costs due to different fouling conditions were estimated based on the similarity law analysis and compared with other costs associated with antifouling activities. The results indicated that the costs related to hull cleaning and painting are much lower than the added fuel costs due to hull fouling. Recently, (Demirel et al., 2019) generated added resistance diagrams to predict the effect of different hull fouling conditions on the resistance and powering of ships with

arbitrary lengths and speeds. The similarity law analysis was conducted using the roughness length scales of different fouled surfaces proposed by (Schultz, 2007).

Several simplifications limit Granville's theoretical method due to its assumption of a flat plate (Atlar et al., 2018). First, this method only considers the roughness effect on frictional resistance, while the hull roughness also affects the other pressure-related resistance components (Andersson et al., 2020; Farkas et al., 2020, 2018; Demirel et al., 2017b). Another limitation of this scaling method is that it considers only a uniform roughness Reynolds number k^+ over the flat plate of ship length. However, a constant k^+ is not realistic as the local friction velocity varies by the flow being developed along with the flat plate (White, 2011). In fact, Granville's assumption of a constant roughness function along the flat plate may lead to scaling problems and inaccurate added resistance predictions, as underlined by (Demirel et al., 2017b). Furthermore, the 2D flat plate assumption neglects the 3D effect, as criticised by (Atlar et al., 2018).

In conclusion, another disadvantage of the similarity law scaling procedures is that it is an empirical correlation and is therefore not universally applicable. It is based on assumptions and approximations that may not be accurate in all situations. When the model fails, it is usually due to deviations from the assumptions, such as changes in the fluid flow regime, the geometry of the system, or the roughness of the surface. Therefore, Granville's similarity law scaling procedure is useful tools in fluid mechanics even if deviations from these assumptions can lead to inaccurate predictions.

2.7.2. Computational Fluid Dynamics

The Computational Fluid Dynamics (CFD) approach is a valid alternative to Granville's method as it avoids the non-linear problems of theoretical studies and dynamically computes the roughness function for each discretised cell (Stern et al., 2015). Furthermore, as suggested by (Atlar et al., 2018), CFD is as cost-efficient and can overcome Granville's related shortcomings. According to (Song et al., 2020c, 2019; Atlar et al., 2018; Demirel et al., 2017a), ship resistance predictions are more accurate in CFD since the 3D effect of the hull is considered, and the ship can be modelled in full-scale. Different studies, such as (Eça and Hoekstra, 2011),

demonstrated that the surface roughness could be simulated in CFD using either near-wall resolution or wall-functions (wall boundary conditions). However, the modified wall-function approach can better represent the surface's roughness in CFD simulations (Demirel, 2015).

(Demirel, 2015) validated the modified wall-function approach by comparing the results obtained in CFD with the experimental data obtained from a series of towing tests of flat plates coated with antifouling coatings. Similarly, (Vargas and Shan, 2016) implemented a modified wall-function in their CFD models based on the equivalent sand-grain roughness approach in conjunction with the SST k-ω turbulence model. Their roughness model was validated against the experiments on rough towed plates covered with sand-grain using towing tank and flow channel (Schultz and Flack, 2007; Schultz, 2004). However, the ITTC (ITTC, 2011a) continues raising concerns about using the equivalent sand grain roughness to represent surface roughness. In fact, real ships' hull surfaces do not show the behaviour of tightly packed sand roughness. Recently, in (Song et al., 2021b), CFD simulations were performed using the modified wall-function approach and the roughness function model of (Song et al., 2020b). In their study, the CFD model was validated to predict the effect of roughness on ship resistance for 3D hulls. Their findings also showed good agreement between the modified wall-function approach, Granville's similarity law, and measurements from a ship model towing tests with a rough surface (Song et al., 2021a).

It is of note that further investigations into the effect of hull roughness on ship resistance to characterise possible real-life conditions in terms of surface roughness are recommended (ITTC, 2011a). Furthermore, regardless of the in-service ships' inherently heterogeneous hull roughness distribution, most studies dealing with hull roughness assume that the hull roughness is homogeneous (Song et al., 2020a, Demirel et al., 2019; Farkas et al., 2018). Only in recent studies such as (Kim et al., 2022; Ravenna et al., 2022c; Song et al., 2021c, 2021b; Östman et al., 2019; Vargas et al., 2019), the effect of heterogeneous distributions of hull roughness on ship resistance is investigated using CFD with a modified wall-function approach. However, these studies mainly consider the effect of wetted surface areas of the different roughness

regions, not their roughness location. Furthermore, they dealt with limited ship types, velocity characteristics and hull roughness scenarios.

2.8. Literature Gap Identification

The literature review on the effects of hull roughness on ship resistance highlighted several limitations, including the lack of roughness function models that can represent all types of fouling control coatings and hull roughness conditions. The review also noted limited research on developing roughness functions using Fully Turbulent Flow Channels (FTFC), which are valid alternatives to other indirect methods such as towing tank flat plate tests.

Additionally, the review also pointed out that to improve our understanding, further numerical predictions of hull roughness effects on ships at different scales and velocities should be performed and validated by comparing computational fluid dynamics (CFD) simulations to Granville's similarity law predictions.

Last but not least, the review highlighted the need to extend studies beyond the uniform distribution of hull roughness conditions to heterogeneous hull roughness distributions that more accurately represent real ships' surfaces. Investigating the impacts of roughness on different hull regions is essential to achieve targeted hull maintenance strategies. CFD simulations in heterogeneously distributed hull roughness conditions can enable investigation of flow characteristics around the roughness. Developing new approaches to consider the impact of roughness location on different hull regions would also improve our understanding of the effect of heterogeneous hull roughness on ship resistance.

Overall, these research gaps are addressed in the PhD thesis.

2.9. Motivations Behind this Work

Following the literature gap identification, this section gives an overview of the general motivations of this PhD thesis in bullet points:

- Existing roughness function models cannot represent all surfaces, so experimental data must be developed. In fact, the International Towing Tank Conference has recommended the development of new experimental data to investigate the effect of hull roughness on ship resistance (ITTC, 2017a). Additionally, the use of Fully Turbulent Flow Channels (FTFCs) to develop roughness function models is an economical solution, yet limited studies have compared FTFC to towing tank roughness functions results.

- While CFD-based prediction methods have been effective in predicting ship resistance in rough conditions, further study is needed to understand the correlation between roughness and drag. Similarity law scaling and CFD-based methods are the most rational approach to understanding the impact of hull roughness, yet limited studies have compared the two.

- Previous studies have not adequately addressed the heterogeneity of roughness distribution on ship hull surfaces. In other words, the impact of heterogeneous distribution of hull roughness on ship resistance is not well understood, and strategies to mitigate its effects are incomplete. Additionally, there is no defined parameter to describe the impact of roughness on different parts of the hull.

2.10. Research Aims and Objectives

Above all the literature gaps and motivations given in the previous sections, this PhD thesis aims to:

- Investigate the effects of fouling control coatings and heterogeneous hull roughness on ship hydrodynamics.

Further objectives have been identified as follows:

- To obtain new experimental roughness functions for commonly used marine coatings, including a recently developed hard foul-release coating and mimicked biofouled hull conditions using the state-of-the art Fully Turbulent Flow Channel facility (FTFC) of the University of Strathclyde to contribute to the international database of the roughness functions. Additionally, to carry out flat plate towing test in smooth and rough surface conditions by conducting hydrodynamic experiments with the state-of-the art towing tank facility of the University of Strathclyde (UoS) to compare the roughness functions obtained from FTFC for the same surface and demonstrate the advantages of the FTFC (Chapter 4-5).

- To investigate the resistance and powering characteristics of the full-scale KRISO containership (KCS) using Granville's similarity law scaling procedure and CFD in realistic hull roughness conditions by embedding the FTFC experimental results Additionally, to compare the results obtained from the two methods and demonstrate their effectiveness in understanding the impact of hull roughness on ship resistance (Chapters 6-7).

- To investigate the hydrodynamics effects of heterogeneously distributed hull roughness on KCS and KVLCC2 (KRISO very large crude carrier) models and introduce a new factor to correlate the added resistance of the heterogeneous roughness areas to their rough wetted surface area and corresponding increased added resistance. Additionally, to discuss the results of the study in order to shed light on possible biofouling management strategies for ship owners and operators and to critically summarise the main findings and novelty of this thesis in order to identify the opportunities for future research (Chapter 8-9).

2.11. Chapter Summary

A comprehensive literature survey has been conducted, and the research gaps have been identified in this chapter.

3. Methodology

3.1. Introduction

This chapter depicts the general methodology used throughout the present PhD thesis.

3.2. Approach

The aim of this thesis has been realised by achieving several milestones using Experimental Fluid Dynamics (EFD) and Computational Fluid Dynamics (CFD). In order to demonstrate the bigger picture to the reader, *Figure 3-1* illustrates the schematic of the global methodology adopted in the present thesis.

As shown in *Figure 3-1*, the thesis can be divided into three parts. The chapters in Part I provide roughness function data for different rough surfaces obtained through experimental methods: fully turbulent flow channel (flow cell) pressure drop tests (Chapter 4) and towing tank resistance tests (Chapter 5). The chapters in Part II present the full-scale ship resistance and powering predictions of the KCS hull in realistic hull roughness conditions at different speeds conducted using numerical methods: CFD simulations using the modified wall-function approach (Chapter 6) and Granville's similarity law scaling method (Chapter 7). Finally, Part III presents extended investigations into the effects of heterogeneous hull roughness on ship hydrodynamics at design speed to provide biofouling management strategies: model-scale CFD simulations on the KCS and KVLCC2 hulls (Chapter 8) in different hull roughness scenarios.

Numerical methods such as CFD and Granville's similarity law can be successfully adopted to investigate the effect of hull roughness on ship resistance, provided that the roughness functions of the surfaces in question are known. In other words, the first requirement for the prediction of the effect of any hull roughness on ship resistance is to determine the roughness functions, ΔU^+, and roughness Reynolds numbers, k^+, of the surfaces in question.
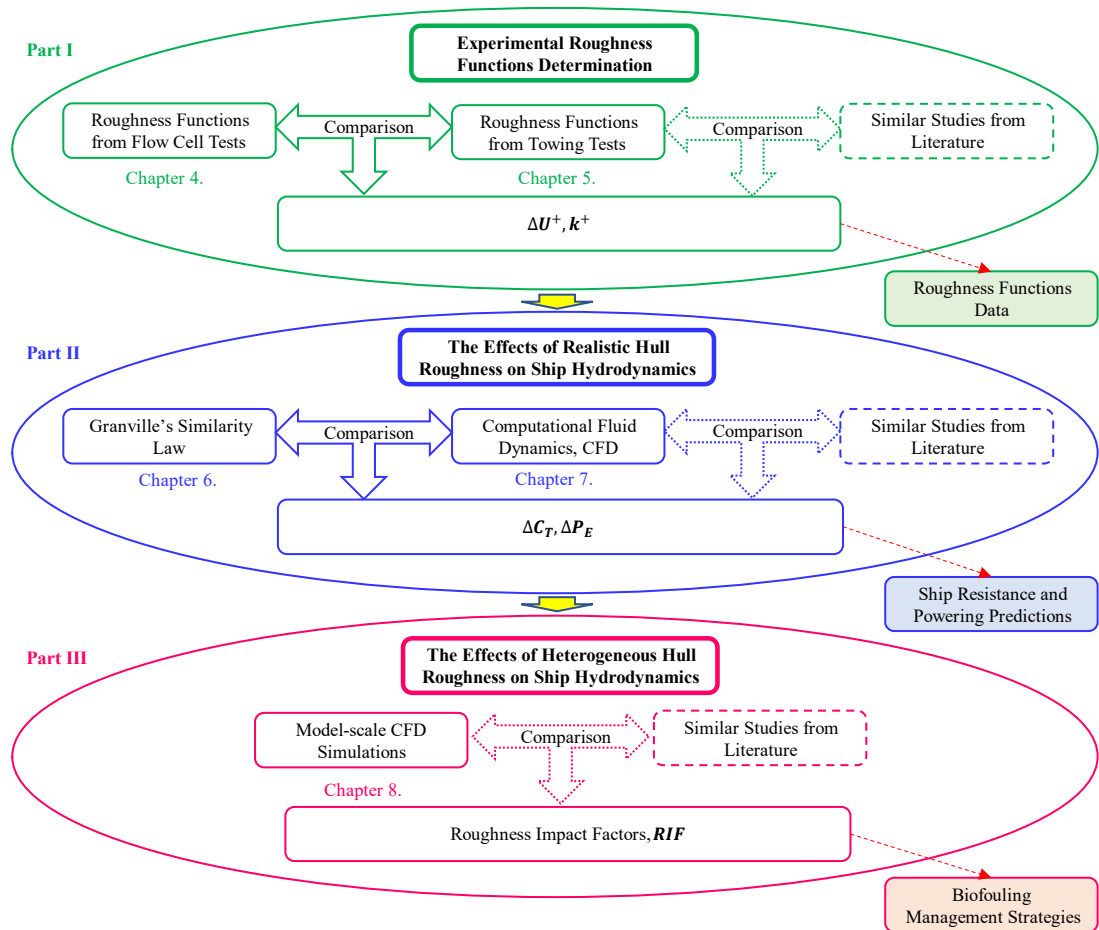
Figure 3-1 Schematic of the global methodology adopted in the present thesis.

3.3. Roughness Function Development: FTFC

In order to determine the roughness functions of a number of fouling control coatings, including the new *FR02* surface (hard-foul release coating) and sanded surfaces mimicking biofouling, flow cell (FTFC) pressure drop tests of flat plates coated with these coatings are performed. The pairs of roughness functions and roughness Reynolds numbers for the *FR02* paint by Graphite International Technologies (GIT), for the existing commercial paints by Dalhousie University and in-house sanded surfaces by the University of Strathclyde, are therefore experimentally obtained using Granville's overall method for pipes (Granville, 1987, 1978). Finally, in-house roughness function models for the different surfaces tested are developed by curve-

fitting the present experimental results to the roughness functions models of Nikuradse (Cebeci and Bradshaw, 1977; Nikuradse, 1933), as presented in Chapter 4.

Figure 3-2 shows a schematic illustration of the experimental and numerical methodology adopted to investigate the roughness effects of marine coatings and mimicked biofouling on ship hydrodynamics with a fully turbulent flow channel. It is of note that the following key tasks are carried out in Chapter 4 to obtain the roughness functions values from the FTFC experiments: physically conducting the pressure drop measurements, Δp, calculating the skin friction coefficients, c_f, and finally calculating the roughness function values, $\Delta U^+, k^+$, to be implemented in numerical methods.
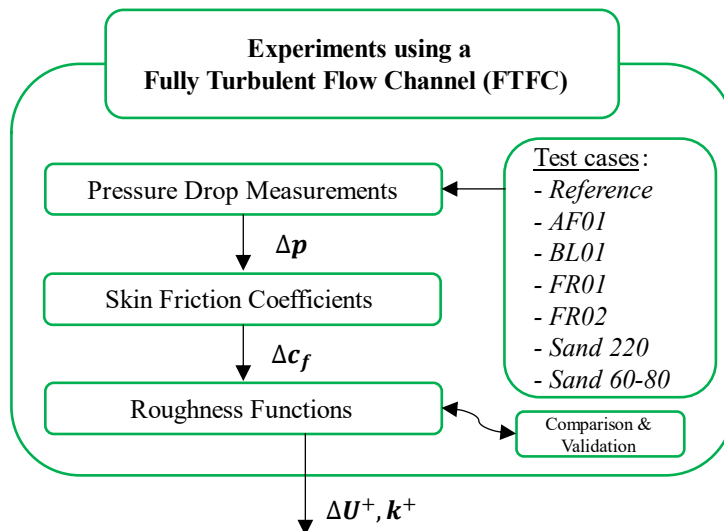
Figure 3-2: Schematic illustration of the methodology adopted in the Chapter 4 to obtain the roughness functions of the test surfaces from FTFC experiments.

Drag characterisation of arbitrary rough surfaces on flat plates can be evaluated by the indirect method for pipes (Granville, 1987) that uses the pressure drop Δp, which can be measured along the coatings (i.e., the pressure drop method). The FTFC was used to determine the skin friction coefficients c_f, by measuring the pressure drop Δp on the test surfaces. Eventually, the roughness functions obtained for the test surfaces (i.e., roughness functions, ΔU^+, roughness Reynolds numbers k^+, roughness length scale, k, etc.), were compared and validated (Ravenna, 2019). Eventually, the roughness functions developed can then be embedded in numerical methods to predict

the effect of such surfaces on ship resistance and powering, as it will be done later in this thesis.

3.4. Roughness Function Development: Towing Tank

Similarly, Chapter 5 presents the experimental roughness functions developed for the *Sand 220* surface (mimicked medium-light slime biofouling) from towing tank resistance tests on a flat plate using Granville's overall method (Granville, 1958). The pairs of roughness functions and roughness Reynolds numbers for the *Sand 220* surface are therefore compared with the results obtained for the same surface from the FTFC tests detailed in Chapter 4. Further comparison across the roughness functions data obtained in the present study from the FTFC tests, the towing tank tests and similar studies in the literature are presented at the end of Chapter 5.

The towing tank tests at the Kelvin Hydrodynamics Laboratory (KHL) of the University of Strathclyde (UK) were carried out following the state-of-the-art procedures suggested in (ITTC, 2011b). A sand-coated flat plate was towed at a range of speed, and the drag was measured. For reference, the bare plate was towed at the same speed range (from 1.5 to 4.5 m/s with an increment of 0.2 m/s). Notably, the actual speed reached by the carriage was considered rather than the input one. The uncertainties of the results were evaluated by repeating the runs at the lowest and highest speeds at least two more times for each configuration.

The total resistance (drag) of a flat plate, R_T, can be decomposed into two major components: frictional resistance, R_F, and the residuary resistance, R_R, as given in Equation (3-1):

$$R_T = R_F + R_R \qquad\qquad (3\text{-}1)$$

The frictional resistance occurs due to shear stresses on the plate's surface. On the other hand, the residuary resistance arises due to the wave-making resistance since the pressure resistance component is negligible for thin bodies (van Manen and van

Oossanen, 1988). Similarly to R_T, the total resistance coefficient, C_T, is made up of the frictional coefficient, C_F, function of the Froude number, Fr, and residuary resitance coefficient, C_R, function of the Reynolds number, Rn, as in equation (2-1).

The differences between the C_T values obtained from experiments and the C_F values obtained using a frictional line such as in equation (3-2) (Hughes, 1952) or equation (3-3) (Schoenherr, 1932). For a smooth plate, the frictional resistance coefficients can be predicted using the frictional correlation line of Hughes (Hughes, 1952), equation (3-2):

$$C_F = \frac{0,066}{(log(Rn)-2.03)^2} \qquad (3-2)$$

However, the frictional resistance coefficients of the reference smooth plate of the sand-grain equivalent roughness configuration were obtained from the Karman-Schoenherr friction line (Schoenherr, 1932) given by equation (3-3):

$$\frac{0.242}{\sqrt{C_F}} = log(Rn\, C_F) \qquad (3-3)$$

Equation (3-3) was solved using the iterative method of Newton-Raphson, and it is of note that Candries, (2004) and Schultz, (2004) also confirmed that it is suitable for flat plates. Since they were not expected to be effectively affected by roughness (Schultz and Flack, 2007), the values of the residual resistance coefficients, C_R, of the bare flat plate (reference) were assumed to be the same for all the configurations. Consequently, the C_R values for the reference plate and the sand roughness plate are calculated as shown in the equation (3-4):

$$C_R = C_T - C_F \qquad (3-4)$$

The experimental resistance coefficients are the essential input data of the procedure from Granville (1987) to find the roughness function of the flat plate tested. The actual frictional coefficients C_F were found substracting C_R to the experimental C_T, equation (3-5):

$$C_F = C_T - C_R \qquad (3-5)$$

Where the values of the residuary resistance coefficients C_R computed for the reference plate adopting the Karman-Schoenherr friction line (Schoenherr, 1932) were taken to be the C_R values for the tested surface. As discussed, this is a reasonable assumption since the residuary resistances of the smooth plate were not expected to be significantly different from the values obtained for the rough plate (Schultz, 2007). Notably, the results of the tests were considered at a nominal water temperature of 15°C to make them more readable by other researchers.

Provided that the roughness function of the flat plate is known, as suggested by (Schultz and Flack, 2007), the boundary layer similarity law scaling indirect method from Granville (1958) can be used to predict the effect of the tested roughness on the frictional resistance of flat plates of ship lengths. In order to model the change in frictional resistance of an arbitrary ship, the increments of frictional coefficients ΔC_F need to be found for a flat plate of the ship length, provided that its roughness is considered equal to that of the rough plate tested.

Granville's similarity law scaling procedure (1958) allowed the evaluation of the added resistance, providing the resistance coefficients of a given ship in smooth conditions. Some examples of the use of this method are given by (Flack and Schultz, 2010; Schultz, 2007, 2004, 2002; Shapiro, 2004). The details of the roughness function, similarity law scaling and powering analysis will be discussed later.

3.5. Ship Resistance Predictions: Similarity Law

Chapter 6 describes the effects of hull roughness on the full-scale ship resistance and power requirements of the full-scale KCS hull. Different hull roughness conditions at both design and slow speed are predicted using Granville's similarity law scaling procedure (Granville, 1958).

The hydrodynamic characteristics of the 0.36 m rough plates coated with different surfaces tested in the FTFC in Chapter 4 were scaled to full-scale ship length using Granville's similarity law scaling procedure (Granville, 1978, 1958). As mentioned

earlier, the roughness function, ΔU^+, and roughness Reynolds number, $k+$, values obtained for the test surfaces from the FTFC experiments were used. In fact, apart from the desired ship length and velocity, the main inputs of the procedure are the ΔU^+ and corresponding k^+. Consequently, the resistance coefficients and power requirements of any ship at different speeds with given hull surface conditions can be calculated by solving Granville's similarity law scaling procedure. *Figure 3-3* gives an overview of the methodology adopted to investigate the effects of fouling control coatings and hull roughness on ship resistance.
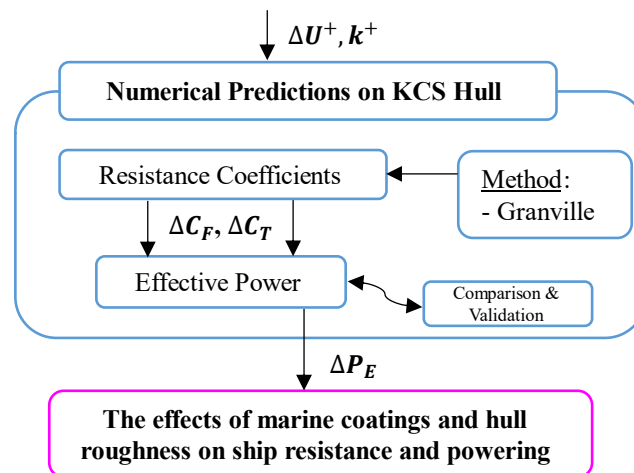
Figure 3-3: Schematic illustration of the methodology adopted in Chapter 6 to predict the effect of fouling control coatings and hull roughness on the full-scale KCS hull.

Numerical predictions were conducted on the benchmark KRISO containership hull at the design speed of 24 knots (12.35 m/s), Froude number $Fr = 0.260$ and the lower speed of 16 knots (8.23 m/s), $Fr = 0.173$. The Reynolds numbers based on the ship speed and length were in the range of Re_L equals to 2.72×10^9, and 1.59×10^9, respectively. *Table 3-1* presents the particulars of the full-scale and model KCS adapted from (Kim et al., 2001). The ship examined represents a medium size feeder container ship that would fit around 3000 TEUs.

Table 3-1: KRISO Container Ship (KCS) full-scale hull principal characteristics.

Parameters		
Scale factor	λ	1
Length between the perpendiculars	$L_{PP}\ [m]$	230
Length of waterline	$L_{WL}\ [m]$	232.5
Beam at waterline	$B_{WL}\ (m)$	32.2
Depth	$D\ (m]$	19.0
Design draft	$T\ (m]$	10.8
Wetted surface area w/o rudder	$WSA_{Total}\ [m^2)$	9424
Displacement	$\nabla\ [m^3]$	52,030
Block coefficient	C_B	0.6505
Design speed	$V\ [kn]$	24
Froude number	F_n	0.260
Reynolds number	Re	$2.72x10^9$
Centre of gravity	$KG\ [m]$	7.28
Metacentric height	$GM\ [m]$	0.6

3.6. Ship Resistance Predictions: CFD

Chapter 7 presents the roughness function models of the surfaces tested in Chapter 4. To characterise the rough surfaces in CFD, these models are then written in the parametric form required by the solver (StarCCM+) and embedded in the code. Full-scale CFD predictions for the KRISO containership (KCS) hull in different hull roughness conditions at both design and slow speed are detailed in Chapter 7. Finally, further comparison across the predictions obtained from the CFD modified wall-function approach, Granville's similarity law scaling method and similar studies from the literature are presented at the end of Chapter 7.

Notably, the well-known KRISO Container Ship (KCS) ("KCS Geometry and Conditions," 2008) full-scale hull in homogeneous conditions (i.e., smooth and rough) was used. Additionally, the present simulations were developed in the Star-CCM+ software package (Versions 15.06.007-R8 and 16.06.010-R8), adopting the Unsteady Reynolds Averaged Navier–Stokes (URANS)-based CFD with the modified wall-function model recently validated by Song et al. (Song et al., 2020b). The governing equations of the present CFD simulations are as in (Ferziger et al., 2020). Furthermore, the k-ω SST (Shear Stress Transport) turbulence model was used with a second-order convection scheme and the Volume of Fluid (VOF) model with Eulerian multiphase

was used to simulate surface gravity waves on the interface between air and water. Finally, the free surface effects were modelled using High-Resolution Interface Capturing (HRIC). It is also of note that the rationale behind the present CFD modelling choices are discussed extensively in (Ravenna et al., 2022c).

The roughness functions characteristics for the test surfaces were obtained as detailed in Chapter 4 (i.e., roughness functions, ΔU^+, roughness Reynolds numbers k^+, roughness length scale, k, etc.). Afterwards, the modified wall function CFD simulations were adopted in Chapter 7 to predict the effect of the test surfaces on the full-scale KCS hull. Specifically, the experimental roughness functions were embedded in CFD using the modified wall function approach to predict the effect of such surfaces on ship resistance and powering. Furthermore, the resistance coefficient results of the numerical predictions were then compared and validated across similar studies assessing the KCS resistance in smooth and rough conditions (Ravenna et al., 2022b; Song et al., 2020a; Yeginbayeva et al., 2020).

Finally, the variations in effective power, ΔP_E due to each test surface were estimated to give an immediate understanding of the effects of marine coatings and hull roughness on ship resistance and powering. Comparison and validation of the ΔP_E values were conducted across the two numerical methods adopted and among similar studies (Schultz et al., 2011).

3.7. Mathematical Formulations

As discussed in (Ravenna et al., 2022c), the governing equations of this hydrodynamics study are given in tensor notation and Cartesian coordinates by equation (3-6) and (3-7), (Ferziger et al., 2020):

$$\frac{\partial(\rho \bar{u}_i)}{\partial x_i} = 0 \tag{3-6}$$

$$\frac{\partial(\rho\bar{u}_i)}{\partial t} + \frac{\partial}{\partial x_j}\left(\rho\bar{u}_i\bar{u}_j + \rho\overline{u_i'u_j'}\right) = -\frac{\partial\bar{p}}{\partial x_i} + \frac{\partial\bar{\tau}_{ij}}{\partial x_j} \tag{3-7}$$

where, ρ is the density, $\bar{u}_i$ is the averaged velocity vector, $\rho\overline{u_i'u_j'}$ is the Reynolds stress, $\bar{p}$ is the averaged pressure, $\bar{\tau}_{ij}$ is the mean viscous stress tensor components. Newtonian fluid's viscous stress can be expressed as in equation (3-8):

$$\bar{\tau}_{ij} = \mu\left(\frac{\partial\bar{u}_i}{\partial x_j} + \frac{\partial\bar{u}_j}{\partial x_i}\right) \tag{3-8}$$

where, μ is the dynamic viscosity. The Reynolds stress can be written as in equation (3-9), using the Boussinesq hypothesis:

$$-\rho\overline{u_i'u_j'} = \mu_t\left(\frac{\partial\bar{u}_i}{\partial x_j} + \frac{\partial\bar{u}_j}{\partial x_i}\right) - \frac{2}{3}\left(\rho k + \mu_t\frac{\partial\bar{u}_k}{\partial x_k}\right)\delta_{ij} \tag{3-9}$$

where, μ_t is the turbulent eddy viscosity, k is turbulent kinetic energy, and δ_{ij} is the Kronecker delta.

The CFD solver used a second-order upwind convection scheme and a first-order temporal discretisation for the momentum equations. On the other hand, the continuity equations were solved in a segregated manner and linked to the momentum equations with a predictor-corrector algorithm. The k-ω SST (Shear Stress Transport) turbulence model (Menter, 1994) was used with a second-order convection scheme. This turbulent model combines k-ω and k-ε formulations for an accurate near wall treatment of the effects of turbulence, and an overall enhanced prediction of adverse pressure gradients and separating flow.

Although the effect of hull roughness on frictional resistance is dominant compared to other resistance components, recent studies claim that its effect on other resistance components is still essential for accurate prediction of the ship resistance (Farkas et al., 2020; Song et al., 2020c ; Oliveira et al., 2018). The Volume of Fluid (VOF) model with Eulerian multiphase was used to simulate surface gravity waves on the interface between air and water. The VOF model allows specifying wave initial and boundary conditions, and as in this study, the ship is towed through calm water, and a flat VOF

wave was defined. In other words, the VOF model guarantees more accurate predictions of the effect of hull roughness on ship resistance. Furthermore, the free surface water level changes over time during the simulation. Hence, it is of note that the free surface effects were modelled using High-Resolution Interface Capturing (HRIC).

3.8. Geometry and Boundary Conditions: KCS Full-Scale

It is of note that the particulars of the full-scale and model KCS were described in *Table 3-1*. The computational domain of the present simulations is a virtual towing tank (*Figure 3-4*), and the size of the domain was chosen following the International Towing Tank Committee (ITTC) recommendations (ITTC, 2011c) and similar studies (Song et al., 2021a, 2021b, 2020a). For the clean hull case, the smooth type of wall-function was used, whereas the rough type of wall-functions, containing the roughness functions of the test surfaces, were used for the rough surfaces of the hull. Finally, the model ship was free to sink and trim, as no constraints were given.
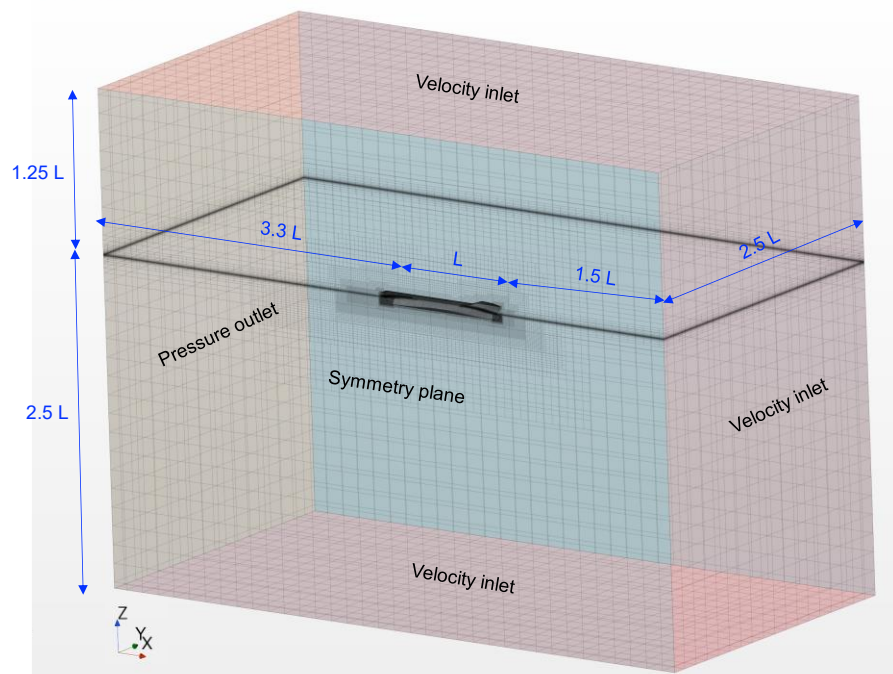
Figure 3-4: Computational domain and boundary conditions of the full-scale KCS simulations.

3.9. Mesh Generations: KCS Full-Scale

The built-in automated mesher of Star-CCM+ software was used to generate the trimmed hexahedral-dominant finite element mesh. Further near-wall mesh refinements were applied using prism layer meshes on the critical regions such as the free surface, the bulbous bow, and the stern. Furthermore, the number of cells selected after the verification study is in the range of 1.4 million (*Table 3-2)* and these values are in close agreement with (Dogrul et al., 2020). Finally, all the simulations used the same mesh regardless of the hull roughness scenarios.

It is of note that for the present simulations, the wall y^+ values were kept between 30 and 300 and higher than k^+ values, as recommended by (Siemens, 2020) the y^+ values of the full-scale KCS hull coated with the FCCs tested earlier. Hence, the average wall y^+ value is around 190 at design speed and 120 at low speed. Notably, the wall y^+ values for the *Sand 60-80* and *Sand 220* cases, and other characteristics will be detailed later in this thesis. Finally, *Figure 3-5* shows the volume mesh of this CFD analysis. Finally, *Figure 3-5* shows the volume mesh of the present CFD analysis.
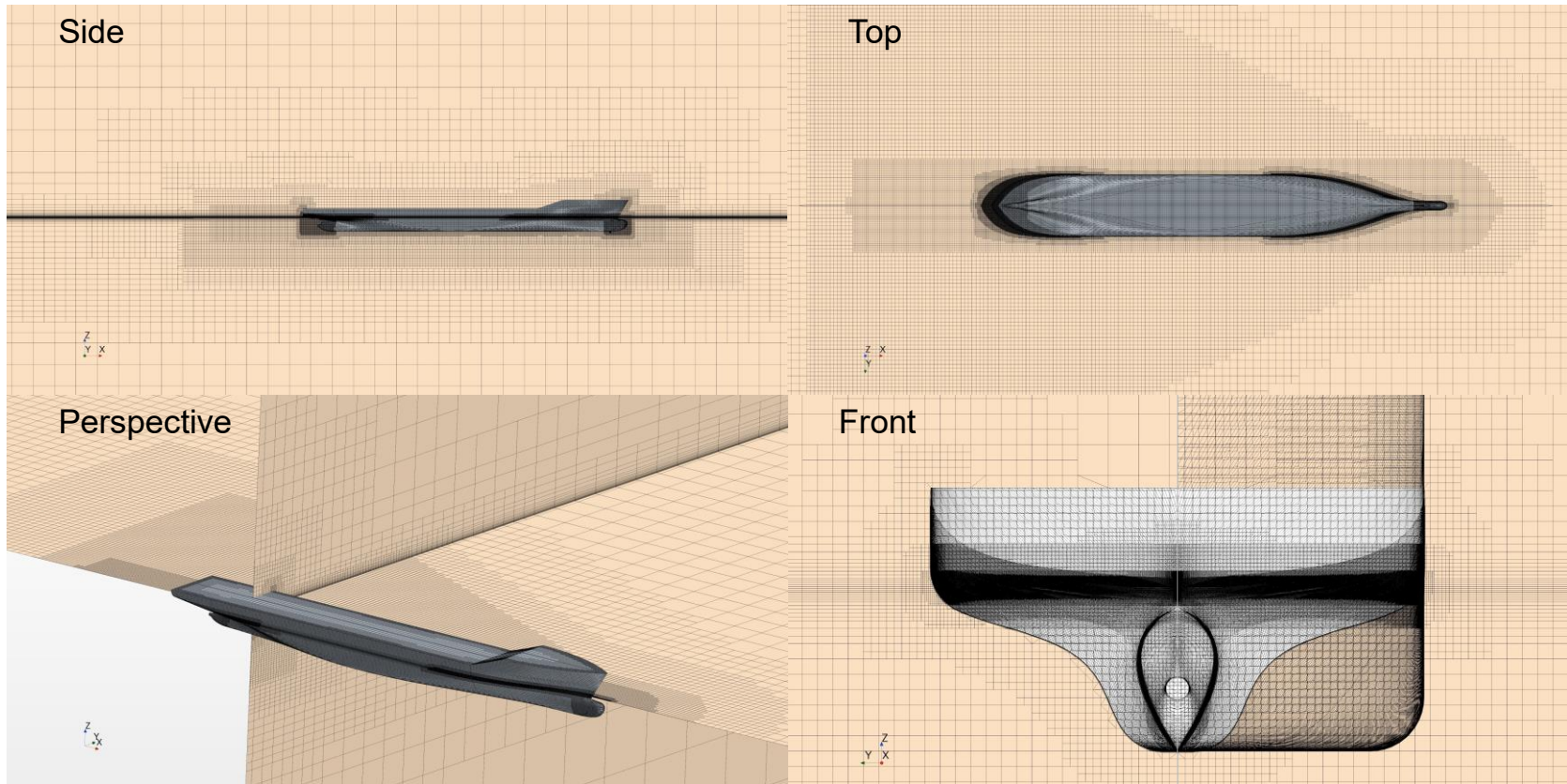
Figure 3-5: Volume mesh used for the KCS full-scale simulation.

3.10. Verification Study of Full-Scale CFD Simulations

The verification procedure of the present CFD study was carried out to assess the spatial uncertainty of the simulations. Richardson's Grid Convergence Index (GCI) method (Richardson, 1911) was adopted as below. According to (Celik et al., 2008), the final expression for the fine-grid convergence index is defined as in equation (3-10):

$$GCI_{fine}^{21} = \frac{1.25e_a^{21}}{r_{21}^{p_a} - 1} \tag{3-10}$$

where, e_a^{21} is the approximate relative error of the key variables, ϕ_k, obtained by equation (3-11), i.e., total resistance coefficient, C_T, as in equation (2-1):

$$e_a^{21} = \left| \frac{\phi_1 - \phi_2}{\phi_1} \right| \tag{3-11}$$

r_{21} is the refinement factor given by $r_{21} = \sqrt[3]{N_1/N_2}$, where N_1 and N_2 are the fine and medium cell numbers, respectively. Also, the apparent order of the method, p_a, is determined by solving equations (3-12) and (3-13) iteratively:

$$p_a = \frac{1}{ln(r_{21})} | \, ln \left| \frac{\varepsilon_{32}}{\varepsilon_{21}} \right| + q(p_a) \, | \tag{3-12}$$

$$q(p_a) = ln \left(\frac{r_{21}^{p_a} - s}{r_{32}^{p_a} - s} \right) \tag{3-13}$$

where $s = sign(\varepsilon_{32}/\varepsilon_{21})$, $\varepsilon_{32} = \phi_3 - \phi_2$, $\varepsilon_{21} = \phi_2 - \phi_1$ and r_{32} is the refinement factor given by $r_{32} = \sqrt[3]{N_2/N_3}$, where N_3 is the coarse cell number.

The extrapolated value of the key variables is calculated by equation (3-14):

$$\phi_{ext}^{21} = \frac{r_{21}\phi_1 - \phi_2}{r_{21} - 1} \tag{3-14}$$

The extrapolated relative error, e_{ext}^{21}, is obtained by equation (3-15):

$$e_{ext}^{21} = \left| \frac{\phi_{ext}^{21} - \phi_1}{\phi_{ext}^{21}} \right| \qquad (3\text{-}15)$$

Table 3-2: Parameters used for the discretisation error for the spatial convergence study of the full-scale KCS hull simulations, key variable: C_T.

Parameter	Full-scale KCS
N_1	2,287,881
N_2	1,413,800
N_3	729,830
r_{21}	1.17
r_{32}	1.25
ϕ_1	1.988×10^{-3}
ϕ_2	1.996×10^{-3}
ϕ_3	1.965×10^{-3}
ε_{32}	-3.07×10^{-5}
ε_{21}	7.10×10^{-6}
s	-1
e_a^{21}	0.36%
q	-0.33
p_a	7.04
ϕ_{ext}^{21}	1.985×10^{-3}
e_{ext}^{21}	0.17%
GCI_{fine}^{21}	0.53%

Table 3-2 depicts the required parameters for the calculation of the spatial uncertainty of the simulation. A grid convergence index, $GCI_{N_2}^{21}$, of 0.53% was estimated for the medium-grid simulations conducted in the smooth surface condition with the inlet speed of 24 kn ($Fr = 0.260, Rn = 2.72 \times 10^9$), when using ten iterations every time step of $0.1\,s$. It is of note that the time step was selected following the recommendations of (ITTC, 2011c), for which $\Delta t = 0.005 \sim 0.01\, L_{WL}/V$, where L_{WL} is the ship length at waterline and V is the ship speed.

Furthermore, the number of cells in the present study is considerably compared to the simulations in (Song et al., 2020b). Therefore, guaranteeing a reduced computational cost without compromising the accuracy of the results. In fact, the estimated spatial GCI value of 0.53% indicates the great accuracy of the present CFD predictions. Furthermore, the resistance coefficient results of the smooth case agree with the results found in the literature. In fact, the discretisation errors for the spatial convergence study, GCI, found by (Dogrul et al., 2020; Song et al., 2020a) for the KCS model scale hull were 0.40% and 0.10%, respectively.

Table 3-3: Parameters used for the discretisation error for the temporal convergence study of the full-scale KCS hull simulations, key variable: C_T.

Parameter	Full-scale KCS hull
Δt_1	0.08s
Δt_2	0.10s
Δt_3	0.12s
r_{12}	2
r_{23}	2
ϕ_1	2.002×10^{-3}
ϕ_2	1.996×10^{-3}
ϕ_3	1.975×10^{-3}
ε_{32}	-2.10×10^{-5}
ε_{21}	-6.15×10^{-6}
e_a^{21}	0.31%
e_a^{32}	1.05%
p_a	-1.77
ϕ_{ext}^{21}	2.004×10^{-3}
e_{ext}^{21}	-0.13%
$GCI_{\Delta t_2}^{21}$	0.16%

Similar to the spatial convergence study, *Table 3-3* presents the parameters used for the discretisation error for the temporal convergency on the key variable: C_T. For the temporal convergence study, three different time steps, namely Δt_1, Δt_2, and Δt_3, were used for the simulations using the medium mesh (N_2). The simulations were conducted in the smooth surface condition, with the inlet speeds of 24 kn ($Fr = 0.260, Rn = 2.72 x 10^9$), for the full-scale KCS hull simulations. The total resistance coefficients, C_T, were used as the key variables.

As indicated in the table, the numerical uncertainties, $GCI_{\Delta t_2}^{21}$, of the KCS hull simulations is 0.16% when the time step Δt_2 is used. Therefore, for accurate predictions, the time step, Δt_2, was used for further simulations in this study. Above all, the present CFD simulations to predict the effect of hull roughness on ship resistance and powering are further reasonably validated.

Model-scale CFD simulations at design speed conducted for the KCS hull and the KRISO Very Large Crude Carrier (KVLCC2) in heterogeneous hull roughness are presented in Chapter 8. Notably, the heterogeneous hull roughness scenarios are designed to investigate the potential of low-cost targeted hull maintenance.

3.11. Heterogeneous Hull Roughness Simulations

Figure 3-6 shows a schematic illustration of the CFD methodology adopted to investigate the effect of heterogeneous distributions of hull roughness on the well-known KRISO Container Ship (KCS) and KRISO Very Large Crude Carrier (KVLCC2) ("KCS Geometry and Conditions," 2008).

Notably, the rough areas selected for the heterogeneous scenarios are distinctive features of a ship's hull. The hull's bulbous bow, fore, midship, aft, stern, and flat bottom parts follow specific design considerations. They are designed based on rigorous considerations such as hydrodynamics optimisations, structural requirements, and equipment placement. Therefore, the rough areas chosen for the heterogeneous hull roughness cases reflect an intuitive subdivision of the ship's hull. However, it is also of note that the subdivision adopted in this thesis is unique, and no evidence of the same heterogeneous scenarios is found in the literature.

It is also of note that the KCS and KVLCC2 hulls were selected as they are popular choices for CFD-based resistance predictions because they are well-documented and widely available geometries that have been extensively tested and validated through experimental studies. These hulls have been used as benchmark test cases in various research studies, and their data has been widely published, making it easier for researchers to validate their numerical results against the experimental data.

Furthermore, the KCS and KVLCC2 hulls are representative of different types of ships that are commonly used in the industry, such as a Panamax containership and ultra-large crude carrier, respectively. As such, they are good choices for testing and comparing the performance of CFD models and numerical methods for resistance prediction of different types of ships.
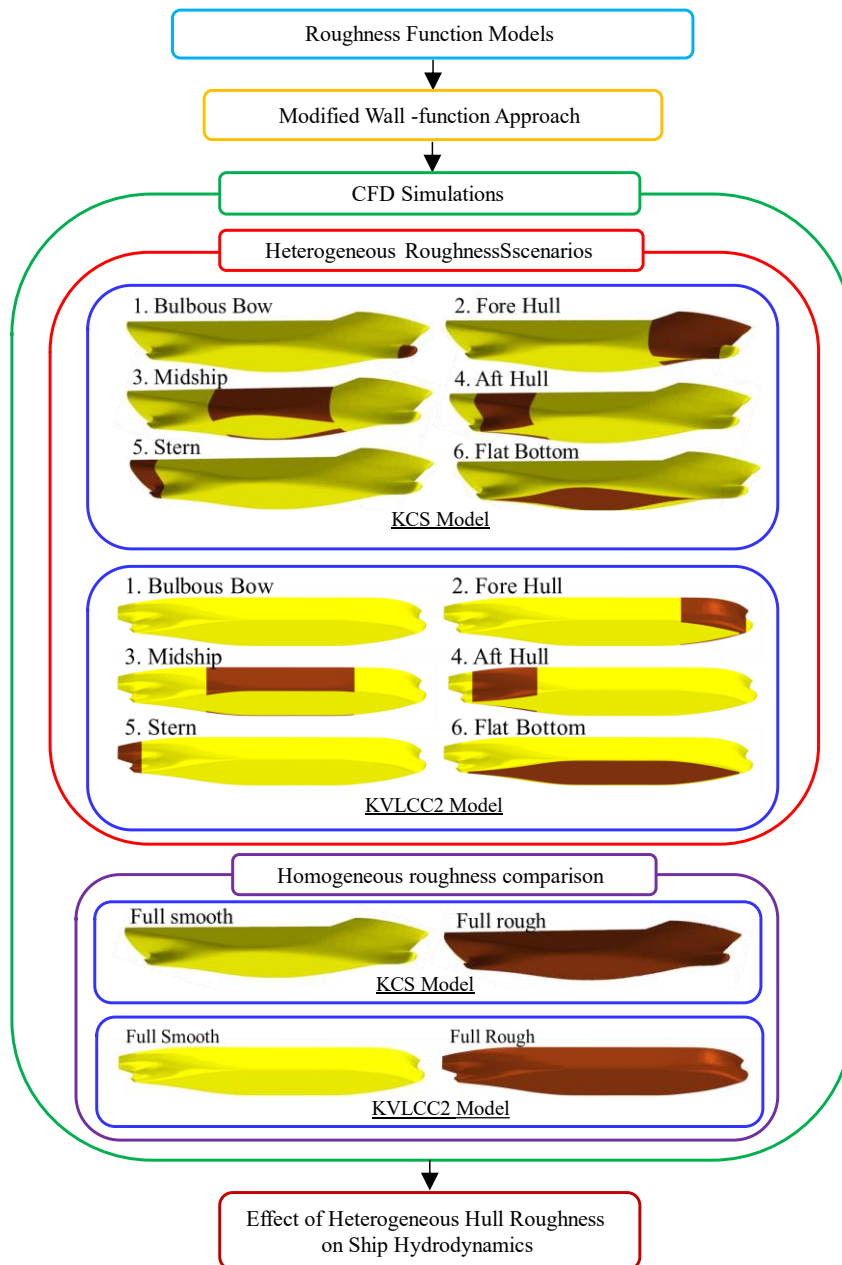
Figure 3-6: Schematic illustration of the methodology adopted for the KCS and KVLCC2 model-scale simulations in heterogeneous conditions.

In the figure, the rough areas of the tested scenarios are denoted in brown, and the smooth ones are in yellow. The model-scale numerical towing tests investigated the impact of various heterogeneous hull roughness conditions (different smooth/rough wetted surface coverage ratios) and effects on ship resistance. These roughness scenarios were designed to investigate the potential of low-cost targeted hull maintenance.

A so-called *roughness impact factor* (*RIF*) is introduced to quantify the impact of increased hull roughness in specific areas on the ship's hydrodynamics performances. Comparison between the two hull models in similar heterogeneous hull roughness conditions is given to the reader for a better perspective on the findings. Finally, further comparison between the results of the present CFD simulations and the towing tank experiments conducted for the KVLCC2 model in full-rough conditions are detailed at the end of Chapter 8.

It is of note that the velocity U^+ in the turbulent boundary layer is not uniform on the rough surface due to differences in the friction velocity distribution. The effect of U^+ varying along the surface can be simulated using CFD-based models as the friction velocity is dynamically computed for each discretised cell. CFD-based URANS are essential to simulate the surface roughness phenomenon by means of a fully non-linear method. The URANS solution is time accurate as it is based on the Implicit Unsteady approach. In the Implicit Unsteady method, each physical time-step involves some number of inner iterations to converge the solution for that given instant of time. Therefore, the resulting frictional resistance can be computed using URANS CFD methods. Finally, it is of note that the mathematical formulations behind the present CFD simulations are as detailed in Chapter 7.

The simulations were developed in the StarCCM+ software package (Versions 15.06.007-R8 and 16.06.010-R8), adopting the Unsteady Reynolds Averaged Navier–Stokes (URANS)-based CFD with the modified wall-function model recently validated in (Song et al., 2020b). The wall shear stress, τ_w, skin friction coefficient, c_f, roughness Reynolds number, k^+, and boundary layer on the hull surfaces were examined and correlated with the findings. Finally, the wake elevation figures will support a better comprehension of the impact of the increased roughness of different hull conditions on ship resistance.

3.12. Geometry and Boundary Conditions: Hull Models

The CFD simulations were carried out on the well-known container ship KCS and crude carrier KVLCC2, modelled on the scale factor of 75 and 110, respectively. *Table 3-4* presents the particulars of the KCS and KVLCC2 models adapted from (Larsson et al., 2013) and (Kim et al., 2001). Furthermore, *Table 3-5.* depict the characteristics of the different hull roughness scenarios of the CFD simulations.

Table 3-4: KCS and KVLCC2 model-scale principal characteristics.

Parameters		KCS Model	KVLCC2 Model
Scale factor	λ	75	110
Length between the perpendiculars	$L_{PP}\ (m)$	3.0667	2.909
Length of waterline	$L_{WL}\ (m)$	3.1	2.955
Beam at waterline	$B_{WL}\ (m)$	0.4293	0.527
Depth	$D\ (m)$	0.2533	0.273
Design draft	$T\ (m)$	0.144	0.189
Wetted surface area w/o rudder	$WSA_{Total}\ (m^2)$	1.6753	2.265
Displacement	$\nabla\ (m^3)$	0.123	0.235
Block coefficient	C_B	0.6505	0.810
Design speed	$V\ (m/s)$	1.426	0.760
Froude number	F_n	0.260	0.142
Reynolds number	R_n	$3.7x10^6$	$1.9x10^6$

Table 3-5: Test scenarios of the KCS and KVLCC2 models simulations in heterogeneous hull roughness conditions.

Roughness scenario	% Rough wetted surface area	
	KCS Model	KVLCC2 Model
1. Bulbous Bow	2.57	1.02
2. Fore Hull	17.68	13.83
3. Midship	29.50	26.43
4. Aft Hull	19.13	14.82
5. Stern	8.14	3.86
6. Flat Bottom	22.92	39.97
Full Rough	100	100
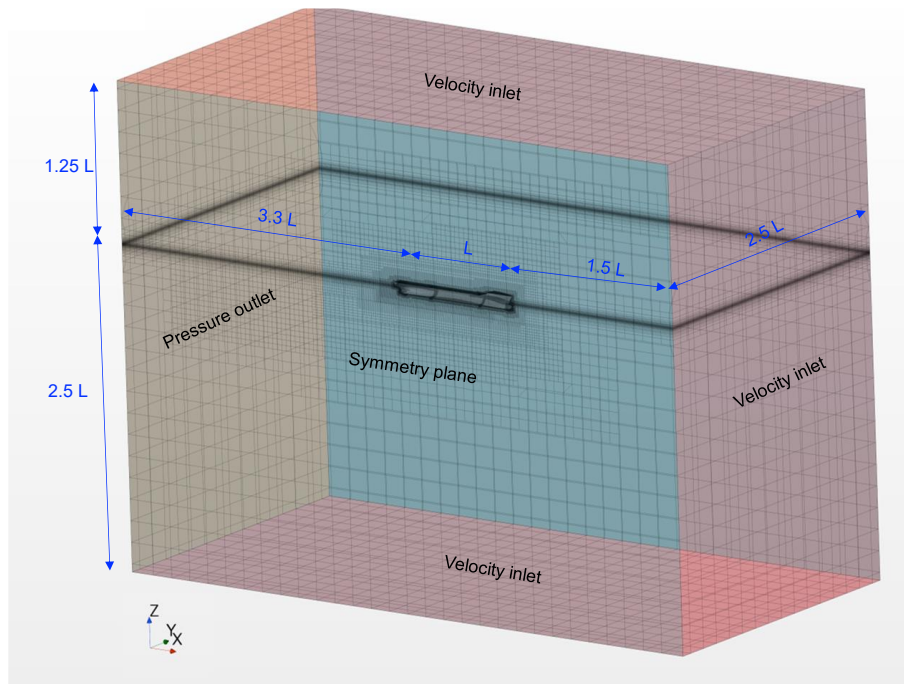
(a) KCS model
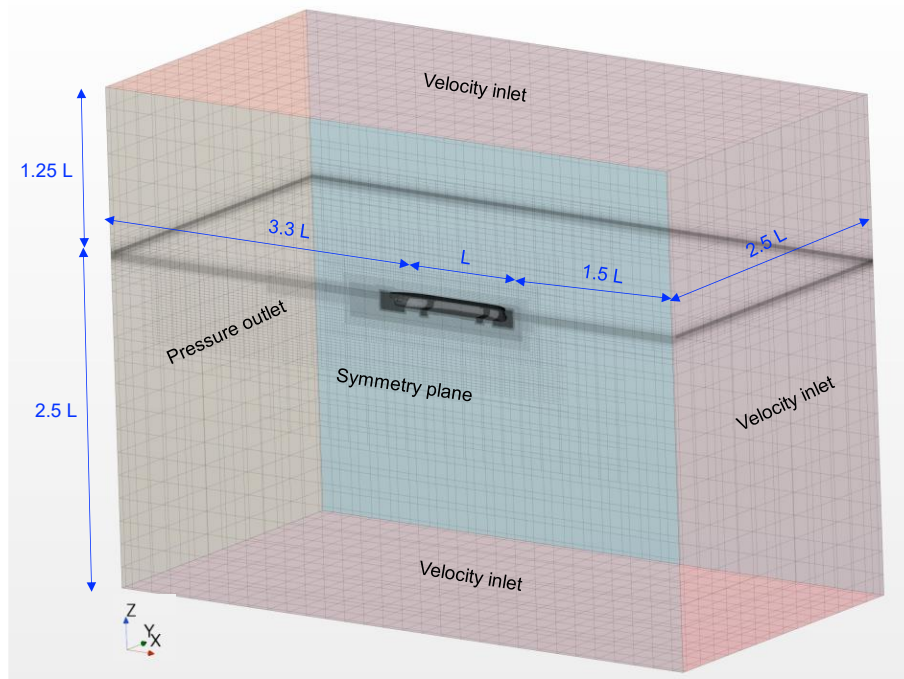
(b) KVLCC2 model

Figure 3-7: Computational domain and boundary conditions of the KCS and KVLCC2 model simulation.

It is noted that the difference between the geometry of the hull in the present study (without rudder) and in the literature (with rudder), (Song et al., 2020b), does not compromise the validity of the CFD modified-wall function approach used as shown later. Notably, the results of the present CFD simulations were calculated using the same the WSA values given in the literature, *Table 3-5*. Using universally adopted WSAs for the calculations guarantees more straightforward comparisons across different studies.

Figure 3-7 shows the computational domain, a towing tank with the size chosen following the International Towing Tank Committee (ITTC) recommendations (ITTC, 2011c) and similar studies (Song et al., 2021c, 2021b, 2020b). A pressure outlet was selected for the outlet boundary condition, while a velocity inlet was applied for all the other surfaces of the domain (inlet, sidewalls, bottom and top). These boundary conditions simulated the deep water and infinite air conditions. The tank's bottom, top and sidewalls were selected as slip-walls, whilst for free-surface modelling, the no-slip wall type boundary condition was used on the hull surfaces. The symmetry boundary condition was applied on the vertical centre plane of the domain to shorten the computational time. The model ship was free to sink and trim, as no constraints were given.

3.13. Mesh Generation: KCS & KVLC2 Hull Models

The built-in automated mesher of Star-CCM+ software was used to generate the trimmed hexahedral-dominant finite element mesh. Further near-wall mesh refinements were applied using prism layer meshes on the critical regions such as the free surface, the bulbous bow, and the stern. Furthermore, the number of cells selected after the verification study is in the range of 1.5 million for the KCS model and 1.9 million for the KVLCC2 model (*Table 3-6*), and these values are in close agreement with (Dogrul et al., 2020). Finally, all the simulations used the same mesh regardless of the hull roughness scenarios.

It is of note that for the present simulations, the wall y^+ values were kept between 30 and 300 and higher than k^+ values, as recommended by (Siemens, 2020) for the y^+ values of the full-scale KCS hull coated with the FCCs tested earlier. Hence, the average wall y^+ value is around 90 for the KCS model and 100 for the KVLCC2 model in smooth conditions. Notably, the wall k^+ values for the *Sand 60-80* and *Sand 220* cases, and other characteristics will be detailed later in this thesis. Finally, *Figure 3-8* and *Figure 3-9* show the volume meshes of the present CFD analysis.

.
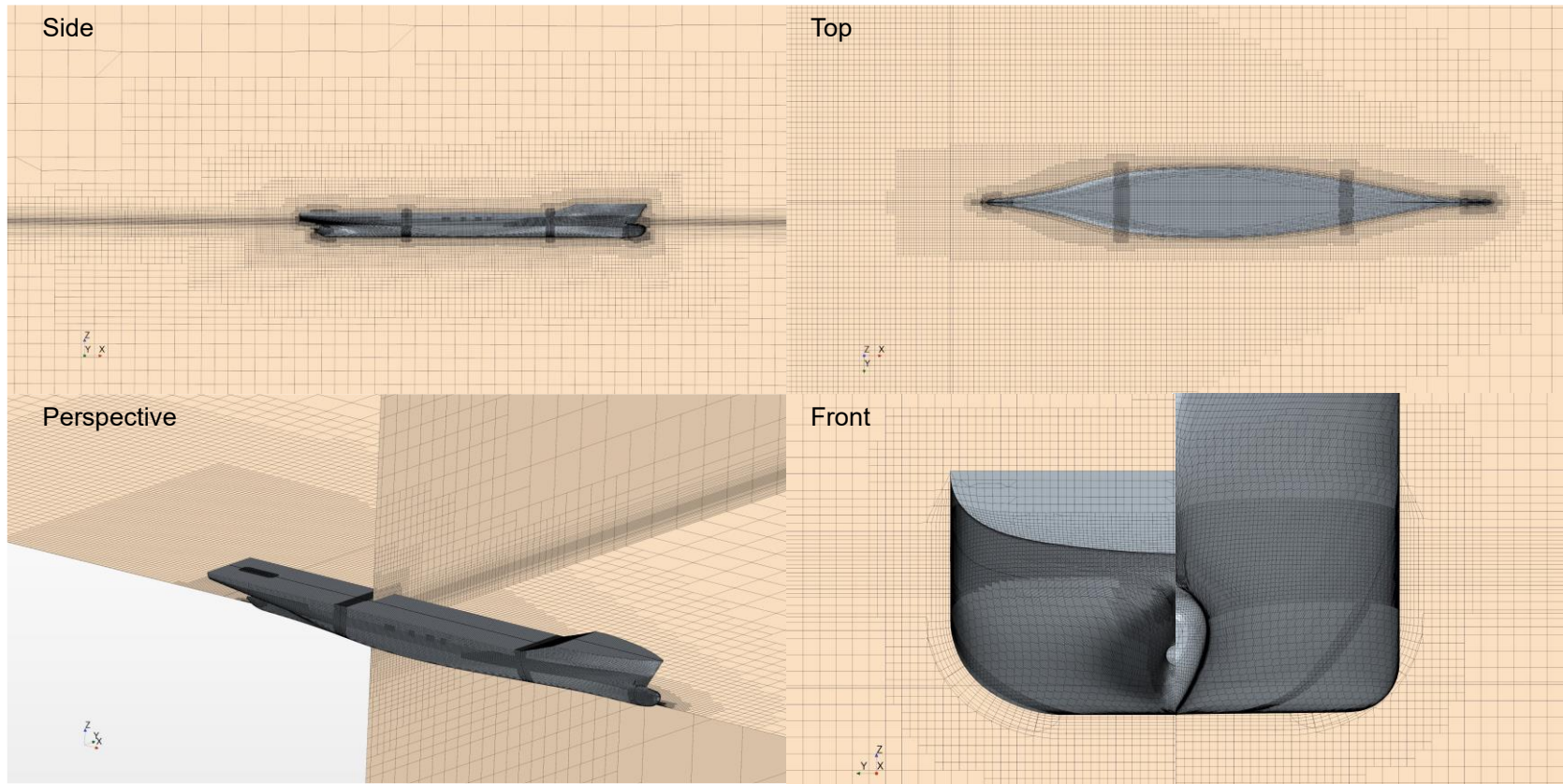
Figure 3-8: Volume mesh used for the KCS model simulations.
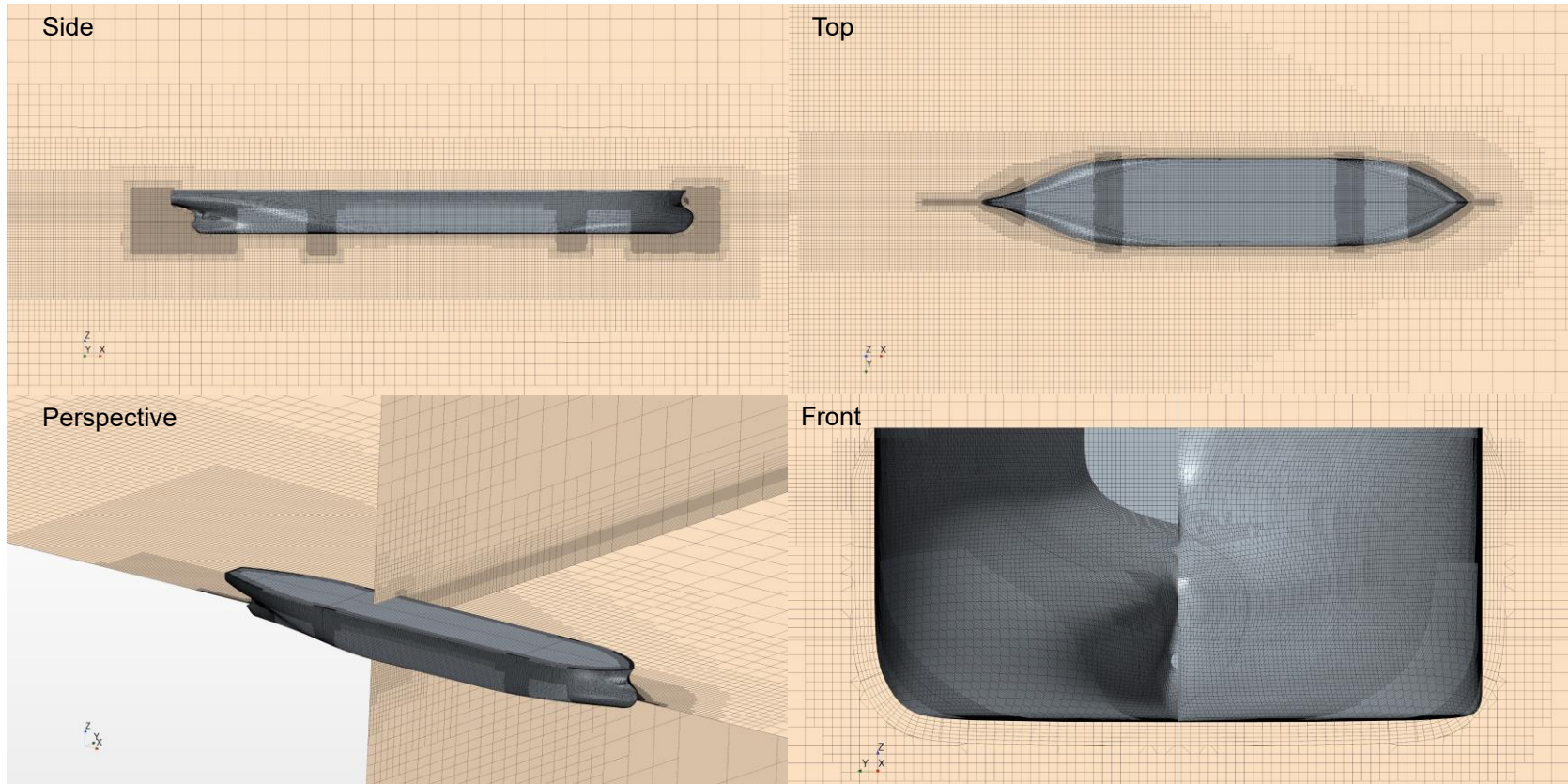
Figure 3-9: Volume mesh used for the KVLCC2 model simulation.

3.14. Verification Study of Model Scale Simulations

Table 3-6 depicts the required parameters for calculating the spatial uncertainty of the KCS and KVLCC2 models simulations. For the KCS model simulations, a grid convergence index, GCI_{fine}^{21}, of 0.20% was estimated for the fine-grid simulations conducted in the smooth surface condition with the inlet speed of 1.426 m/s ($Fr = 0.260$, $Re = 3.7x10^6$), when using ten iterations every time step of $0.01\ s$. In comparison to the simulation in (Song et al., 2020b), the number of cells in the present study has registered an 11% increase, from 1,306,433 to 1,462,274. The increase is due to the extra mesh refinements added at strategic locations of the hull, where the transition from smooth to rough conditions is expected. The estimated GCI value of 0.20% indicates the accuracy of the resistance prediction of the effect of the heterogeneous distribution of hull roughness on the KCS model.

Similarly, for the KVLCC2 model simulations, a grid convergence index, GCI_{fine}^{21}, of 0.31% was estimated. Fine-grid simulations were conducted in the smooth surface condition with an inlet speed of 0.760 m/s ($Fr = 0.142$, $Re = 1.9x10^6$), using ten iterations every time step of $0.04\ s$. In comparison to the KCS model simulation, the number of cells is higher for the KVLCC2 simulations. The increase is due to the bigger hull surfaces and mesh refinements around them. Finally, the estimated uncertainty indicates the validity of the resistance prediction of the effect of the heterogeneous hull roughness on the model KVLCC2 hull.

On the other hand, *Table 3-7* depicts the required parameters for the calculation of the temporal uncertainty of the KCS and KVLCC2 models simulations. For the KCS model simulations, a grid convergence index, $GCI_{\Delta t_1}^{21}$, of 0.35% was estimated for the simulations conducted with a time step of $0.01\ s$. Similarly, for the KVLCC2 model simulations, a temporal uncertainty of 0.47% was estimated when the simulations were conducted in with a time step of $0.04\ s$. As of the discussions above, the simulations for both the cases (KCS and KVLCC2 models) were considered verified.

Table 3-6: Parameters used for the discretisation error for the spatial convergence study, key variable: C_T.

Parameter	KCS Model	KVLCC2 Model
N_1	410,448	471,461
N_2	764,370	935,009
N_3	1,462,274	1,868,998
r_{21}	1.24	1.26
r_{32}	1.23	1.26
ϕ_1	$4.365x10^{-3}$	$4.783x10^{-3}$
ϕ_2	$4.232\ x10^{-3}$	$4.819x10^{-3}$
ϕ_3	$4.226x10^{-3}$	$4.674x10^{-3}$
ε_{32}	$-5.83x10^{-6}$	$-1.45x10^{-4}$
ε_{21}	$-1.33x10^{-4}$	$3.62x10^{-5}$
s	1	-1
e_a^{21}	3.04%	0.76%
q	0.13	0.01
p_a	13.85	6.05
ϕ_{ext}^{21}	$4.372x10^{-3}$	$4.771x10^{-3}$
e_{ext}^{21}	-0.16%	0.25%
GCI_{fine}^{21}	0.20%	0.31%

Table 3-7: Parameters used for the discretisation error for the temporal convergence study, key variable: C_T.

Parameter	KCS Model	KVLCC2 Model
Δt_1	0.01s	0.02s
Δt_2	0.02s	0.04s
Δt_3	0.04s	0.08s
r_{12}	2	2
r_{23}	2	2
ϕ_1	$4.485x10^{-3}$	$4.819x10^{-3}$
ϕ_2	$4.514x10^{-3}$	$4.783x10^{-3}$
ϕ_3	$4.612x10^{-3}$	$4.674x10^{-3}$
ε_{32}	$9.82x10^{-5}$	$-1.08x10^{-4}$
ε_{21}	$2.93x10^{-5}$	$-3.62\ x10^{-5}$
e_a^{21}	0.65%	0.75%
e_a^{32}	2.18%	2.27%
p_a	1.746	1.581
ϕ_{ext}^{21}	$4.472x10^{-3}$	$4.837x10^{-3}$
e_{ext}^{21}	0.28%	-0.38%
$GCI_{\Delta t_2}^{21}$	0.35%	0.47%

Further validation with other studies is discussed below: *Table 3-8* compares the total resistance coefficient, C_T, values predicted from the present CFD simulations of the KCS model and the results of (Song et al., 2021a). The comparison was conducted for total resistance coefficients of the full smooth and full rough surface conditions (i.e., C_{T_S} and C_{T_R}) conducted at the design speed of KCS with the corresponding Froude number of 0.26. The EFD towing tank tests were adapted from (Song et al., 2021a) for comparisons.

Table 3-8: Comparison between CFD and EFD average total resistance coefficients, C_T, in smooth and rough conditions for the KCS model at design speed ($Fr = 0.260$).

Parameter	CFD simulations	EFD towing tests (Song et al., 2021a)	$\%(C_{T,CFD} - C_{T,EFD})$
$C_{T_{Smooth}(KCS)}$	$4.366x10^{-03}$	$4.39x10^{-3}$	-0.39%
$C_{T_{Rough}(KCS)}$	$6.034x10^{-03}$	$6.02x10^{-3}$	-0.033%

As said earlier, the present CFD resistance coefficients were calculated using the same WSA of (Song et al., 2021a). The table shows that the differences are acceptable, especially given the uncertainties evaluated in the experimental resistance coefficients. In other words, the total resistance coefficient values, C_T, predicted from the present CFD simulations, agrees well with experimental C_T values. Therefore, this agreement confirms that the modified wall-function approach adopted in this study can predict the increased skin friction due to the heterogeneous surface roughness.

Similarly, *Figure 3-10* and *Table 3-9* compare the present KVLCC2 model simulations to the EFD towing tank tests in smooth and rough conditions conducted at Kelvin Hydrodynamics Laboratory (KHL). (Papantoniou, 2022) extensively discussed the results of this experimental campaign in his thesis submitted to fulfil the requirements for the master's degree achieved at the University of Strathclyde in 2022. As can be seen, the discrepancies between CFD and EFD results are minimum in both the smooth and rough conditions. Specifically, the CFD results underestimate the total resistance coefficient by only 0.409% for the rough case compared to the EFD measurements. The difference is smaller for the rough case: 0.043%.
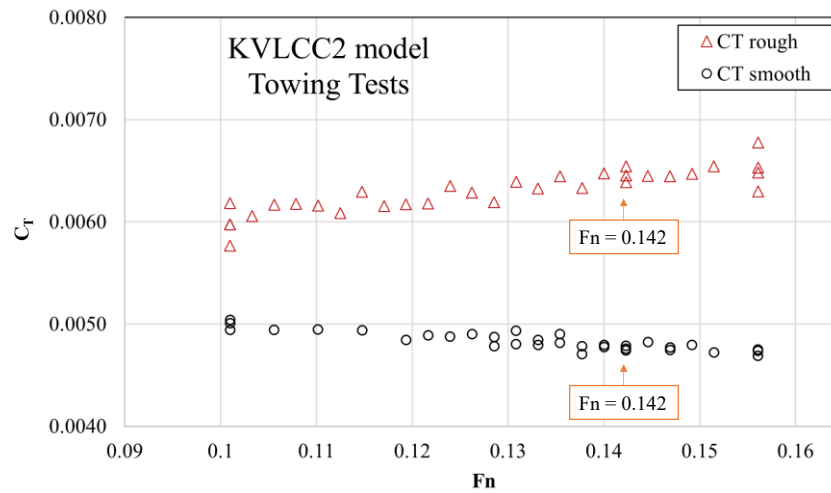
Figure 3-10: EFD towing tank tests results of the KVLCC2 model in smooth and rough conditions (Sand 60-80) adapted from (Papantoniou, 2022).

Table 3-9: Comparison between CFD and EFD average total resistance coefficients, C_T, in smooth and rough conditions for the KVLCC2 model at design speed ($Fr = 0.142$).

Parameter	CFD simulations	EFD towing tests (Papantoniou 2022)	$\%(C_{T,CFD} - C_{T,EFD})$
$C_{T,smooth(KVLCC2)}$	$4.783x10^{-03}$	$4.763x10^{-03}$	-0.409%
$C_{T,rough(KVLCC2)}$	$6.465x10^{-03}$	$6.463x10^{-03}$	-0.043%

3.15. Chapter Summary

The methodology followed in the chapters of this thesis has been presented in this chapter. It can be seen from *Figure 3-1* and the explanations above that each part of the thesis has interactions with the other parts, each independently presents contributions of its own, and they are all tied up within the general scope of the study.

Part I

(Chapters 4-5)

Key Publication:

Ravenna, R., Ingham, R., Song, S., Johnston, C., De Marco Muscat-Fenech, C., Tezdogan, T., Atlar, M., Demirel, Y. K. (2022) "*Predicting the Effect of Hull Roughness on Ship Resistance using a Fully Turbulent Flow Channel*", Journal of Marine Science and Engineering, 10, 1863.

Ravenna, R., Marino, A., Song, S., Atlar, M., Turan, O., Day, S., Demirel, Y. K., (2022) "*Experimental Study on the Effect of Biomimetic Tubercles on the Drag of a Flat Plate*", Ocean Engineering, 225, 111445.

4. Modelling the Hydrodynamics Characteristics of Realistic Surfaces: Fully Turbulent Flow Channel

4.1. Introduction

Granville's method (Granville, 1978, 1958) can be used to predict the hull roughness effect on ship resistance, provided that the roughness function is known. Such a method is based on the turbulent boundary layer similarity law scaling technique. The roughness function is the difference between the velocities in the boundary layer between a rough surface and a hydraulically smooth reference surface (Demirel, 2015). Furthermore, Granville's method owes its merit to its robustness and practicality (Oliveira et al., 2018). Additionally, it allows for predicting the roughness effect on the frictional resistance for ships of arbitrary lengths and speeds (Song et al., 2021a).

The specific roughness function models can effectively represent hull surface conditions. However, no universal roughness function can represent all surfaces. Therefore, the roughness function can be seen as the hydrodynamic fingerprint of any given surface. Consequently, several theoretical and experimental methods have been developed for determining the roughness function of rough surfaces. Ref. (Lindholdt et al., 2015) gave a comprehensive overview of these experimental methods, and their advantages and disadvantages, and (Yeginbayeva et al., 2018) presented a historical overview of the experimental facilities used in hull coating hydrodynamic tests. Among the literature, a recurrent successful alternative to determine the roughness functions of given surfaces is a fully turbulent flow channel (FTFC) facility. By offering rapid experimental turn-around times combined with high Reynolds numbers, FTFCs can provide reliable results combined with significant financial savings.

Therefore, several investigators have studied turbulent channel flow experimentally. For example, Dean et al. (Dean, 1978) provided us with a widely adopted reference equation. However, much of this research had focused on the Reynolds-number

dependence of the skin friction and the mean flow, as reported in (Zanoun et al., 2009). In (Flack et al., 2016) an investigation was conducted on the skin-friction behaviour in the transitionally rough regime using a turbulent channel flow facility installed in the United States Naval Academy using Granville's indirect method for pipes (Granville, 1987). Results were analogous to the Nikuradse-type roughness function (Cebeci and Bradshaw, 1977), which were obtained when investigating the effect of wall roughness on turbulent flows by measuring the pressure drop across a pipe.

Additionally, in a recent investigation on the effect of hull roughness on ship resistance using an FTFC. (Yeginbayeva and Atlar, 2018) recommended a procedure to estimate the effect of roughness on ship hull resistance based on Granville's procedure (Granville, 1987) by using the experimentally determined database for roughness functions of rough surfaces. Recently, ref. (Yeginbayeva et al., 2021) conducted skin friction measurements with an FTFC on two different sizes of silicon carbide particles (i.e., F220 silicon carbide particles with an average grain size of 53–75 μm and F80 silicon carbide particles with an average grain size of 150–212 μm), proving that roughness amplitude parameters alone are not enough to explain the hydrodynamic performance of surfaces. Furthermore, ref. (Zhang et al., 2021) developed roughness functions for different antifouling coatings by conducting flow cell experiments and predicted the frictional performance of a KVLCC2 hull (Korean Very Large Crude Carrier) model case.

Within this, it is clear that the most rational current approach to tackling the effect of ship hull roughness, including biofouling, is to combine experimental and numerical methods. This would require determining the roughness functions using experimental methods, such as cost-effective and practical FTFCs. Therefore, this study aims to obtain new roughness functions for a hard foul-release coating, other commonly used marine coatings and mimicked biofouled hull conditions. Furthermore, this chapter aimed to demonstrate the advantages of FTFC experiments to predict the effect of hull roughness on full-scale ship resistance and powering.

An important objective was to use the FTFC of the UoS, which is a more practical facility than, e.g., a towing tank. To the best of the author's knowledge, only limited (and unpublished) research has been conducted using the FTFC of the UoS. Hence,

the sophisticated new FTFC designed and custom-built (Marino et al., 2019) at the University of Strathclyde (UoS) was used in the present study. While the facility supports drag reduction studies, another aim of such a facility is to contribute to the international database of the roughness functions for different FCCs and biofouling, as recommended, e.g., by the 21st ITTC Surface Treatment Committee (ITTC, 2011a).

Therefore, different FCCs produced by Graphite Innovation and Technologies (GIT, 2021), including antifouling, foul-release and barrier resin coatings and the newly developed hard foul-release coating (*FR02*), were tested in the FTFC. Roughness functions were developed from FTFC tests for widely adopted sandpaper-like surfaces mimicking biofouled conditions (medium light slime and medium slime) as similarly done in towing tests (Schultz, 2004). Furthermore, the roughness functions developed for a sandpaper-like surface (*Sand 220*) from the FTFC experiments were compared with previous towing tank tests. Finally, the present study also aims to confirm the robustness of Granville's method to predict the effect of hull roughness on ship resistance and powering.

The remaining chapter is structured as follows: Section 2 presents the methodology adopted, including the experimental setup, roughness functions development, Granville's similarity law scaling procedure, and experimental uncertainty analysis. Section 3 discusses the current experimental and numerical investigation results and presents the roughness functions of the test surfaces. Finally, Section 4 presents the conclusions, final remarks, and recommendations for future studies.

4.2. Experimental Setup

4.2.1. Fully Turbulent Flow Channel

The University of Strathclyde's Fully Turbulent Flow Channel (FTFC), as shown in *Figure 4-1*a from repository, was designed and installed at the KHL of the NAOME Dept (UoS) to conduct a series of measurements for various types of fouling control coatings and rough surfaces in the freshly applied condition. Delivered to the UoS in

2019, the FTFC is a closed-circuit flow channel that can accommodate two opposing panels in its test section (*Figure 4-1*b-c from repository) located downstream of a single centrifugal pump. The channel has a speed range of 1.5–13.5 m/s, thus able to reach high Reynolds numbers $Re_M \approx 3.0x10^5$. Re_M is the channel height-based Reynolds number based on mean bulk velocity of the flow, U_M. The resulting wall shear stress over 300 Pa in the facility with smooth panels. This creates wall shear stress conditions that are similar to average conditions on a smooth ship, 150 m in length, travelling at up to 17 m s^{-1} (33 knots), as observed by (Schultz et al., 2015).

The UoS - FTFC ensures the development of a two-dimensional flow at its test section located at the upper limb downstream (tail end), where the flow becomes fully turbulent. This is due to its features, e.g., a relatively large test section with a channel height (22.5 mm), an aspect ratio of 8:1, water speed (13.5 m/s) and laser-based measurement access as well as a capability for circulating seawater. *Table 4-1* summarises the main particulars of the FTFC upper limb section. The volume of the system (main tank, auxiliary tank, etc.) is 2.58 m^3. For information on the FTFC design, operation and calibration, the reader is advised to see (Marino et al., 2019).

Table 4-1: Main particulars of the FTFC upper limb.

Name	Symbol	Unit	Value
Length (Tolerance)	l	mm	3000 ($\pm$0.05)
Height (Tolerance)	h	mm	22.5 ($\pm$0.05)
Beam (Tolerance)	b	mm	180 ($\pm$0.05)
Speed range	U	m/s	$1.5 - 13.5$
Flow rate	Q	l/s	$10 - 60$
Channel height-based Reynolds number	Re_M	-	$\approx 3.0x10^5$
Material	-	-	Stainless steel (316 L)
Centrifugal Pump power	P	kW	22

(a)

Test section

(b)

22.5 mm
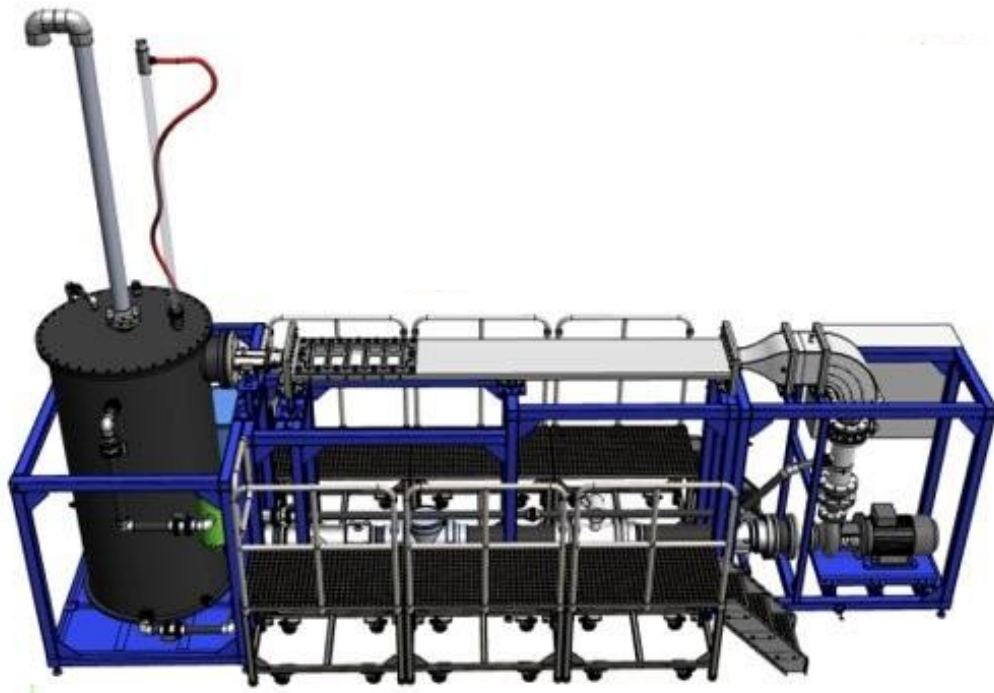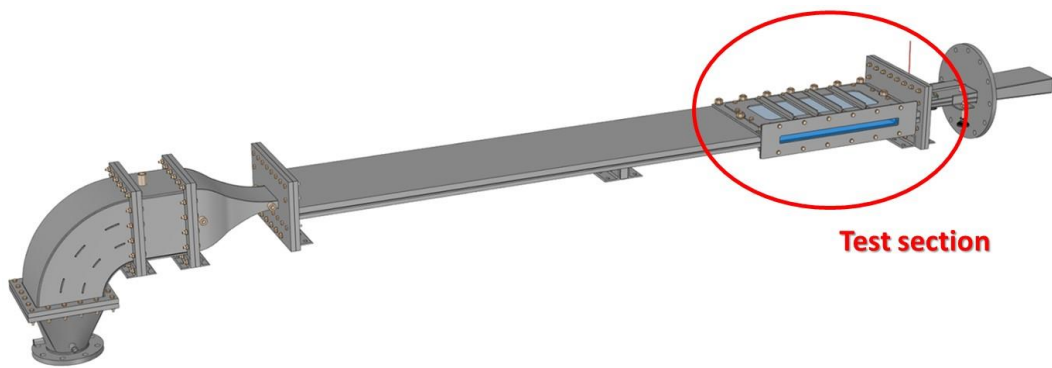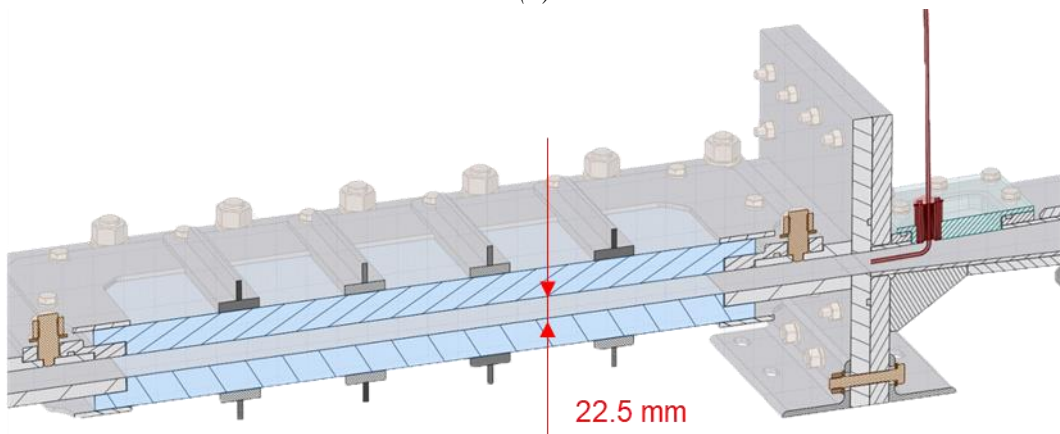
(c)

Figure 4-1: The Fully Turbulent Flow Channel (FTFC) of the University of Strathclyde (UoS). Images adapted from (Atlar, 2008). (a) 3D schematic of the FTFC. (b) and (c): 3D view of the test section.

4.2.2. Test Panels Design and Preparation

In the present experimental campaign, four different types of FCCs were tested in the FTFC, including the newly developed hard foul-release coating (*FR02*) manufactured by Graphite international Technologies, GIT, (GIT, 2021) and marine coatings type that are commonly used in the shipping industry manufactured at Dalhousie University, DU, i.e., a self-polishing antifouling coating (*AF01*), a gelcoat barrier coating (*BL01*), and a soft foul-release coating (*FR01*). Furthermore, two sandpaper-like surfaces mimicking slime biofouling, i.e., *Sand 220* (medium light slime) and the coarser *Sand 60-80* (medium slime) manufactured at the University of Strathclyde, UoS, were tested. The coated panels (*Figure 4-2*a) were tested along with an uncoated "control surface" or the "reference" to represent hydraulically smooth surfaces, *Figure 4-2*b. Additionally, the sanded control panels (*Sand 220* and *Sand 60-80*) and the reference panel were of acrylic (i.e., Polymethyl Methacrylate, PMMA) sheets. On the other hand, high-density polyethene was used as the material to manufacture the test panels for marine coating applications.

Table 4-2 describes the dimensions of the test panels, while a breakdown of the type of each marine coating applied and the method of application is provided in *Table 4-3*. It is of note that in *Table 4-3*, the arithmetic mean roughness, R_a, for the FCCs was measured using the Surtronic 25 gauge by Taylor & Hobson over a cut-off length of 0.8 mm, *Figure 4-3*. The filtering is often carried out because the long wavelength component of the roughness is not expected to contribute significantly to the frictional drag. However, it is worth noting that selecting the optimum cut-off length to characterise a surface in a hydrodynamic sense is still an unresolved debate (Schultz et al., 2015). A review article by (Howell and Behrends, 2006) discusses this issue in the context of ship hull paints. For example, the Gaussian filter with a 2.5 mm cut-off length is used by (Li et al., 2018), whilst (Schultz et al., 2015) uses a 5 mm cut-off length for similar hull paints. Further surface statistics studies could be carried in future studies. Different cut-off lengths could be used to filter the measured data.

(a)
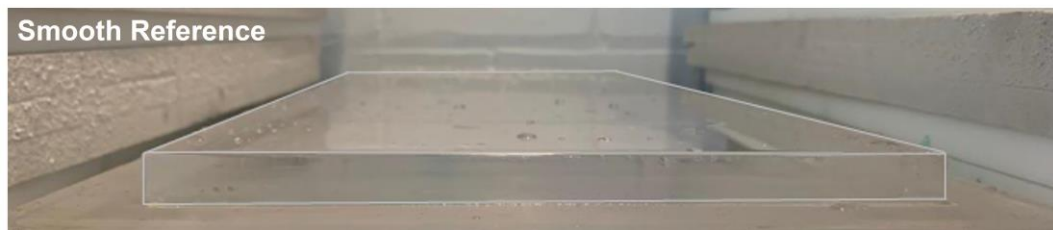
(b)

Figure 4-2: Surfaces tested in the FTFC. (a) Test panels coated with different fouling control coatings and sand grit. (b) Uncoated smooth reference panel.

Table 4-2: Dimensions of the FTFC test panels.

Dimension	[mm]
Inner length	599
Inner breadth	218
Inner thickness	14
Outer length	662
Outer breadth	282
Outer thickness	16
Tolerance	0.1
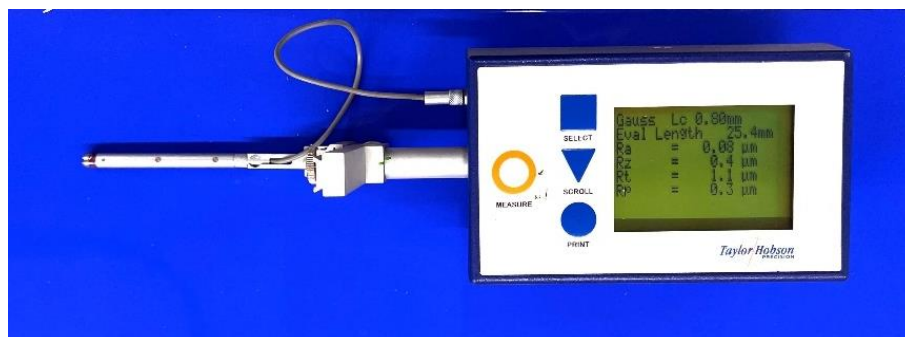
Figure 4-3 Surtronic 25 roughness measurement gauge by Taylor & Hobson measuring the FR01 coating.

Table 4-3: Overview of each test panel set. Similar test surfaces can be found in (Schultz et al., 2015).

Panel Set Name	Description (Manufactured by)	Panel Material	Coating Type (Topcoat, Underlayers)	Method of Application (Topcoat, Underlayers)	Colour	R_a [μm]
Reference	Smooth reference panel (UoS)	Acrylic	N/A	N/A	Transparent	0.04
AF01	Self-Polishing antifouling coating (DU)	High Density Polyethylene	Self-polishing antifouling, anticorrosive primer	Airless spray, Airless spray	Red matt	0.96
BL01	Gelcoat barrier coating (DU)	High Density Polyethylene	Vinyl ester resin barrier	Airless spray	Green matt	1.44
FR01	Soft foul-release coating (DU)	High Density Polyethylene	Fluoropolymer/silicone foul-release, elastomeric tie coat, anticorrosive primer	Roller, Roller, Airless spray	Blue lucid	0.10
FR02	Hard foul-release coating (DU/GIT)	High Density Polyethylene	Hard foul-release, anticorrosive primer	Airless spray, Airless spray	White lucid	0.22
Sand 220	Medium light slime surface (UoS)	Acrylic	Sanded rough, Aluminium oxide sand grit 220	Scattering, Roller resin	Gray matt	101
Sand 60-80	Medium slime surface (UoS)	Acrylic	Sanded rough, Aluminium oxide sand grit 60-80	Scattering, Roller resin	Brown matt	294

4.2.3. Roughness Statistics

A more extensive statistical analysis of surface roughness was carried out for rough plates coated with uniform sand (*Sand 220* and *Sand 60-80*) using a TQC Hull Roughness Gauge. Specifically, the surface roughness of the plates used for towing tank test (stainless steel) and FTFC measurements (acrylic) was investigated. *Table 4-4* presents the roughness statistics of the *Sand 220* and *Sand 60-80* surfaces measured with the TQC gauge on the towing tank and FTFC plates. The arithmetic mean roughness height R_a and the roughness height over 50 mm sample, $R_t(50)$ (measured using a TQC Hull Roughness Gauge were calculated according to (ISO, 1997). It should be noted that the presented parameters are not the only parameter to assess the roughness characteristics of different surfaces but are good references.

Table 4-4: Roughness statistics of the Sand 60-80 and Sand 220 surfaces measured with the TQC gauge on the towing tank and FTFC plates.

Roughness Statistics	*Sand 220*		*Sand 60-80*	
	FTFC	Towing Tank	FTFC	Towing Tank
R_a [μm]	101	100	355	354
$R_t(50)$ [μm]	294	184	509	408

Figure 4-4 shows the process of taking a roughness measurement of Sand 220 with the TQC Hull Roughness Gauge ("TQC," 2022). The sensor unit of the TQC is moved horizontally over the plates from the leading edge to the trailing edge thanks to its three non-slip wheels. Moreover, the maximum peak-to-trough roughness height over a 50 mm interval is measured by a carbide-tipped stylus while moving the sensor unit. It is of note that the range of the TQC device is from 0 to 2500 mm with an accuracy of ±5mm or ±2% of the measured data, whichever is greater.

Figure 4-5 demonstrates the probability density functions (pdf) of the roughness data of the *Sand 220* and *Sand 60-80* test surfaces for towing tank and FTFC experiments. As seen in *Figure 4-5*, the *Sand 220* surfaces have a lower mean roughness height, and their roughness distribution is narrower than the others. This is expected since *Sand 220* is smoother than *Sand 60-80*. *Sand 60-80* surfaces have higher mean roughness values than the *Sand 220* surface. Hence, they were expected to have a relatively more homogenous roughness distribution.

Figure 4-4: Process of taking a roughness measurement of Sand 220 with the TQC Hull Roughness Gauge ("TQC," 2022).
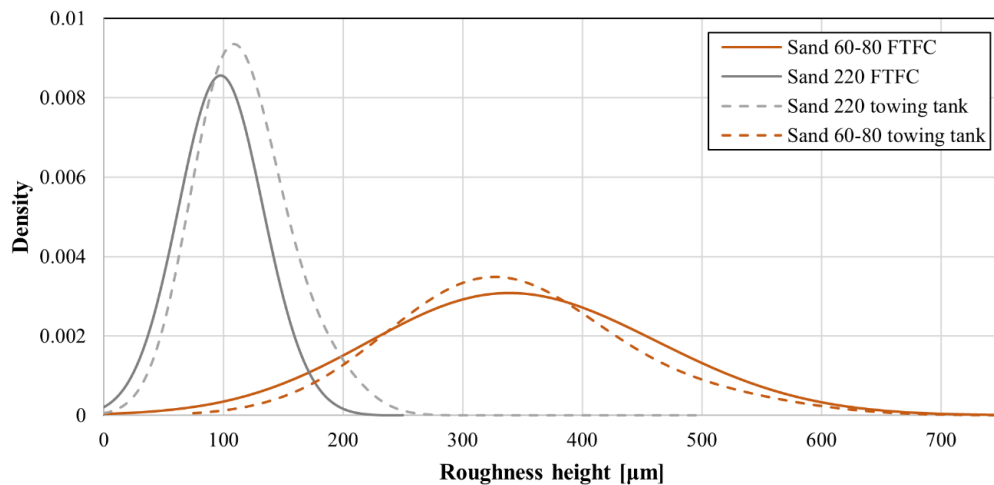
Figure 4-5: Probability density functions (pdf) of the roughness data of the Sand 220 and Sand 60-80 test surfaces.

On the other hand, all the test surfaces applied on the FTFC panels were profiled with an OSP100 optical profilometer (Uniscan Instruments Ltd., Buxton, UK) of the University of Newcastle, utilising laser interferometry *Figure 4-6*. The optical laser sensor was adjusted on the two-axis traverse with a positioning range of 90mm × 40mm *Figure 4-7*. Eighty linear profiles were measured at a scanning speed of 15mm/s, giving 3600 points on the x-axis. Representative images of the surface topography for the test surfaces, including the FCCs and sanded plates, are presented in *Figure 4-9*. The roughness maps in the figure are 90 mm by 40 mm and the origin for the topography maps is detailed in *Figure 4-8*. Furthermore, the vertical colour scale for surface elevation represents the unfiltered surface roughness.
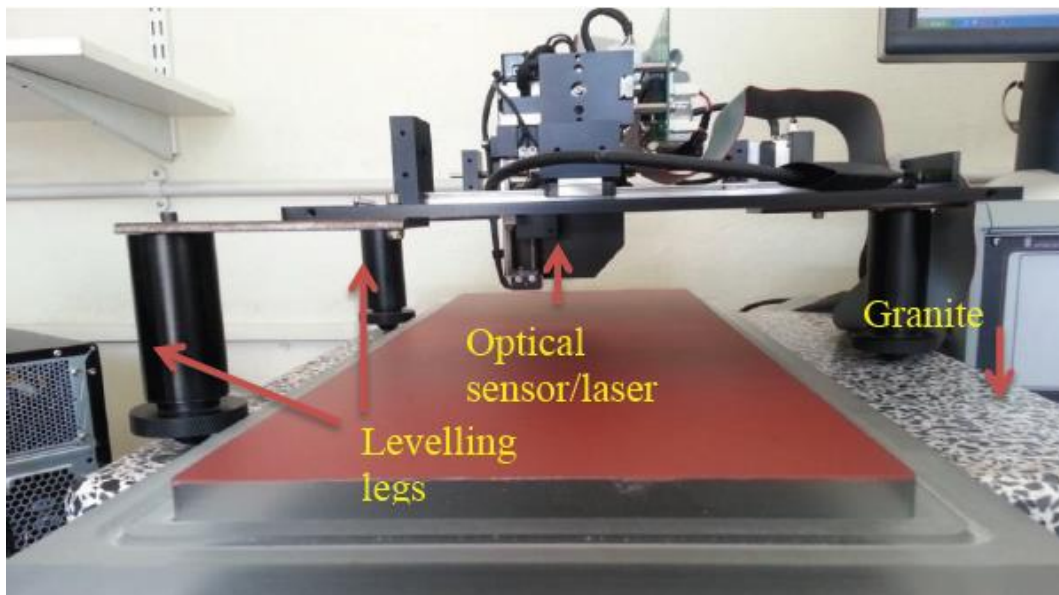
Figure 4-6: Schematic of the OSP100 optical profilometer (Uniscan Instruments Ltd., Buxton, UK) of the University of Newcastle (Atlar, 2008).
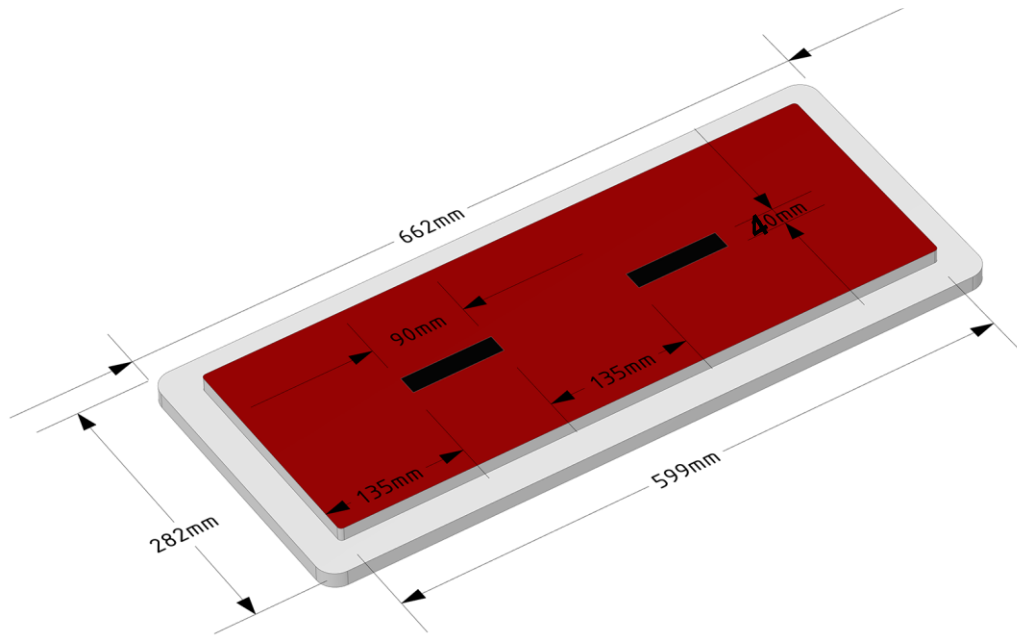
Figure 4-7: Schematic of the typical profiled areas on the FTFC plate. Adapted from (Atlar, 2008)
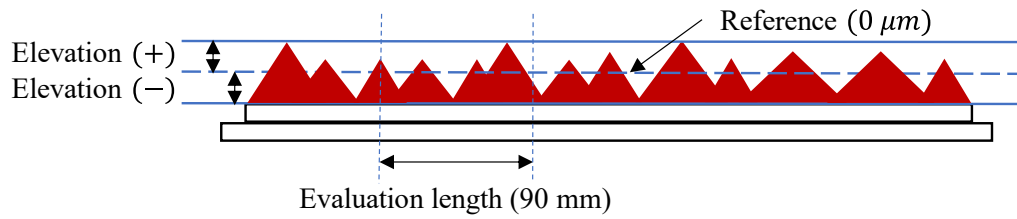
Figure 4-8: Schematic showing the origin (median reference between the highest peak and lowest trough) for the surface topography on the FTFC plate.

Sand 60-80

(a)

Sand 220

(b)

AF01

(c)

BL01
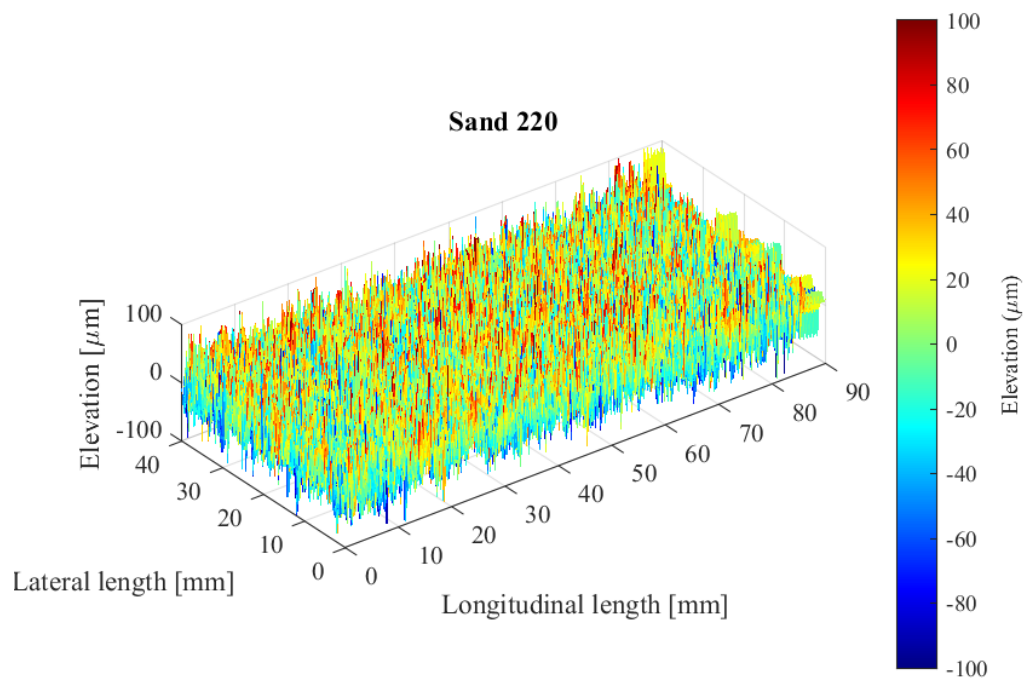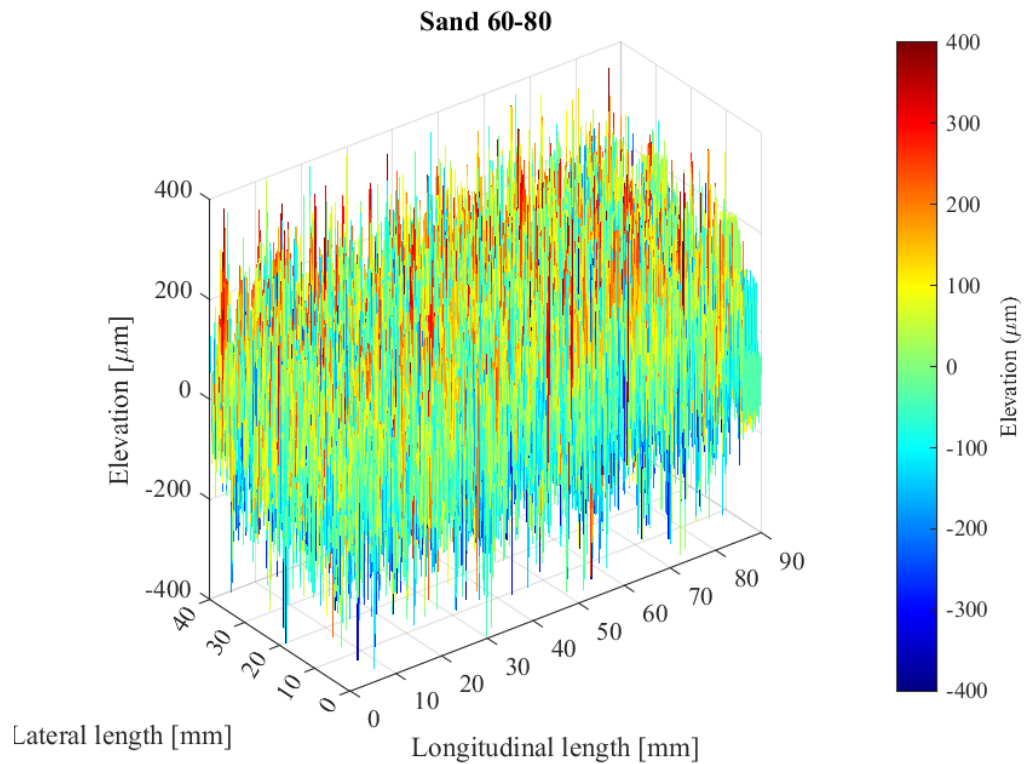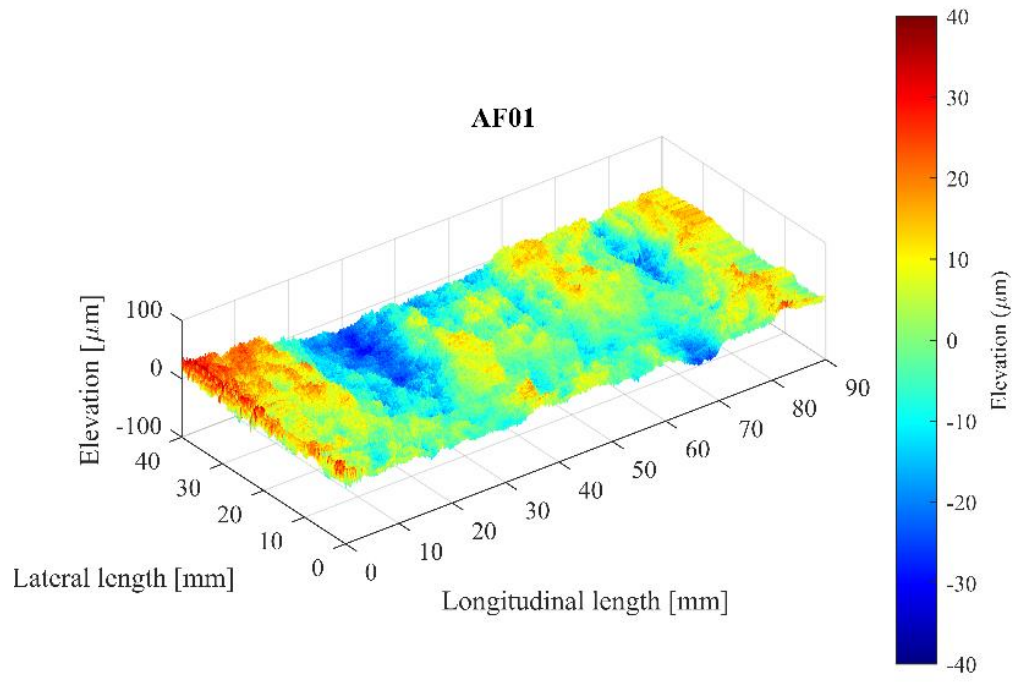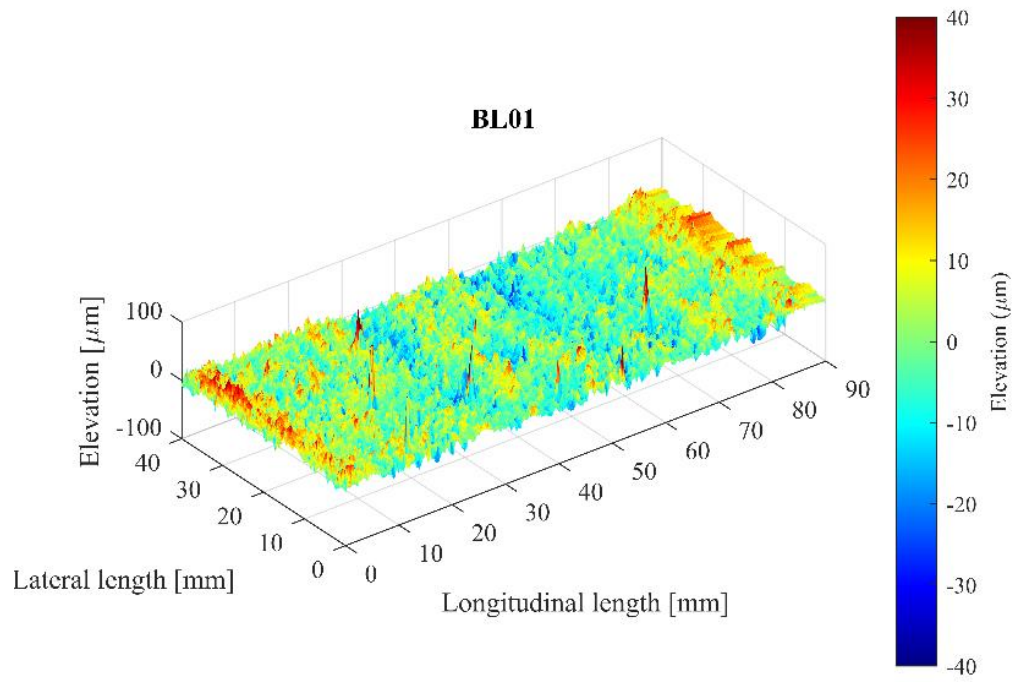
(d)
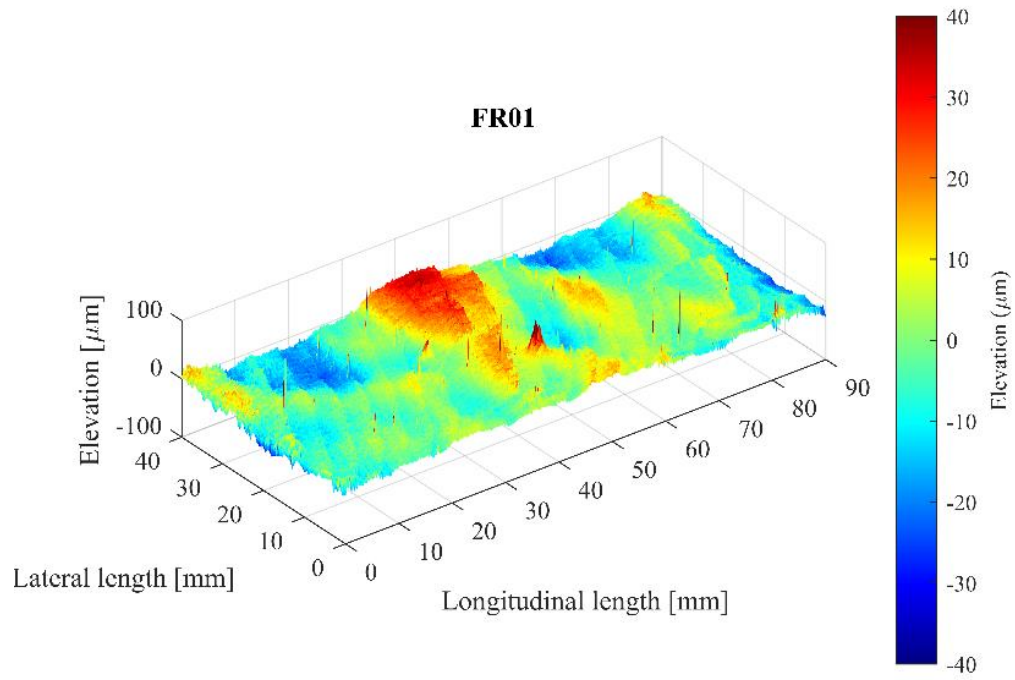
(e)
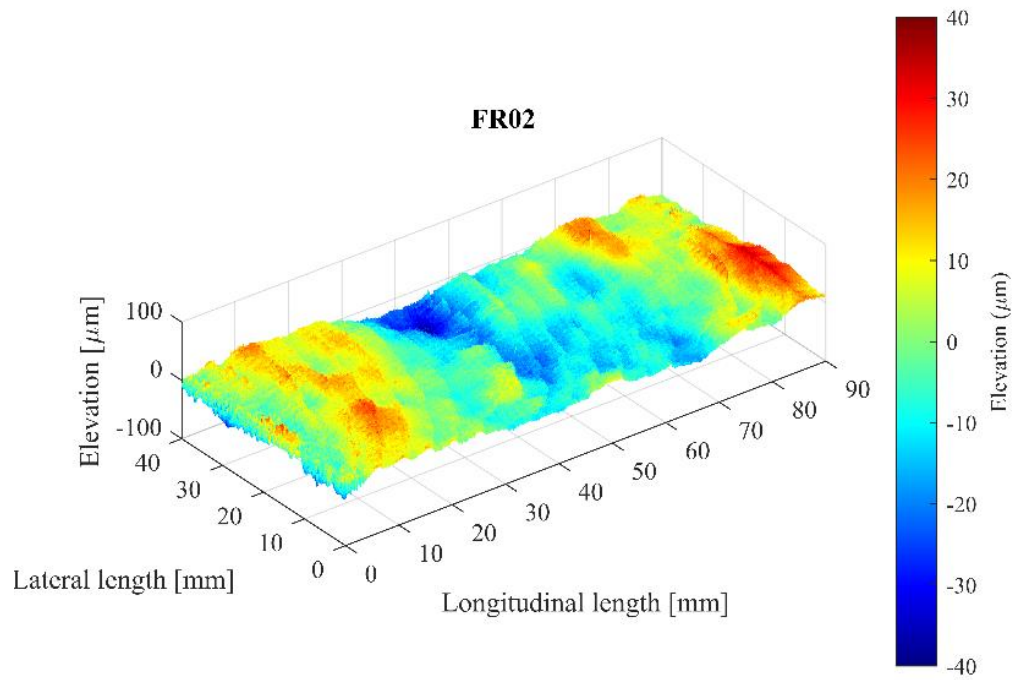
(f)

Figure 4-9: Unfiltered surface topography maps of the test surfaces.

4.2.4. Pressure Drop Measurements

The UoS' FTFC facility is fitted with six pressure taps on the test section. Theses taps are located on the side opposite the laser window to measure (*Figure 4-10*). Notably, the test section of the FTFC is located the furthest away from the centrifugal pump and just before the discharge tank. A honeycomb triggers the turbulence in the flow in the curved section above the centrifugal pump. This configuration allows to reach a fully developed turbulent flow.

Figure 4-10: Pressure taps distribution numbered from 1 to 6 (left to right) on the test section of the FTFC.

Pressure taps 2 and 5 were chosen for pressure drop measurements to avoid pressure waves and noise disturbances at the ends of the measuring section. In fact, taps 2–5 also provided the lowest uncertainty in pressure drop values at the mid-range pump frequency (16 Hz) (Marino et al., 2019). Each pair of taps can be connected to a differential pressure transducer with a range of 0–400 mbar via plastic hoses. Notably, each data point has been recorded at least twice (morning and afternoon convection cycles) with extra repeats at the lowest and highest speed of the range for uncertainty analysis. However, only one set of data is presented in the *Results* section. Additionally, the sampling rate used by the LabView data acquisition code to record each data point is 1000 Hz. It is also of note that the pressure taps are 120 mm apart from each other, and the pressure drop Δp is used in relation to the streamwise linear distance Δx to assess the skin friction of the surfaces, according to the following formulae from Equations (4-1)–(4-4), (Dean, 1978):

$$c_f = \frac{\tau_w}{\frac{1}{2}\rho U_M^2} \qquad (4\text{-}1)$$

$$\tau_w = -\frac{D_h}{4}\frac{\Delta p}{\Delta x} \qquad (4\text{-}2)$$

$$D_h = \frac{2\,hb}{h+b} \qquad (4\text{-}3)$$

$$Re_M = \frac{U_M\,h}{\nu} \qquad (4\text{-}4)$$

where h and b are, respectively, the channel height ($h = 22.5$ mm) and channel width ($b = 180$ mm), ρ, the water density, and U_M, the mean bulk velocity of the flow in the test section. Notably, U_M is measured by a magnetic flow meter and a resistance thermometer monitors the water temperature. The water density, ρ, is specified based on the formulae provided by (ITTC, 2011d), including the correction for the temperature of the channel flow, which is continuously recorded by the channel sensor.

Furthermore, the pressure drop measurements were conducted for a range of mean bulk velocities, U_M, calculated by using the data obtained from the magnetic flowmeter. For each set of test panels, the full range of pump frequencies was assessed (5–40 Hz) to give 36 different mean bulk velocity values (approx. 1.5–13.5 m/s). The variation of the mean bulk velocity at the test section of the FTFC with the smooth reference (uncoated) panel against the pump frequency (rotation per second) is shown in *Figure 4-11*.
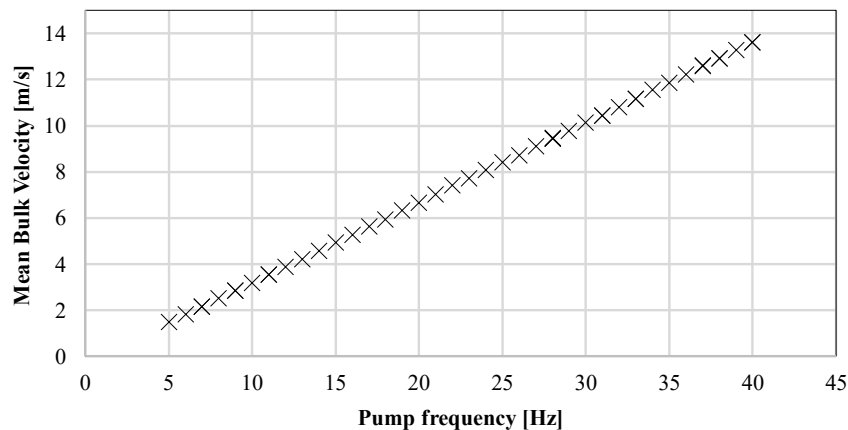
Figure 4-11: Centrifugal pump frequencies and corresponding mean bulk velocities at the test section of the FTFC with the smooth reference (uncoated) panel.

Notably, the time required to get out a sufficiently populated data matrix for each set of panels is about 2 hours. This time accounts for half an hour to mount/dismount the panels to carry out repeats (approx. one minute is sufficient to record the data at one flow speed). Finally, it can be recommended that future studies consider the kinetic Reynolds number (i.e., Valensi number) to correlate the oscillating frequency with the flow velocity.

4.2.5. Experimental Uncertainty Analysis

The uncertainties of the measurements in the FTFC tests were assessed following the ITTC-recommended procedures (ITTC, 2014). The standard errors for the coefficient of friction were calculated based on a two to six replicate runs of the panel at low and maximum flow velocities, respectively. *Table 4-5* and *Table 4-6* and Table XX presents the standard deviation errors to be considered when assessing the skin friction results. Notably, to exclude the impact of convection cycles on experimental data, the repeats tests were carried with a minimum of 6 hours gap. Furthermore, the plates were dismounted and remounted to the test section before running the repeat tests. However, in the results section, the data points presented will correspond to a single set of experiments.

The precision uncertainty in the skin friction coefficient was calculated at a 95% confidence interval by multiplying the standard error by the two-tailed t values ($t =$ 3.182, 2.571) for three to five degrees of freedom, according to (Coleman and Steele, 2012). The accuracy of the differential pressure sensor is ±0.075%, and the accuracy of the magnetic flow meter was ±0.2% according to the manufacturer's specifications, *Table 4-7*. The total uncertainty was calculated using equation (4-5) and typical error propagation techniques (ITTC, 2002):

$$(U_A)^2 = (B_A)^2 + (P_A)^2 \qquad (4-5)$$

where B_A is the bias uncertainty limit, P_A is the precision uncertainty limit and U_A is the total uncertainty. The overall uncertainty in the roughness function, ΔU^+ is ±14.4% or 0.04 (whichever is larger) at the lowest Re_M, ±6.5% or 0.04 (whichever is larger) at

the highest Re_M. The total bias limit and precision limit for the skin friction coefficients c_f were combined using equation (4-5) to give a total uncertainty of maximum $\pm 1.64\%$ at the lowest Re_M and $\pm 0.75\%$ at the highest Re_M, respectively. For comparison, the high Reynolds number turbulent flow facility at the US Naval Academy achieved a relatively similar level of uncertainty, with their skin friction data being $\pm 1.2\%$ at Re_M between $4.0x10^4 - 3.0x10^5$ (Schultz et al., 2015).

Table 4-5: Uncertainty in the c_f with 95% confidence level at the highest flow speed of the FTFC $(U_M = 13.5\ m/s)$.

		B_A	P_A	U_A
AF01	Absolute	$1.47x10^{-5}$	$1.13\ x10^{-5}$	$1.85\ x10^{-5}$
	Relative	$\pm 0.40\%$	$\pm 0.31\%$	$\pm 0.50\%$
BL01	Absolute	$1.64x10^{-5}$	$1.53\ x10^{-5}$	$2.25\ x10^{-5}$
	Relative	$\pm 0.40\%$	$\pm 0.37\%$	$\pm 0.54\%$
FR01	Absolute	$1.60x10^{-5}$	$1.23\ x10^{-5}$	$2.02\ x10^{-5}$
	Relative	$\pm 0.40\%$	$\pm 0.31\%$	$\pm 0.50\%$
FR02	Absolute	$1.40x10^{-5}$	$2.26\ x10^{-5}$	$2.66\ x10^{-5}$
	Relative	$\pm 0.40\%$	$\pm 0.64\%$	$\pm 0.75\%$

Table 4-6: Uncertainty in the c_f with 95% confidence level at a low flow speed of the FTFC $(U_M = 3.9\ m/s)$.

		B_A	P_A	U_A
AF01	Absolute	$3.15x10^{-5}$	$2.76\ x10^{-5}$	$4.19\ x10^{-5}$
	Relative	$\pm 0.79\%$	$\pm 0.69\%$	$\pm 1.05\%$
BL01	Absolute	$3.43x10^{-5}$	$5.87\ x10^{-5}$	$6.80x10^{-5}$
	Relative	$\pm 0.79\%$	$\pm 1.35\%$	$\pm 1.56\%$
FR01	Absolute	$3.43x10^{-5}$	$2.88x10^{-5}$	$4.47\ x10^{-5}$
	Relative	$\pm 0.79\%$	$\pm 0.67\%$	$\pm 1.03\%$
FR02	Absolute	$3.17x10^{-5}$	$5.80\ x10^{-5}$	$6.61\ x10^{-5}$
	Relative	$\pm 0.79\%$	$\pm 1.44\%$	$\pm 1.64\%$

Table 4-7: Manufacturer specification of all measuring instruments of the FTFC.

Measuring and Control Instrument	Accuracy
Magnetic flow meter	±0.2%
Differential pressure sensor	±0.075%
Pressure sensor	±0.5%
Temperature transmitter with a resistance thermometer	±0.1%

It is also of note that roughness changes the height of the flow channel slightly which changes the Re_M in return. *Figure 4-12* shows the change in Reynolds number at three different speeds (medium to maximum flow speed) for each surface tested compared to the smooth reference plates. The changes measured are considered negligible as are in the range of 0.05% to 2.15%. However, the shift in the data points presented for skin friction might be caused by this change in Reynolds numbers due to the presence of roughness reducing the channel height. Furthermore, the variation in channel height could also stem from the panels' thickness tolerance. When significant roughness is introduced, such as in the case of the coarsest sand (Sand 60-80), the Reynolds numbers (Re) consistently decrease as anticipated.
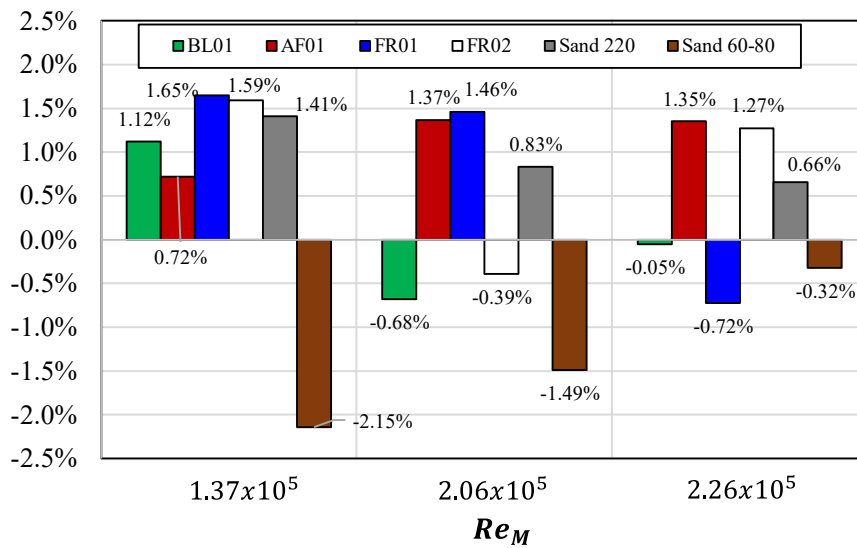
Figure 4-12: Change in Reynolds number based on channel height at three different speeds for each surface tested compared to the smooth reference plates.

4.3. Results and Discussion

4.3.1. Wall Shear Stress

The wall shear stress of each panel set was calculated by Equation (4-2) based on the hydraulic diameter of the channel defined in Equation (4-3) and the resulting longitudinal pressure drop ($\Delta p/\Delta x$). In *Figure 4-13* a plot of τ_w vs. flow speed for each panel set is shown, including the 1957 ITTC skin friction formulation for a 232.5 m long flat plate.

As shown, the wall shear stress of a 232.5 m long flat plate representing the full-scale KCS at a ship speed, V, of 24 knots (12.35 m/s) can be achieved in the FTFC at a considerably low flow speed (4.8–7.2 m/s). In fact, the horizontal dashed red line represents the constant τ_w achieved by KCS at 24 knots. This line crosses the τ_w curves of the FTFC-tested panels at considerably lower velocities than the ITTC curve. In other words, at a constant speed of 24 knots (indicated by the vertical dashed red line at 12.35 m/s), the τ_w values of the tested panels in the FTFC are much higher than the value from the ITTC formulation. Therefore, the results from the FTFC can be analogised to the turbulent boundary layer formed on a ship's hull at cruising speed. In fact, the FTFC enables the measurement of much higher flow speeds and τ_w values that would not be otherwise achievable in a typical towing tank with flat friction test plates. Overall, the wall shear stress trend of all the FCCs surfaces tested is quite similar. The very subtle differences are related to minor differences in surface roughness that likely arise from the application rather than being inherent in any differences in the coatings themselves. Similar observations were made in (Schultz et al., 2015).
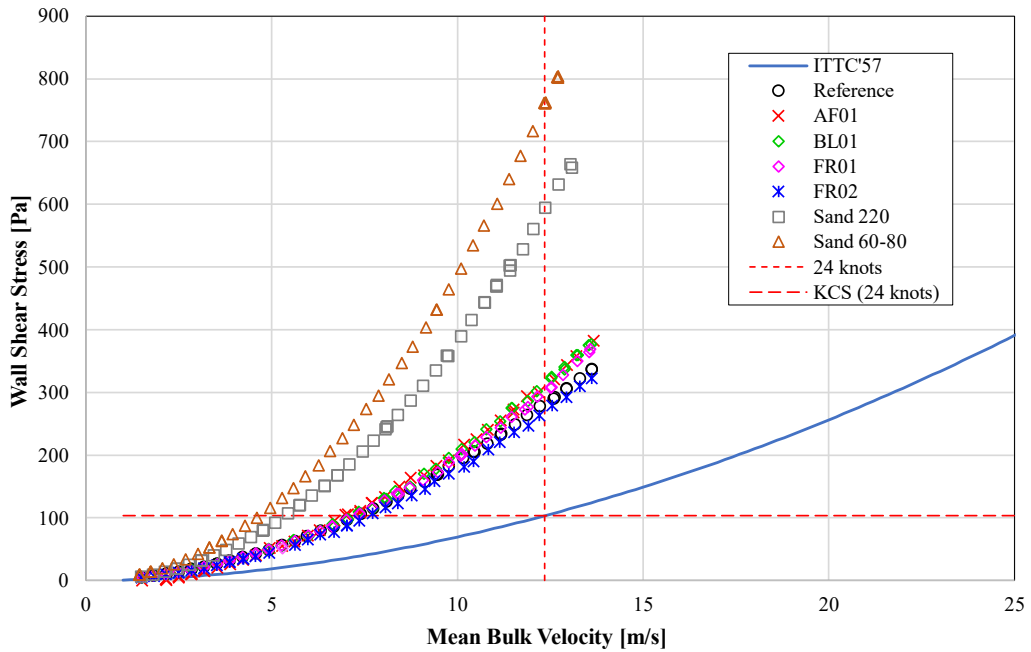
Figure 4-13: Wall shear stress achieved in FTFC compared to a 232.5 m long flat plate using the ITTC formulation.

4.3.2. Skin Friction Coefficients

Figure 4-14 shows the skin friction coefficient, c_f of each test surface plotted against the Reynolds number, Re_M compared to the hydraulically smooth acrylic panel and reference data taken from (Schultz and Flack, 2013). It is of note that the almost unitary R^2 value in Figure 8 refers to the polynomial trendline fitted for the experimental reference data. Interestingly, all the test surfaces had skin friction coefficient values beneath the smooth friction line at low Reynolds numbers except for the sanded surfaces. It can be noted that the *AF01* displayed unique frictional coefficients behaviour below values of $Re_M < 10^5$, which its surface condition appearance could not explain. The *FR01* and *BL01* coatings had skin friction curves that followed the behaviour of the smooth acrylic reference panel up until $Re_M = 2x10^5$ where the surfaces showed an increase in skin friction compared to the reference surface.

Furthermore, all the surfaces had skin friction coefficient values above the smooth friction line at higher Re values ($Re_M > 2x10^5$) except for the *AF01* and *FR02* surfaces. In fact, *AF01* and *FR02* were the only surfaces to maintain a lower skin

friction coefficient than the smooth reference surface over the entire Reynolds number range $(3x10^4 < Re_M < 3x10^5)$. These coatings (*AF01* and *FR02*) probably have lower friction than the smooth reference because their surface is amphiphilic and hydrophobic, while the reference is neutral. It is of note that each panel set separated from the hydraulically smooth condition at slightly different values of Reynolds numbers. On the other hand, *Sand 220,* and *Sand 60–80* considerably increased skin friction from the smooth reference panel. As expected, the increase in skin friction is more significant for the coarsest of the two surfaces, *Sand 60–80*, than the smoothest, *Sand 220*. Note that each panel set is separated from the hydraulically smooth condition at slightly different values of Reynolds numbers.
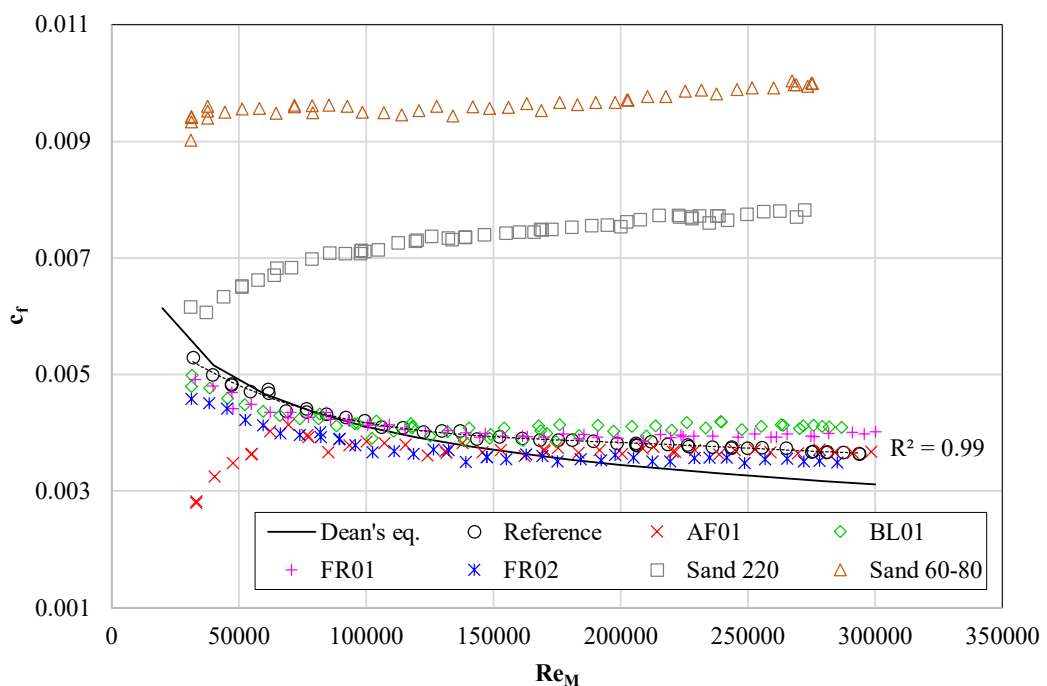
Figure 4-14: Skin friction coefficients (c_f) vs. Reynolds number (Re_M) for all marine coating surfaces.

As discussed, the *AF01* and *FR02* coatings had an interesting skin friction behaviour compared the smooth reference panel. The author believes that it is possible that experimental errors are the cause of the virtuous behaviour. Furthermore, the chemistry of the surfaces (hydrophobics) and the application method affect the surface roughness and hence the frictional resistance. In other words, as discussed in the methodology section, it is also important to note that these surfaces were applied in a largely isolated (i.e., laboratory) environment which is not representative of the

conditions of a real-world coating application in a dockyard. In fact, a dockyard environment can be subject to various external factors, including high winds, temperature, and pre-existing hull roughness (macro roughness). Therefore, the coating surfaces presented in this study and those compared in other studies, especially the coatings that were airless sprayed (*FR02 & AF01*), should be taken as a better finish than one that would be achieved on the surface of a ship in drydock (Schultz et al., 2015; Walker et al., 2014).

It is worth noting that all the FCCs tested exhibited decreasing c_f with increasing Reynolds number until $Re_M < 10^4$. This indicates surfaces that have not yet reached the fully rough flow regime. For $Re_M > 10^4$ the c_f of the FCCs become independent of the Reynolds number. This could prove that the Reynolds number of these tests is high enough to achieve fully rough behaviour. On the other hand, this was not the case for the *Sand 220* and *Sand 60–80* that were tested at the same Reynolds numbers. In fact, it could be indicative of a fundamental change in flow regimes. *Sand 220* and *Sand 60-80* do not display typical fully rough behaviour, at least over the range of the Reynolds number assessed here. Instead, c_f continues to increase with the Reynolds number over the entire range.

4.3.3. Roughness Function Models

As discussed in the methodology section, provided that the roughness functions of the test surfaces are known, Granville's similarity law can be used to predict the effect of hull roughness on ship resistance. Once the roughness functions have been calculated, they were directly compared with both Colebrook-type (Grigson, 1992) and Nikuradse-type (Cebeci and Bradshaw, 1977) roughness functions

Figure 4-15 shows the experimental roughness functions, ΔU^+, vs. roughness Reynolds numbers, k^+ obtained from the FTFC pressure drop measurements following Granville's approach (Granville, 1987). Notably, the experimental roughness functions of *Sand 60-80* and *Sand 220* surfaces show a similar trend as the Nikuradse type roughness function, *Figure 4-15*a.

On the other hand, the FCCs tested (*Figure 4-15*b) show a deviation between the experimental results with the Nikuradse model in the vicinity of 0.4 to 5 (k^+). This is probably due to the special amphiphilic and hydrophobic characteristics of the coatings, which exhibited lower friction than the smooth reference. To overcome the deviation from Nikuradse's model, the roughness functions were modelled by adapting the roughness function model of (Demirel et al., 2017a) with the curve fitting coefficients in Table 6. Finally, as previously mentioned, the roughness length scale values, k, were selected so that the roughness function models obtained were in agreement with the Nikuradse (Cebeci and Bradshaw, 1977; Nikuradse, 1933) or Colebrook type (Colebrook et al., 1939), *Table 4-8*. An exaggerated difference between the roughness functions of the smoothest and roughest coated panels is given in *Figure 4-16*.

Table 4-8: Curve fitting coefficients of the roughness functions for the test surfaces.

Test Surface	Roughness Length Scale, k [m]
AF01	$9.598 \ x10^{-6}$
BL01	$1.822 \ x10^{-5}$
FR01	$1.544x10^{-5}$
FR02	$5.840x10^{-6}$
Sand 220	$1.532x10^{-4}$
Sand 60-80	$3.530x10^{-4}$
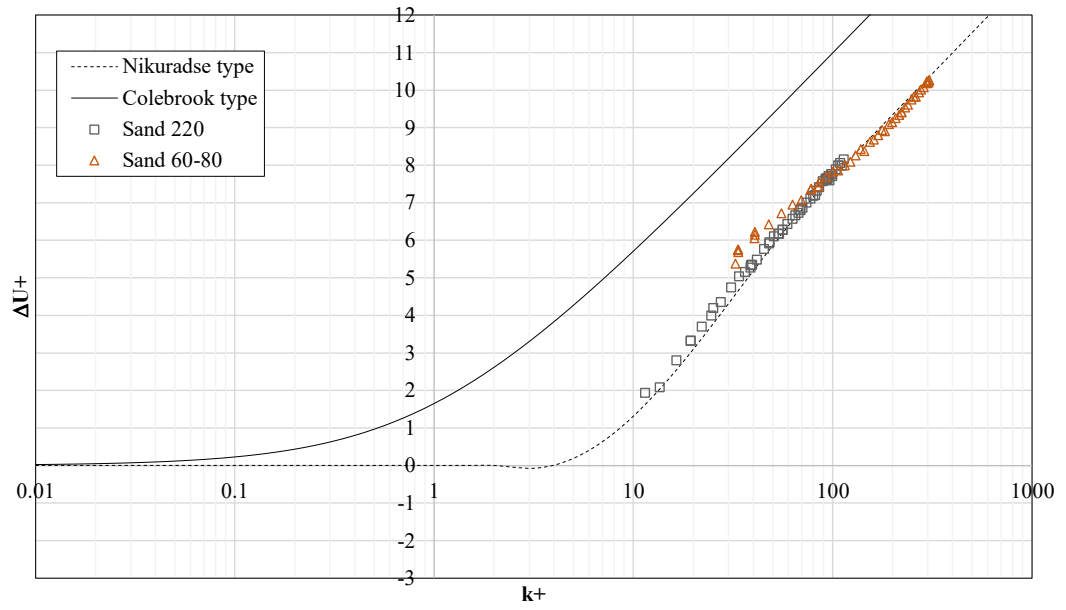
(a)
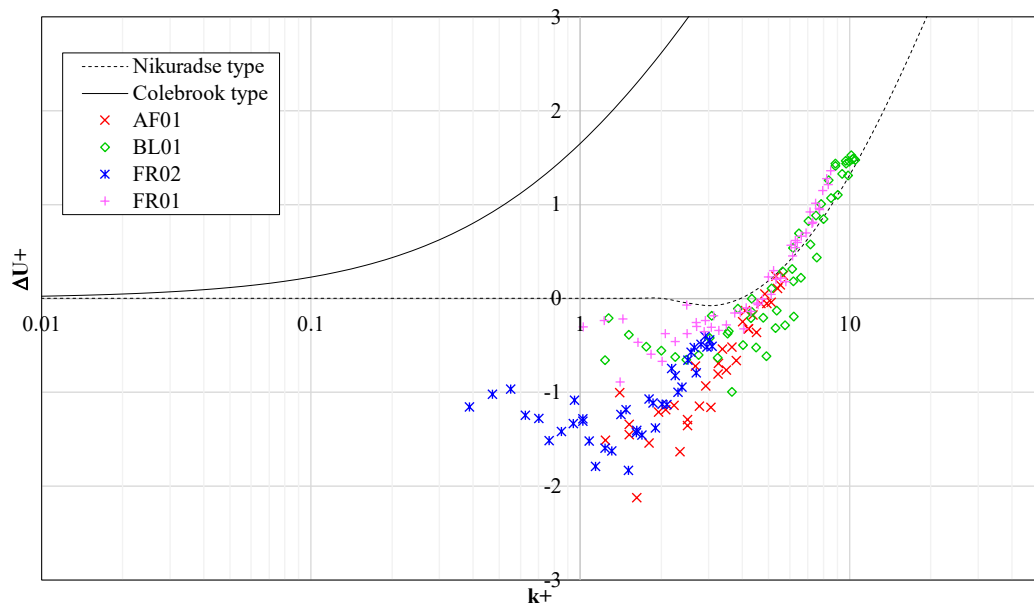
(b)

Figure 4-15: Experimental roughness functions of the test surfaces developed from FTFC pressure drop measurements; (a) sanded rough; (b) FCCs.
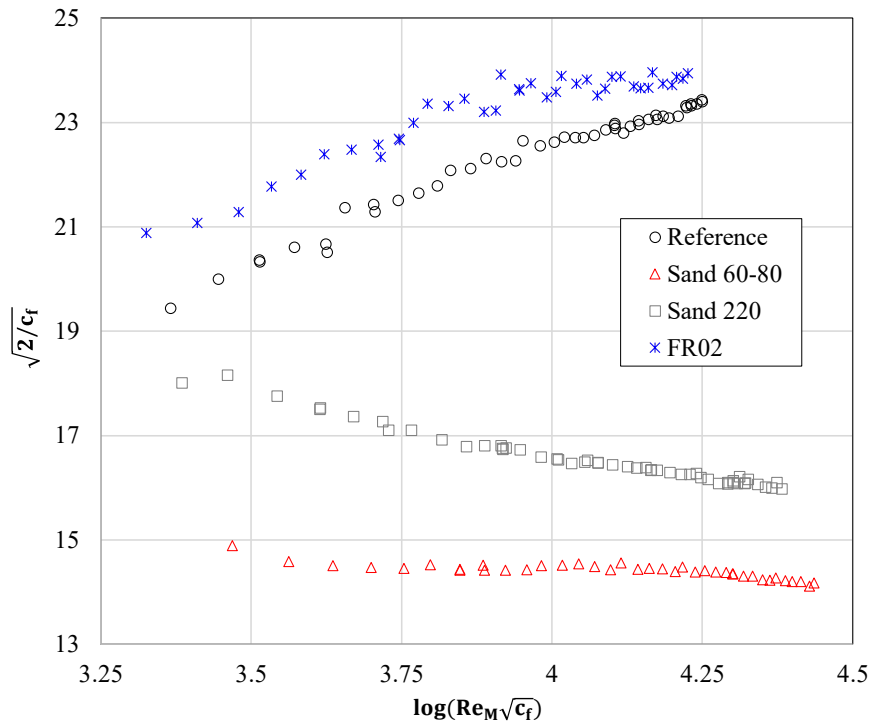
Figure 4-16: Exaggerated difference between the roughness functions of the smoothest and roughest coated panels.

4.4. Conclusions

The present chapter confirmed that the most rational approach to tackling the effect of ship hull roughness, including biofouling, combines experimental and numerical methods. The practical and sophisticated FTFC facility recently installed at the UoS was adopted for this scope. In fact, roughness functions for a hard foul-release coating, other commonly used marine coatings, and mimicked biofouled hull conditions were developed. Furthermore, this chapter exploited the advantages of FTFC experiments to predict the effect of hull roughness on full-scale ship resistance and powering. To the best of the author's knowledge, only limited (and unpublished) research was conducted using the FTFC of the UoS before the present study. Hence, the urgency to use the FTFC designed and custom-built (Marino et al., 2019) at the University of Strathclyde (UoS).

Furthermore, the experimental data produced supports drag reduction studies and contributes to the international database of the roughness functions for different FCCs

and biofouling. Producing experimental data was indeed recommended, e.g., by the 21st ITTC Surface Treatment Committee (ITTC, 2011a). Finally, the goal of developing transferrable expertise with the FTFC of the UoS was met.

Hence, the chapter introduced experimental roughness functions for the FCCs tested, including GIT's (*FR02* hard foul-release coating). Each surface's wall shear stress values and specific friction coefficients relative to the smooth uncoated reference surface were presented for completeness. Furthermore, the roughness function developed for a sandpaper-like surface (*Sand 220*) from the FTFC experiments was compared with previous towing tank tests. It is of note that this was the first time the same surface was tested in two different facilities of KHL.

Among the four fouling control coatings (FCCs) that were tested in the FTFC, the *FR02* coating (hard foul-release) displayed the best hydrodynamic performance across the entire Reynolds number range. In contrast, *Sand 220* (medium light slime) and *Sand 60-80* (medium slime) have, as expected, the highest resistance due to their rougher characteristics.

It would be beneficial to investigate the hydrodynamic performance of the same FCC under the effect of biofouling growth. Exposing surfaces to dynamically grown biofouling would give shipowners and operators a better indication of what powering penalty they should expect from these coatings after a specific time in active service. It is of note that such real biofouling could soon be simulated in the biofouling farm under development at the University of Strathclyde. Applying different mimicked biofouling to the panels before or after the coating application could also serve as a better method to predict the resistance behaviour of the as-applied condition to an existing rough ship hull.

It is also of note that fully turbulent flow channels are useful for testing the resistance of a flat plate, but their applicability for predicting the resistance of a curved plate or a ship hull is limited. This is because the flow over a curved surface is more complex and three-dimensional than that over a flat plate, and other features of the hull can significantly affect the flow behaviour and resistance.

However, results from flat plate experiments can guide the design of ship hulls. By developing roughness functions that relate the drag coefficient to the surface roughness using flat plate experiments, researchers can account for the effects of surface roughness on the resistance of ship hulls in CFD simulations, even though the shape of the hull is different. Additionally, researchers can use scaled-down models of ship hulls in fully turbulent flow channels to develop empirical correlations between the drag coefficient and hull shape, which can then be used to estimate the resistance of full-scale ships based on their geometry.

Above all, the present chapter has provided several significant findings, including the procedure to conduct pressure drop measurements with an FTFC, the application of Granville's method for pipes to develop roughness functions, as well as the introduction of roughness functions for marine coatings and mimicked biofouling. The findings presented can help predict the required power, fuel consumption and greenhouse gas emissions of ships with hulls coated with certain fouling control coatings and/or in the fouled condition. As a final remark, the author would like to emphasise that there is an enormous opportunity for growth in the area of research on FTFCs. Indeed, the test cases in this chapter only represent an infinitesimal fraction of the number of coating products and surface roughness conditions that can be tested.

4.5. Chapter Summary

The consequences of poor hull surface conditions on fuel consumption and emissions are well-known. However, their rationales are yet to be thoroughly understood. The present chapter investigated the hydrodynamics of fouling control coatings and mimicked biofouling. Experimental roughness function data were developed from the "young" fully turbulent flow channel facility of the University of Strathclyde (UoS). Different surfaces, including a hard foul-release coating, were tested. The present chapter can also serve as a valuable guide for future experimental campaigns using the fully turbulent flow channel facility of the UoS and the corresponding development of roughness functions.

5. Modelling the Hydrodynamics Characteristics of Realistic Surfaces: Towing Tank Tests

5.1. Introduction

The effect of hull roughness can be particularly detrimental to ship performance in terms of fuel consumption and greenhouse gas emission. Skin frictional resistance is critically dependent on the roughness of the surface. An increase in roughness leads to an increase in turbulence, turbulent stress, and wall shear stress and finally, skin friction increases. The previous chapter's flow channel experiments confirmed skin friction's importance. Despite the progress of modern marine coatings and active or passive protection against corrosion, the increase in roughness of the hull of a ship in-service is inevitable.

In order to gain a deeper understanding of the effects of roughness on the skin friction of ships, the fundamentals of the studies in the literature (Ünal, 2012; Candries and Atlar, 2004; Schultz and Swain, 1999) suggest conducting experimental studies on lab-scale plates with a focus in the turbulent boundary layer. According to the literature, the effect of deteriorated coating or light slime of a ship can be reproduced by coating sand on the surfaces of flat plates for towing tank experiments. For example, the equivalent sand-grain roughness found by (Monty et al., 2016) was used to reproduce the light calcareous fouling. Physical roughness can be controlled easier than biological roughness (fouling), which is time dependent.

Furthermore, the impact of fouling on ship performance is greatly dependent on the type and coverage of fouling (Schultz, 2007). In this thesis, a stainless-steel flat plate was coated with sand to obtain the model's desired surface roughness finish. Furthermore, as mentioned earlier, ITTC recommends that researchers generate an extensive experimental database of the roughness functions of different surfaces (ITTC, 2011b). This is because the roughness functions of a given surface assessed

must be known in order to predict the roughness effect that those surfaces have on ship resistance.

Measurements during full-scale trials conducted in several existing studies have investigated the roughness effect on ship resistance and powering. The unreliability of the results due to different experimental conditions can be seen in the literature (Busch et al., 2019; Munk, 2006). Above all, the data from towing tank experiments are considered more reliable than sea trial measurements since the lab-scale setups provide known uncertainties and excellent repeatability. Therefore, considering the recommendations of ITTC (2017a), in this chapter, the effects of roughness on a flat plate were investigated using towing tank tests. Finally, the roughness function values of the *Sand 220* surface were developed from towing tests and compared with the roughness function values of the same surface developed from FTFC experiments.

The rest of the chapter is structured as follows: Section 2 presents the methodology adopted. Section 3 details the towing tank experimental facilities, calibration of instruments, test design and experimental uncertainty analysis. Section 4 discusses the results of the experimental and numerical investigation. Finally, Section 5 gives the chapter's conclusions, final remarks, and summary.

5.2. Experimental Facilities

5.2.1. Towing Tank

The flat plate models and their towing tests were prepared at the Kelvin Hydrodynamics Laboratory (KHL) of the University of Strathclyde (UoS). The freshwater test tank is 76.0 metres long, 4.6 metres wide, and 2.5 metres deep (*Figure 5-1*). The digitally controlled towing carriage (*Figure 5-2*) has a velocity range of 0÷5 m/s, while the speeds used in the present experiments ranged between 1.5 and 4.5 m/s.

The technicians of KHL operated the carriage under the author's directions. Furthermore, the actual temperature of the water was monitored in order to evaluate the corresponding drag coefficients. It is of note that the temperature gauge of the tank

water registered a practically stable temperature of 17.0°C during all the tests. Daily morning reads of the gauge showed that the oscillations were always less than 0.3°C, which is the precision limit of the instrument.

Figure 5-1 - Test Tank of KHL.

Figure 5-2 - Towing Carriage of KHL.

5.2.2. Calibration of Instruments

Two displacement transducers were interposed between the test plate and the carriage to measure the towed plate's drag and side force. The resistance transducers were separately calibrated with weights (*Figure 5-3*) following the procedure of (ITTC, 2002) and (ITTC, 2017b) at a 95% confidence level. Furthermore, the relationship between the known loads and output voltage for the side force transducer (*Figure 5-4*) and drag transducer (*Figure 5-5*) were used to evaluate the calibration factors. It is of note that the transducers were manufactured by Cambridge Electronic Design (CED) 1988-2016 – Data Acquisition & Analysis and used the Linear Variable Differential Transformer (LVDT) principle. Finally, Spike2 version 8.09b x64 Unicode was the software utilised to digitalise the signals.
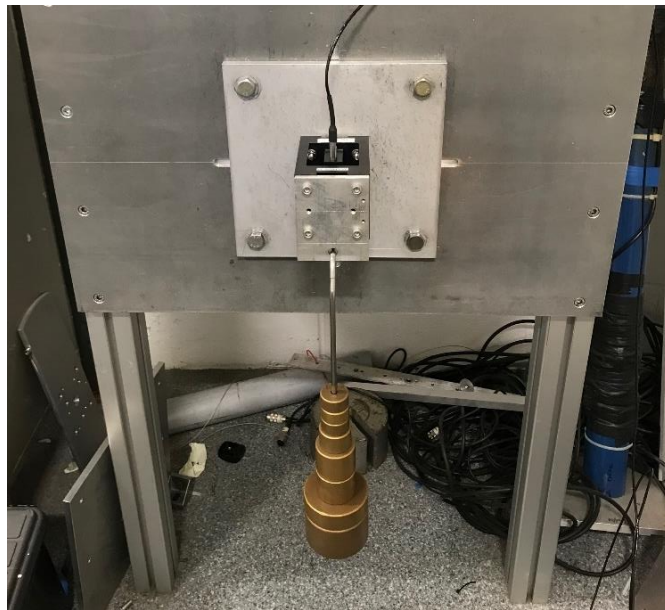
Figure 5-3: Calibration of a force transducer.
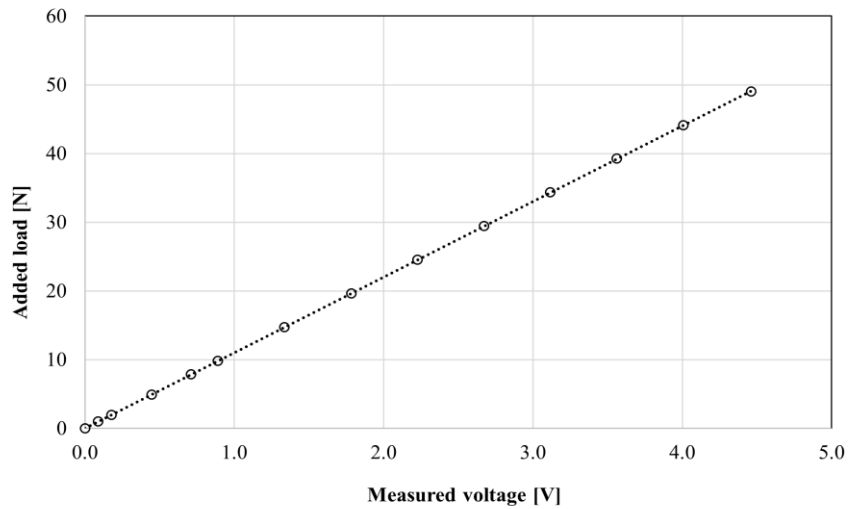
Figure 5-4: Side force transducer calibration.
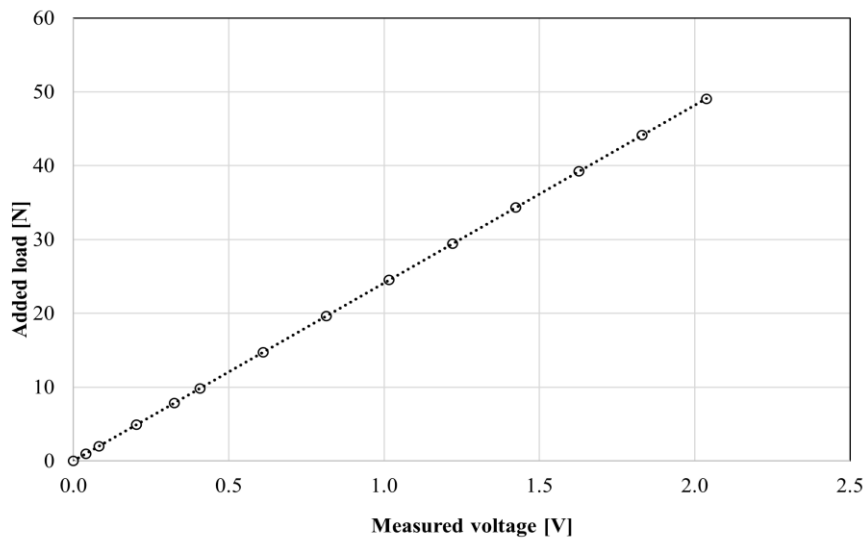
Figure 5-5: Drag transducer calibration.

5.2.3. Test Panels Design and Preparations

Figure 5-6 from Demirel et al., (2017) gives a schematic of the flat plate setup on the towing carriage. Notably, the angle of attack of the towed plate was zero during the experiments. The flat plate was manufactured from 304 stainless steel grade sheet stock and had the dimensions given in *Table 5-1*. The leading and trailing edges of the flat plate were milled, and the whole plate was polished with acetone solvent. Specifically, the leading-edge (*Figure 5-8*a) was rounded with a radius of 2.5 mm,

while the trailing edge (*Figure 5-8*b) was kept flat and sharp. The flatness of the plate was checked before starting the tests. All these steps were done in order to reduce the undesired extra drag and lift of the bare flat plate. Finally, once the plate was installed on the rig of the carriage (*Figure 5-7*), repeated runs were conducted to find the correct alignment.

Table 5-1: Dimensions of the flat plate used for the towing tests.

Length [m]	Height [m]	Thickness [m]	Draught [m]
1.495	0.805	0.005	0.588
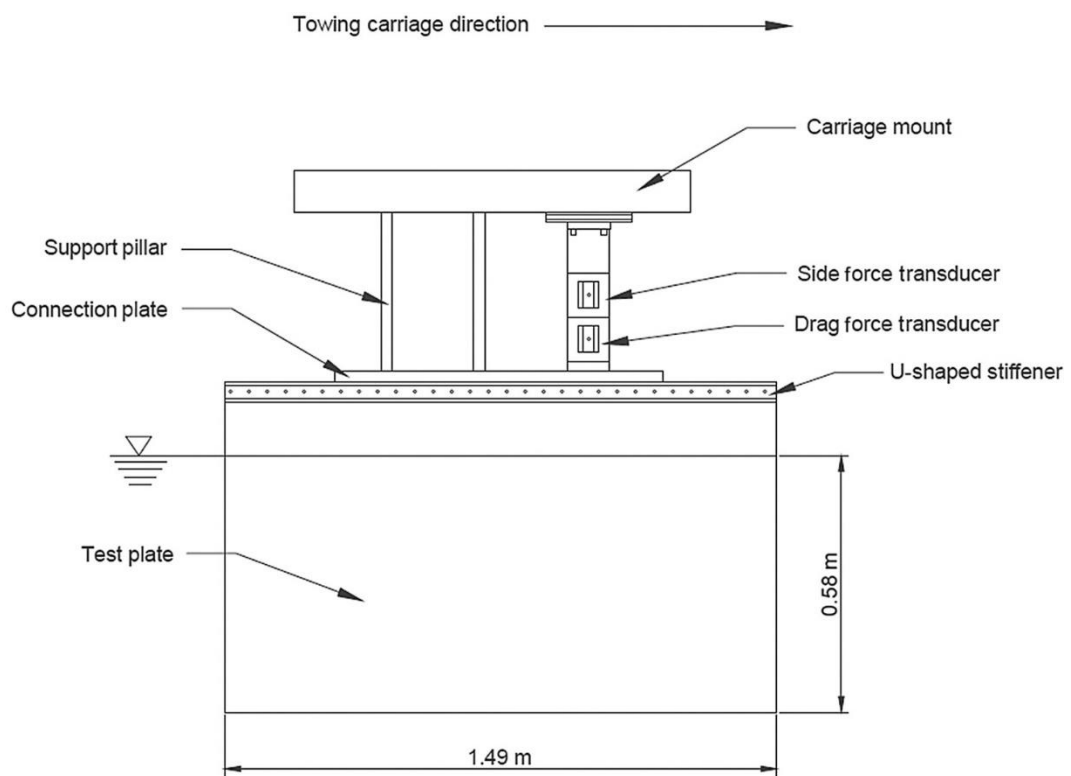
Figure 5-6: Schematic of the tests setup adapted from Demirel et al., (2017).

Figure 5-7: Rigging operations of the flat plate on the carriage.

The handling and preparation of the plate were performed by the specialised technicians of KHL, following state-of-the-art procedures (*Figure 5-7*). All the plate surfaces were coated with the mentioned sand-grit except for the rigging area. Having enough sand coating above the waterline of the plate made it possible even for the small waves that overpassed the waterline to be influenced by the roughness. Chapter 4 presented the statistical analysis of surface roughness for the towing tank rough plates coated with uniform sand (*Sand 220* and *Sand 60-80*) using a TQC Hull Roughness Gauge. Furthermore, *Figure 4-5* demonstrated the probability density functions (pdf) of the roughness data of the *Sand 220* and *Sand 60-80* test surfaces for towing tank and FTFC experiments.

(a)   *(b)*

Figure 5-8: Flat plate details: (a) Leading-edge; (b) Trailing-edge.

It is of note that the plate was carefully aligned to minimise the side forces. Hence, the side forces were monitored during all the sets of runs, and once the optimal position was found, no further adjustments were made to the alignment of the plate. Finally, the total resistance coefficients of the bare flat plate derived from the data collected during the tests are plotted in *Figure 5-9* below, together with the actual frictional resistance coefficients and the correlation lines of Schoenherr, (1932), Hughes, (1952) and ITTC, (1957). Despite the oscillations, especially at medium speeds, the trend of the C_T curve derived from the present experiments for the smooth flat plate is similar to the trends of the frictional correlation lines plotted.
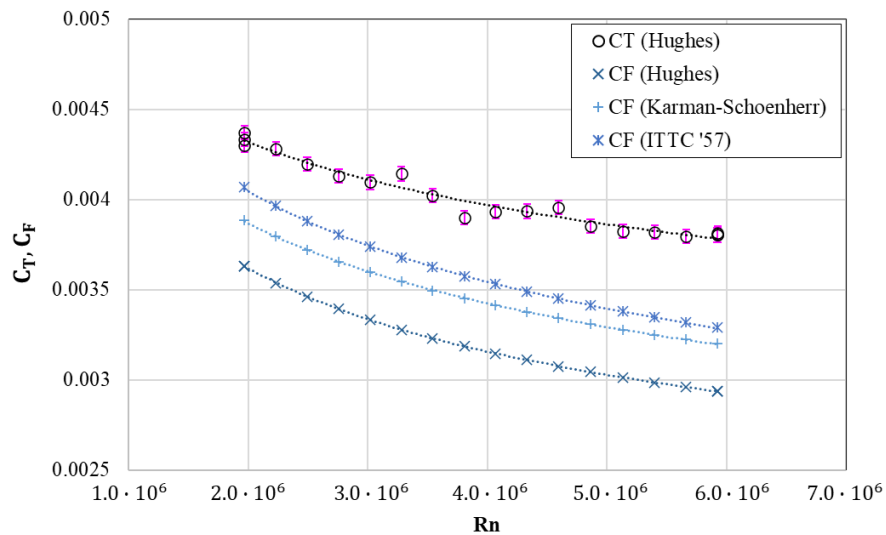
Figure 5-9: The smooth reference plate's total resistance coefficients and frictional correlation lines.

Once the tests for the smooth reference flat plate were completed, the rough conditions were prepared. According to literature, e.g. (Demirel, 2015), the effect of a ship's deteriorated coating or light slime can be reproduced by coating sand on the surfaces of flat plates for towing tank experiments. Therefore, the smooth stainless-steel flat plate described earlier was now coated with silicon carbide sand, 220 grit (the grit represents the density and size of sharp particles that characterise the sand coating of a surface, e.g., classic sandpapers). The *Sand 220* surface represents a medium-light slime and is considered a relatively small grit for resistance experiments. Hence, the increment produced by the total resistance of the reference plate was not expected to be as dramatic as other types of sand resembling more fouled conditions of the hull, such as *Sand 60-80*.

Figure 5-10: Coating operations of the flat plate with Sand 220.

5.2.4. Towing Tests

The present experiments were conducted at Kelvin Hydrodynamics Laboratory (KHL) of the University of Strathclyde (UoS) on a flat plate of typical dimensions (*Table 5-1*). The sand-coated flat plate was used according to the major assumption of Froude, which proposes that the skin friction of a hull is equal to that of a flat plate of the same length and area as the wetted surface of the ship (Lackenby, 1962). The rough plate was rigged on the carriage and towed longitudinally at a speed range from 1.5 to 4.5 m/s (*Figure 5-11*). Notably, the plate was towed longitudinally at a range of speeds for each configuration, and the drag was measured. With an increment of 0.2 m/s, the entire range of speed from 1.5 to 4.5 m/s was tested (16 speeds). The transducers measured the drag during the towing tests to obtain the total resistance coefficients. Furthermore, the lift and side forces are monitored to check on the alignment of the plate. The experimental data obtained for the smooth plate were used for reference to check on the drag increase when evaluating the rough plate. The actual speed of the carriage and tank water temperature was considered for the derived data, such as Reynolds numbers Rn and total resistance coefficients C_T.

It is of note that several more speeds of the range were repeated for repeatability and uncertainty analysis. In particular, in the later sections, the results will be discussed at the lower and higher speed of the range. Furthermore, the drag of sand roughness is assumed to qualify purely as skin friction drag since the pressure drag is expected to be insignificant compared to the plate's frictional drag. In fact, two repeats at the lowest and highest speeds of the range were always conducted for repeatability and uncertainty analysis. The repeats at the same speed were neve consequent but a time interval was respected.

It is also of note. the experiment duration for a single speed typically ranged from two to five minutes, which was determined by the time it took for the carriage to travel back and forth to the start position, as well as the need to wait for the water surface to settle between runs. Collecting data for the entire range of 16 speeds in the test matrix required approximately two to five hours. With repeated tests for both the smooth reference plate and the rough plate, the total time spent conducting tests on board the

carriage was approximately three workdays. Additionally, considering the time required to calibrate instruments and align the plate, the minimum time needed for the towing tests of a flat plate was approximately five days, excluding surface preparation.

| (a) | (b) |
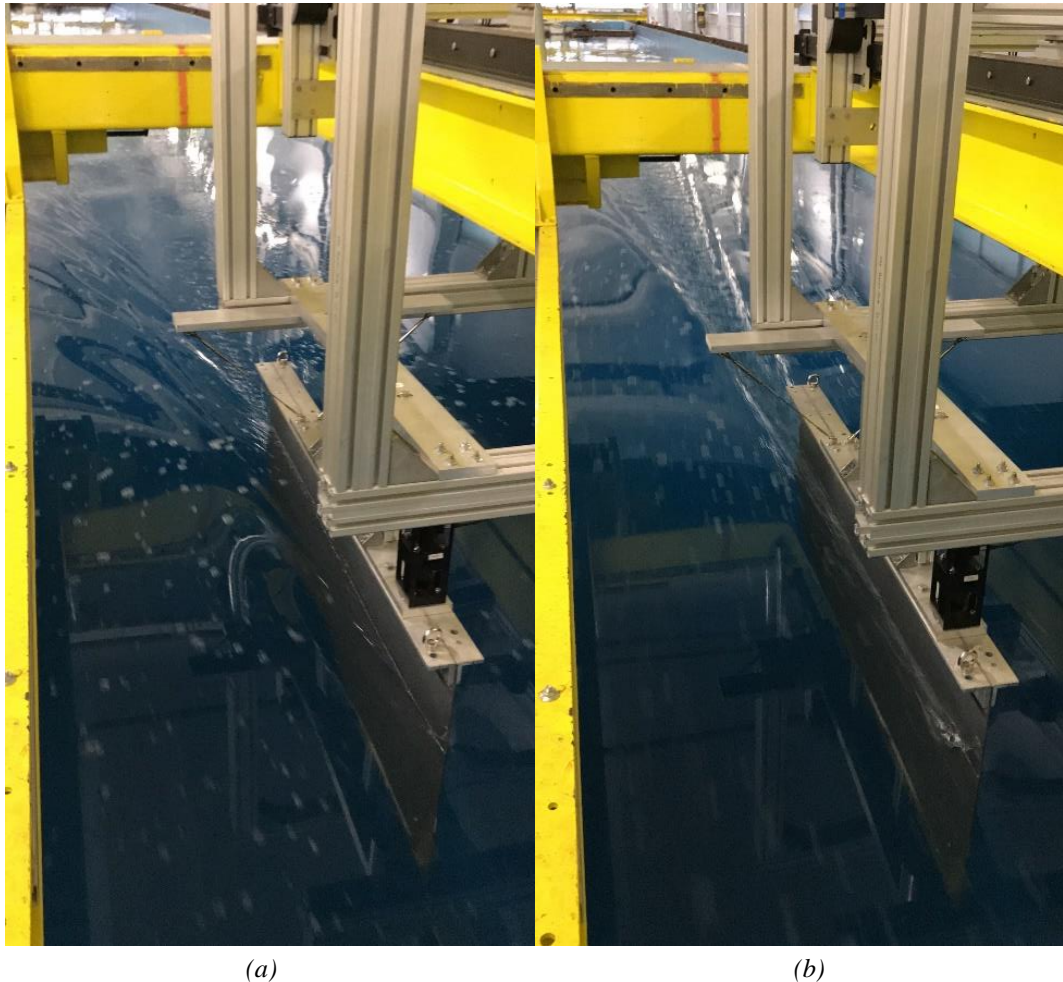
Figure 5-11: Towing tank experiments of a flat plate coated with Sand 220 towed at (a) 1.5 m/s; (b) 4.5 m/s.

5.2.5. Repeatability and Uncertainty Estimates

Repeated tests were performed to estimate the drag coefficients' uncertainty at the range's lowest and highest speeds (1.5 and 4.5 m/s, respectively). For this estimate, the procedure of (ITTC, 2017b, 2002; Coleman and Steele, 1999) was followed, similarly as for the calibration of instruments. Therefore, uncertainty estimates for the drag coefficients were made through repeatability tests using the procedure defined by the

ITTC, (2002). Equation (5-1) from ITTC, (2002) relates, for a quantity A, the total uncertainty U_A to the bias limit B_A and the precision limit P_A.

$$U_A^2 = B_A^2 + P_A^2 \tag{5-1}$$

B_A can also be called systematic errors and occurs due to the errors of measurement devices. On the other hand, P_A is caused by random errors with regard to the repeatability of the experiment. Therefore, *Table 5-2* presents the details of the uncertainty estimates for the total resistance coefficients in rough conditions at the lowest and highest speeds of the range.

Following the procedure of (ITTC, 2002) and (Coleman and Steele, 1999) to carry out an uncertainty analysis as explained in the methodology section, the results for the rough plate tested are presented, which are overall acceptable compared to other studies in the literature. Eventually, the combined bias uncertainty of the devices for C_T ranges between ±0,7%. As it can be seen from *Table 5-2*, the overall uncertainty in C_T ranges between ±0.9% at the lowest speed, and between ±0.7% at the highest speed. Finally, it is of note that for the frictional resistance coefficient C_F the overall uncertainty results are generally lower than those of the total resistance coefficient.

Table 5-2: Uncertainty Analysis of C_T at the lowest and highest speed of the range.

		1.5 m/s			4,5 m/s		
		Bias	Precision	Uncertainty	Bias	Precision	Uncertainty
Reference	[-]	$3.215\,x10^{-5}$	$3.367x10^{-5}$	$4.655x10^{-5}$	$1.929x10^{-5}$	$5.353x10^{-6}$	$2.002x10^{-5}$
	[%]	0.736	0.771	1.062	0.504	0.140	0.528
Rough	[-]	$3.308x10^{-5}$	$2.806x10^{-5}$	$4.337x10^{-5}$	$2.472x10^{-5}$	$2.516\,x10^{-5}$	$3.528x10^{-5}$
(*Sand 220)*	[%]	0.720	0.611	0.942	0.505	0.514	0.719

5.3. Results and Discussion

5.3.1. Flat plate towing test

Table 5-3 reports the experimental data at 15°C for the rough plate for velocities between 3.7-4.5 m/s. Furthermore, *Figure 5-12* presents the drag curves measured from towing tests on the smooth reference and rough (*Sand 220*) flat plate. On the other hand, *Figure 5-13* presents the total resistance coefficients derived from the drag values. Furthermore, the percentage of variation of total resistance (drag), R_T, and total resistance coefficients, C_T from the reference plate is given in the table. As expected, the roughness effect manifests as an increase in drag for the whole speed range.
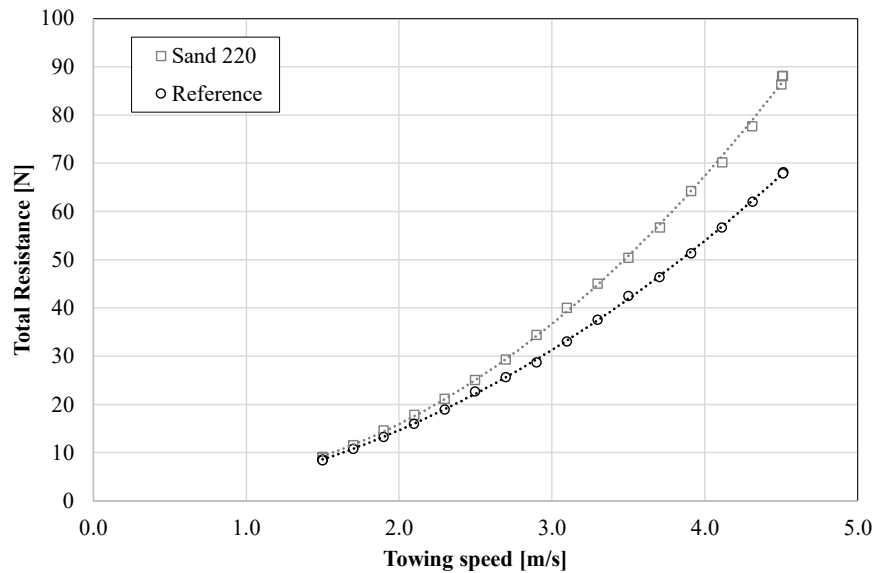
Figure 5-12 - Drag curves of the smooth (uncoated plate: Reference) and rough conditions (Sand 220) from towing tests on a flat plate.
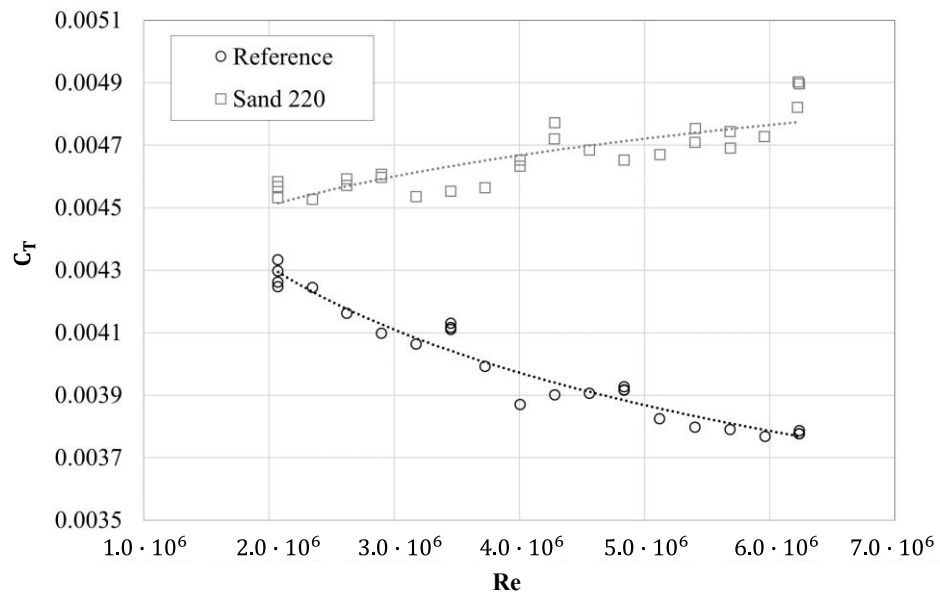
Figure 5-13 – Total resistance coefficients of the smooth (uncoated plate: Reference) and rough conditions (Sand 220) from towing tests on a flat plate.

Table 5-3: Rough plate experimental data (Sand 220) for velocities between 1.5 and 4.5 m/s; variation of drag and C_T with respect to the reference plate.

Speed [m/s]	Drag [N]	C_T	Rn	ΔDrag %	ΔC$_T$ %
1.500 m/s	9.12	$4.583x10^{-3}$	$2.074x10^6$	7.5	7.0
1.700 m/s	11.58	$4.526x10^{-3}$	$2.351x10^6$	6.7	5.8
1.899 m/s	14.65	$4.591x10^{-3}$	$2.626x10^6$	10.4	9.4
2.099 m/s	17.92	$4.595x10^{-3}$	$2.902x10^6$	12.2	11.3
2.300 m/s	21.21	$4.534x10^{-3}$	$3.179x10^6$	11.6	10.8
2.498 m/s	25.13	$4.552x10^{-3}$	$3.454x10^6$	10.7	9.9
2.698 m/s	29.38	$4.563x10^{-3}$	$3.730x10^6$	14.3	13.4
2.900 m/s	34.46	$4.631x10^{-3}$	$4.010x10^6$	19.7	18.8
3.099 m/s	40.08	$4.719x10^{-3}$	$4.284x10^6$	21.0	20.1
3.300 m/s	45.11	$4.683x10^{-3}$	$4.562x10^6$	20.0	19.0
3.501 m/s	50.43	$4.651x10^{-3}$	$4.840x10^6$	18.5	17.6
3.706 m/s	56.73	$4.669x10^{-3}$	$5.124x10^6$	22.1	21.2
3.911 m/s	64.36	$4.752x10^{-3}$	$5.407x10^6$	25.2	24.3
4.114 m/s	70.24	$4.690x10^{-3}$	$5.689x10^6$	23.8	22.9
4.310 m/s	77.69	$4.726x10^{-3}$	$5.960x10^6$	25.2	24.6
4.501 m/s	86.39	$4.820x10^{-3}$	$6.223x10^6$	27.0	26.8

5.3.2. Roughness Functions Determination

As described previously, provided that the roughness function of a specific surface is known, the procedure from Granville (1958) can be used to predict the roughness effect on the frictional resistance of a ship covered with given roughness (Demirel et al., 2017). The roughness function ΔU^+ is defined as the downward shift of the velocity profile in the log-law region caused by the roughness effect. Roughness Reynolds numbers, k^+, and roughness function values, ΔU^+, were obtained iteratively using equations (2-15) and (2-16) following the overall drag method procedure of Granville (1987) using the present experimental data.

In *Figure 5-14* are shown the roughness functions against roughness Reynolds numbers for the same rough surface tested, with values plotted for four different roughness length scales, namely k_1, k_2, k_3, k_4. The value of k_4 ($k_4 = 1.532\, R_{t_{50}} = 1.532 x 10^{-4} m$) was such that the roughness function observed behaviour was appropriate with respect to the model of Nikuradse (Cebeci and Bradshaw, 1977). It is of note that, as *Figure 5-14* shows, the selected roughness Reynolds number, k, only affects the abscissa of the profile of roughness functions against roughness Reynolds numbers (Demirel et al., 2014).
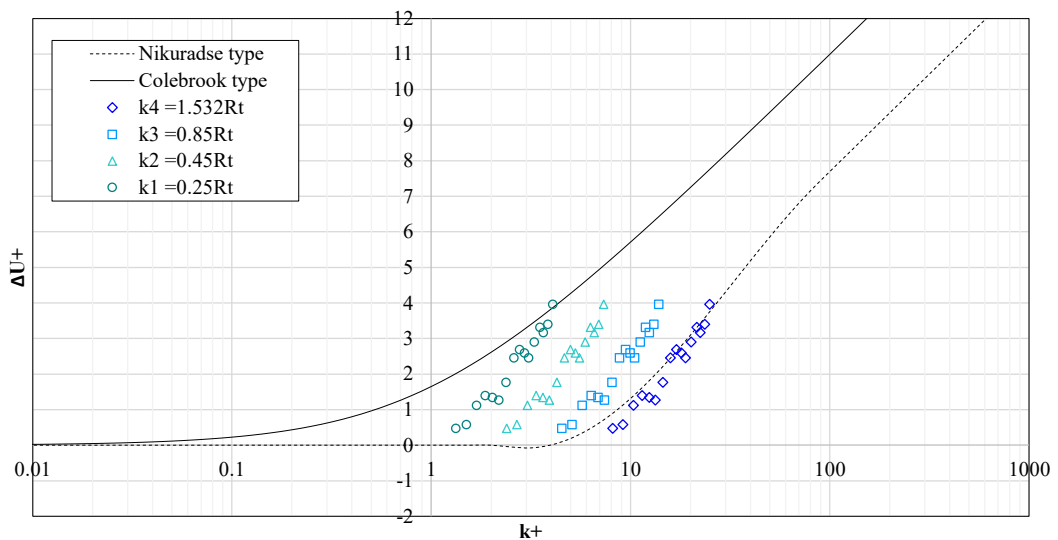
Figure 5-14: Experimental roughness functions of the Sand 220 surface at different roughness length scale values, developed from flat plate towing tank tests.

5.3.3. Comparison Between Towing Tank and FTFC Roughness Functions

When comparing results obtained from these two types of tests, it is important to take into account the differences in testing conditions, including the presence of free-surface effects and the associated wave-induced drag. The presence of waves can create complex flow patterns around the ship's hull, which can make it more difficult to accurately measure the forces acting on the ship. Additionally, it is also important to consider the limitations and assumptions of each testing method when interpreting the results.

Another difference between FTFC and towing tank resistance tests is the flow conditions. In a towing tank, the flow is generally steady and unidirectional, while in a turbulence tunnel, the flow is turbulent and can vary in direction and intensity. This can lead to differences in the boundary layer development and separation behaviour on the flat plate, which affects the measured drag and lift forces. Additionally, the test set up and instrumentation is different between the two types of tests. In a towing tank, the test model is mounted on a carriage and towed through the water, while in a turbulence tunnel, the test model is fixed in place, and the flow is generated by a centrifugal pump. The instrumentation used to measure the forces acting on the flat plate is also different between the two types of tests.

Therefore, it is important to note that the 2D assumption may not hold in towing tank tests with free-surface effects, as the waves can create a 3D flow field around the ship's hull. This can lead to differences in the results obtained from towing tank tests compared to turbulence tunnel tests. Another major difference is the size of the test model. In general, towing tank tests are conducted on larger flat plates than turbulence tunnel tests. This is because the towing tank has a larger test section and can accommodate larger flat plates. As a result, the scale effects may be different between the two types of tests, and the results obtained from the tests may not be directly comparable. However, this limitation is overcome when comparing the roughness function values of the surfaces tested.

That being said, the roughness functions of the sandpaper-like surface *Sand 220* obtained in this chapter from towing tests were compared for validation purposes with the results obtained from previous Fully Turbulent Flow Channel (FTFC) experiments (Ravenna et al., 2022a). In fact, the FTFC experiments in (Ravenna et al., 2022a) were conducted for the same surface roughness (*Sand 220*) but, obviously, on different kinds of panels. Specifically, stainless steel flat plate was used for the towing tank tests and acrylic panels for the FTFC experiments.

Hence, a comparison between the towing tank and FTFC roughness functions is shown in *Figure 5-15*. As expected, the roughness functions obtained from FTFC tests reach higher values than those obtained from towing tests. This is because higher flow velocities can be reached in the FTFC, representing an advantage of such a sophisticated facility. This is particularly important when studying high-speed flows, where the effects of surface roughness can have a significant impact on the overall performance of the system. Eventually, excellent agreement across the trends of the experimental roughness functions and the Nikuradse type is shown. Additionally, it is of note that the same roughness length scale, $k = 1.532 x 10^{-4}\ m$ was used to collapse both the experimental roughness functions on the Nikuradse reference.

Similar observations were made comparing the experimental roughness functions developed in the present thesis for the coarser sand surface tested (*Sand 60*-80) using the FTFC to the roughness function model developed by (Song et al., 2020b) for the same surface but using towing tests. Hence, it was possible to use the same roughness length scale, $k = 3.530 x 10^{-4}\ m$ to collapse the experimental roughness functions on the Nikuradse reference.

In summary, fully turbulent flow channels are a valid alternative to towing tanks for roughness function development. FTFCs provide a more realistic and controlled environment for studying the effects of surface roughness on fluid flow. Also, they allow researchers to quickly vary the roughness of the test surface over a wide range of values while maintaining high accuracy in their measurements.
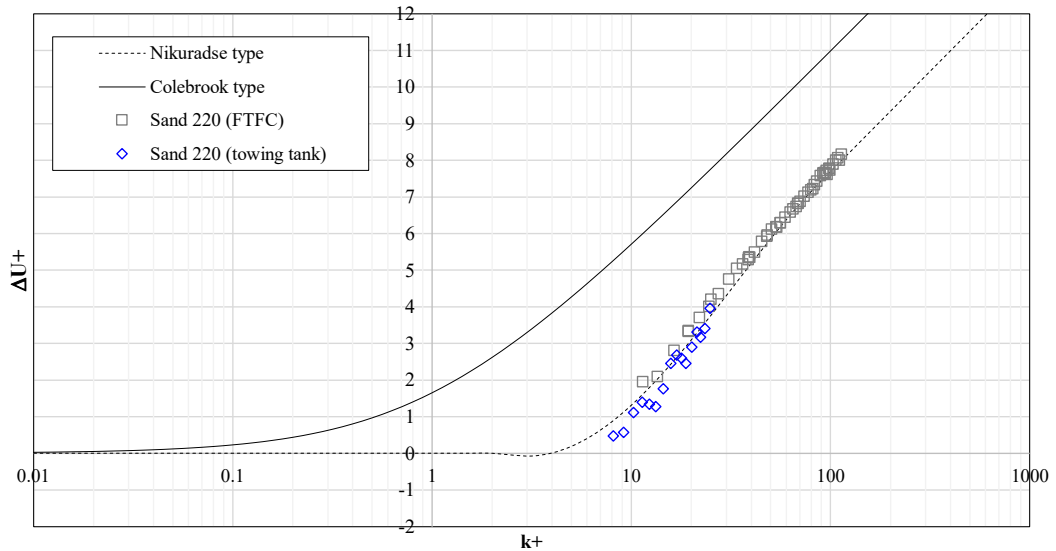
Figure 5-15: Experimental roughness function of the Sand 220 surface developed from FTFC pressure drop measurements and towing tank tests.

5.4. Chapter Summary and Conclusions

The present chapter investigated the hydrodynamics of mimicked biofouling on a flat plate. Towing tank experiments were conducted to investigate the effect of increased roughness on the drag characteristics of a flat plate with the towing tank facilities of Kelvin Hydrodynamics Laboratory (KHL) of the University of Strathclyde. The towing tank experiments were conducted on a stainless steel flat plate at a range of speeds as used in similar studies (Ravenna et al., 2022b).

Experimental roughness function data were developed from the towing tests on a flat plate homogenously coated with 220-grit sand-grain equivalent roughness (*Sand 220*). Eventually, the results of the experimental campaign in terms of roughness functions values were compared with those obtained from Fully Turbulent Flow Channel (FTFC) tests and showed excellent agreement. The present chapter can also serve as a valuable guide for future towing tests using flat plates in smooth and rough conditions and the corresponding roughness functions development.

As mentioned, the flat plate tested was homogenously covered with 220-grit sand-grain equivalent roughness (*Sand 220*). However, the homogenous distribution of

roughness on the flat plates of ships' hulls may not necessarily be the case on real ships. Hence, the sand-grain equivalent roughness approach should be improved in further studies by focusing on more complex surfaces and roughness models, such as considering the spatial distribution of hull roughness or its percentage coverage on a real hull. This thesis will deal with the heterogeneous distribution of hull roughness using CFD.

Part II

(Chapters 6-7)

Key Publications:

Ravenna, R., Ingham, R., Song, S., Johnston, C., De Marco Muscat-Fenech, C., Tezdogan, T., Atlar, M., Demirel, Y. K. (2022) *"Predicting the Effect of Hull Roughness on Ship Resistance using a Fully Turbulent Flow Channel"*, Journal of Marine Science and Engineering, 10, 1863.

Ravenna, R., Ingham, R., Song, S., Johnston, C., De Marco Muscat-Fenech, C., Tezdogan, T., Atlar, M., Demirel, Y.K., *"Predicting the Effect of Hull Roughness on Ship Resistance using a Fully Turbulent Flow Channel and CFD"*, 4th International Meeting of the A. Yucel Odabasi Colloquium Series on Ship Design & Optimization and Energy Efficient Devices for Fuel Economy (AYOCOL 2022), 15-16 December 2022, Istanbul, Turkey.

6. Predicting the Effect of Fouling Control Coatings on Ship Hydrodynamics: Similarity Law Scaling

6.1. Introduction

A ship's hull surface condition is crucial to its hydrodynamic performance (Schultz, 2007). Hence, choosing suitable fouling control coatings (FCCs) and drydock strategies for a vessel can offer significant economic and environmental advantages. Furthermore, improving hull performances associated with surface conditions enables the vessels to comply with IMO regulations (IMO, 2021), such as the operating expense index (OPEX), Energy Efficiency Existing Ship Index (EEXI) and the Carbon Intensity Indicator (CII).

In this chapter, the boundary layer similarity law scaling technique, originally proposed by Granville, (Granville, 1978, 1958)) is utilized to anticipate the impact of different test surfaces on the complete-scale KCS hull. The predictions are made for various rough surfaces, such as a recently created fouling control coating (known in this thesis as *FR02* hard-foul release from Graphite International Technologies), and simulated biofouling conditions on the KCS full-scale hull. It's worth noting that the roughness functions of these rough surfaces were derived from the FTFC experiments explained earlier. Finally, the alterations in effective power, ΔP_E, attributed to each test surface are evaluated to gain a quick comprehension of the impact of the marine coatings and hull roughness conditions that were tested on the ship's resistance and powering.

The boundary layer similarity law scaling procedure of Granville (Granville, 1978, 1958) is adopted in this chapter to predict the effect of different test surfaces on the full-scale KCS hull. The effects of various rough surfaces, including a newly developed fouling control coating (hard-foul release from Graphite International Technologies) and mimicked biofouling conditions, are predicted on the KCS full-

scale hull. Notably, the roughness functions of these rough surfaces were developed from the FTFC experiments detailed earlier. Finally, the variations in effective power, ΔP_E due to each test surface are estimated to give an immediate understanding of the effects of the marine coatings and hull roughness conditions tested on ship resistance and powering.

Additionally, the resistance coefficient results of the numerical predictions are compared and validated across similar studies assessing the KCS resistance in smooth and rough conditions (Song et al., 2020c; Yeginbayeva et al., 2020). Furthermore, comparison and validation of the ΔP_E values obtained were also conducted among similar studies, such as (Schultz et al., 2011). Notably, the next chapter will give a detailed comparison of the results obtained from Granville's similarity law scaling procedure with the in-house CFD simulations.

The structure of this chapter is as follows: Section 2 presents the methodology adopted, including the full-scale KCS hull geometry details. Section 3 gives an overview of Granville's similarity law scaling procedure. Section 4 discussed the results of the numerical predictions. Finally, the chapter's conclusions, final remarks, and summary are given in Section 5.

6.2. Granville's Similarity Law Scaling Procedure

The variance of resistance and powering requirements for the full-scale KCS due to different test surfaces were calculated using Granville's similarity law. It is of note that the newly developed roughness functions were incorporated into the procedure. The process for Granville's scale-up method (Granville, 1978, 1958) is explained in detail in (Demirel, 2015). However, an insight into the main steps is given in this section, as shown in *Figure 6-1*.

:

Step 1: to obtain the smooth frictional resistance coefficients, $C_{F_{smooth}}$, of the full-scale ship for varying speeds iteratively solving equation (3-3), ((Schoenherr, 1932), where Re is the Reynolds number based on ship speed and ship length at the waterline.

Step 2: Shift the $C_{F_{smooth}}$ curve by $\Delta U^+ \kappa [\ln(10)]^{-1}$ to create a $C_{F_{rough}}$ curve by selecting the experimental ΔU^+, k^+ pair of the given surface that guarantees the desired ship scale Reynolds number.

Step 3: Draw a curve of constant L_{plate}^+ by solving the implicit form of the following equation:

$$Re = \frac{L_{plate}^+}{\sqrt{\frac{C_{F_{smooth}}}{2}}\left(1 - \frac{1}{\kappa}\sqrt{\frac{C_{F_{smooth}}}{2}}\right)} \tag{6-1}$$

where, L_{plate}^+ is a non-dimensional length of the plate defined by:

$$L_{plate}^+ = L_{plate}\frac{k^+}{k} \tag{6-2}$$

Step 4: Shift the L_{plate}^+ line by a distance of $log(L_{ship}/L_{plate})$ in the $log(Re)$ direction, creating a new line of L_{ship}^+. The intersection point between the $C_{F_{rough}}$ curve and the line of L_{ship}^+ gives the C_F value at ship scale in rough conditions,
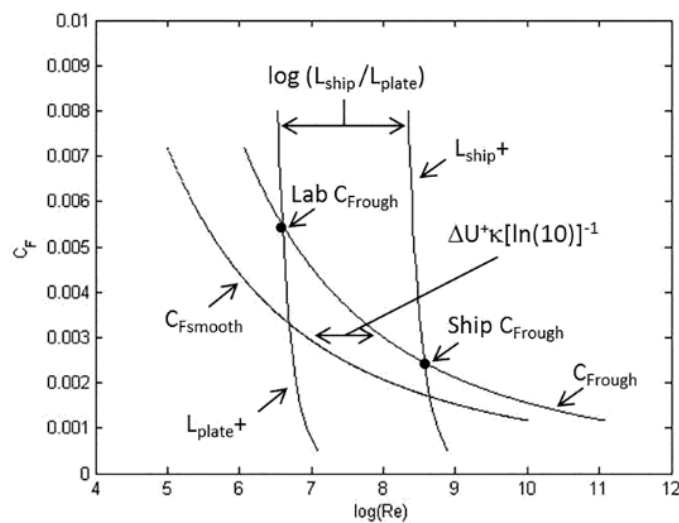
Figure 6-1: Outline of the Granville's similarity law scaling procedure (Demirel, 2015).

6.3. Results and Discussion

6.3.1. Ship Resistance Coefficients

The difference between the $C_{F_{rough}}$ value obtained from Granville's procedure and the $C_{F_{smooth}}$ calculated using equation (3-3) for the same Reynolds number gives the added frictional resistance coefficient, ΔC_F, of the ship due to roughness. Hence, the variation of the frictional resistance due to the presence of roughness can also be expressed in percentage, as in equation (6-3):

$$\frac{C_{F_{rough}} - C_{F_{smooth}}}{C_{F_{smooth}}} \, 100 = \%\Delta C_F \qquad (6\text{-}3)$$

Finally, the total resistance for the rough ship, $C_{T_{rough}}$, is determined by equation (6-4):

$$C_{T_{rough}} = C_{T_{smooth}} + \Delta C_F \qquad (6\text{-}4)$$

Like $\%\Delta C_F$, the variation of the total resistance due to the presence of roughness can also be expressed as in equation (6-5):

$$\frac{C_{T_{rough}} - C_{T_{smooth}}}{C_{T_{smooth}}} \, 100 = \frac{\Delta C_F}{C_{T_{smooth}}} \, 100 = \%\Delta C_T \qquad (6\text{-}5)$$

Figure 6-2 shows the resistance coefficients of the test surfaces on the full-scale KCS hull at 24 knots obtained from Granville's similarity law compared to a hydrodynamically smooth ship hull. Interestingly, the test cases *AF01* and *FR02* show a ΔC_T of -2.3% and -3.8%, respectively. On the other hand, the *BL01* and *FR01* cases lead to light ΔC_T increases (0.7% for *BL01* and 0.2% for *FR01*) compared to the total added resistance due to mimicked slime (27.0% for *Sand 220* and 38.9% *Sand 60–80* cases). It is of note that all the results of the present scaling procedure were considered at a nominal water temperature of 15°C.

As expected, the *FR02* is the best-performing FCCs tested, while the sanded surface, Sand 60-80, leads to a higher increase in the total resistance coefficients. Indeed, the phenomena of reduced ΔC_T values are due to the negative roughness functions, ΔU^+

observed from the experimental measurements. Furthermore, *Figure 6-3* shows the absolute values and percentage variation (relative values) of frictional and total resistance coefficients obtained for the test surfaces at design speed. Notably, the total resistance coefficient results are in good agreement and show similar trends to the frictional resistance coefficients.
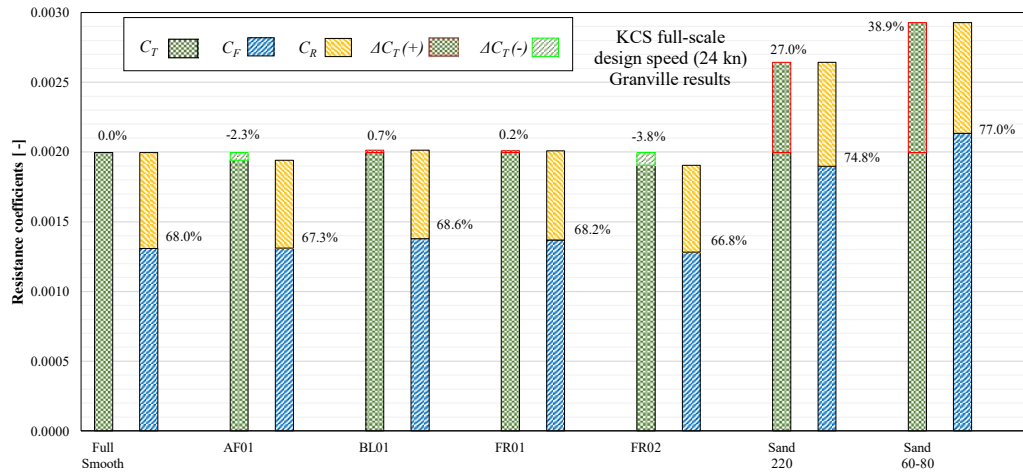
Figure 6-2: Percentage bar diagram of the resistance coefficients for the full-scale KCS in different hull roughness conditions at design speed ($V = 24\ kn$, $Fr = 0.260$).
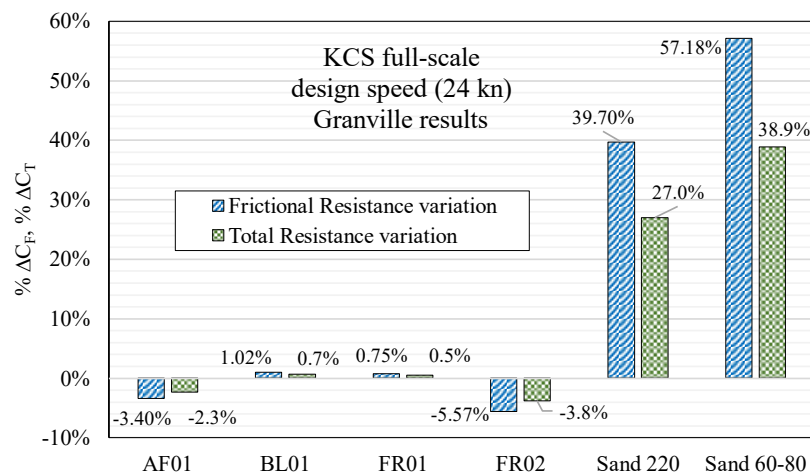
Figure 6-3: Percentage variation of frictional and total resistance coefficients for the full-scale KCS in different hull roughness conditions at design speed ($V = 24\ kn$, $Fr = 0.260$).

Table 6-1: Frictional resistance coefficients for the full-scale KCS in different hull roughness conditions at design speed ($V = 24\ kn$, $Fr = 0.260$).

Test Surface	Granville Similarity Law		
	C_F	ΔC_F	$\%\Delta C_F$
Reference	$1.358x10^{-3}$	-	-
AF01	$1.312x10^{-3}$	$-4.620x10^{-5}$	-3.40%
BL01	$1.378x10^{-3}$	$1.387x10^{-5}$	1.02%
FR01	$1.368x10^{-3}$	$1.013\ x10^{-5}$	0.75%
FR02	$1.282x10^{-3}$	$-7.557x10^{-5}$	-5.57%
Sand 220	$1.897x10^{-3}$	$5.390x10^{-4}$	39.70%
Sand 60-80	$2.135x10^{-3}$	$7.765x10^{-4}$	57.18%

Table 6-2: Total resistance coefficients for the full-scale KCS in different hull roughness conditions at design speed ($V = 24\ kn$, $Fr = 0.260$).

Test Surface	Granville Similarity Law		
	C_T	ΔC_T	$\%\Delta C_T$ ($\%\Delta P_E$)
Reference	$1.996x10^{-3}$	-	-
AF01	$1.950x10^{-3}$	$-4.620x10^{-5}$	-2.31%
BL01	$2.010x10^{-3}$	$1.387x10^{-5}$	0.69%
FR01	$2.006x10^{-3}$	$1.013\ x10^{-5}$	0.51%
FR02	$1.920x10^{-3}$	$-7.557x10^{-5}$	-3.79%
Sand 220	$2.535x10^{-3}$	$5.390x10^{-4}$	27.01%
Sand 60-80	$2.772x10^{-3}$	$7.765x10^{-4}$	38.90%

Similarly, *Figure 6-4* shows the resistance coefficients of the test surfaces on the full-scale KCS hull at 16 knots obtained from Granville's similarity law compared to a hydrodynamically smooth ship hull. At low ship speed, the test cases *AF01* and *FR02* show a more significant benefit on the ship hydrodynamics. A ΔC_T of -3.5% and -5.7% is calculated, respectively. Furthermore, the *BL01* and *FR01* cases that lead to light ΔC_T increases for the design speed case, are manifesting drag reductions of 0.1% and 1.3%, respectively. It is noted that the mimicked slime surfaces (Sand 60-80 and Sand 220) have a greater impact on ship hydrodynamics at a lower speed than at a higher one. In fact, the total added resistance for the full-scale KCS hull at low speed (16 knots) is 31.1% for *Sand 220* and 46.1% for *Sand 60–80* cases). The rationale behind the relation between the impact of hull roughness on ship efficiency and ship speed was discussed in the literature review.

Once again, it can be noted that the *FR02* is the best-performing FCCs tested at low ship speed, too. On the other hand, the sanded surface, *Sand 60-80*, as expected, leads to the highest increase in the total resistance coefficients. Furthermore, *Figure 6-5* shows the percentage variation of frictional and total resistance coefficients obtained for the test surfaces at design speed. Notably, the total resistance coefficient results are in good agreement and show similar trends to the frictional resistance coefficients.
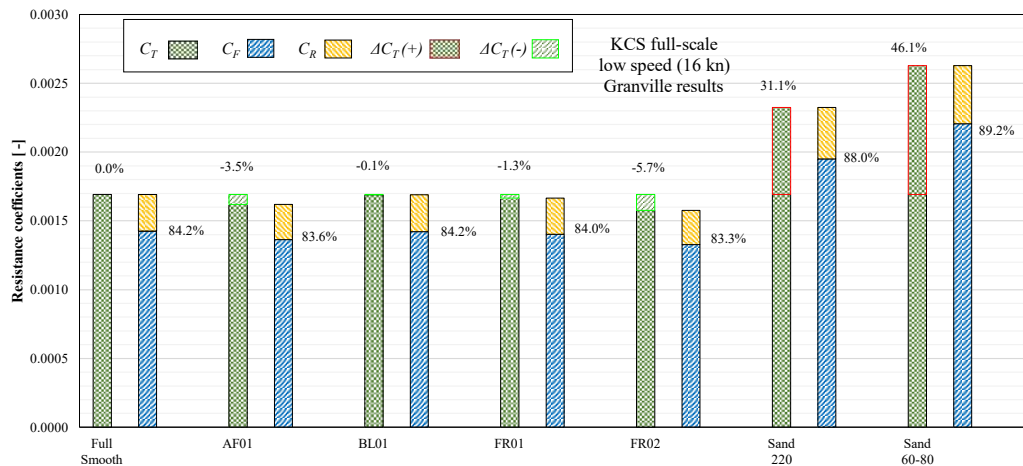
Figure 6-4: Percentage bar diagram of the resistance coefficients for the full-scale KCS in different hull roughness conditions at low speed (16 kn, $Fr = 0.173$).
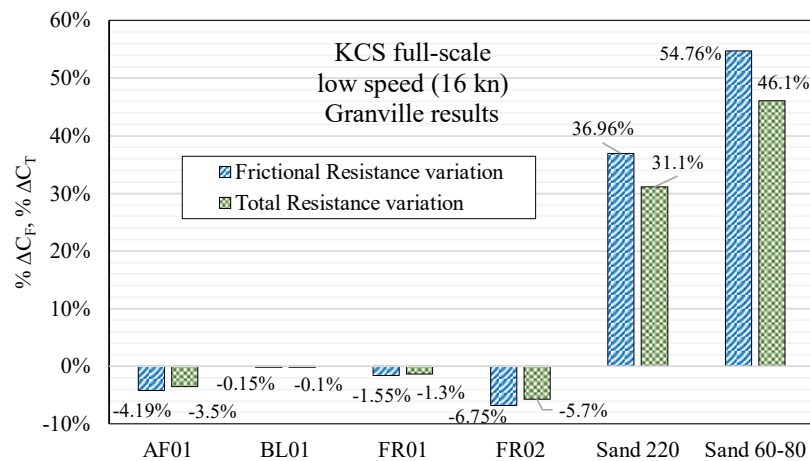
Figure 6-5: Percentage variation of frictional and total resistance coefficients for the full-scale KCS in different hull roughness conditions at slow speed (16 kn, $Fr = 0.173$).

Table 6-3: Frictional resistance coefficients for the full-scale KCS in different hull roughness conditions at slow speed (16 kn, $Fr = 0.173$).

Test Surface	Granville Similarity Law		
	C_F	ΔC_F	$\%\Delta C_F$
Reference	$1.425x10^{-3}$	-	-
AF01	$1.365x10^{-3}$	$-5.967x10^{-5}$	-4.19%
BL01	$1.422x10^{-3}$	$-2.128x10^{-6}$	-0.15%
FR01	$1.402x10^{-3}$	$-2.214\ x10^{-5}$	-1.55%
FR02	$1.328x10^{-3}$	$-9.618x10^{-5}$	-6.75%
Sand 220	$1.951x10^{-3}$	$5.267x10^{-4}$	36.96%
Sand 60-80	$2.206x10^{-3}$	$7.803x10^{-4}$	54.76%

Table 6-4: Total resistance coefficients for the full-scale KCS in different hull roughness conditions at slow speed (16 kn, $Fr = 0.173$).

Test Surface	Granville Similarity Law		
	C_T	ΔC_T	$\%\Delta C_T\ (\%\Delta P_E)$
Reference	$1.692x10^{-3}$	-	-
AF01	$1.632x10^{-3}$	$-5.967\ x10^{-5}$	-3.53%
BL01	$1.689x10^{-3}$	$-2.128\ x10^{-6}$	-0.13%
FR01	$1.669x10^{-3}$	$-2.214\ x10^{-5}$	-1.31%
FR02	$1.595x10^{-3}$	$-9.618x10^{-5}$	-5.69%
Sand 220	$2.218x10^{-3}$	$5.267\ x10^{-4}$	31.14%
Sand 60-80	$2.472x10^{-3}$	$7.803\ x10^{-4}$	46.13%

Finally, the results are reasonably in agreement with other studies found in the literature, such as (Yeginbayeva and Atlar, 2018; Schultz, 2004) found that a foul-release coating as applied measured an added frictional resistance $\%\Delta C_F$ equal to 2.6%, and for a 150 m flat plate at 12 knots coated with *Sand 60-80* calculated $\%\Delta C_F = 59\%$.

6.3.2. Ship Effective Power

Ship resistance is a complex phenomenon that depends on a multitude of factors, including the shape and size of the ship, the speed at which it is traveling, the properties of the hull surfaces, waves, currents, etc. Power, on the other hand, is simply the rate at which work is being done and is often used as a proxy for the amount of energy required to overcome the resistance of the ship. As a ship increases in speed, its resistance typically increases as well, but the relationship between speed and resistance is not linear ($P_E = R_T V$). At some point, the resistance will begin to increase at an accelerating rate, requiring significantly more power to maintain the same speed. Additionally, the efficiency of the ship's propulsion system can also have a significant impact on the amount of power required to achieve a given speed. A more efficient propulsion system may require less power to achieve the same speed as a less efficient system, even if the resistance of the ship is the same in both cases. Nevertheless, the change in effective power, $\%\Delta P_E$ due to the different surfaces tested can be expressed by equation (6-6):

$$\%\Delta P_E = \frac{\Delta C_F}{C_{T_{smooth}}} \, x100 = \%\Delta C_T \tag{6-6}$$

similar to that used by (Tezdogan et al., 2015), where $C_{T_{smooth}}$ is the total resistance coefficient of the hull in smooth conditions. $C_{T_{smooth}}$ values are obtained from CFD simulations as will be detailed in the following chapter. It can be noted that $\%\Delta P_E$ is equal to $\%\Delta C_T$. *Figure 6-6* shows the change in effective power, $\%\Delta P_E$ due to the different test cases obtained from Granville's approach. It is of note that the largest reduction of effective power among all the coating types is 5.7% given by *FR02* at slow speed (16 kn). Furthermore, the coating *AF01* also shows excellent performance when applied on the ship hull, reducing effective power requirements of 3.5% at 16 kn.

Despite the analogy between ship resistance and power in equation (6-6) is often used in the literature, it is important to understand its limitations. In fact, the relationship between power and resistance is not always straightforward. For example, as a ship increases in speed, its resistance typically increases as well, but at a certain point the

resistance may begin to decrease due to the phenomenon of wave-making resistance. This means that the relationship between power and resistance may not be linear, and that the amount of power required to achieve a given speed may vary depending on the specific conditions.

Therefore, *AF01* and *FR02* are the best-performing fouling control coatings tests. These findings are justified by the roughness functions of the test surfaces developed from FTFC experiments, as presented in the previous chapter. Specifically, as expected, the phenomena of improved ship hydrodynamics characteristics are due to the negative roughness functions values observed throughout most of the k^+ range, which corresponds to reduced resistance coefficient values.

On the other hand, the *BL01* and *FR01* surfaces exhibit mostly positive roughness function values, which translates into increases in effective power requirements of 0.69% and 0.51%, respectively, at design speed ($V = 24\ kn$). Furthermore, the total added effective power due to mimicked slime is 27.0% for *Sand 220* and 38.9% *Sand 60-80* cases at design speed. Furthermore, the *FR02* is the best-performing FCCs assessed ($\%\Delta P_E = -3.79\%$), while the sanded surface, *Sand 60-80*, would lead to the highest increase in the effective power ($\%\Delta P_E = 38.90\%$). Finally, it can also be noted that the rate $\%\Delta P_E/\%\Delta C_F$ is in the range of $65\% \div 70\%$, as would be expected according to the literature (Schultz et al., 2011).
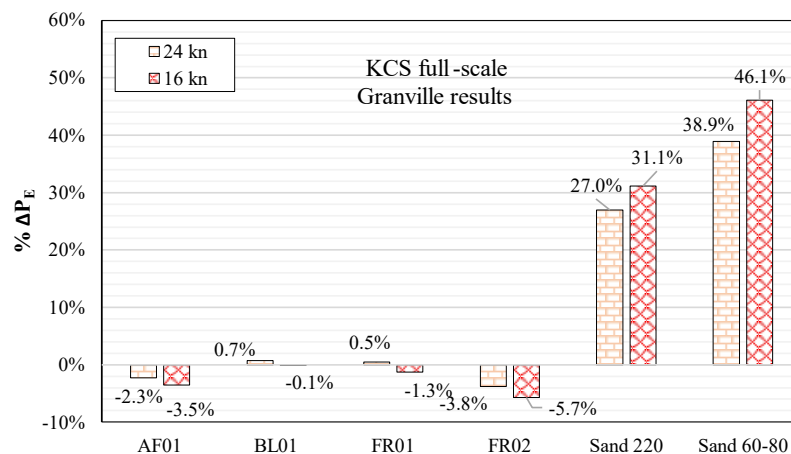
Figure 6-6: Effective power percentage variation for the full-scale KCS in different hull roughness conditions at design ($V = 24\ kn$, $Fr = 0.260$) and slow speed (16 kn, $Fr = 0.173$).

6.4. Chapter Summary and Conclusions

The present chapter presented the similarity law scaling procedure (Granville, 1978) conducted to investigate the effect of hull roughness on ship hydrodynamics. Notably, the roughness characteristics of the surfaces previously tested in the Fully Turbulent Flow Channel were used in Granville's scaling procedure. Furthermore, the procedure scaled up the laboratory results to the size of a full ship length. The full-scale KCS hull was selected for the numerical predictions, and different speeds were investigated. Hence, a design speed of 24 knots ($Fr = 0.260$) as used in similar studies (Ravenna et al., 2022a; Song et al., 2020c). Furthermore, a lower and less investigated speed of 16 knots ($Fr = 0.173$) was considered.

Among the four fouling control coatings (FCCs) that were tested in the FTFC, the *FR02* coating (hard foul-release) displayed the best hydrodynamic performance across the entire Reynolds number range. Furthermore, the *FR02* surface led to a maximum decrease in effective power requirements of 3.8% and 5.7% at 24 kn and 16 kn speeds, respectively. The numerical prediction results also show that the *AF01* (self-polishing antifouling coating) has better hydrodynamic performance than the smooth reference case (maximum decrease in effective power requirements of 3.5% at 16 kn). In contrast, *Sand 220* (medium light slime) and *Sand 60-80* (medium slime) have, as expected, the highest resistance due to their rougher characteristics. In fact, a containership such as the KCS hull with medium light slime (*Sand 220*) and medium slime (*Sand 60-80*) surface roughness characteristics as the test surfaces would experience a maximum increase in effective power requirements of 27.01% and 38.90% at design speed, respectively. At this point, it important to consider that experimental results are affected by numerical error, error in roughness model determination, and assumptions that have been made. Therefore, one needs to be mindful of the uncertainties when utilising these results. A generally safe range of validity in ship power predictions of this thesis could be $\pm 5\%$.

However, several simplifications limit Granville's theoretical method, e.g., its assumption of a flat plate (Atlar et al., 2018). The 2D flat plate assumption neglects the 3D effect of a ship's hull, as criticised by (Atlar et al., 2018). Furthermore,

Granville's method only considers the roughness effect on frictional resistance, while the hull roughness also affects the other pressure-related resistance components (Andersson et al., 2020; Farkas et al., 2020, 2018; Demirel et al., 2017b). Another limitation of this scaling method is that it considers only a uniform roughness Reynolds number k^+ over the flat plate of ship length. Hence the ship hull is considered homogeneously covered with a constant k^+, which is not realistic and may lead to scaling problems and inaccurate added resistance predictions, as underlined by (Demirel et al., 2017b). Finally, it is of note that the Granville method is limited to the assumption that the velocity is constant for the length of the plate (i.e., ship).

Above all, the present study has provided several significant findings, including the application of Granville's similarity law scaling procedure with high-performing fouling control coatings (FCC) exhibiting negative roughness functions and the effects of FCCs on the hydrodynamics of a full-scale ship. Eventually, the findings presented can help predict the required power, fuel consumption and greenhouse gas emissions of ships with hulls coated with certain fouling control coatings and/or in the fouled condition. Further investigation could also be conducted on predicting the resistance of fouling control coatings (FCCs) at different speeds and hulls.

7. Predicting the Effect of Fouling Control Coatings on Ship Hydrodynamics: Computational Fluid Dynamics

7.1. Introduction

Granville's similarity law scaling procedure is a robust method to predict the effects of hull roughness on ship resistance and powering, as highlighted by many researchers such as (Song, 2020). Nevertheless, as suggested by (Atlar et al., 2018), CFD is a more cost-efficient solution that can overcome Granville's related shortcomings. Furthermore, the ship resistance predictions are expected to be more accurate in CFD since the 3D effect of the hull is considered, and the ship can be simulated on a full-scale (Song et al., 2020c, 2019; Atlar et al., 2018; Demirel et al., 2017a).

Therefore, CFD simulations were carried out on the container ship KCS in full-scale, at the design speed of 24 knots (12.35 m/s), Froude number $Fr = 0.260$, and low speed of 16 knots (8.23 m/s), $Fr = 0.173$. The Reynolds number based on the ship speed and length was in the range of $Re_L = 2.72 \times 10^9$ for the design speed of the full-scale KCS hull, and $Re_L = 1.59 \times 10^9$. Eventually, the results in the present chapter will represent a valid comparison and alternative to Granville's results given earlier.

The structure of this chapter is as follows: Section 2 presents the methodology adopted, including the mathematical formulations, mesh details, and verification study. Section 3 details the modified wall function procedure followed in the simulations adopting the roughness functions developed experimentally. Section 4 presents the results of the numerical predictions, including detailed figures of the effect of hull roughness on the flow. Finally, the chapter's conclusions, final remarks, and summary are given in Section 5.

7.2. Modified Wall Function Approach

Equation (7-1) shows the roughness function model employed in the CFD software to represent the roughness conditions examined and obtain the variance in frictional resistance coefficients. Furthermore, (Cebeci and Bradshaw, 1977) recommended the following constants: $k_{smooth}^+ = 2.25$, $k_{rough}^+ = 90$, $A = 0$ and $C_s = 0.253$ for traditional Nikuradse roughness function and $C_s = 0.5$ for other roughness types. (Demirel et al., 2017b) proposed $k_{smooth}^+ = 3$, $k_{rough}^+ = 15$ and $C_s = 0.26$ when fitting the roughness function proposed by (Schultz and Flack, 2007). Different constants to develop the roughness function models for the surfaces tested in the FTFC are introduced in the following section.

$$\Delta U^+ = \begin{cases} A & \rightarrow & k^+ < k_{smooth}^+ \\ \frac{1}{\kappa} \ln C_s k^{+^{sin\left[\frac{\pi}{2}\frac{log(k^+/3)}{log(25/3)}\right]}} & \rightarrow & k_{smooth}^+ \leq k^+ < k_{rough}^+ \\ \frac{1}{\kappa} \ln C_s k^+ & \rightarrow & k_{rough}^+ \leq k^+ \end{cases} \qquad (7\text{-}1)$$

In which κ is the von-Karman constant ($\kappa = 0.42$).

7.2.1. Roughness Function Models

Once the roughness functions had been calculated from experiments, they were directly compared with both Colebrook-type (Grigson, 1992) and Nikuradse-type (Cebeci and Bradshaw, 1977) roughness functions. In the present study, all the experimental roughness functions of the fouling control coatings and mimicked biofouled surfaces tested were modelled by curve fitting to the roughness function model of Nikuradse. Specifically, the new roughness function models have been developed using STAR-CCM+'s built-in features, as in equation (7-1).

Table 7-1 presents the curve fitting coefficients used for all the surfaces tested, where *E* is the so-called turbulent wall function coefficient. In fact, in StarCCM+, the wall roughness is modelled by moving the logarithmic region of the boundary layer closer

to the wall. To decrease roughness, E must be increased to incorporate this effect. Therefore, for the smoother and best-performing surfaces (*AF01* and *FR02*) to which corresponded negative roughness function values, E was increased from the standard $E = 9$ to $E = 12$ and $E = 15$, respectively. Finally, *Figure 7-1* shows the roughness Reynolds numbers, k^+, of the full-scale KCS hull coated with the fouling control coatings investigated earlier by means of fully turbulent flow channel experiments. Notably, as mentioned earlier, the k^+ values for the *Sand 60-80* and *Sand 220* cases, and other characteristics will be detailed later in this thesis.

(a) Design speed

(b) Low speed
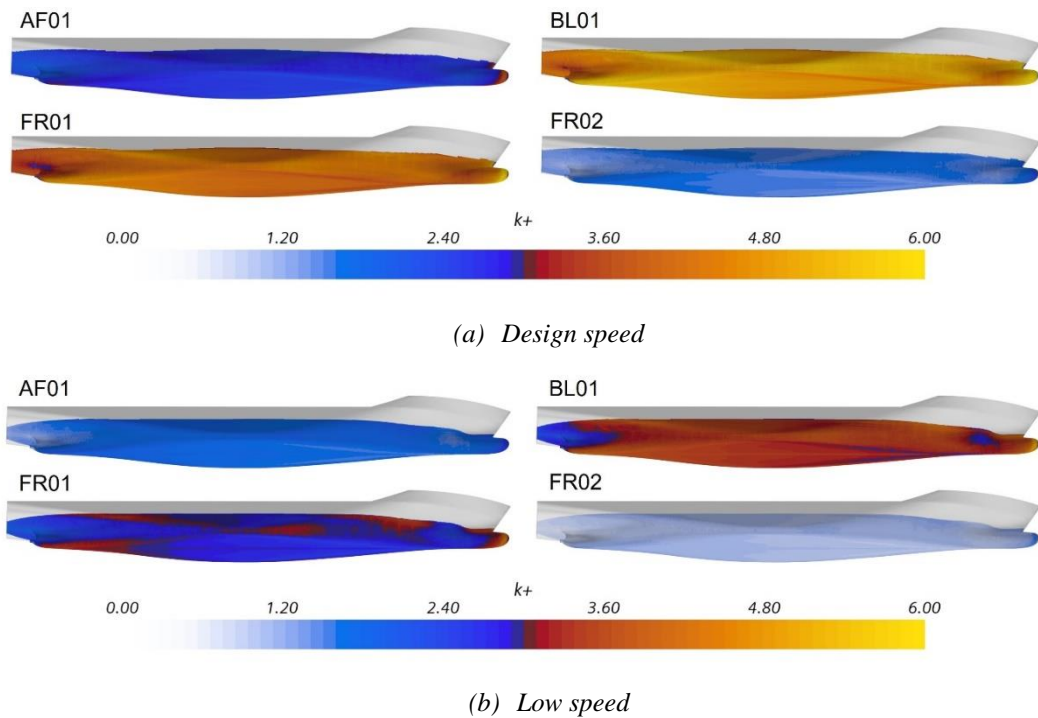
Figure 7-1: Local roughness Reynolds number characteristics, k^+, on the full-scale KCS hull at: (a) $V = 24\ kn$, $(Fr = 0.260)$; (b) $V = 16\ kn$, $(Fr = 0.173)$.

Table 7-1: Curve fitting coefficients of the roughness function model for the test surfaces.

Test Surface	Roughness length scale, $k\ [m]$	A	C_s	E	k_s^+	k_r^+
AF01	$9.598\ x10^{-6}$	-1.5	0.2	12	1	15
BL01	$1.822\ x10^{-5}$	-0.5	0.26	9	3	25
FR01	$1.544x10^{-5}$	-0.5	0.2	15	3	25
FR02	$5.840x10^{-6}$	-1.5	0.26	9	1	15
Sand 220	$1.532x10^{-4}$	0	0.35	9	3	25
Sand 60-80	$3.530x10^{-4}$	0	0.49	9	3	25

7.3. Results and Discussion

7.3.1. Ship Resistance Coefficients

Numerical predictions were conducted on the benchmark KRISO containership hull at a towing speed of 24 knots ($Fr = 0.260$) and 16 knots ($Fr = 0.173$). The variance of resistance and powering requirements due to different test surfaces were calculated by incorporating the newly developed roughness functions into the Granville similarity law. *Figure 7-2* and *Figure 7-3* present the local characteristics of the wall shear stress, τ_w, and skin friction coefficients, c_f, of the *FR02* coating on the full-scale KCS hull at design and low speed, respectively. To higher speeds correspond higher τ_w, and c_f values. Additionally, τ_w and c_f increase with flow speed and surface roughness. However, it can be noted from the figures that there are negligible variations between the design and low-speed cases.

(a)

(b)
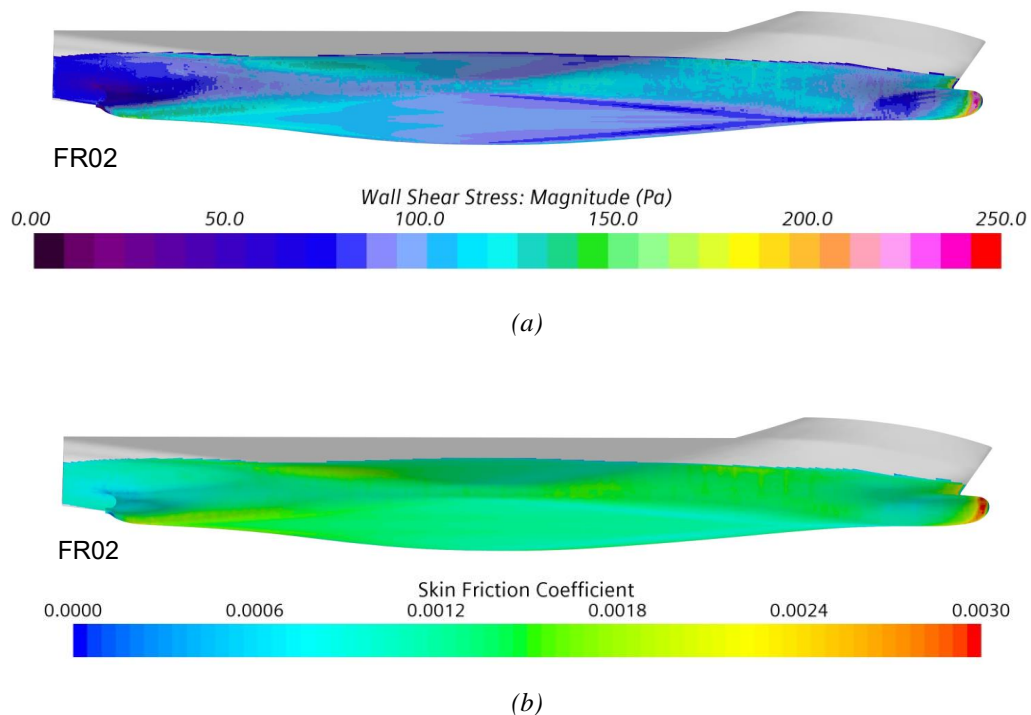
Figure 7-2: Local characteristics of the wall shear stress, τ_w, (a), and skin friction coefficients, c_f, (b) of the FR02 coating on the full-scale KCS hull at design speed, 24 kn ($Fn = 0.260$).

(a)

(b)
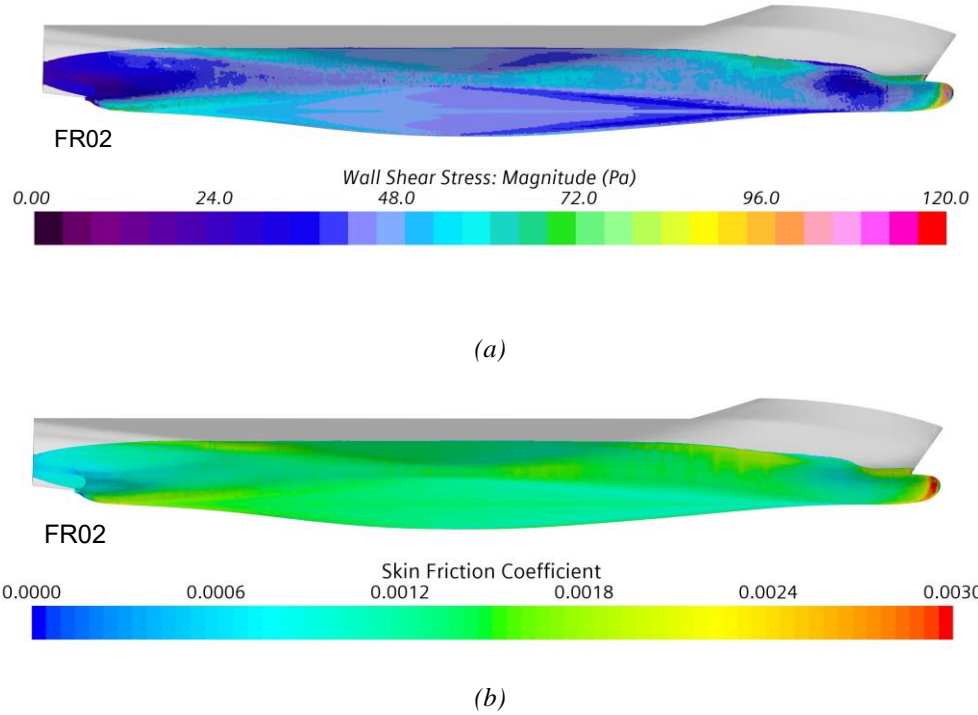
Figure 7-3: Local characteristics of the wall shear stress, τ_w, (a), and skin friction coefficients, c_f, (b) of the FR02 coating on the full-scale KCS hull at low speed, 16 kn ($Fn = 0.173$).

The total resistance coefficient, C_T, is defined in equation (2-1) as a function of the total drag, R_T, the dynamic pressure, $1/2\ \rho V^2$, the hull wetted surface area, S, is the towing speed V (i.e., the inlet velocity). Furthermore, it is well-known that the total ship resistance coefficient, C_T, can be decomposed into the frictional, C_F, and the residuary, C_R resistance coefficients, as given by equation (2-2). The variation of the frictional resistance coefficient ΔC_F is the difference between the rough, $C_{F_{rough}}$, and smooth, $C_{F_{smooth}}$, conditions at the same Froude number can be given by equation (2-4). Hence, the frictional resistance variation due to roughness can also be expressed in percentage, as in equation (6-3). The total resistance for the rough ship, $C_{T_{rough}}$, is determined by equation (7-2):

$$C_{T_{rough}} = C_{T_{smooth}} + \Delta C_T \tag{7-2}$$

where the total roughness allowance, ΔC_T is the variation in the total resistance coefficient between the rough, $C_{T_{rough}}$, and smooth, $C_{T_{smooth}}$, conditions, and can be given by equation (7-3):

$$\Delta C_T = C_{T_{rough}} - C_{T_{smooth}} \qquad (7\text{-}3)$$

Table 7-2 shows the frictional resistance coefficients obtained for the test surfaces at the design speed of 24 knots, $Fr = 0.260$. The results obtained from the CFD simulations analysis are compared to the hydrodynamically smooth ship hull. Interestingly, the test cases *AF01* and *FR02* show a negative ΔC_F of 3.1% and 5.4%, respectively. As expected, the phenomena of reduced ΔC_F values are due to the negative roughness functions, ΔU^+ observed from the experimental measurements. On the other hand, the *BL01* and *FR01* cases lead to light ΔC_F increases (1.5% for *BL01* and 0.4% for *FR01*) compared to the added frictional resistance due to mimicked slime (40.3% for *Sand 220* and 56.7% for *Sand 60-80* cases). Similar observations can be made for the low-speed case (16 kn, $Fr = 0.26$) in *Table 7-3*.

Table 7-4 presents the total resistance coefficients of the test cases at the design speed of 24 knots, $Fr = 0.26$. Notably, the total resistance coefficient results are in good agreement and show similar trends to the frictional resistance coefficients. Interestingly, the test cases *AF01* and *FR02* show a negative ΔC_T of 2.1% and 3.6%, respectively. As expected, the phenomena of reduced ΔC_T values are due to the negative roughness functions, ΔU^+ observed from the experimental measurements.

On the other hand, the *BL01* and *FR01* cases lead to light ΔC_T increases (0.9% for *BL01* and 0.2% for *FR01*) compared to the total added resistance due to mimicked slime (27.7% for *Sand 220* and 36.1% *Sand 60-80* cases). Above all, it can be noted that at both design and low speed, the *FR02* is the best-performing FCCs tested, while the sanded surface, *Sand 60-80,* leads to the highest increase in the total resistance coefficients. Furthermore, it can be noted that the impact of hull roughness at low speed is greater than at design speed. Similar observations can be made for the low-speed case (16 kn, $Fr = 0.26$) in *Table 7-5*.

Table 7-2: Frictional resistance coefficients of the full-scale KCS hull at 24 knots ($Fr = 0.26$).

Test Surface	C_F	ΔC_F	$\%\Delta C_F$
Reference	$1.309x10^{-3}$	-	-
AF01	$1.268x10^{-3}$	$-4.05x10^{-5}$	-3.09%
BL01	$1.328\ x10^{-3}$	$1.91x10^{-5}$	1.46%
FR01	$1.314x10^{-3}$	$5.44x10^{-6}$	0.42%
FR02	$1.238x10^{-3}$	$-7.08x10^{-5}$	-5.41%
Sand 220	$1.835x10^{-3}$	$5.27x10^{-4}$	40.26%
Sand 60-80	$2.051x10^{-3}$	$7.42x10^{-4}$	56.72%

Table 7-3: Frictional resistance coefficients of the full-scale KCS hull at 16 knots ($Fr = 0.173$).

Test Surface	C_F	ΔC_F	$\%\Delta C_F$
Reference	$1.348x10^{-3}$	-	-
AF01	$1.328x10^{-3}$	$-1.969\ x10^{-5}$	-1.46%
BL01	$1.371\ x10^{-3}$	$2.387x10^{-5}$	1.77%
FR01	$1.371x10^{-3}$	$2.366x10^{-6}$	1.76%
FR02	$1.305x10^{-3}$	$-4.223x10^{-5}$	-3.13%
Sand 220	$1.852x10^{-3}$	$5.042x10^{-4}$	37.41%
Sand 60-80	$2.196x10^{-3}$	$8.481x10^{-4}$	62.94%

Table 7-4: Total resistance coefficients of the full-scale KCS at 24 knots ($Fr = 0.26$).

Test Surface	C_T	ΔC_T	$\%\Delta C_T$
Reference	$1.996x10^{-3}$	-	-
AF01	$1.955\ x10^{-3}$	$-4.096\ x10^{-5}$	-2.05%
BL01	$2.015x10^{-3}$	$1.860\ x10^{-5}$	0.93%
FR01	$2.001x10^{-3}$	$4.668\ x10^{-6}$	0.23%
FR02	$1.925x10^{-3}$	$-7.096x10^{-5}$	-3.56%
Sand 220	$2.528x10^{-3}$	$5.320\ x10^{-4}$	26.66%
Sand 60-80	$2.717x10^{-3}$	$7.210\ x10^{-4}$	36.12%

Table 7-5: Total resistance coefficients of the full-scale KCS at 16 knots ($Fr = 0.173$).

Test Surface	C_T	ΔC_T	$\%\Delta C_T$
Reference	$1.692x10^{-3}$	-	-
AF01	$1.655x10^{-3}$	$-3.702x10^{-5}$	-2.19%
BL01	$1.698x10^{-3}$	$6.223x10^{-6}$	0.37%
FR01	$1.698x10^{-3}$	$5.967x10^{-6}$	0.35%
FR02	$1.632x10^{-3}$	$-5.936x10^{-5}$	-3.51%
Sand 220	$2.186x10^{-3}$	$4.944x10^{-4}$	29.23%
Sand 60-80	$2.543x10^{-3}$	$8.511x10^{-4}$	50.31%

Further details of the resistance coefficients at design and low speed can be seen in *Figure 7-4* and *Figure 7-5*, respectively. It is also notable from the figures that the total resistance coefficient results are generally in good agreement and show similar trends to the frictional resistance coefficients. Furthermore, the results are reasonably in agreement with other studies found in the literature such as (Yeginbayeva and Atlar, 2018; Schultz, 2004). In fact, (Yeginbayeva and Atlar, 2018; Schultz, 2004) found that a foul-release coating as applied measured an added frictional resistance %ΔC_F equal to 2.6%, and for a 150 m flat plate at 12 knots coated with sand 60-80 calculated %$\Delta C_F = 59\%$.
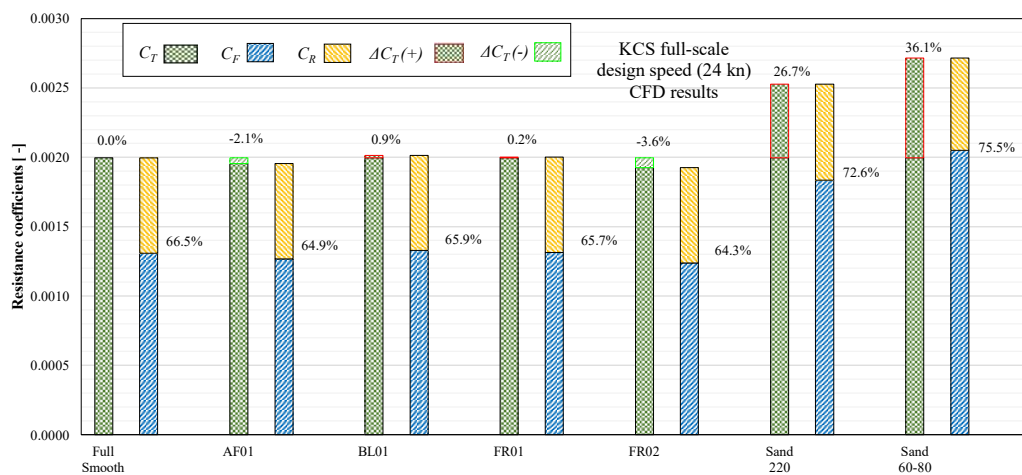
Figure 7-4: Percentage bar diagram of the resistance coefficients for the full-scale KCS with FCCs at design speed ($V = 24\ kn$, $Fr = 0.260$) from CFD simulations in homogeneous conditions.
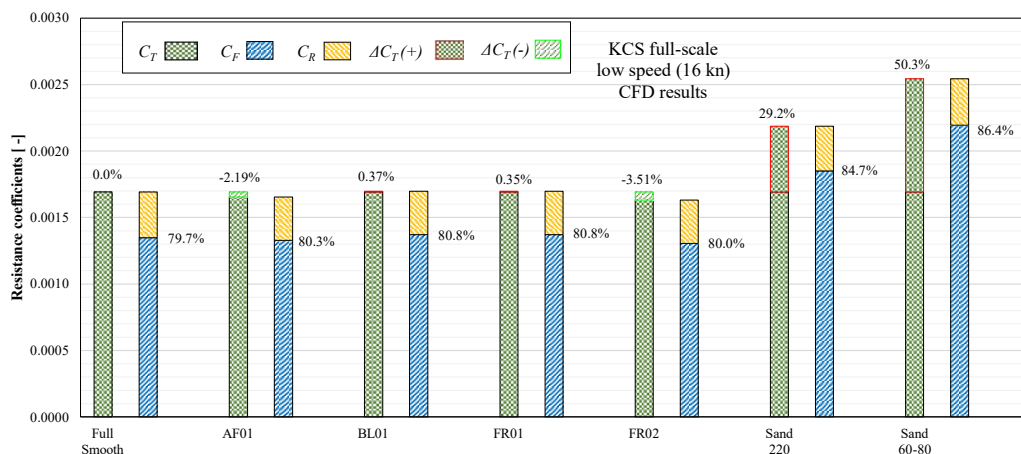
Figure 7-5: Percentage bar diagram of the resistance coefficients for the full-scale KCS with FCCs at low speed ($V = 16\ kn$, $Fr = 0.173$) from CFD simulations in homogeneous condition.

7.4. Ship Effective Power

The change in effective power, $\%\Delta P_E$ due to the different surfaces tested can be expressed by equation (7-4):

$$\%\Delta P_E = \frac{C_{T_{rough}} - C_{T_{smooth}}}{C_{T_{smooth}}} \, x100 = \frac{\Delta C_T}{C_{T_{smooth}}} \, x100 \qquad (7\text{-}4)$$

similar to that used by (Tezdogan et al., 2015), where $C_{T_{smooth}}$ is the total resistance coefficient of the hull in smooth conditions obtained from the present CFD simulations. It is of note that $\%\Delta P_E$ is equal to $\%\Delta C_T$. Notably, equation (7-4) is a based on different simplification such as assuming that ship speed and resistance are linearly related to the power requirements, the shortcomings of which were presented in the previous chapter.

Table 7-6, *Table 7-7* and *Figure 7-6* present the change in effective power, $\%\Delta P_E$ due to the different test cases obtained from the CFD simulations and Granville's approach. Notably, the largest difference between coating types for powering requirements is an average of 4.75% between *FR02* and *BL01*. As expected, if the coatings *AF01* and *FR02* were applied on the ship hull, they would reduce effective power requirements. In fact, *AF01* guarantees a maximum decrease of power requirements of 2.31%, while *FR02* of 3.79%. As mentioned earlier, the phenomena are due to the negative roughness functions, ΔU^+ observed from the experimental measurements, to which correspond negative ΔC_T values.

On the other hand, the *BL01* and *FR01* cases lead to positive $\%\Delta P_E$, which translates into increases in effective power requirements of 0.93% for *BL01* and 0.23% for *FR01*. Furthermore, the total added effective power due to mimicked slime is 26.66% for *Sand 220* and 36.12% *Sand 60-80* cases at design speed. Above all, the *FR02* is the best-performing FCCs tested while the sanded surface, *Sand 60-80,* would lead to a higher increase in the effective power. Finally, it can also be noted that the ratio $\%\Delta P_E/\%\Delta C_F$ is in the range of $65\% \div 70\%$, as would be expected (Schultz et al., 2011).

Table 7-6: Effective power variation (%ΔP$_E$) of the full-scale KCS at 24 knots (Fr = 0.260).

Test Surfaces	Design speed %ΔP$_{E_{CFD}}$
AF01	-2.05%
BL01	0.93%
FR01	0.23%
FR02	-3.56%
Sand 220	26.66%
Sand 60-80	36.12%

Table 7-7: Effective power variation (%ΔP$_E$) of the full-scale KCS at 16 knots (Fr = 0.173).

Test Surfaces	Low speed %ΔP$_{E_{CFD}}$
AF01	−2.19%
BL01	0.37%
FR01	0.35%
FR02	−3.51%
Sand 220	29.23%
Sand 60-80	50.31%
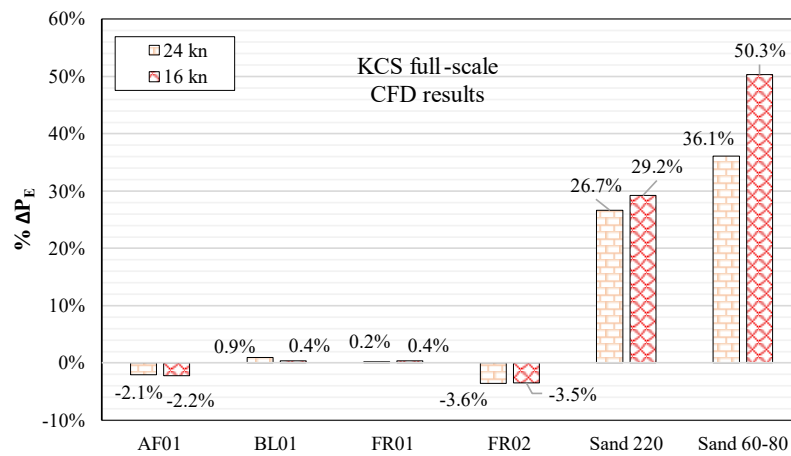
Figure 7-6: Effective power variation (%ΔP$_E$) of the full-scale KCS at design speed (V = 24 kn, Fr = 0.260) and low speed (V = 16 kn, Fr = 0.173).

150

7.4.1. Comparison and Validation

Table 7-8 compares the total resistance coefficient, C_T, values predicted from the present CFD simulations of the full-scale KCS and the results of (Song et al., 2020c). The results are presented for different speeds including the design speed of 24 knots and low speed of 19 knots. It is of note that the results of (Song et al., 2020c) in *Table 7-8* and *Figure 7-7* are adapted to consider the same wetted surface area of the present simulations. Notably, the comparisons show that the differences are acceptable, especially given the uncertainties evaluated in the analysis and the different geometries (KCS hull with/without rudder), boundary conditions and meshes. In other words, the total resistance coefficient values, C_T, predicted from the present CFD simulations agrees well with C_T values in the literature. Therefore, the modified wall-function approach adopted in this study can predict the effects of hull roughness on hydrodynamics of the full-scale KCS hull.

Table 7-8: Comparison between CFD average total resistance coefficients, C_T, in smooth conditions for the KCS full-scale hull.

Parameter	Present CFD simulations	CFD simulations (Song et al. 2020)	%($C_T - C_{T,Song}$)
$C_{T,smooth}(16\ kn)$	$1.692x10^{-3}$	$1.751x10^{-3}$	-3.46%
$C_{T,smooth}(24\ kn)$	$1.996x10^{-3}$	$2.045x10^{-3}$	-2.48%
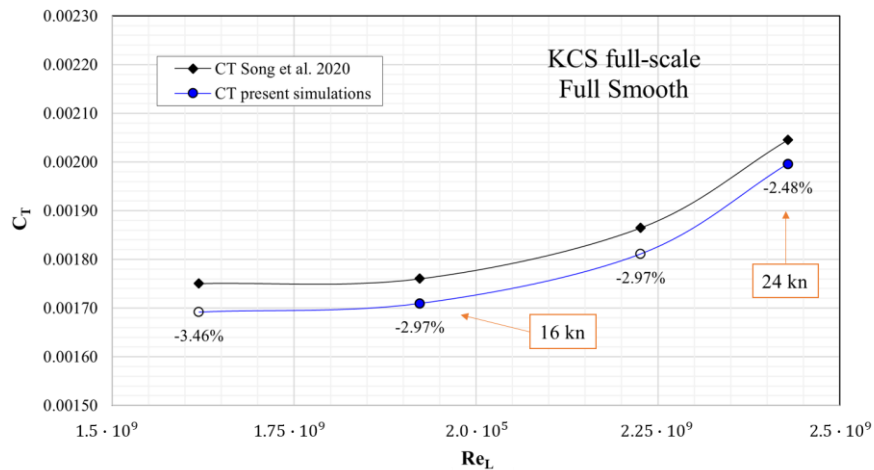
Figure 7-7: Comparison between CFD average total resistance coefficients, C_T, in smooth conditions for the KCS full-scale hull.

Further comparisons across the resistance coefficients and effective power variations obtained from the present CFD simulations and similarity law scaling procedure (Granville's method detailed in Chapter 6) are presented in the tables below. Notably, there is generally excellent agreement across the results. For example, *Table 7-9* shows that for all the surfaces investigated at design speed, the difference in $\%\Delta C_F$ is in the range of $-0.45 \div 0.57\%$.

Table 7-9: Comparison between the frictional resistance coefficients of the full-scale KCS at $V = 24\ kn$ obtained from CFD and Granville numerical methods.

Test Surface	Frictional Resistance Coefficients (design speed) $\%\Delta C_{F_{(CFD)}} - \%\Delta C_{F_{(Granville)}}$
AF01	0.31%
BL01	0.45%
FR01	−0.33%
FR02	0.16%
Sand 220	0.57%
Sand 60-80	−0.45%

Notably, more significant differences are seen in *Table 7-10* for low speed (16 knots). In this case, the comparison between the frictional resistance coefficients obtained from CFD and Granville numerical methods exhibited a minimum difference of 0.45% for the *Sand 220* surface and 8.18% for the *Sand 60-80.* This discrepancy predicted for rougher surfaces such as the *Sand 60-80* is expected to derive from the fact that hull roughness affects different components of ship resistance, including the frictional one.

Table 7-10: Comparison between the frictional resistance coefficients of the full-scale KCS at $V = 16\ kn$ obtained from CFD and Granville numerical methods.

Test Surface	Frictional Resistance Coefficients (low speed) $\%\Delta C_{F_{(CFD)}} - \%\Delta C_{F_{(Granville)}}$
AF01	2.73%
BL01	1.92%
FR01	3.31%
FR02	3.62%
Sand 220	0.45%
Sand 60-80	8.18%

Similarly, *Table 7-11* and *Table 7-12* present comparisons of the results obtained from the CFD and Granville numerical predictions for the effective power variation ($\%\Delta P_E$) of the full-scale KCS at design and low speed, respectively. As mentioned earlier, $\%\Delta P_E = \%\Delta C_T$. It is of note that at design speed, the variations of $\%\Delta P_E$ for the fouling control coatings tested is in the range of $-0.24 \div 0.29\%$ at design speed and $0.49 \div 2.18\%$ at low speed. Slightly more significant discrepancies are exhibited for the *Sand 220* and *Sand 60-80* cases.

Table 7-11: Effective power variation ($\%\Delta P_E$) of the full-scale KCS at $V = 24\ kn$ (Fr = 0.26) and comparisons of results obtained from the CFD and Granville numerical methods.

Test Surface	Effective Power Variation (design speed) $\%\Delta P_{E_{CFD}} - \%\Delta P_{E_{Granville}}$
AF01	0.29%
BL01	0.26%
FR01	−0.24%
FR02	0.24%
Sand 220	−0.61%
Sand 60-80	−1.72%

Table 7-12: Comparisons of the results obtained from the CFD and Granville numerical predictions for the effective power variation ($\%\Delta P_E$) of the full-scale KCS at 16 knots (Fr = 0.173).

Test Surface	Effective Power Variation (low speed) $\%\Delta P_{E_{CFD}} - \%\Delta P_{E_{Granville}}$
AF01	1.34%
BL01	0.49%
FR01	1.66%
FR02	2.18%
Sand 220	−1.91%
Sand 60-80	4.18%

7.4.2. Effects of Fouling Control Coatings on Flow Characteristics

Figure 7-8 and *Figure 7-9* compare the wave patterns around the full-scale KCS hull at design speed and low speed, respectively. It is seen from the figures that the wave elevations around the hull are reduced at low speed. As the fouling control coatings are almost as smooth as the reference surface, the behaviour of the wave patterns was expected to be unchanged. On the other hand, the sanded surfaces (*Sand 220* and *Sand 60-80*) do affect the wave patterns more, as will be discussed in the next chapter. Furthermore, in the following chapter, the roughness effect on the wave pattern will be investigated in different scenarios.

(a)

(b)
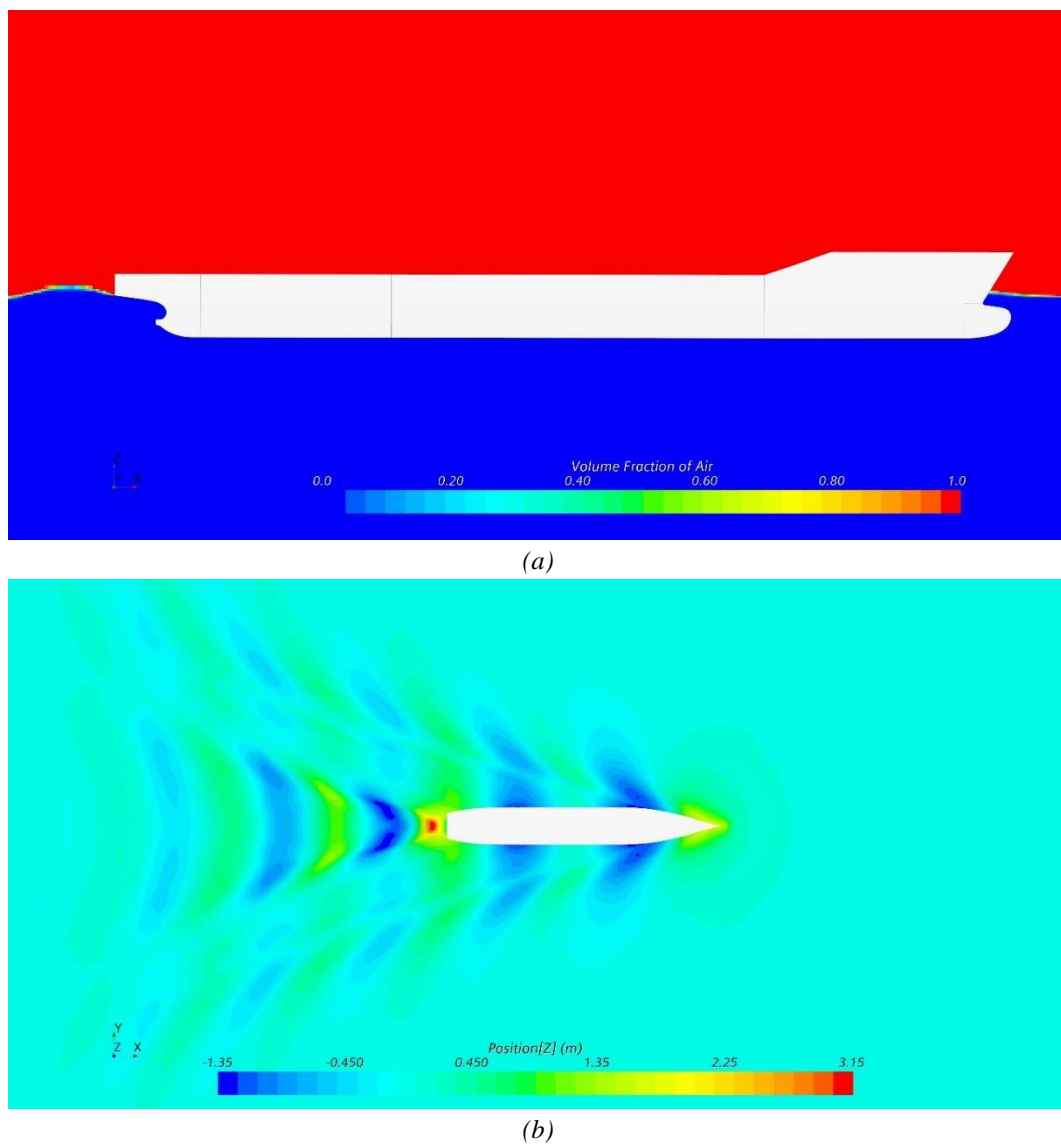
Figure 7-8: Free surface (a) and Kelvin wake pattern (b) around the full-scale KCS hull at design speed ($V = 24\ kn$, $Fr = 0.260$) with smooth conditions.
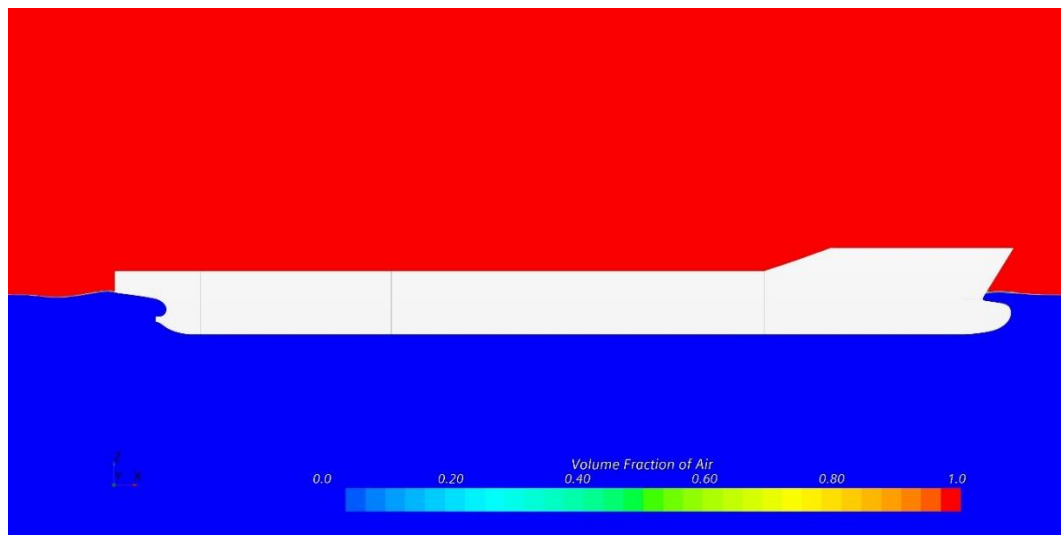
(a)
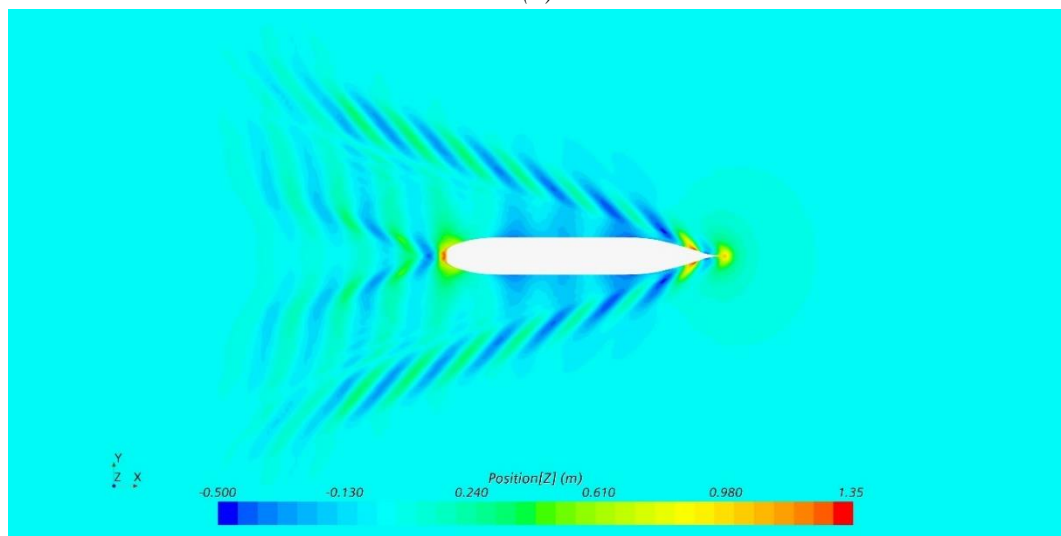
(b)

Figure 7-9: Free surface (a) and Kelvin wake pattern (b) around the full-scale KCS hull at low speed (V = 16 kn, Fr = 0.173) with smooth conditions.

Figure 7-10 and *Figure 7-11* compare the boundary layer contours around the hull of the KCS ship with the *FR02* coating at different speeds. The mean axial velocity, V_x, was normalised by dividing the ship speed, V_{ship}. The figures show similar boundary layer characteristics. However, a more significant difference between the design and low-speed cases can be noted in the boundary layer thickness. Finally, in the following chapter, the boundary layer characteristics will be investigated with *Sand 220* and *Sand 60-80* in different conditions, including different hulls, model scales and heterogeneous conditions.
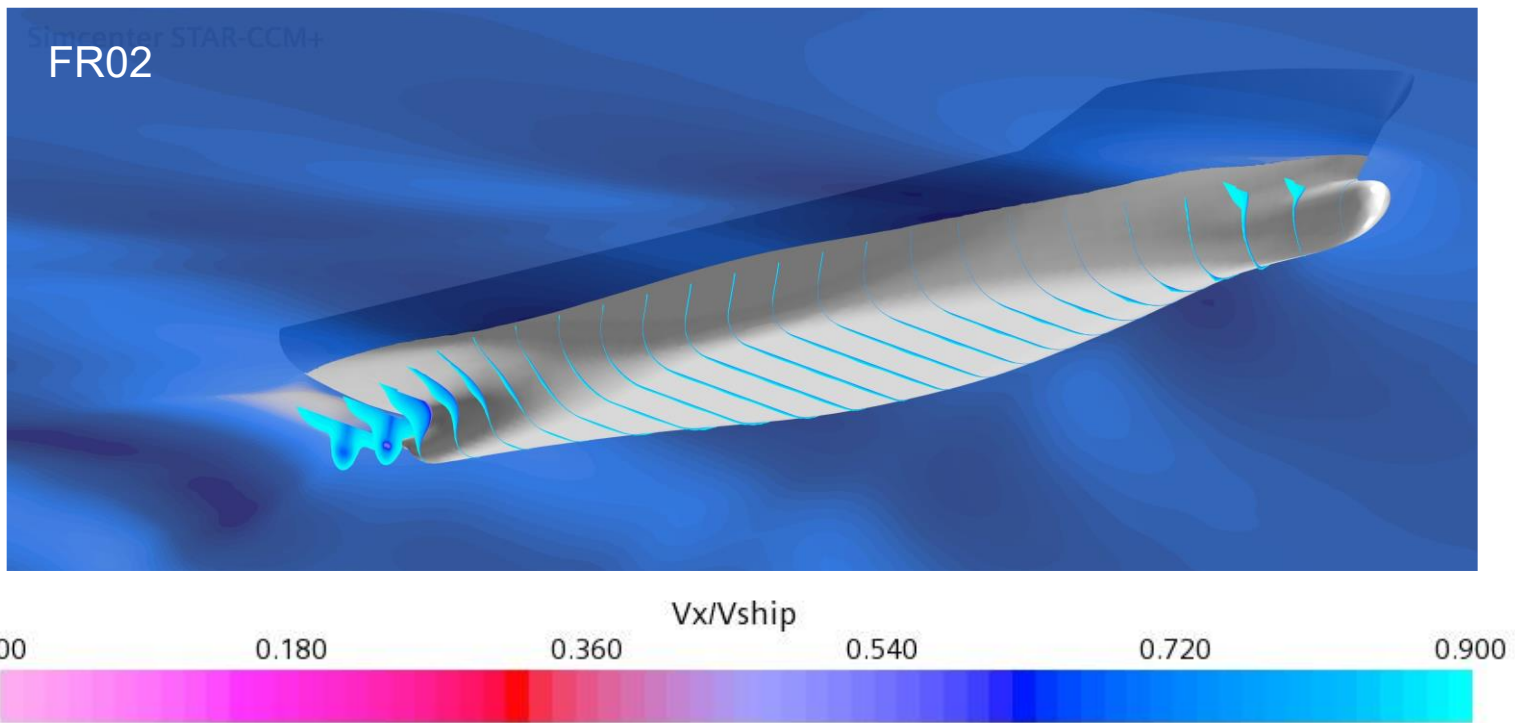
Figure 7-10: Boundary layer of the FR02 coating on the full-scale KCS hull with at the design speed (V = 24 kn, Fr = 0.260).
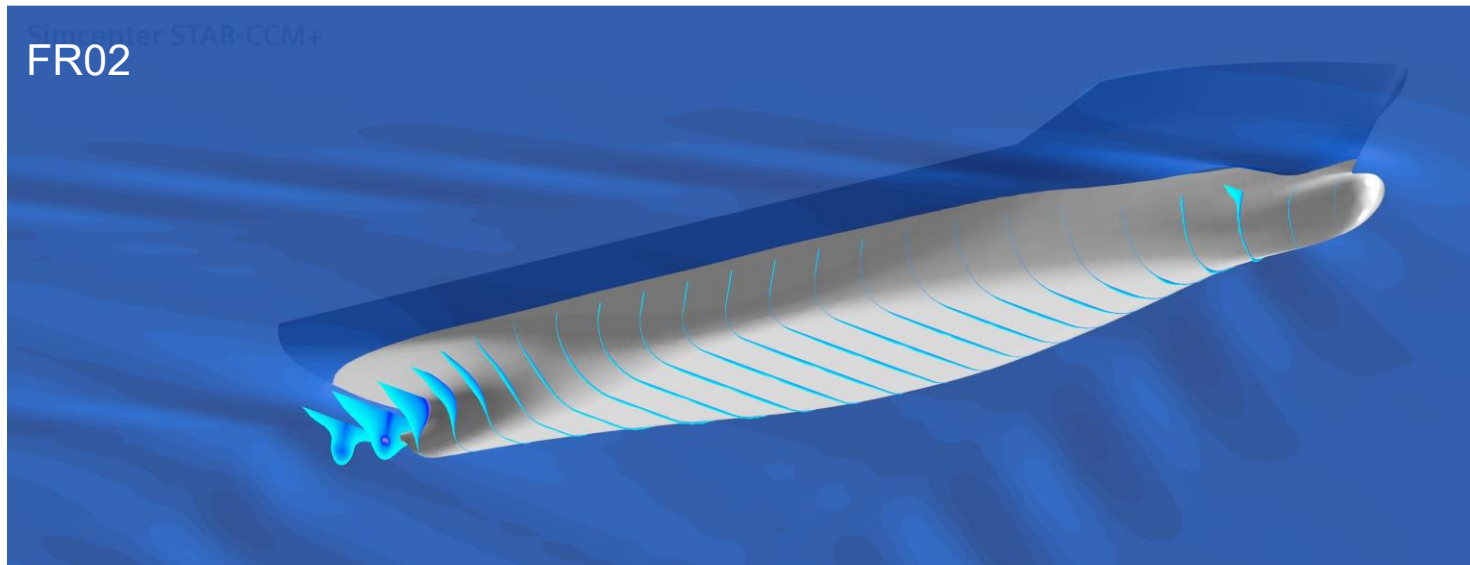
Figure 7-11: Boundary layer of the FR02 coating on the full-scale KCS hull with at the low speed (V = 16 kn, Fr = 0.173).

7.4. Chapter Summary and Conclusions

A CFD study was carried out to investigate the full ship hydrodynamic performance of different fouling control coatings and mimicked biofouling. The newly developed roughness functions of the fouling control coatings and sanded surfaces were implemented into CFD's modified wall function approach using the Star-CCM+ software to provide scale-up results to ship length. The benchmark KRISO containership (KCS) hull in full-scale was chosen to calculate the variance of resistance and powering requirements due to different test surfaces at the design speed of 24 knots ($Fr = 0.260, Re = 2.39x10^9$) and low speed of 16 knots ($Fr = 0.173, Re = 1.59x10^9$)

Among the four fouling control coatings (FCCs) that were tested in the FTFC, GIT's hard foul-release coating (*FR02*) displayed the best hydrodynamic performance across the entire Reynolds number range. In fact, *FR02* displayed lower frictional resistance coefficients than if the ship was considered as smooth as the acrylic reference panel (5.57% decrease). Furthermore, *FR02* led to a maximum decrease in effective power requirements of 3.6%. The numerical prediction results also show that the *AF01* (self-polishing antifouling coating) have better hydrodynamic performance than the smooth reference case (maximum decrease in effective power requirements of 2.1%).

In contrast, *Sand 220* (medium light slime) and *Sand 60-80* (medium slime) have, as expected, the highest resistance due to their rougher characteristics. In fact, a ship hull with medium light slime (*Sand 220*) and medium slime (*Sand 60-80*) surface roughness characteristics as the test surfaces would experience a maximum increase in effective power requirements of 26.7% and 36.1%, respectively.

Above all, the present chapter has provided several important findings, including the procedure to conduct CFD hydrodynamics prediction on full-scale ships and the introduction of roughness functions model for marine surfaces. The findings presented can help predict the required power, fuel consumption and greenhouse gas emissions of ships with hulls coated with certain fouling control coatings and/or in the fouled condition.

Further investigation could be conducted on the prediction of resistance of the coatings at different speeds, on different hulls, and using heterogeneous patch distribution of the roughness. It will also be beneficial to investigate the hydrodynamic performance of the same fouling control coating under the effect of biofouling growth. Exposing surfaces to dynamically grown biofouling will give shipowners and operators a better indication of what powering penalty they should expect from these coatings after a specific time in active service. Finally, applying different mimicked biofouling to the panels before or after the coating application could also serve as a better method to predict the resistance behaviour of the as-applied condition to an existing rough ship hull.

Part III

(Chapter 8)

Key Publications:

Ravenna, R., Song, S., Shi W., Sant, T., De Marco Muscat-Fenech, C., Demirel, Y. K. (2022) CFD analysis of the effect of heterogeneous hull roughness on ship resistance. Ocean Engineering, 257, 111733.

Song, S., **Ravenna, R.**, Dai, S., DeMarco Muscat-Fenech, C., Tani, G., Demirel, Y. K., Mehmet, A., Day, S., Incecik, A. (2021). Experimental investigation on the effect of heterogeneous hull roughness on ship resistance. Ocean Engineering, 223, 108590.

8. Heterogeneous Hull Roughness

8.1. Introduction

Heterogeneous hull roughness refers to the variation in the roughness characteristics of a ship's hull surface, where the roughness can vary in terms of size, shape, and distribution of surface irregularities. Additionally, heterogeneous hull roughness can arise due to a number of factors, including variations in paint thickness, surface imperfections, weld seams, and marine growth. However, in the present thesis, for heterogeneous hull roughness is intended that the roughness varies only in terms of distribution over the hull surfaces. Therefore, the same roughness type is used for a patch. In other words, in the present thesis, heterogeneous hull roughness means that the hull's surface texture is irregular, with areas of smoothness and roughness.

The effects of the heterogeneous distribution of roughness and the benefits of partial hull cleaning were first investigated by dividing the hull into different sections (Vargas et al., 2019). They conducted CFD simulations on a surface combatant exposed to different roughness scenarios. The findings indicated that the increase in the skin friction resulting from localised roughness is highest at the bow, followed by sides, flat bottom, stern, and transom. In (Östman et al., 2019), the author carried out a CFD analysis investigating the potential of a selective application of different quality coatings on a full-scale tanker. The regions with concentrated high skin friction were modelled with a high-quality coating (low roughness), while the rest of the hull was modelled with a low-quality coating. The results confirmed the expectations: this selective approach can reduce the ship resistance compared to when the inferior coating is applied to the entire hull.

As mentioned in the literature review, state-of-the-art studies investigating heterogeneous hull roughness have highlighted the importance of hull roughness on ship resistance and hydrodynamic performance. These studies have also shown that small-scale roughness features can significantly impact resistance and that numerical simulations can be useful tools for investigating these effects. However, further

research is needed to fully understand hull roughness's complex and nonlinear effects on ship resistance. The location and distribution of roughness on the hull can also impact resistance. For example, roughness at the bow and stern can have a more significant impact than roughness in the middle of the hull.

(Song et al., 2021c, 2021b) investigated the heterogeneous hull roughness effect on ship hydrodynamics through experimental fluid dynamics (EFD) and CFD was investigated. In our previous study, (Song et al., 2021c), the Wigley hull was modelled with different hull roughness conditions by applying sand-grit on the hull surface in various configurations (i.e., smooth and full-rough, ¼-bow-rough, ¼-aft-rough, ½-bow-rough and ½-aft-rough). The increased roughness in the forward wetted surface of the Wigley hull caused more added resistance than the hull roughness in its other parts. Hence, the findings suggest the possibility of prioritising a partial hull cleaning depending on the impact of the roughness in different hull regions.

Similarly to the roughness impact factor (*RIF*), which will be introduced later in the present study (Ravenna et al., 2022c), a recent paper investigated some of the issues of heterogeneous hull roughness on the benchmark tanker KVLCC2, (Kim et al., 2022). Their study included self-propulsion simulations with SHIPFLOW, a code developed by FLOWTECH, on the induced relation between hull surface roughness and ship performance. They estimated the attainable reduction of propulsion power by hull surface treatment as a cleaning efficiency index (CEI), which is defined as the ratio between the delivered horsepower reduction per unit cleaning area. Similarly to the roughness impact factor (*RIF*), the CEI number recommends partial hull treatment based on cost-benefit analysis. Furthermore, the study showed the economic viability of partial hull treatment. However, only the heterogeneous roughness effect on the KVLCC2 hull was investigated. Different ship types should be investigated to better understand the optimum hull surface maintenance strategy.

The promising findings of the few studies addressing the effect of heterogeneous distribution of hull roughness are limited to the ship types considered (the Wigley hull, the KVLCC2 tanker, and a surface combatant). Despite these recent studies, our understanding of the effect of heterogeneous hull roughness is still limited. The different impacts of hull roughness on different hull regions need to be investigated

for better comprehension. The present study aims to fill this research gap by investigating the effect of heterogeneous roughness on the hydrodynamic resistance of the well-known KRISO Container Ship (KCS) hull using CFD, also supporting a targeted strategy for hull maintenance. Furthermore, the CFD simulations in this study will provide data to assess how the heterogeneous hull roughness affects the flow regime around the hull.

The present chapter details a CFD investigation conducted on the benchmark KCS and KVLCC2 hulls in model scale with heterogeneously distributed hull roughness conditions. Unsteady Reynolds Averaged Navier–Stokes (URANS)-based CFD simulations with a modified wall-function approach were developed in StarCCM+. The scenarios modelled include homogeneous (i.e., smooth, and full rough conditions) and heterogeneous conditions (i.e., different smooth/rough wetted surface ratios). A so-called *Roughness Impact Factor, RIF,* was introduced to correlate the added resistance of the heterogeneous roughness scenarios to the corresponding rough wetted surface area. Chapter 8 is structured as follows:

It is also of note that conducting both model scale and full-scale CFD-based ship resistance simulations is important because it allows for more accurate predictions of the performance of real-world ships. Model scale simulations provide a cost-effective and efficient way to test the hydrodynamic behaviour of scaled-down ship models. These tests can be also experimentally replicated in controlled environments such as towing tank laboratories. Model-scale CFD simulations can help in identifying potential issues with the design early on, and guide improvements before the actual construction of the ship. On the other hand, the full-scale CFD-based ship resistance simulations detailed earlier use the actual ship geometry and operating conditions, providing more realistic results. They enable the evaluation of ship performance under various scenarios and operating conditions and can help in optimizing the ship design for improved performance and fuel efficiency. By combining both model scale and full-scale CFD-based simulations, ship designers and naval architects can gain a more comprehensive understanding of the ship's behaviour and optimize its performance, resulting in more efficient and safer ships. Hence, as more cost effective but yet accurate and easy to validate against experiments, the model-scale geometries have

been preferred for the extensive CFD investigation on the heterogeneous hull roughness effects on ship resistance.

Section 2 presents the methodology adopted, including the geometry and boundary conditions, mesh generations, verification, and validation. Section 3 presents the roughness function model adopted in the modified wall-function approach of the present CFD simulations. Section 4 discusses the results of the current CFD investigation. The effects of heterogeneous hull roughness on the hydrodynamics of the KCS and KVLCC2 models were assessed and discussed in this section. Moreover, the so-called *Roughness Impact Factor* (RIF) was defined to correlate the various hull roughness conditions with the predicted resistance coefficients. Notably, the rationale behind the heterogeneous hull roughness effects is discussed by graphically comparing the local wall shear stress, skin friction coefficients, roughness Reynolds number values and boundary layer distributions of the heterogeneous configurations with the homogeneous full rough and full smooth cases. Finally, Section 5 gives the conclusions of the present chapter. In this section, the results are further summarised and discussed, along with recommendations for future studies.

8.2. Modified Wall Function Approach

8.2.1. Roughness Function Models

Equation (8-1) shows the roughness function model employed in this study for the *Sand 60-80* scenario using STAR-CCM+'s built-in roughness function model. (Song et al., 2020b) developed the model in equation (8-1) from the towing tests of a flat plate covered with sand (aluminium oxide, 60/80 grit) (Song et al., 2021a). As mentioned earlier, the hull surface condition represented by *Sand 60-80* is a medium rough case ($R_a = 353$ μm) as of a medium developed slime (Schultz, 2004). As mentioned earlier, this roughness function model agrees well with the FTFC tests depicted in Chapter 4 for the same surface, *Sand 60-80*. Hence, the k^+ value for the *Sand 60-80* case is shown in *Table 4-8*.

$$\Delta U^+ = \begin{cases} 0 & \rightarrow & k^+ < 3 \\ \dfrac{1}{\kappa}\ln\left[0.49k^+ - 3\left(\dfrac{k^+ - 3}{25 - 3}\right)\right]^{\sin\left[\frac{\pi}{2}\frac{\log(k^+/3)}{\log(25/3)}\right]} & \rightarrow & 3 \le k^+ < 25 \\ \dfrac{1}{\kappa}\ln(0.49k^+ - 3) & \rightarrow & 25 \le k^+ \end{cases} \quad (8\text{-}1)$$

In which κ is the von-Karman constant ($\kappa = 0.42$).

8.3. Results and Discussion

8.3.1. Heterogeneous Hull Roughness Effects on Ship Resistance

The conventional simplification of treating hull surfaces as uniformly rough may introduce uncertainties in the added resistance prediction. Heterogeneous hull roughness affects the ship's performance in a complicated, non-linear way as it influences both frictional and wave-making resistance (Schultz and Flack, 2007). Furthermore, the location of the increased roughness on the hull profoundly influences its overall effect on ship resistance (Kim et al., 2022; Song et al., 2021c).

This study examined the impact of the uneven distribution of hull roughness on ship resistance, which can be influenced by factors such as coating type, age, surface condition, and marine growth. Certain areas of a ship, such as the flat bottom, bilge keels, sea chests, and thrusters, are more prone to marine growth due to prolonged water submersion and slow-moving water. Based on the author's experience in drydock activities, the hulls have been observed to have vertical patches of varying roughness from the deepest to the highest draft, likely due to differences in submerged area at different prolonged loading conditions. These differences are less apparent longitudinally and may be attributed to variations in flow characteristics around the hull, such as speed, stagnation, and turbulence.

Specifically, this section discusses and compares the results of the towing tests conducted in CFD on the KCS and KVLCC2 model in heterogeneous hull roughness

conditions with the homogeneous fully smooth and fully rough cases. As reported in *Table 3-4*, the simulations for the KCS model were carried out at a towing speed of $1.426\ m/s$, Froude number $Fr = 0.260$, and Reynolds number $Re_L = 3.74 \times 10^6$, which correspond to the full-scale design speed of 24 knots and $Re_L = 2.39 \times 10^9$. On the other hand, , the simulations for the KVLCC2 model were carried out at a towing speed of $0.760\ m/s$, Froude number $Fr = 0.142$, and Reynolds number $Re_L = 1.89 \times 10^6$, which correspond to the full-scale design speed of 15.5 knots and $Re_L = 2.15 \times 10^9$.

Figure 8-1 and *Table 8-1*compare the resistance coefficients of the KCS model in heterogeneous roughness configurations calculated using the WSA of the present simulations. Different ΔC_T values were found across the fore-rough conditions (*Bulbous Bow*, *Fore Hull*), the midship-rough conditions (*Midship*, *Flat Bottom*), and the aft-rough conditions (*Aft Hull*, *Stern*) due to the different local increased hull roughness and hence locally increased skin friction of the hull. It would be expected that larger rough/smooth wetted surface area ratios would correspond to more significant resistance coefficients.
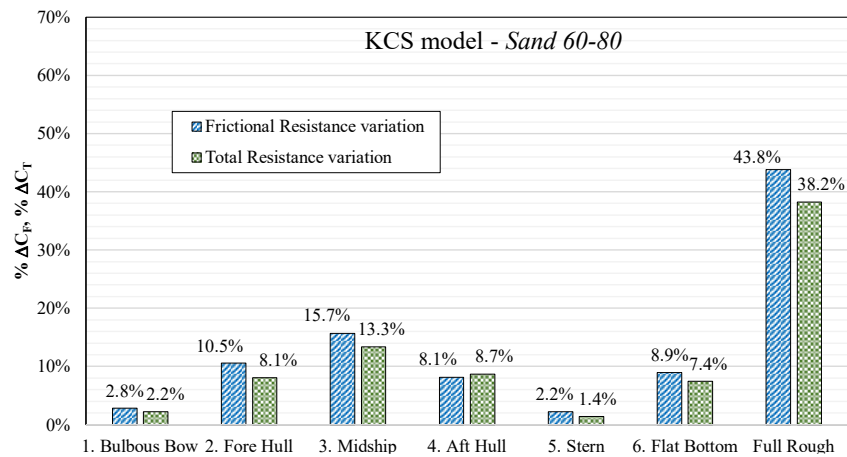
Figure 8-1: Resistance coefficients for the KCS model hull simulations in different hull roughness conditions (Sand 60-80) at design speed ($Fr = 0.260$).

Roughness scenario	Total resistance coefficient C_T	Frictional resistance coefficient C_F		Residuary resistance coefficient C_R		Added resistance coefficient ΔC_T	
Full smooth	$4.37x10^{-3}$	$3.67x10^{-3}$	84.1%	$6.93x10^{-4}$	15.9%	0.00	0.00%
1. Bulbous Bow	$4.46x10^{-3}$	$3.78x10^{-3}$	82.3%	$6.87x10^{-4}$	15.5%	$9.68x10^{-5}$	2.17%
2. Fore Hull	$4.72x10^{-3}$	$4.06x10^{-3}$	77.9%	$6.57x10^{-4}$	14.7%	$3.52x10^{-4}$	7.45%
3. Midship	$4.95x10^{-3}$	$4.25x10^{-3}$	74.2%	$7.00x10^{-4}$	14.0%	$5.82x10^{-4}$	11.77%
4. Aft Hull	$4.74x10^{-3}$	$3.97x10^{-3}$	77.4%	$7.73x10^{-4}$	14.6%	$3.78x10^{-4}$	7.97%
5. Stern	$4.43x10^{-3}$	$3.75x10^{-3}$	83.0%	$6.72x10^{-4}$	15.7%	$6.01x10^{-5}$	1.36%
6. Flat Bottom	$4.69x10^{-3}$	$4.00x10^{-3}$	78.3%	$6.90x10^{-4}$	14.8%	$3.24x10^{-4}$	6.91%
Full Rough	$6.03x10^{-3}$	$5.28x10^{-3}$	60.9%	$7.51x10^{-4}$	11.5%	$1.67x10^{-5}$	27.64%

Similarly, *Figure 8-2* and *Table 8-2* compare the resistance coefficients of the KVLCC2 model in heterogeneous roughness configurations calculated using the WSA of the present simulations. As for the KCS model case, different ΔC_T values were found across the configurations tested due to the different local increased hull roughness and hence locally increased wall shear stress and skin friction of the hull.
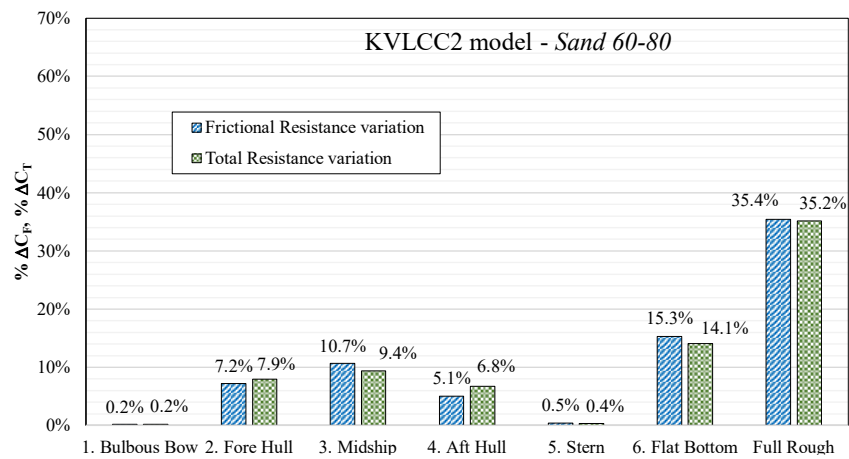
Figure 8-2: Resistance coefficients for the KVLCC2 model hull simulations in different hull roughness conditions (Sand 60-80) at design speed ($Fr = 142$).

Table 8-2: Resistance coefficients for the KVLCC2 model simulations in different hull roughness conditions.

Roughness scenario	Total resistance coefficient C_T	Frictional resistance coefficient C_F		Residuary resistance coefficient C_R		Added resistance coefficient ΔC_T	
Full smooth	$4.78x10^{-3}$	$3.87x10^{-3}$	80.8%	$9.16x10^{-4}$	19.2%	0.00	0.00%
1. Bulbous Bow	$4.79x10^{-3}$	$3.87x10^{-3}$	80.8%	$9.19x10^{-4}$	19.2%	$1.11x10^{-5}$	0.23%
2. Fore Hull	$5.16x10^{-3}$	$4.15x10^{-3}$	80.3%	$1.02x10^{-3}$	19.7%	$3.80x10^{-4}$	7.94%
3. Midship	$5.23x10^{-3}$	$4.28x10^{-3}$	81.8%	$9.54x10^{-4}$	18.2%	$4.50x10^{-4}$	9.42%
4. Aft Hull	$5.11x10^{-3}$	$4.06x10^{-3}$	79.6%	$1.04x10^{-3}$	20.4%	$3.23x10^{-4}$	6.75%
5. Stern	$4.80x10^{-3}$	$3.88x10^{-3}$	80.9%	$9.17x10^{-4}$	19.1%	$1.82x10^{-5}$	0.38%
6. Flat Bottom	$5.46x10^{-3}$	$4.46x10^{-3}$	81.7%	$9.97x10^{-4}$	18.3%	$6.73x10^{-4}$	14.07%
Full Rough	$6.47x10^{-3}$	$5.24x10^{-3}$	81.0%	$1.23x10^{-3}$	19.0%	$1.68x10^{-5}$	35.19%

Finally, *Figure 8-3* and *Figure 8-4* give an overview of all the resistance coefficients of the KCS and KVLCC2 models, respectively, in heterogeneous roughness configurations calculated using the WSA of the present simulations. As mentioned earlier, it would be expected that larger rough/smooth wetted surface area ratios would correspond to more significant resistance coefficients. On the other hand, the present CFD simulations discredited the simplistic assumption that the larger the area, the more significant the impact. This concept will be elaborated on afterwards.
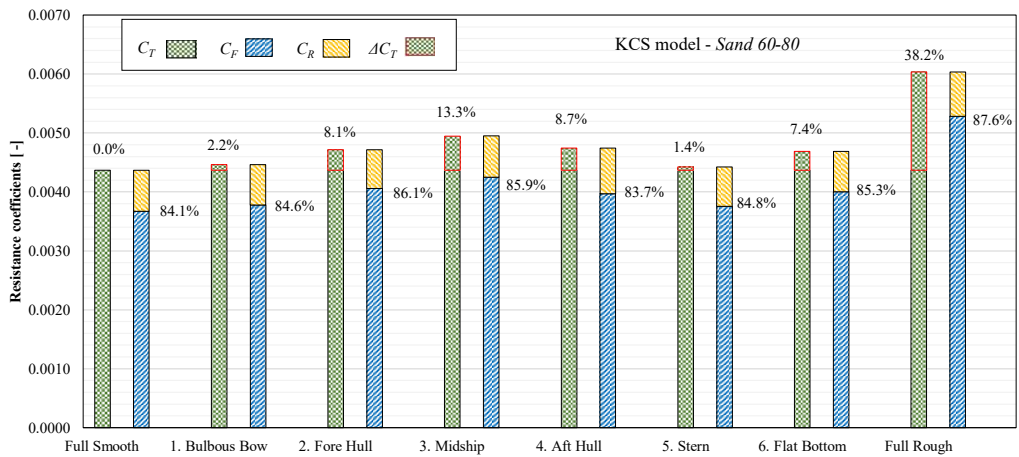
Figure 8-3. Percentage bar diagram of the resistance coefficients of the KCS model in heterogeneous hull roughness conditions (Sand 60-80) at design speed ($Fr = 0.260$).
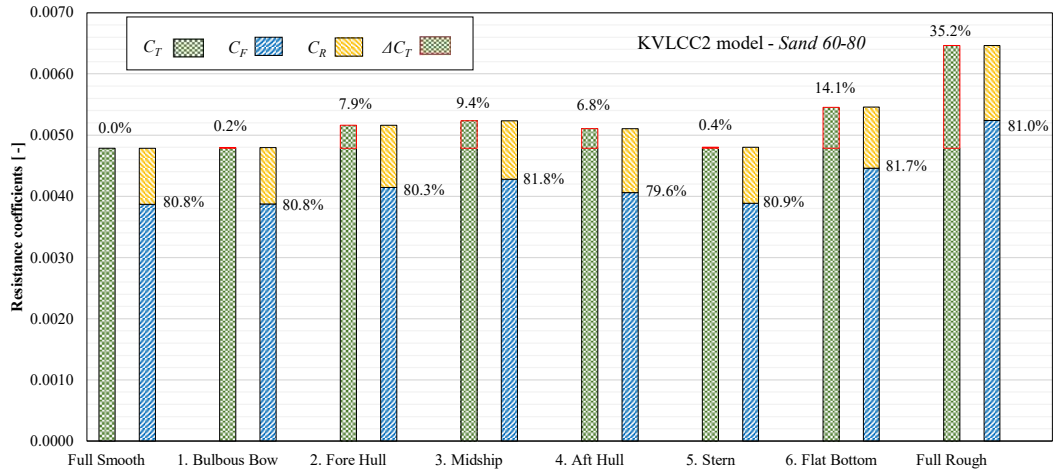
Figure 8-4: Percentage bar diagram of the resistance coefficients of the KVLCC2 model in heterogeneous hull roughness conditions (Sand 60-80) at design speed ($Fr = 0.142$).

8.3.2. Novel Parameter for Assessing Heterogeneous Hull Roughness

Recently, (Ravenna et al., 2022c) proposed a new measure called *Roughness Impact Factor* to quantify the relative impacts of heterogeneous hull roughness varying with rough surface's position. In the determination process of the RIF, a hull surface consisting of *n* surface regions ($c = 1,2,3,...,n$) is considered. When the ith surface is rough while the other regions remain smooth, the *Roughness Impact Factor*, RIF of the ith surface, RIF_i, has been defined as in equation (8-2):

$$RIF_i = \frac{(\Delta C_T)_i}{\left(WSA_{Rough}\right)_i} \bigg/ \frac{(\Delta C_T)_{Full\ Rough}}{WSA_{Total}} \tag{8-2}$$

In which $(\Delta C_T)_i$ and $(WSA_{Rough})_i$ are, respectively, the total added resistance and the rough wetted surface area of the ith surface. $(\Delta C_T)_{Full\ Rough}$ is the added resistance when the entire hull is covered with the given roughness, and WSA_{Total} is the total wetted surface area of the hull. In other words, RIF correlates the added resistance coefficient to the rough wetted surface area of any given roughness condition.

In this method, $RIF = 1$ for the *Full Rough* scenario and it indicates that the corresponding surface has an average impact. On the other hand, $RIF > 1$ indicates that the corresponding region has a greater impact than the average. Similarly, $RIF <$

1 suggests that the region has a lower impact than the average. *Figure 8-5*, *Table 8-3* and *Table 8-4* highlight the non-proportional impact of increased roughness of the heterogeneous configurations. Notably, the *Bulbous Bow* cases accounts for a smaller rough/smooth wetted surface area ratio than the *Stern* configurations, but their corresponding added resistance values are more significant than those of the *Stern* scenarios. As shown in *Figure 8-5*, and *Table 8-3* for the KCS model, the *Bulbous Bow* rough/smooth wetted surface area ratio is 2.57%, and the added resistance coefficient is $9.68x10^{-5}$ while for the *Stern* case, these parameters are 8.14% and $6.01x10^{-5}$, respectively. In other words, the results of this study showed that the position of the selected area of the hull with increased surface roughness strongly affects its impact on the ship's hydrodynamics.

Moreover, while being the smallest area with increased hull roughness, the *Bulbous Bow* scenario has the most significant impact on ship resistance (impact factor of 2.26) of all the scenarios. The *Fore Hull* and *Aft Hull* cases have the second-largest effect (impact factor of 1.19). On the other hand, despite being the largest rough wetted surface area tested, the *Midship* configuration only gives an impact factor of 1.18. Similarly, the *Stern* and *Flat Bottom* configurations showed the lowest impact factors of the heterogeneous scenarios tested. For these configurations, *RIF* is lower than unity (0.44, 0.85, respectively).

Similarly, for the KVLCC2 model, as shown in *Figure 8-6* and *Table 8-4*, the *Bulbous Bow* rough/smooth wetted surface area ratio is 1.02%, and the added resistance coefficient is $1.11x10^{-5}$ while for the *Stern* case, these parameters are 8.14% and $1.82x10^{-5}$, respectively. In other words, again, it is evident that the position of the selected area of the hull with increased surface roughness strongly affects its impact on the ship's hydrodynamics. It can be noted that *Fore Hull* has the largest effect (impact factor of 1.63). On the other hand, despite being the largest rough wetted surface area tested, the *Flat Bottom* configuration only gives an impact factor of 1.00. Similarly, the *Midship,* configuration showed an impact factor of 1.01. Finally, as expected, the *RIF* for the *Stern* configuration is lower than unity (0.28).
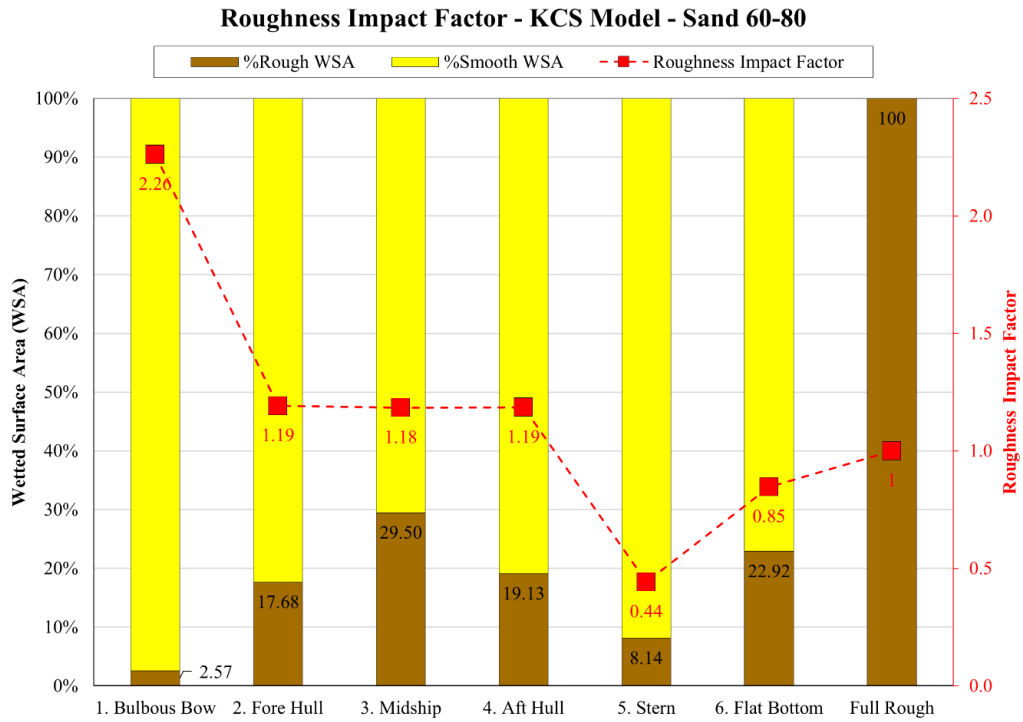
Figure 8-5: Roughness impact factors and wetted surface area ratios of the roughness scenario tested (Sand 60-80) for the KCS model hull at design speed ($Fr = 0.260$).

Table 8-3: Roughness impact factors and wetted surface area ratios of the roughness scenario tested (Sand 60-80) for the KCS model hull ($Fr = 0.260$).

Roughness scenario	Rough wetted surface area % WSA_R	Added effective power % ΔC_T , % ΔP_e	Roughness Impact Factor RIF
Full Smooth	0	0	0
1. Bulbous Bow	2.57	2.22	2.26
2. Fore Hull	17.68	8.05	1.19
3. Midship	29.49	13.34	1.18
4. Aft Hull	19.12	8.66	1.19
5. Stern	8.14	1.38	0.44
6. Flat Bottom	22.91	7.42	0.85
Full Rough	100	38.20	1

171
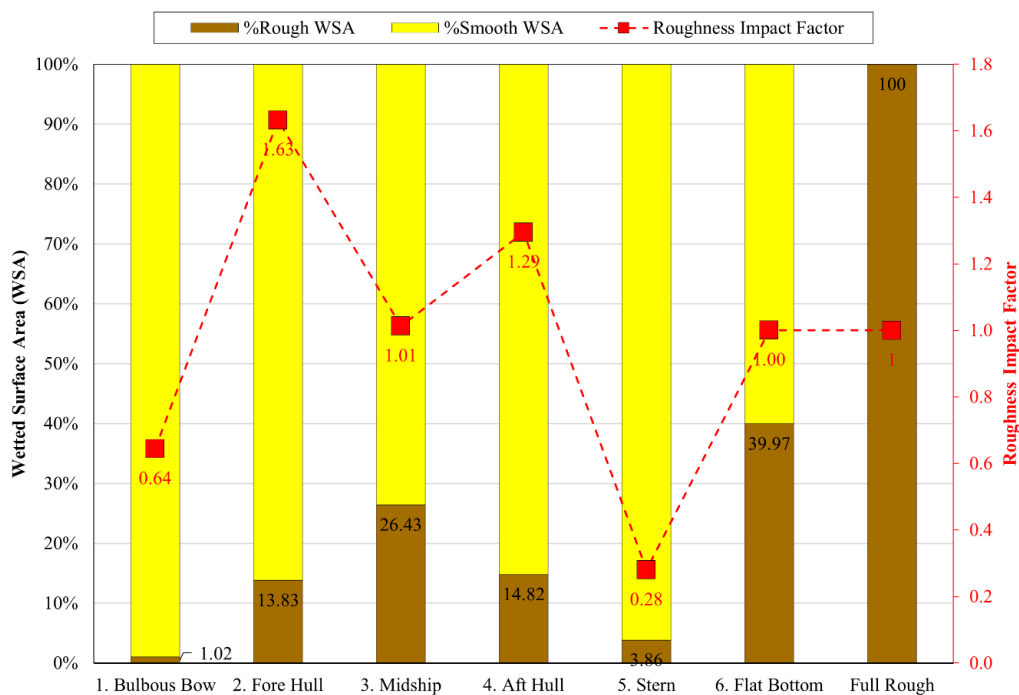
Figure 8-6: Roughness impact factors and wetted surface area ratios of the roughness scenario tested (Sand 60-80) for the KVLCC2 model hull at design speed ($Fr = 0.142$).

Table 8-4: Roughness impact factors and wetted surface area ratios of the roughness scenario tested (Sand 60-80) for the KVLCC2 model hull at design speed ($Fr = 0.142$).

Roughness scenario	Rough wetted surface area % WSA_R	Added effective power % ΔC_T, % ΔP_e	Roughness Impact Factor RIF
Full Smooth	0	0.00%	0
1. Bulbous Bow	1.02	0.23%	0.64
2. Fore Hull	13.83	7.94%	1.63
3. Midship	26.43	9.42%	1.01
4. Aft Hull	14.82	6.75%	1.29
5. Stern	3.86	0.38%	0.28
6. Flat Bottom	39.97	14.07%	1.00
Full Rough	100	35.19%	1

As mentioned above, (Ravenna et al., 2022c) proposed the "*Roughness Impact Factor*" (RIF) as a new measure to quantify the impact of heterogeneous hull roughness that varies with the position of rough surfaces. Through CFD simulations on a model-scale containership, they determined RIF values for different hull regions, providing useful insights on hull roughness. However, future research could develop a practical method to predict added resistance due to such roughness, possibly by incorporating Granville's similarity law scaling and RIF values on different regions to weigh up their relative impacts. It is of note that a key limitation of RIF is that its values may vary with hull shapes and speeds. Therefore, future studies should investigate RIF values for different hull types at various velocities.

8.3.3. Heterogeneous Hull Roughness Effects on Ship Powering

Finally, similarly to (Tezdogan et al., 2015), the effective power penalties for the KCS and KVLCC2 models, ΔP_E, were estimated as in equation (8-3):

$$\frac{\Delta C_T}{C_{T_S}} 100 = \%\Delta P_E \tag{8-3}$$

The impact of the different roughness scenarios on the effective power of the two models tested is presented in *Figure 8-7*, *Table 8-3* and *Table 8-4*. Once again, the *Bulbous Bow* rough case, regardless of the limited rough wetted area (2.57%), has a significant impact on the hydrodynamic performances of the KCS model. Hence, the added effective power of the KCS model with a rough bulbous bow is 2.22%. Therefore, assuming a similar outcome for full-scale conditions, it seems reasonable to promptly tackle the increased hull roughness on the bulbous bow region.
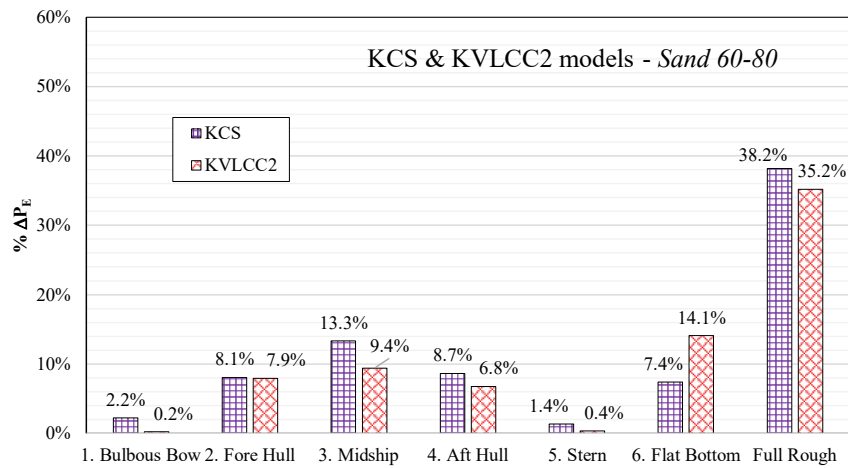
Figure 8-7: Effective power variation $(\%\Delta P_E)$ *of the KCS and KVLCC2 models at design speed in heterogeneous hull roughness conditions (Sand 60-80).*

8.3.4. Rationale behind the Heterogeneous Roughness Effects

The effect of hull roughness on ship resistance is closely related to the heterogeneous distribution of the increased roughness. Locally increased roughness affects the wall shear stress and, hence, the local skin friction coefficients, the Roughness Reynolds number values (k^+) and the boundary layer characteristics. The rationale behind the roughness effects of the KCS hull with heterogeneous hull roughness scenarios is presented. *Figure 7-8* and *Figure 8-9*, show the free surface and Kelvin wave pattern around the KCS and KVLCC2 models in smooth conditions at design speed. Considerable differences were observed between the KCS and KVLCC2 models, as expected. Notably, the faster KCS model , *Figure 8-8*, presents higher waves around the hull than the KVLCC2 model, *Figure 8-9*.
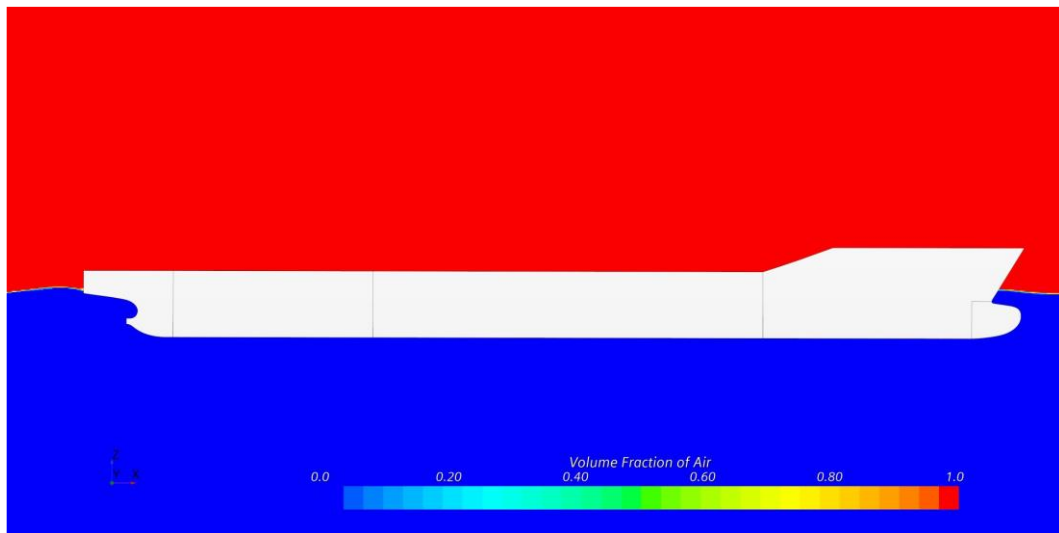
(a)
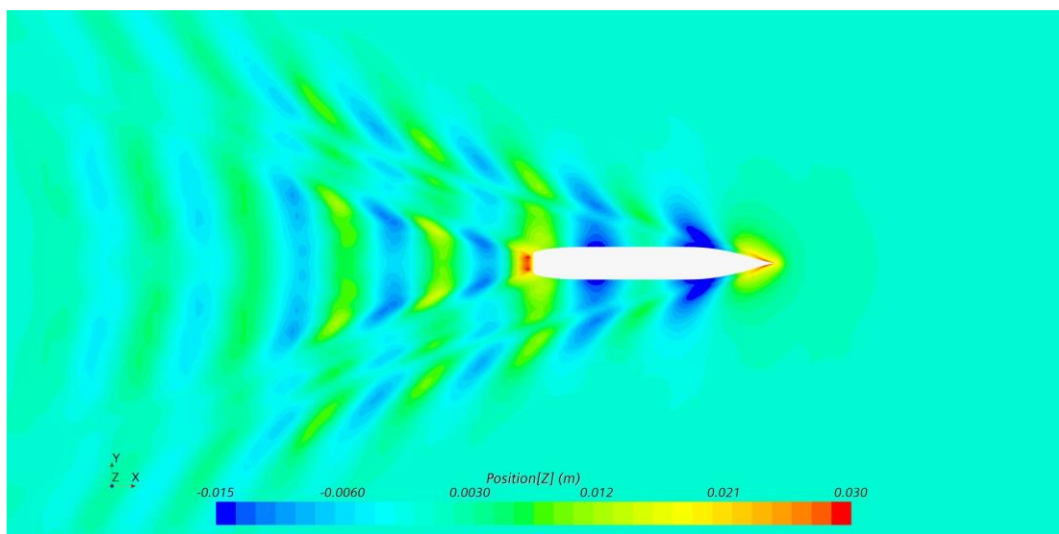
(b)

Figure 8-8: Free surface (a) and Kelvin wake pattern (b) around the model KCS hull at design speed ($Fn = 0.260$) with smooth conditions.
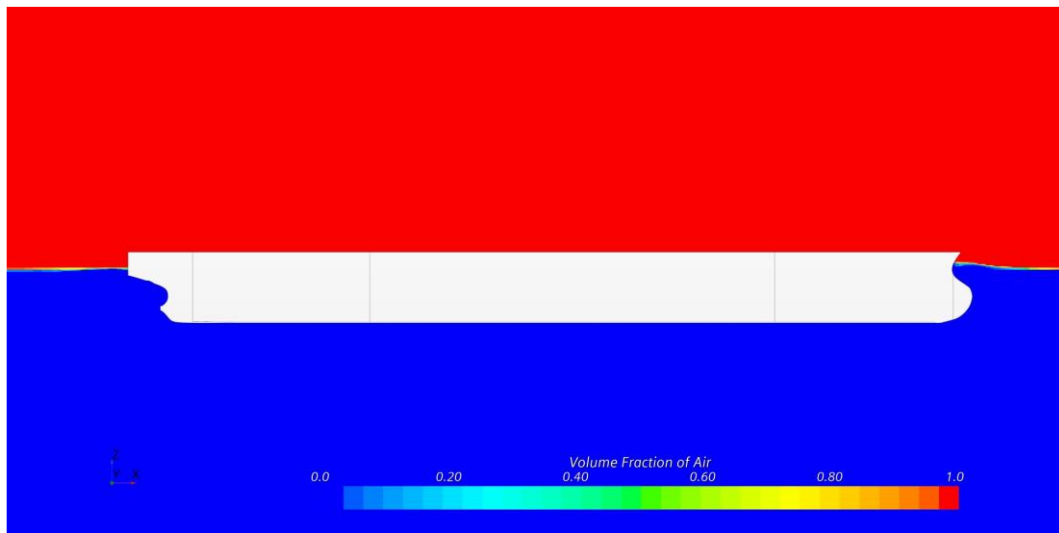
(a)
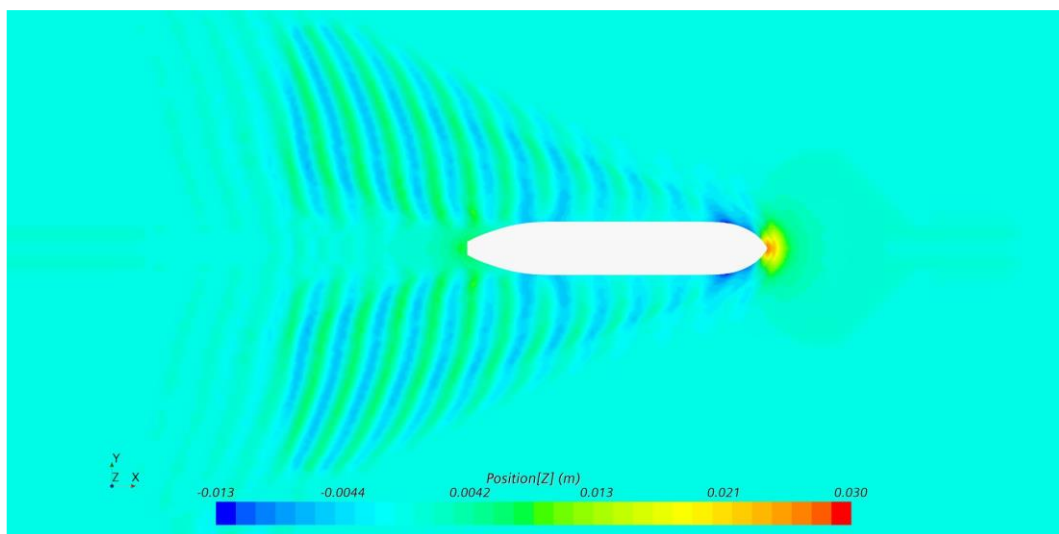
(b)

Figure 8-9: Free surface (a) and Kelvin wake pattern (b) around the model KVLCC2 hull at design speed ($Fr = 0.142$) with smooth conditions

Figure 8-10 compares the local wall shear stress, τ_w, and skin friction coefficients, c_f, on the KCS hull in heterogeneous hull roughness conditions with the homogeneous full smooth and full rough cases (scalar field distribution on the hull surfaces limited to $c_f = 0.01$). The Bulbous Bow and Fore Hull roughness conditions in *Figure 8-10-*a and *Figure 8-10*-b show similar c_f distributions as that of the Full Rough condition in the rough regions.
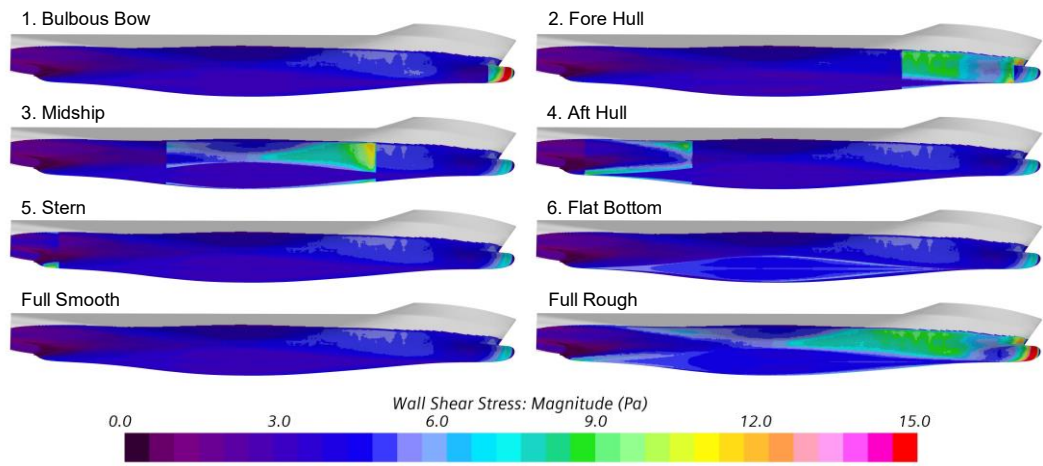
(a)
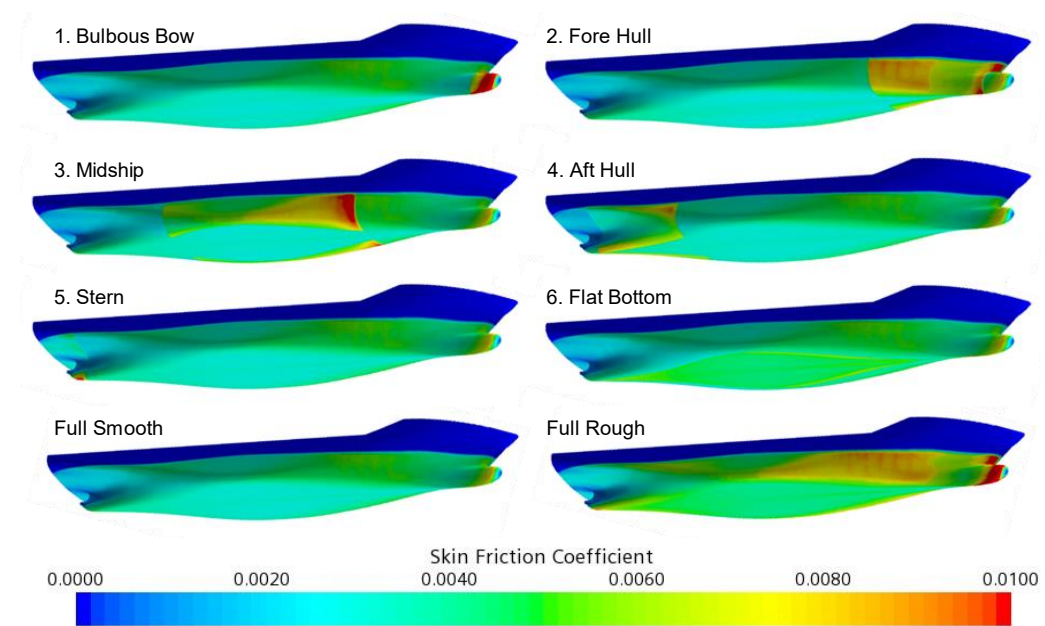
(b)

Figure 8-10: Local characteristics of the wall shear stress, τ_w, (a), and skin friction coefficients, c_f, (b) on the model KCS hull at design speed ($Fr = 0.260$).

Furthermore, the most significant increases in the local c_f values were observed for the upstream regions of the *Midship* configuration. In this case, the effect of the heterogeneous increase of hull roughness is dramatic, as shown in *Figure 8-10*-3. On the other hand, the *Aft Hull*, *Stern,* and *Flat Bottom* scenarios (*Figure 8-10*-4,5,6) are less impactful on the skin friction coefficient distribution. Hence, c_f distributions are more similar to the *Full Smooth* homogeneous condition than to the *Full Rough*.
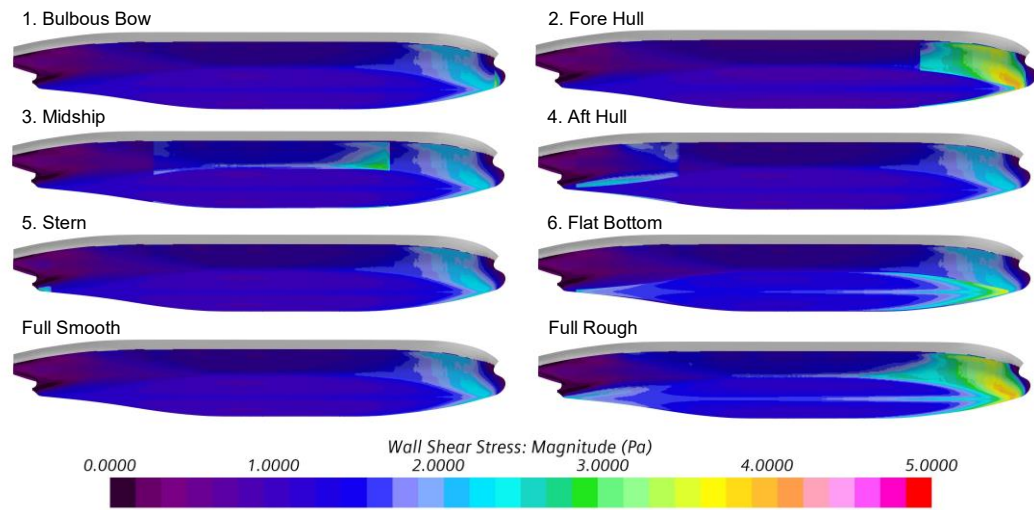
(a)
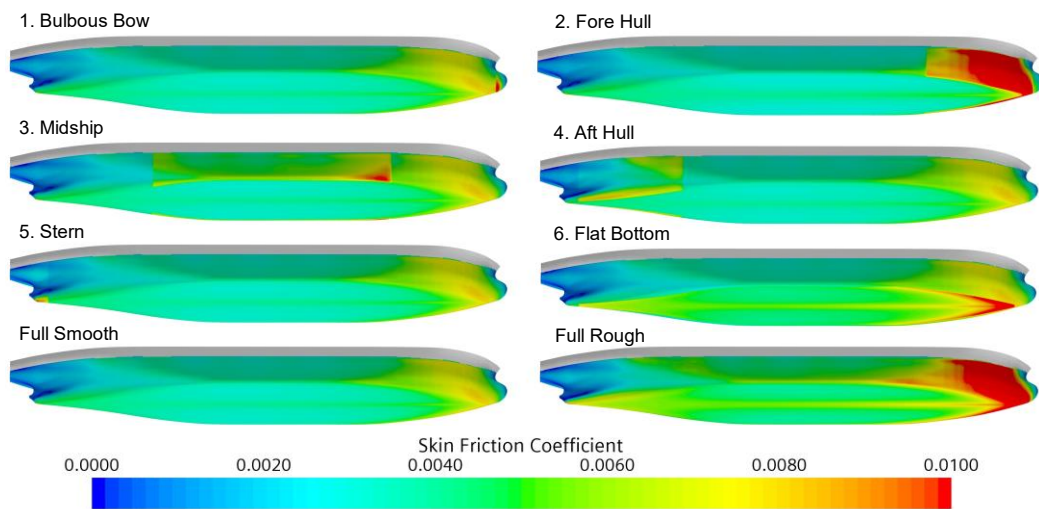
(b)

Figure 8-11. Local characteristics of the wall shear stress, τ_w, (a), and skin friction coefficients, c_f, (b) on the model KVLCC2 hull at design speed ($Fr = 0.142$).

Similarly, *Figure 8-11* presents the local wall shear stress, τ_w, and skin friction coefficients, c_f, on the KVLCC2 hull. Notably, the *Bulbous Bow* case is such as the rough region is very small compared to the whole wetted surface area. Hence, the effects of this scenario on the hydrodynamics of the KVLCC2 are minor. On the other hand, the *Fore Hull* scenario leads to the evident detriment of the hull performance. Furthermore, the c_f distribution of the *Fore Hull* case is similar to the *Full Rough* homogeneous condition.
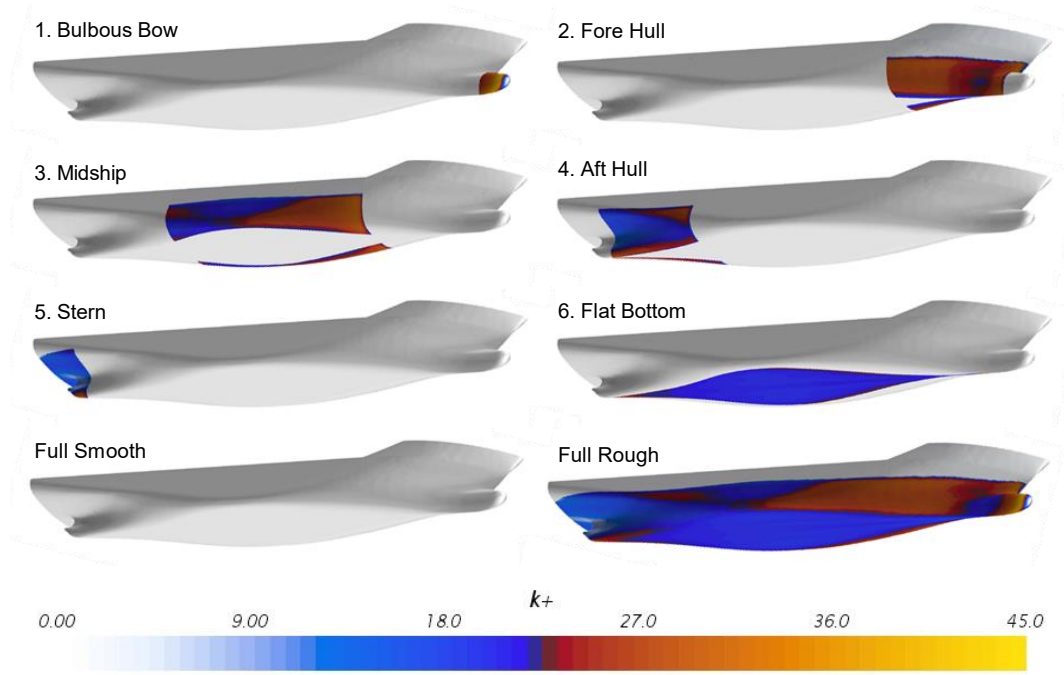
(a) KCS model
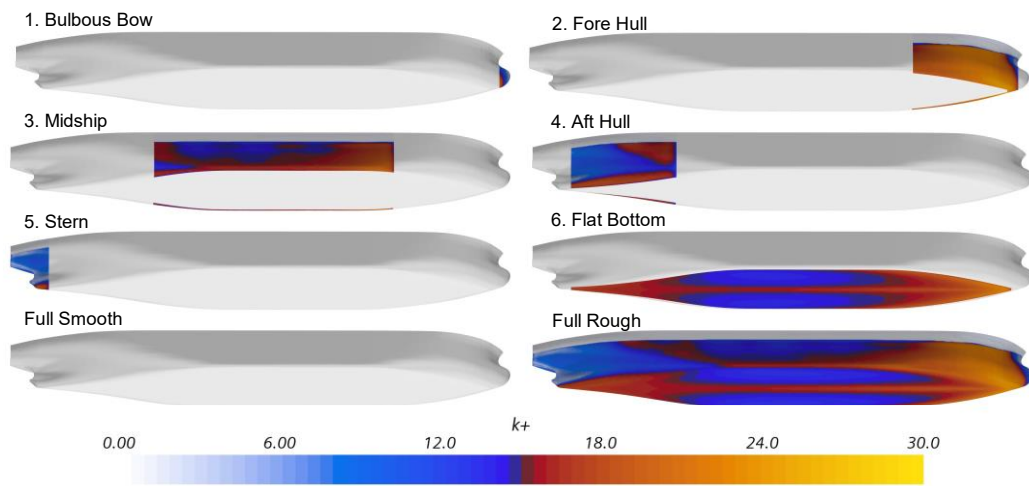
(b) KVLCC2 model

Figure 8-12. Local roughness Reynolds number characteristics, k^+, on the (a) KCS model at $Fr = 0.260$; (b) KVLCC2 model at $Fr = 0.142$.

Figure 8-12 shows the distributions of the roughness Reynolds number, k^+, on the KCS and KVLCC2 models in heterogeneous hull roughness conditions (scalar field distribution on the hull surfaces limited to $k^+ = 45.0$ and $k^+ = 30.0$, respectively). As shown in equation (8-1), the fully rough regime is reached when k^+ value is higher than 25. For the KCS model, the distributions of k^+ on the heterogeneous rough surfaces is similar to the bow regions of the homogeneous *Full Rough* case. Accordingly, configurations 1, 2 and 3 show larger k^+ values than the scenarios 4, 5 and 6 due to the observed roughness effect. Similarly, for the KVLCC2 model, the distributions of k^+ on the heterogeneous rough surfaces is complementary to the *Full Rough* case.

The observation of the local skin friction coefficients, c_f, and the roughness Reynolds numbers, k^+, are strictly related to the wall shear stress values. It is well-known that the wall shear stress, τ_w, is more significant in the bow region of ship hulls due to the active transition behaviours, and it decreases as the flow develops along the hull. Furthermore, the flow is less de-accelerated in the bow area resulting in a less developed boundary layer, i.e., a thinner boundary layer. Hence, the roughness height will occupy a larger fraction of the boundary layer, resulting in a higher skin friction coefficient. As the wall shear stress, τ_w, increases, it results in more significant local skin friction coefficients and roughness Reynolds numbers in the bow regions. Accordingly, the roughness effect in the fore regions becomes more critical than in the stern areas. Eventually, the Full Rough scenario shows a thicker boundary layer than the Full Smooth condition for the homogeneous cases.

The roughness increase affects the boundary layer thickness around the hull, which is defined as the distance between the wall and the point where the velocity magnitude of the flow parallel to the wall, V_x, reaches the proportion of 0.99 of the free-stream velocity, V_{ship}, i.e., $V_x = 0.99 V_{ship}$. *Figure 8-13* and *Figure 8-14* show another notable feature of the effect of heterogeneous hull roughness on the ship resistance, i.e., the boundary layer contours on the KCS hull in different hull roughness conditions. The boundary layer is represented by portions of transversal planes limited to the axial velocity, $V_x/V_{ship} = 0.9$
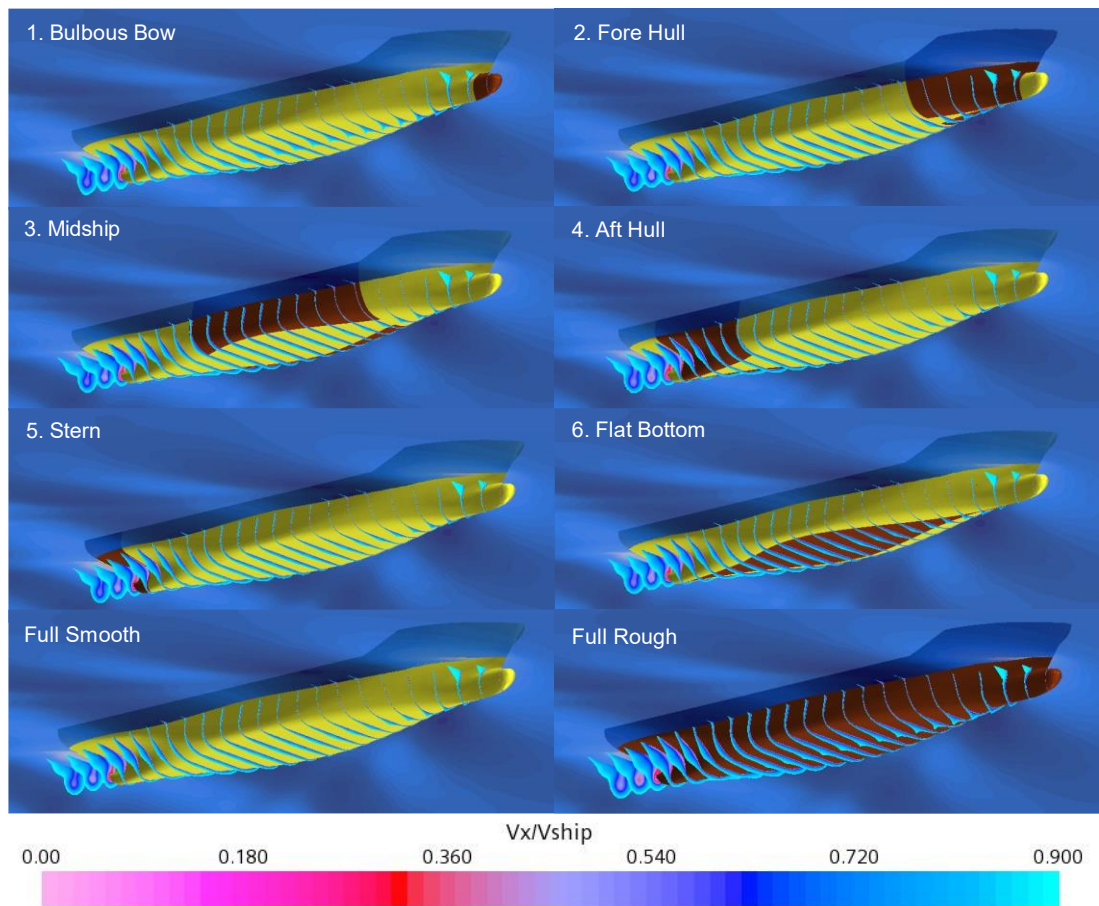
Figure 8-13. Boundary layer on the KCS model in different hull roughness conditions at design speed
$(Fr = 0.260)$.

As shown in *Figure 8-13* and *Figure 8-14*, the velocity in the turbulent boundary layer decreases with roughness on the hull surface. This velocity decrease manifests itself as an increase in frictional resistance. On the other hand, the roughness increases turbulence and turbulent kinetic energy, which means that the turbulent stress and wall shear stress increase. The present findings are in agreement with previous studies of other researchers (Song et al., 2021a, 2019; Demirel et al., 2017b; Schultz and Flack, 2007, 2005). The Full Rough scenario shows a thicker boundary layer than the Full Smooth condition for the homogeneous cases. Furthermore, for the KCS model, *Figure 8-13*, the differences between *Full Rough* and *Full Smooth* configurations become apparent in the bow regions where the increased roughness causes a thicker boundary layer, peak-shaped on the symmetry plane.
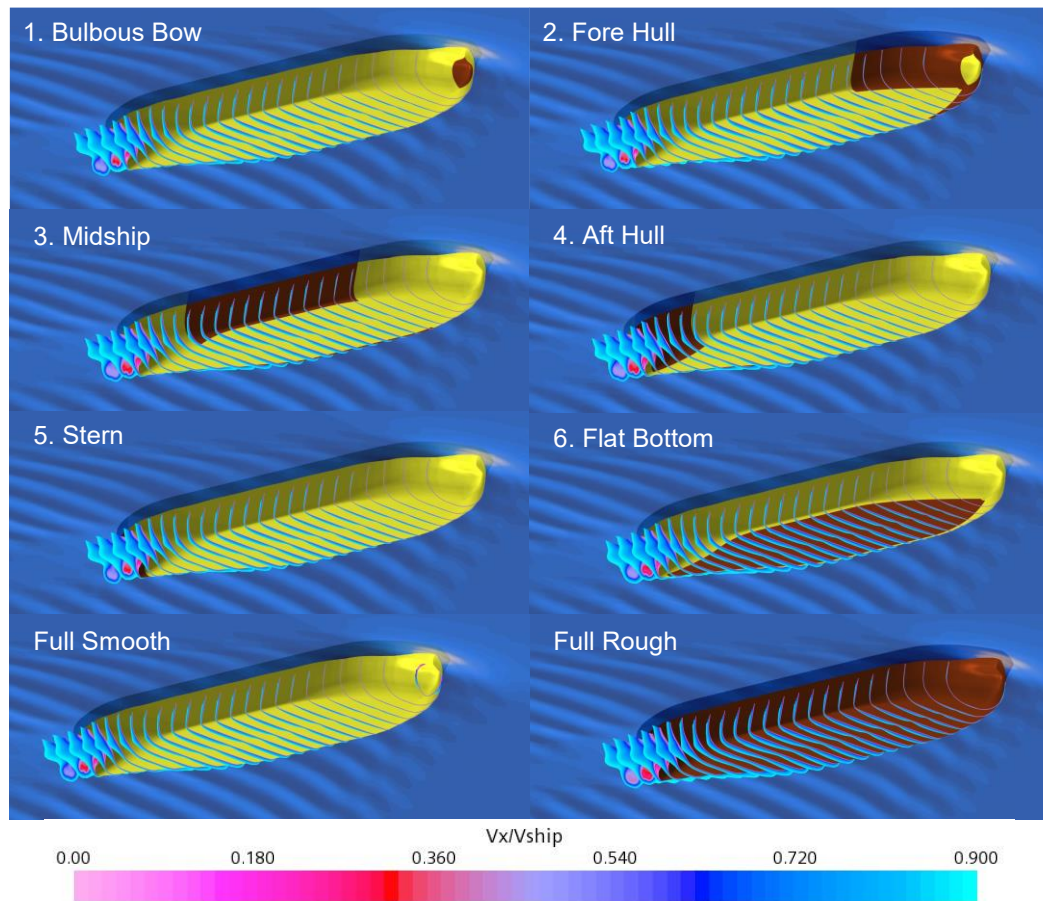
Figure 8-14: Boundary layer on the KVLCC2 model in different hull roughness conditions at design speed ($Fr = 0.142$).

Notably, the boundary layer contours shown in *Figure 8-13* present a spike at the centre plane, particularly evident in the midship area of the hull. Similarly to the spike-shaped boundary layer of the KCS case, such a recognisable shape is due to the implementation of symmetry conditions at the symmetry plane, as discussed in other research studies such as (Demirel et al., 2017a) and (Song et al., 2020c). Hence, the rationale behind the significant Roughness Impact Factor of the bulbous bow and fore regions of the hull may lie in its extensive influence on the boundary layer characteristics. Interestingly, the boundary layer of the *Bulbous Bow* case (*Figure 8-13*-1) is similar to that of the *Full Rough* condition. While, despite a similar thickness of the boundary layer, the *Fore Hull* case shows a much less evident pointy shape (*Figure 8-13*-2). On the other hand, as shown in *Figure 8-13*-3,4,5,6, the boundary layer thickness around the hull showed almost no differences compared to that of the *Full Smooth* case.

On the other hand, for the KVLCC2 model, *Figure 8-14*, the differences between *Full Rough* and *Full Smooth* configurations are minor. Notably, the boundary layer contours shown in *Figure 8-13* present a shrinkage at the centre plane, particularly evident in the Bulbous Bow and Full Rough cases. Such a recognisable shape is due to the implementation of symmetry conditions at the symmetry plane, as discussed in other research studies such as (Demirel et al., 2017a) and (Song et al., 2020c).

One may notice that understanding the roughness effect on various hydrodynamic aspects, such as the boundary layer thickness, is still limited. Therefore, additional analyses could be carried out, including broad variations in speeds, scales, and hull forms. Further investigation could exclude the free surface in the viscous pressure resistance, C_{VP}, term to illustrate that the viscous pressure resistance ratio changes (akin to the form factor). Hence, an expected result would be that roughness in the stern area would have the highest ratio of C_{VP}.

8.4. Chapter Summary and Conclusions

An investigation was carried out on the effect of heterogeneous hull roughness on ship resistance components and the characteristics of the flow around the hull. URANS-based CFD simulations were carried out on the well-known KCS and KVLCCS hull models in different hull roughness conditions. A modified wall-function approach was adopted to implement the roughness characteristics of the surfaces in the CFD model. The different scenarios studied were intended to assess the roughness effect of different parts of the hull on the ship's hydrodynamics. The observations on the effects of heterogeneous hull roughness were correlated with the rough wetted surface areas, the distributions of the local wall shear stress and skin friction coefficients, the roughness Reynolds number values, and the boundary layer characteristics. Furthermore, comparisons with the homogeneous full rough-smooth cases were presented.

The CFD towing tests showed that the rough regions tested (*Bulbous Bow*, *Fore Hull*, *Midship*, *Aft Hull*, *Stern* and *Flat Bottom*) had a different impact on the ship

resistance due to their position on the hull. A *roughness impact factor*, *RIF*, was defined to quantify this impact. The added resistance observed for the fore-rough regions was proportionately greater than for the aft-rough regions with the same surface roughness conditions. In other words, the roughness conditions of the fore regions proportionally affect the ship hydrodynamics more than the aft regions. The present chapter supported similar observations of other researchers (Song et al., 2021a, 2019; Demirel et al., 2017b; Schultz and Flack, 2007, 2005).

The numerical investigation presented in this chapter provides valuable results from a practical point of view. The roughness impact of different hull regions has been investigated, adopting a widely accepted and validated CFD approach. Interestingly, the present findings showed that among all the scenarios, the rough *Bulbous Bow* condition of the KCS model presents the greatest roughness impact factor ($RIF =$ 2.26), despite the smallest percentage of rough wetted surface area. Thus, the rough bulbous bow scenario led to proportionately greater added resistance than other rough regions of the hull.

Therefore, partial hull cleaning of the bow part would be more beneficial than cleaning an equal surface area in another part of the wetted surface. On the other hand, the rough *Stern* case of the KCS model presents a smaller roughness impact factor ($RIF =$ 0.44), suggesting the surface conditions of the aft regions of the hull have a minor impact on ship resistance. Naval architects, ship owners, and operators could benefit from this chapter's insight and target limited-time maintenance on the fore-hull regions affecting the ship resistance the most. When complete maintenance on the entire hull is not feasible, it could be worth cleaning the fore hull parts first.

This chapter provided several significant findings, including the definition of the roughness impact factor to assess the effect of heterogeneous hull roughness on ship resistance. Intuitively, the hull roughness causes substantial increases in the frictional resistance regardless of the heterogeneous configurations. However, it is worth considering that hull areas are characterised by specific wall shear stress and heterogeneous surface roughness distributions affecting the ship resistance differently. Areas of the hull with low wall shear stress would likely be heavily fouled and vice-

versa. A rougher surface would characterise the most degraded areas. Detailed correlations between heterogeneous hull roughness distributions and the occurrence probability on specific hull parts could be further analysed.

It may be demonstrated that the higher the wall-shear stress, the lower the probability of that hull region experiencing severely increased roughness. Although this phenomenon is not yet well documented in the literature, it is known that higher stress on "Foul Release Coatings" implies minor biofouling accumulation. On the other hand, for vessels coated with "Self-Polishing Coatings", higher stress implies that these coatings are worn off faster and, when wholly depleted, would increase bioaccumulation. Nevertheless, it is well demonstrated that fouling organisms attach more easily to stationary vessels as neither "Self-Polishing Coatings" nor "Foul Release coatings" are effective for stationary vessels. It is evident that the parameter most influencing the hull roughness for ships that spend longer time stationary would not be the wall-shear stress. For stationary ships, other parameters, such as light exposure, would perhaps lead to a more severe heterogeneous distribution of hull roughness.

It is expected that, for the propulsion of ships, the hull surface roughness will significantly affect ship resistance as the wake can be affected significantly. Therefore, the numbers presented in the present study are not the whole story leading to assessing fuel consumption effects. Future studies could compare the numerical results presented in this research with measurements obtained from EFD tow tests and investigate self-propulsion simulations. Further heterogeneous hull roughness configurations, in model and full scale, and their effect on ship resistance could be investigated. Further investigations could also exploit the relationship between hull roughness distribution and vortex development, pressure distribution, turbulence kinetic energy, vorticity, flow recovery, and wake development.

9. Discussions and Conclusions

9.1. Introduction

This chapter summarises and discusses the work carried out within this thesis. In Section 9.2 the achievement of specific research aims and objectives is discussed. Section 9.3 discusses the main conclusions of this thesis, while the novelties and contributions to the field are defined in Section 9.4 Section 9.5 presents the general discussions, and recommendations for future work are given in Section 9.6. Finally, Section 10.7 lists the main research outputs produced throughout this PhD study.

9.2. Achievement of Research Aims and Objectives

The main aim of this PhD was defined in Chapter 1 as being "*to investigate the effect of fouling control coatings and heterogeneous hull roughness on ship hydrodynamics*". This ultimate aim was achieved by realising specific objectives within each chapter and combining them to form one complete investigation.

The specific objectives listed in Chapter 1 were achieved as follows:

- Chapter 4 achieved the objective "*to obtain new experimental roughness functions for commonly used marine coatings, including a recently developed hard foul-release coating and mimicked biofouled hull conditions using the state-of-the art Fully Turbulent Flow Channel facility (FTFC) of the University of Strathclyde to contribute to the international database of the roughness functions*" by investigating the hydrodynamics of fouling control coatings and mimicked biofouling using a flow cell. Experimental roughness function data were developed from the "young" fully turbulent flow channel facility of the University of Strathclyde (UoS). Different surfaces, including a hard foul-release coating, were tested. Finally, Chapter 4 can also serve as a valuable

guide for future experimental campaigns using the fully turbulent flow channel facility of the UoS and the corresponding development of roughness functions.

- Chapter 5 achieved the objective "*to carry out flat plate towing test in smooth and rough surface conditions by conducting hydrodynamic experiments with the state-of-the art towing tank facility of the University of Strathclyde (UoS) to compare the roughness functions obtained from FTFC for the same surface and demonstrate the advantages of the FTFC*" by investigating the hydrodynamics of mimicked biofouling on a flat plate using towing tank experiments. The towing tank facilities of Kelvin Hydrodynamics Laboratory (KHL) of the University of Strathclyde were used. Experimental roughness function data were developed from the towing tests on a flat plate homogenously coated with 220-grit sand-grain equivalent roughness (*Sand 220*). Eventually, the results of the experimental campaign in terms of roughness functions values were compared with those obtained from FTFC tests. Finally, Chapter 5 can also serve as a valuable guide for future towing tests using flat plates in smooth and rough conditions and the corresponding roughness functions development.

- Chapter 6 and Chapter 7 achieved the objective "*to investigate the resistance and powering characteristics of the full-scale KRISO containership (KCS) using Granville's similarity law scaling procedure and CFD in realistic hull roughness conditions by embedding the FTFC experimental results Additionally, to compare the results obtained from the two methods and demonstrate their effectiveness in understanding the impact of hull roughness on ship resistance*" by conducting Granville's similarity law scaling procedure (Granville, 1978) to investigate the effect of hull roughness on ship hydrodynamics. Notably, the roughness characteristics of the surfaces tested in the Fully Turbulent Flow Channel from Chapter 4 were used. Finally, the full-scale KCS hull was selected for the numerical predictions, and different speeds were investigated. Hence, a design speed of 24 knots ($Fr = 0.260$) as used in similar studies (Ravenna et al., 2022a; Song et al., 2020c). Notably, a lower and less investigated speed of 16 knots ($Fr = 0.173$) was considered in

Chapter 6. Furthermore, by embedding the newly developed roughness functions of the fouling control coatings and sanded surfaces from Chapter 4 in CFD simulations. Notably, the modified wall function approach was used in Star-CCM+ software to provide scale-up results to ship length for the full-scale KCS hull at 24 and 16 knots. Finally, the results obtained from CFD simulations in Chapter 7 and Granville's method on the full-scale KCS hull were compared and discussed.

- Chapter 8 achieved objective "t*o investigate the hydrodynamics effects of heterogeneously distributed hull roughness on KCS and KVLCC2 (KRISO very large crude carrier) models and introduce a new factor to correlate the added resistance of the heterogeneous roughness areas to their rough wetted surface area and corresponding increased added resistance. Additionally, to discuss the results of the study in order to shed light on possible biofouling management strategies for ship owners and operators and to critically summarise the main findings and novelty of this thesis in order to identify the opportunities for future research*" by carrying out URANS-based CFD simulations on the well-known KCS and KVLCCS hull models in heterogeneous hull roughness conditions. A modified wall-function approach was adopted to implement the roughness characteristics of the surfaces tested in Chapter 4 in the CFD model. The different scenarios studied were intended to assess the roughness effect of different parts of the hull on the ship's hydrodynamics. The observations on the effects of heterogeneous hull roughness were correlated with the rough wetted surface areas, the distributions of the local skin friction coefficients, the roughness Reynolds number values, and the boundary layer characteristics. Furthermore, comparisons with the homogeneous full rough-smooth cases were presented. Last but not least, a new measure called *Roughness Impact Factor*, *RIF*, was defined in Chapter 8 to predict the impact of different rough regions on ship resistance.

9.3. Novelties and Contributions

The main novelty introduced within this PhD research ia given as follows:

- To the best of the author's knowledge, this is the first time that a measure to quantify the relative impact of heterogeneous hull roughness varying with rough surface's position has been proposed. The so-called *Roughness Impact Factor* (*RIF*) can be used as a practical tool to make an informed decision on biofouling maintenance strategies.

This was achieved by conducting extensive URANS CFD simulations with the modified wall function approach in several heterogeneously distributed hull roughness conditions on the KCS and KVLCC2 hulls. Model and full-scale simulations were conducted at different speeds with different roughness functions mimicking biofouled surfaces.

Other main contributions made to the field within this PhD study are listed below:

- The first-ever roughness functions of a new-generation hard-foul release marine coating and other fouling control coatings (FCCs) were determined and provided.

- A flat plate coated with mimicked medium-light slime was towed in the KHL test tank at different speeds, and in-house roughness functions data was determined.

- The results of the towing test on a flat plate coated with mimicked medium-light slime were compared with the FTFC results for the same surface, confirming the accuracy of the roughness function models determined.

- The findings from the first-ever extensive CFD study on KCS and KVLCC2 hulls of the impact of the roughness locations on the ship added resistance can be useful to increase the understanding of the roughness effect on ship resistance.

9.4. General Discussion

This work was based on a balanced combination of experimental and numerical methods. The experiments, including the pressure drop measurements with the Fully Turbulent Flow Channel, were carried out to develop the roughness functions (i.e., hydrodynamics fingerprints) of the conveniently prepared test surfaces. Afterwards, Granville's similarity law scaling procedure and CFD-based numerical (i.e., modified wall function approach) were used to predict the effects of the test surfaces on ship hydrodynamics. Notably, the motivations behind this work, literature gaps and overall methodology adopted to achieve the aim and objectives of the present thesis were clearly discussed in Chapter 1, Chapter 2, and Chapter 3, respectively.

Afterwards, Chapter 4 showed that the indirect method for pipes could be used to determine the drag characteristics of surfaces. The first step was to conduct pressure drop measurements on rough surfaces with the Fully Turbulent Flow Channel (FTFC) facility at Kelvin Hydrodynamics Laboratory (KHL), University of Strathclyde (UoS). Several experimental challenges were tackled to carry out these experiments. Above all, leakages from the test frame were the most complicated and were typically avoided by tightening the bold uniformly and in a specific sequence (according to the manufacturer's specifications). Furthermore, as the test plates were outsourced, ensuring manufacturing within specific tolerances was challenging. For example, the inner and outer dimensions of the plates are both relevant to guarantee good outcomes of the experiments (i.e., avoiding leakages). Notably, sometimes it was necessary to smoothen the plates' corners on the spot to guarantee fit within the FTFC test frame. Nevertheless, the tests showed excellent accuracy across all cases once it was guaranteed perfect fit and flushness with the flow.

As mentioned, an advantage of operating the FTFC, compared to the towing tests, is that one person alone is enough to handle the plates and carry out experiments safely and in a short time (sufficient settling time between each run must be guaranteed). Further challenges were also keeping consistent equipment maintenance (i.e., filters, valves, and gauges). Finally, it is of note that the FTFC tests were repeated at a different time of the day following the complete dismantling and remounting of the

test plates to account for the bias of the machinery. Following the pressure drop measurements, the indirect method for pipes (Granville, 1987) depicted in Chapter 4 was used to determine the roughness functions of the rough surfaces tested in the FTFC. Unfortunately, as mentioned earlier, no unique roughness function model exists to describe every surface.

Chapter 5 showed that the overall (towed plate) method could be used to determine the drag characteristics of surfaces. The challenges experienced during the towing tests were numerous compared to the FTFC tests. Firstly, not only driving the carriage but also handling the heavy stainless-steel plates required the support of technicians and special equipment. Furthermore, once mounted on the carriage using expensive ad-hoc supports and transducers, the alignment of the flat plate was checked. Since poor alignment would create side forces and the zero-pressure gradient condition would not be met, the alignment phase is difficult and time-consuming. Afterwards, once the alignment is set, no alterations should be made to the set-up. Therefore, the changing times between different surfaces were very long compared to the turnaround time of the FTFC tests. Hence, e.g., one week of towing tank tests led to the development of roughness function data for a single surface, while at the same time, the drag characteristics of six surfaces were acquired from the FTFC. Finally, a disadvantage of the towing tank (overcome by the FTFC) is the limited maximum Reynolds number achievable.

It was clearly shown in Chapter 6 that Granville's similarity law scaling is an effective prediction method for the effects of hull roughness on ship resistance. As discussed in Chapter 6, the advantage of this method is that the results are immediately obtained by changing the inputs in the prediction code. However, this method can only predict the frictional resistance of flat plates, hence, of flat plates of any given ship length. Another weakness of the method might be attributed to the unrealistic assumption of one single roughness Reynolds number and roughness function for a given speed and surface condition. Furthermore, the roughness effect predicted by this method leads the user to have an assumption that only frictional resistance is affected by the surface roughness. That is to say, the similarity law scaling procedure requires much less time than the CFD simulations. Notably, the longer run times of CFD simulations are not

due to the application of roughness function models. In other words, employing new roughness function models by modifying wall-functions does not cause any additional run-time to the CFD simulations, as shown in Chapter 7.

It was clearly shown in Chapters 7 that CFD could be effectively used to predict the effects of fouling control coatings and heterogeneous hull roughness on ship resistance. Furthermore, it was demonstrated how different types of roughness could be embedded in the CFD software by modifying the wall-function settings once the relationship between the roughness functions and roughness Reynolds numbers of each surface is known. Another challenge was the selection of roughness function models representing the roughness function behaviours of the coatings and biofouling conditions for CFD simulations. The built-in roughness function model of StarCCM+ software described in Chapter 7 is in the form of the roughness functions of the uniform, closely packed sand roughness of Nikuradse (Nikuradse, 1933).

The challenges in processing the roughness functions data for the fouling control coatings (FCCs) and sanded surfaces were rising from curve fitting the results (mainly the negative roughness functions leading to improved ship resistance) to the reference model (i.e., Nikuradse-type roughness function model) by selecting the suitable roughness length scale, k. Hence, reasonable approximations were made that would not significantly affect the results or the validity of the proposed models. Notably, as mentioned earlier, the roughness functions values are independent of the roughness Reynolds number and hence independent of the selection of k since it only affects the roughness Reynolds number values, k^+. It is of note that the roughness function models chosen in the present study were based on the experimental data collected from the present FTFC and towing test compared to those available in the literature, and they may not necessarily work for other surfaces or every kind of coating or fouling condition. Even if models can be developed to correlate the roughness statistics to the roughness functions, the debate behind this correlation between the surfaces and roughness functions was beyond the scope of this thesis.

Having said that, further technical difficulties were experienced while running the CFD simulations. The most challenging issue was the instability of the simulations

when the modified wall-function was applied, especially in heterogeneous scenarios of Chapters 8. This issue was not consistent across different hulls, surface conditions, and heterogeneous scenarios. Therefore, different solutions were used after several trials and errors. On the one hand, generating a very fine mesh would increase the accuracy of the results; on the other hand, it would dramatically increase the run time. Therefore, the most effective solution was applying local mesh refinements where the hull surface conditions transitioned from smooth to rough or vice versa. Notably, by performing grid-dependence studies, it was possible to verify the validity of the simulations. Also, changing the boundary condition to a rough surface after the simulation settles down for the smooth case further helped save computational time.

Further challenges experienced in Chapters 8 for the CFD simulations in heterogeneous conditions were the design of geometry and boundary conditions. Several heterogeneous hull roughness scenarios were designed based on possible biofouling management strategies. Finally, considering that different hull types were tested at different speeds in homogeneous and heterogeneous conditions with the same roughness function model developed experimentally, the resulting test matrix accounted for many test cases. Therefore, it was challenging to post-process the conspicuous data from the numerous CFD simulations and present them in readable tables and figures.

9.5. Main Conclusions

The main conclusions drawn from the present thesis are listed below:

- Chapter 1 "*Introduction*" concluded that ignoring the vessel's underwater hull conditions is a major cause of considerable losses to a fleet's economy. Numerical methods can be used to predict the hull roughness effect on ship resistance, provided that the roughness functions of the hull surfaces are known. However, no universal roughness function can represent all surfaces. Therefore, the roughness functions – hydrodynamic fingerprints of any given surface – must be developed experimentally.

- Chapter 2 "*Literature Review*" concluded that our understanding of the hull roughness effect on ship resistance is limited to date. Several limitations, such as the absence of roughness function models that represent all types of fouling control coatings and conditions, were identified. The review suggested further predictions of hull roughness effects at different scales and velocities using CFD simulations and Granville's similarity law. Last but not least, investigating heterogeneous hull roughness distribution's impact on different regions of the hull could enable targeted maintenance strategies and improved understanding of its effect on resistance.

- Chapter 3 "*Methodology*" concluded that the current approach of this thesis is to tackle the effect of ship hull roughness, including fouling control coatings and biofouling, by combining experimental and numerical methods. Therefore, the results of FTFC and towing tank experiments were combined to similarity law scaling and CFD predictions.

- Chapter 4 "*Modelling the Hydrodynamics Characteristics of Realistic Surfaces: Fully Turbulent Flow Channel*" concluded that the FTFC experiments to predict the effect of hull roughness on full-scale ship resistance and powering have several advantages compared to other methods such as towing tests. Additionally, this chapter introduced experimental roughness functions for the FCCs tested, including the GIT-*FR02* hard foul-release coating.

- Chapter 5 "*Modelling the Hydrodynamics Characteristics of Realistic Surfaces: Towing Tank Tests*" concluded that the roughness functions values obtained from the towing tests showed excellent agreement with the FTFC roughness functions, therefore, validating the methods. Experimental roughness function data were developed from the towing tests on a flat plate homogenously coated with 220 grit sand-grain equivalent roughness (*Sand 220*) as done with the FTFC plates.

- Chapter 6 "*Predicting the Effects of Fouling Control Coatings on Ship Hydrodynamics: Similarity Law Scaling*" concluded that among the four

fouling control coatings (FCCs) that were tested in the FTFC, GIT-*FR02* coating (hard foul-release) displayed the best hydrodynamic performance across the entire Reynolds number range. Furthermore, the chapter showed the application of Granville's similarity law scaling procedure with high-performing FCCs exhibiting negative roughness functions.

- Chapter 7 "*Predicting the Effects of Fouling Control Coatings on Ship Hydrodynamics: Computational Fluid Dynamic*" confirmed that the GIT-*FR02* hard foul-release coating displayed the best hydrodynamic performance. Furthermore, the chapter showed the procedure to conduct CFD hydrodynamics prediction on full-scale ships as well. Finally, roughness functions models for marine surfaces were introduced.

- Chapter 8 "*CFD Predictions of the Effects of Heterogeneous Hull Roughness on the KCS & KVLCC2 Models*" concluded that the rough regions tested had a different impact on the ship resistance due to their position on the hull. Specifically, the surfaces of the fore part of the ship have a greater impact on the ship's hydrodynamics than the surfaces of the aft part. This different impact was quantified by defining a so-called *roughness impact factor (RIF).* Finally, the *RIF* of all the heterogeneous hull roughness scenarios was calculated for the KCS and KVLCC2 models showing high values for the fore parts in both cases, suggesting that these need extra attention within targeted biofouling management strategies.

9.6. Recommendations for Future Research

1. In Chapter 4 and Chapter 5 it was emphasised that there is an enormous opportunity for growth in the area of research on modelling roughness characteristics especially from FTFC experiments. Further coating products and surface roughness conditions can be tested.

2. In Chapter 6 and Chapter 7 it was recommended that further investigation should also be conducted on predicting the resistance of fouling control coatings (FCCs) at different speeds and with different ship hulls at different scales and using heterogeneous patch distribution of the roughness.

3. In Chapter 7 was mentioned that it will also be beneficial to investigate the hydrodynamic performance of the same fouling control coating under the effect of biofouling growth.

4. Chapter 7 suggested that applying different mimicked biofouling to the panels before or after the coating application could also help to predict the resistance behaviour of the as-applied condition to an existing rough ship hull.

5. Chapter 8 emphasised that further investigations could exploit the relationship between hull roughness distribution and vortex development, pressure distribution, turbulence kinetic energy, vorticity, flow recovery, and wake development.

6. In Chapter 8 it was recommended that detailed correlations between heterogeneous hull roughness distributions and the occurrence probability on specific parts of the hull could be analysed.

7. Finally, Chapter 8 suggested that future studies could compare the numerical results presented in this thesis with measurements obtained from towing tank experiments.

9.7. Research Outputs

The following publications were generated throughout the timespan of the PhD study.

9.7.1. Scientific Journal Papers

1. **Ravenna, R.**, Ingham, R., Song, S., Johnston, C., De Marco Muscat-Fenech, C., Tezdogan, T., Atlar, M., Demirel, Y. K. (2022) *"Predicting the Effect of Hull Roughness on Ship Resistance using a Fully Turbulent Flow Channel"*, Journal of Marine Science and Engineering, 10, 1863, https://doi.org/10.3390/jmse10121863.

2. **Ravenna, R.**, Song, S., Shi, W., Sant, T., De Marco M. F., C., Demirel, Y. K., (2022) *"CFD Analysis of the effect of Heterogeneous Hull Roughness on Ship Resistance"*, Ocean Engineering, 257, 111733, https://doi.org/10.1016/j.oceaneng.2022.111733.

3. **Ravenna, R.**, Marino, A., Song, S., Atlar, M., Turan, O., Day, S., Demirel, Y. K., (2022) *"Experimental Study on the Effect of Biomimetic Tubercles on the Drag of a Flat Plate"*, Ocean Engineering, 225, 111445, https://doi.org/10.1016/j.oceaneng.2022.111445.

4. Song, S., **Ravenna, R.,** Dai, S., De Marco Muscat-Fenech, C., Tani, G., Demirel, Y.K., Atlar, M., Day, S., Incecik, A., (2021) *"Experimental investigation on the effect of heterogeneous hull roughness on ship resistance"*, Ocean Engineering, 223, 108590, https://doi.org/10.1016/j.oceaneng.2021.108590.

9.7.2. International Conference Papers

1. **Ravenna, R.**, Marino, A., Song, S., Demirel, Y. K., Atlar, M., & Turan, O., *"Experimental Investigation on the Effect of Biomimetic Tubercles on the Hydrodynamics of a Flat Plate"*. Paper presented at the Sixth International Conference on Advanced Model Measurement Technology for The Maritime Industry (AMT'19), 9-11 October 2019, Rome, Italy.

2. **Ravenna, R.,** Ingham, R., Song, S., Johnston, C., De Marco Muscat-Fenech, C., Tezdogan, T., Atlar, M., Demirel, Y.K., *"Predicting the Effect of Hull Roughness on Ship Resistance using a Fully Turbulent Flow Channel and*

CFD", 4th International Meeting of the A. Yucel Odabasi Colloquium Series on Ship Design & Optimization and Energy Efficient Devices for Fuel Economy (AYOCOL 2022), 15-16 December 2022, Istanbul, Turkey.

3. **Ravenna, R.**, Song, S., Shi, W., Sant, T., De Marco M. F., C., Demirel, Y. K., "*CFD Analysis of the effect of Heterogeneous Hull Roughness on Ship Resistance*", 2nd International Congress on Ship and Marine Technology (GMO-SHIPMAR-2021), 16-17 September 2021, Istanbul, Turkey.

9.7.3. Abstracts / Conference Presentations

1. **Ravenna, R.**, "*CFD Analysis of the effect of Heterogeneous Hull Roughness on Ship Resistance*", a Virtual and physical ExperimeNtal Towing centre for the design of eneRgy Efficient sea-faring vessels (VENtuRE H2020) – Annual Postgraduate Conference, University of Malta, 16-20 May 2022, Malta.

2. **Ravenna, R.**, *"The Effects of Fouling Control Coating and Heterogeneous Hull Roughness on Ship Resistance"* a Virtual and physical ExperimeNtal Towing centre for the design of eneRgy Efficient sea-faring vessels (VENtuRE H2020) – Annual Postgraduate Conference, University of Genova, 12 September 2022, Genoa, Italy.

3. **Ravenna, R.**, *"The Effect of Fouling Control Coating and Heterogeneous Biofouling on Ship Resistance"* a Virtual and physical ExperimeNtal Towing centre for the design of eneRgy Efficient sea-faring vessels (VENtuRE H2020) – Annual Postgraduate Conference, University of Genova, 31 May-1 June 2021, Genoa, Italy.

4. **Ravenna, R.**, "*CFD Analysis of the effect of Heterogeneous Hull Roughness on Ship Resistance*" Ocean Energy and Maritime Transport Conference (OEMT 2022) – Annual Postgraduate Conference, University of Strathclyde, 15-16 June 2022, Glasgow, UK.

5. **Ravenna, R.**, *"Biofouling Management - The Effect of Fouling Control Coating and Heterogeneous Biofouling on Ship Resistance"* Ocean Energy and Maritime Transport Conference (OEMT 2021) – Annual Postgraduate Conference, University of Strathclyde, 16-17 June 2021, Glasgow, UK.

9.7.4. Project Reports / Presentations

1. **Ravenna, R.**, Song, S., Demirel, Y.K., *"Measurements of frictional resistance on Graphite Innovation & Technologies (GIT) marine coatings using a Fully Turbulent Flow Channel (FTFC)"*, 6 December 2022, Halifax, Canada.

2. **Ravenna, R.**, Patryniak, K., Huang, Y., *"IEEE Oceanic Engineering Society (OES) -Strathclyde Chapter Annual Report for the OCEANS 2022 Hampton Roads International Conference for global maritime professional"*, 17-20 October 2022, Virginia Beach, US.

3. **Ravenna, R.**, Atimati, E., Crewdson, G., *"The Doctoral Researchers Group (DRG) in bullet points – Annual Report for the Postgraduate Induction 2022 organised by Strathclyde Doctoral School (SDS)"*, 6 June 2022, University of Strathclyde, Glasgow, UK.

References

Andersson, J., Oliveira, D.R., Yeginbayeva, I., Leer-Andersen, M., Bensow, R.E., 2020. Review and comparison of methods to model ship hull roughness. Applied Ocean Research 99, 102–119.

Andrewartha, J., Perkins, K., Sargison, J., Osborn, J., Walker, G., Henderson, A., Hallegraeff, G., 2010. Drag force and surface roughness measurements on freshwater biofouled surfaces. Biofouling 26, 487–496.

Atlar, M., 2008. An Update on Marine Antifoulings, in: 25th ITTC Group Discussions 3–Global Warming and Impact on ITTC Activities, Fukuoka, Japan.

Atlar, M., Yeginbayeva, I.A., Turkmen, S., Demirel, Y.K., Carchen, A., Marino, A., Williams, D., 2018. A Rational Approach to Predicting the Effect of Fouling Control Systems on "In-Service" Ship Performance. GMO Journal Of Ship And Marine Technology 24, 5–36.

Benson, J.M., Ebert, J.W., Beery, T.D., 1938. Investigation in the NACA Tank of the Effect of Immersion in Salt Water on the Resistance of Plates Coated With Different Shipbottom Paints, N.A.C.A. Memorandum Report C&R C.

Busch, J., Barthlott, W., Brede, M., Terlau, W., Mail, M., 2019. Bionics and green technology in maritime shipping: an assessment of the effect of Salvinia air-layer hull coatings for drag and fuel reduction. Philosophical Transactions of the Royal Society A: Mathematical, Physical and Engineering Sciences 377, 218–263.

Candries, M., 2001. Drag, Boundary-layer and roughness characteristics of marine surfaces coated with antifoulings. University of Newcastle.

Candries, M., Atlar, M., 2004. Experimental Investigation of the Turbulent Boundary Layer of Surfaces Coated With Marine Antifoulings. Journal of Fluids Engineering 127, 219–232.

Candries, M., Atlar, M., Anderson, C.D., 2003. Estimating the impact of new-generation antifoulings on ship performance: the presence of slime. Journal of Marine Engineering & Technology 2, 13–22.

Cebeci, T., Bradshaw, P., 1977. Momentum transfer in boundary layers, Hemisphere Publishing Corporation; Washington, D.C., McGraw-Hill Book Co., New York.

Celik, I., Ghia, U., Roache, P., Freitas, C., Coleman, H., Raad, P., 2008. Procedure for Estimation and Reporting of Uncertainty Due to Discretization in CFD Applications. Journal of Fluids Engineering 130, 11–18.

Chambers, L.D., Stokes, K.R., Walsh, F.C., Wood, R.J.K., 2006a. Modern approaches to marine antifouling coatings. Surface and Coatings Technology 201, 3642–3652.

Chambers, L.D., Walsh, F.C., Wood, R.J.K., Stokes, K.R., 2006b. World maritime technology conference. ICMES Proceedings, The Institute of Marine Engineering, Science and Technology.

Champ, M.A., 2003. Economic and environmental impacts on ports and harbors from

the convention to ban harmful marine anti-fouling systems. Marine Pollution Bulletin 46, 935–940.

Clauser, F.H., 1956. The turbulent boundary layer. Advances in applied mechanics 4, 1–51.

Colebrook, C.F., Inst, A.M.C.E., Thomas, M., 1939. A New Theory of Turbulent Flow in Liquids of Small Viscosity. Journal Inst. C.E 11, 611–630.

Colebrook, C.F., White, C.M., 1937. Experiments with fluid friction in roughened pipes. Proceedings of the Royal Society of London. Series A-Mathematical and Physical Sciences 161, 367–381.

Coleman, H.W., Steele, W.G., 2012. Engineering application of experimental uncertainty analysis. AIAA Journal 33, 1888–1896.

Coleman, H.W., Steele, W.G., 1999. Experimentation, validation, and uncertainty analysis for engineers. John Wiley & Sons, Inc.

Coraddu, A., Oneto, L., Baldi, F., Cipollini, F., Atlar, M., Savio, S., 2019. Data-driven ship digital twin for estimating the speed loss caused by the marine fouling. Ocean Engineering 186, 106063.

Dafforn, K.A., Lewis, J.A., Johnston, E.L., 2011. Antifouling strategies: History and regulation, ecological impacts and mitigation. Marine Pollution Bulletin 62, 453–465.

Davis, A., Williamson, P., 2002. Marine biofouling: a sticky problem. Biologist 49, 1–5.

Dean, R.B., 1978. Reynolds number dependence of skin friction and other bulk flow variables in two-dimensional rectangular duct flow. Journal of Fluids Engineering 100, 215–223.

Demirel, Y.K., 2015. Modelling the Roughness Effects of Marine Coatings and Biofouling on Ship Frictional Resistance. University of Strathclyde, Glasgow, UK.

Demirel, Y.K., Khorasanchi, M., Turan, O., Incecik, A., 2014. CFD approach to resistance prediction as a function of roughness, in: Transport Research Arena CNIT. Puteaux, France.

Demirel, Y.K., Song, S., Turan, O., Incecik, A., 2019. Practical added resistance diagrams to predict fouling impact on ship performance. Ocean Engineering 186, 106–112.

Demirel, Y.K., Turan, O., Incecik, A., 2017a. Predicting the effect of biofouling on ship resistance using CFD. Applied Ocean Research 62, 100–118.

Demirel, Y.K., Uzun, D., Zhang, Y., Fang, H.-C., Day, A.H., Turan, O., 2017b. Effect of barnacle fouling on ship resistance and powering. Biofouling 33, 819–834.

Denny, M.E., 1951. BSRA resistance experiments on the Lucy Ashton: part I–full-scale measurements. Trans INA 93, 40–57.

Doble, M., Kumar, R., 2014. Polymers in a Marine Environment. Smithers Rapra.

Dogrul, A., Song, S., Demirel, Y.K., 2020. Scale effect on ship resistance components

and form factor. Ocean Engineering 209, 107–128.

Eça, L., Hoekstra, M., 2011. Numerical aspects of including wall roughness effects in the SST k–ω eddy-viscosity turbulence model. Computers & Fluids 40, 299–314.

Farkas, A., Degiuli, N., Martić, I., 2018. Towards the prediction of the effect of biofilm on the ship resistance using CFD. Ocean Engineering 167, 169–186.

Farkas, A., Song, S., Degiuli, N., Martić, I., Demirel, Y.K., 2020. Impact of biofilm on the ship propulsion characteristics and the speed reduction. Ocean Engineering 199, 107–133.

Ferziger, J.H., Perić, M., Street, R.L., 2020. Computational Methods for Fluid Dynamics. Springer International Publishing.

Flack, K.A., Schultz, M.P., 2010. Review of Hydraulic Roughness Scales in the Fully Rough Regime. Journal of Fluids Engineering 132.

Flack, K.A., Schultz, M.P., Barros, J.M., Kim, Y.C., 2016. Skin-friction behavior in the transitionally-rough regime. International Journal of Heat and Fluid Flow 61, 21–30.

Froude, W., 1872. Experiments on the surface-friction experienced by a plane moving through water. British Association for the Advancement of Science 42, 118–124.

Ganapathisubramani, B., Hutchins, N., Monty, J.P., Chung, D., Marusic, I., 2012. Amplitude and frequency modulation in wall turbulence. J. Fluid Mech 712, 61.

Gehrke, T., Sand, W., 2003. Interactions between microorganisms and physiochemical factors cause MIC of steel pilings in harbors (ALWC), in: CORROSION 2003. OnePetro, San Diego, California, USA.

George, W.K., 2007. Is there a universal log law for turbulent wall-bounded flows? Philosophical Transactions of the Royal Society A: Mathematical, Physical and Engineering Sciences 789–806.

GIT, 2021. Graphite Innovation and Technologies – Smart protective marine coatings [WWW Document]. URL https://www.grapheneenterprise.ca/ (accessed 11.25.22).

Granville, P.S., 1987. Three indirect methods for the drag characterization of arbitrarily rough surfaces on a flat plates. Journal of Ship Research 31, 70–77.

Granville, P.S., 1978. Similarity-law characterization methods for arbitrary hydrodynamic roughnesses. Bethesda: Rockville, MD, USA.

Granville, P.S., 1958. The Frictional Resistance and Turbulent Boundary Layer of Rough Surfaces. Journal of Ship Research 2, 52–74. https://doi.org/10.5957/jsr.1958.2.4.52

Grigson, C., 1992. Drag Losses of New Ships Caused by Hull Finish. Journal of Ship Research 36, 182–193.

Hama, F.R., 1954. Boundary Layer characteristics for smooth and rough surfaces. The Society of Naval Architects, SNAME, Paper No. 6, New York, USA, Iowa City, USA.

Haslbeck, E.G., Bohlander, G.S., 1992. Microbial Biofilm Effects on Drag-Lab and

Field, in: Proceedings of the Ship Production Symposium. New Orleans, Louisiana.

Hiraga, Y., 1934. Experimental Investigations on the Resistance of Long Planks and Ships. Journal of Zosen Kiokai 55, 159–199.

Howell, D., Behrends, B., 2006. A review of surface roughness in antifouling coatings illustrating the importance of cutoff length. Biofouling 22, 401–410.

Hughes, G., 1952. Frictional resistance of smooth plane surfaces in turbulent flow. Trans. INA.

Hydrex, 2010. The Slime Factor, Hydrex White Paper No. 2, section "No hull or coating immune."

IEA, 2021. Net Zero by 2050. Paris, France.

IMO, 2021. Resolution MEPC.328(76) - Revised MARPOL Annex VI, MEPC 76/15/Add.1 Annex 1.

IMO, 2001. International Convention on the Control of Harmful Anti-Fouling Systems on Ships. AFS/CONF/26.

ISO, 1997. 4287–Geometrical Product Specifications (GPS)–Surface Texture: Profile Method–Terms, Definitions and Surface Texture Parameters, International Organization for Standardization. Geneva, Switzerland.

ITTC, 2017a. Final Report and Recommendations to the 28th ITTC.

ITTC, 2017b. ITTC Quality System Manual Recommended Procedures and Guidelines Procedure.

ITTC, 2014. Executive Committee Final report and recommendations to the 27 th ITTC.

ITTC, 2011a. Specialist Committee on Surface Treatment Final report and recommendations to the 26 th ITTC.

ITTC, 2011b. ITTC-Recommended Procedures and Guidelines.

ITTC, 2011c. ITTC-Recommended Procedures and Guidelines Practical Guidelines for Ship CFD Applications.

ITTC, 2011d. ITTC-Recommended Procedures-Fresh Water and Seawater Properties, in: 26th International Towing Tank Conference. Rio de Janeiro, Brazil.

ITTC, 2002. ITTC Uncertainty Analysis, Example for Resistance Test. ITTC Recommended Procedures and Guidelines.

Izubuchi, T., 1934. Increase in Hull Resistance Through Ship Bottom Fouling. Zosen Kyokai 55.

Jiménez, J., 2004. Turbulent Flows over Rough Walls. Annual Review of Fluid Mechanics 36, 173–96.

KCS Geometry and Conditions [WWW Document], 2008. . SIMMAN 2008, FORCE Technology. URL http://www.simman2008.dk/KCS/kcs_geometry.htm (accessed 11.25.22).

Kempf, I.G., 1937. On the effect of roughness on the resistance of ships. Trans INA 79, 109–119.

Kim, K., Leer-Andersen, M., Werner, S., 2022. A study on the effect of hull surface treatments on ship performances. The 9th Conference on Computational Methods in Marine Engineering.

Kim, W.J., Van, S.H., Kim, D.H., 2001. Measurement of flows around modern commercial ship models. Experiments in Fluids 31, 567–578.

Lackenby, H., 1962. The Thirty-Fourth Thomas Lowe Gray Lecture: Resistance of Ships, with Special Reference to Skin Friction and Hull Surface Condition. Proceedings of the Institution of Mechanical Engineers 176, 981–1014.

Larsson, L., Baba, E., 1996. Ship resistance and flow computations. Advances Marine Hydrodynamics.

Larsson, L., Stern, F., Visonneau, M., 2013. CFD in ship hydrodynamics - Results of the Gothenburg 2010 workshop. Computational Methods in Applied Sciences 29, 237–259.

Lewis, J.A., 1998. Marine biofouling and its prevention on underwater surfaces. Materials Forum 22, 41–61.

Lewkowicz, A.K., Das, D.K., 1986. Turbulent boundary layers on rough surfaces with and without a pliable overlayer: A simulation of marine fouling. International Shipbuilding Progress 33, 174–186.

Li, C., Atlar, M., Haroutunian, M., Anderson, C., Turkmen, S., 2018. An experimental investigation into the effect of Cu2O particle size on antifouling roughness and hydrodynamic characteristics by using a turbulent flow channel. Ocean Engineering 159, 481–495.

Li, C., Atlar, M., Haroutunian, M., Norman, R., Anderson, C., 2019. An investigation into the effects of marine biofilm on the roughness and drag characteristics of surfaces coated with different sized cuprous oxide (Cu2O) particles. Biofouling 35, 15–33.

Lindholdt, A., Dam-Johansen, K., Olsen, S.M., Yebra, D.M., Kiil, S., 2015. Effects of biofouling development on drag forces of hull coatings for ocean-going ships: a review. Journal of Coatings Technology and Research 12, 415–444.

Little, B.J., Depalma, J.R., 2013. Marine biofouling. Materials For Marine Sys-tems and Structures: Treatise on Materials Science and Technology. Elsevier 89–119.

Loeb, G.I., Laster, D., Gracik, T., 1984. The influence of microbial fouling films on hydrodynamic drag of rotating discs. Marine biodeterioration: an interdisciplinary study 88–94.

Marino, A., Shi, W., Atlar, M., Demirel, Y.K., 2019. Design specification, commission and calibration of the University of Strathclyde's Fully Turbulent Flow Channel (FTFC) facility, in: 6th International Conference on Advanced Model Measurements Technologies for The Maritime Industry (AMT'19). Rome, Italy.

Marusic, I., Monty, J.P., Hultmark, M., Smits, A.J., 2012. On the logarithmic region in wall turbulence. Journal of Fluid Mechanics.

McEntee, W., 1916. Variation of frictional resistance of shjps with condition of wetted surface. Journal of the American Society for Naval Engineers 28, 311–314.

McKeon, B.J., Li, J., Jiang, W., Morrison, J.F., Smits, A.J., 2004. Further observations on the mean velocity distribution in fully developed pipe flow. Journal of Fluid Mechanics 501, 135–147.

Menter, F.R., 1994. Two-Equation Eddy-Viscosity Turbulence Models for Engineering Applications. AIA A JOURNAL 32, 1598–1605.

Molland, A.F. (Ed.), 2008. Chapter 5 - Powering, in: The Maritime Engineering Reference Book. Butterworth-Heinemann, Oxford, UK, pp. 181–343.

Monty, J.P., Dogan, E., Hanson, R., Scardino, A.J., Ganapathisubramani, B., Hutchins, N., 2016. An assessment of the ship drag penalty arising from light calcareous tubeworm fouling. Biofouling 32, 451–464.

Morton, L.H.G., Greenway, D.L.A., Gaylarde, C.C., Surman, S.B., 1998. Consideration of some implications of the resistance of biofilms to biocides. International Biodeterioration & Biodegradation 41, 247–259.

Munk, T., 2006. Fuel Conservation through Managing Hull Resistance, in: Motorship Propulsion Conference. Copenhagen, Denmark.

Nikuradse, J., 1933. Laws of Flow in Rough Pipes. Washington, Distric of Columbia, USA.

Okay, O.S., 2004. Antifouling içeren gemi boyalarının uluslararası kurallar çerçevesinde kirletici etkilerinin incelenmesi. Gemi Mühendisliği ve Sanayimiz Sempozyumu 24, 168–178.

Oliveira, D., Larsson, A.I., Granhag, L., 2018. Effect of ship hull form on the resistance penalty from biofouling. Biofouling 34, 262–272.

Östman, A., Koushan, K., Savio, L., 2019. Study on Additional Ship Resistance due to Roughness using CFD. Journal of Ship and Marine Technology Journal 25, 56–65.

Papantoniou, G., 2022. Experimental Investigation on the Effects of Hull Roughness on the Resistance of a Tanker Ship (MSc Thesis). University of Strathclyde, Glasgow, UK.

Ravenna, R., 2019. Experimental Investigation on the Effect of Biomimetic Tubercles and Roughness on the Hydrodynamics of a Flat Plate (MSc Thesis). University of Strathclyde - University of Trieste.

Ravenna, R., Ingham, R., Song, S., Johnston, C., Tezdogan, T., Atlar, M., Demirel, Y.K., 2022a. Predicting the Effect of Hull Roughness on Ship Resistance Using a Fully Turbulent Flow Channel. Journal of Marine Science and Engineering 10, 1863.

Ravenna, R., Marino, A., Song, S., Atlar, M., Turan, O., Day, S., Demirel, Y.K., 2022b. Experimental study on the effect of biomimetic tubercles on the drag of a flat plate. Ocean Engineering 255, 111445.

Ravenna, R., Song, S., Shi, W., Sant, T., De Marco Muscat-Fenech, C., Tezdogan, T., Demirel, Y.K., 2022c. CFD analysis of the effect of heterogeneous hull roughness

on ship resistance. Ocean Engineering 258, 111733.

Richardson, L.F., 1911. IX. The approximate arithmetical solution by finite differences of physical problems involving differential equations, with an application to the stresses in a masonry dam. Philosophical Transactions of the Royal Society of London. Series A, Containing Papers of a Mathematical or Physical Character 210, 307–357.

Schlichting, H., Gersten, K., 2017. Boundary Layer Theory. Springer, Braunschweig, Germany.

Schoenherr, K.E., 1932. Resistance of flat surfaces moving through a fluid. Transactions of the Society of Naval Architects and Marine Engineers 40, 279–313.

Schultz, M.P., 2007. Effects of coating roughness and biofouling on ship resistance and powering. Biofouling 23, 331–341. https://doi.org/10.1080/08927010701461974

Schultz, M.P., 2004. Frictional resistance of antifouling coating systems. Journal of Fluids Engineering, Transactions of the ASME 126, 1039–1047.

Schultz, M.P., 2002. The Relationship Between Frictional Resistance and Roughness for Surfaces Smoothed by Sanding. Journal of Fluids Engineering 124, 492–499.

Schultz, M.P., Bendick, J.A., Holm, E.R., Hertel, W.M., 2011. Economic impact of biofouling on a naval surface ship. Biofouling 27, 87–98. https://doi.org/10.1080/08927014.2010.542809

Schultz, M.P., Flack, K.A., 2013. Reynolds-number scaling of turbulent channel flow. Physics of Fluids 25, 25104.

Schultz, M.P., Flack, K.A., 2007. The rough-wall turbulent boundary layer from the hydraulically smooth to the fully rough regime. Journal of Fluid Mechanics 580, 381–405.

Schultz, M.P., Flack, K.A., 2005. Outer layer similarity in fully rough turbulent boundary layers. Experiments in Fluids 38, 328–340. https://doi.org/10.1007/s00348-004-0903-2

Schultz, M.P., Myers, A., 2003. Comparison of three roughness function determination methods. Experiments in Fluids 35, 372–379.

Schultz, M.P., Swain, G.W., 1999. The Effect of Biofilms on Turbulent Boundary Layers. Journal of Fluids Engineering 121, 44–51.

Schultz, M.P., Walker, J.M., Steppe, C.N., Flack, K.A., 2015. Impact of diatomaceous biofilms on the frictional drag of fouling-release coatings. Biofouling 31, 759–773. https://doi.org/10.1080/08927014.2015.1108407

Shapiro, T., 2004. The Effect of Surface Roughness on Hydrodynamic Drag and Turbulence. US Naval Academy Annapolis.

Siemens, 2020. STAR-CCM+, User Guide. Version 15.06.

Song, S., 2020. Development of computational and experimental techniques to Investigate the effect of biofouling on ship hydrodynamic performance.

University of Strathclyde, Glasgow, UK.

Song, S., Dai, S., Demirel, Y.K., Atlar, M., Day, S., Turan, O., 2021a. Experimental and Theoretical Study of the Effect of Hull Roughness on Ship Resistance. Journal of Ship Research 65, 62–71.

Song, S., Demirel, Y.K., Atlar, M., 2020a. Penalty of hull and propeller fouling on ship self-propulsion performance. Applied Ocean Research 94, 102006.

Song, S., Demirel, Y.K., Atlar, M., 2019. An investigation into the effect of biofouling on the ship hydrodynamic characteristics using CFD. Ocean Engineering 175, 122–137.

Song, S., Demirel, Y.K., Atlar, M., Dai, S., Day, S., Turan, O., 2020b. Validation of the CFD approach for modelling roughness effect on ship resistance. Ocean Engineering 200, 107029.

Song, S., Demirel, Y.K., De Marco Muscat-Fenech, C., Sant, T., Villa, D., 2021b. Investigating the Effect of Heterogeneous Hull Roughness on Ship Resistance Using CFD. Journal of Marine Science and Engineering 9.

Song, S., Demirel, Y.K., De Marco Muscat-Fenech, C., Tezdogan, T., Atlar, M., 2020c. Fouling effect on the resistance of different ship types. Ocean Engineering 216, 107736.

Song, S., Ravenna, R., Dai, S., De Marco Muscat-Fenech, C., Tani, G., Demirel, Y.K., Atlar, M., Day, S., Incecik, A., 2021c. Experimental investigation on the effect of heterogeneous hull roughness on ship resistance. Ocean Engineering 223, 108590.

Stern, F., Wang, Z., Yang, J., Sadat-Hosseini, H., Mousaviraad, M., Bhushan, S., Diez, M., Yoon, S.H., Wu, P.C., Yeon, S.M., Dogan, T., Kim, D.H., Volpi, S., Conger, M., Michael, T., Xing, T., Thodal, R.S., Grenestedt, J.L., 2015. Recent progress in CFD for naval architecture and ocean engineering. Journal of Hydrodynamics. https://doi.org/10.1016/S1001-6058(15)60452-8

Taylan, M., 2010. An overview: effect of roughness and coatings on ship resistance, in: Internatonal Conference on Ship Drag Reduction. pp. 20–21.

Tezdogan, T., Demirel, Y.K., 2014. An overview of marine corrosion protection with a focus on cathodic protection and coatings. Brodogradnja 65, 49–59.

Tezdogan, T., Demirel, Y.K., Kellett, P., Khorasanchi, M., Incecik, A., Turan, O., 2015. Full-scale unsteady RANS CFD simulations of ship behaviour and performance in head seas due to slow steaming. Ocean Engineering 97, 186–206.

Titah-Benbouzid, H., Benbouzid, M., 2015. Marine renewable energy converters and biofouling: A review on impacts and prevention. EWTEC 09, 1–9.

Townsend, A.A.R., 1980. The structure of turbulent shear flow. Cambridge university press.

Townsin, R.L., 2003. The Ship Hull Fouling Penalty. Biofouling 19, 9–15.

TQC [WWW Document], 2022. URL https://industrialphysics.com/product/hull-roughness-gauge/ (accessed 8.8.22).

Ünal, B., 2012. Effect of Surface Roughness on the Turbulent Boundary Layer due to Marine Coatings. Istanbul Technical University.

Uzun, D., Ozyurt, R., Demirel, Y.K., Turan, O., 2020. Does the barnacle settlement pattern affect ship resistance and powering? Applied Ocean Research 95, 102020.

Valchev, I., Coraddu, A., Kalikatzarakis, M., Geertsma, R., Oneto, L., 2022. Numerical methods for monitoring and evaluating the biofouling state and effects on vessels' hull and propeller performance: A review. Ocean Engineering 251, 110883.

van Manen, J.D., van Oossanen, P., 1988. Principles of Naval Architecture, Second Rev. ed. The Society of Naval Architects and Marine Engineers, Jersey City, New Jersey, USA.

Van Rompay, B., 2012. Surface Treated Composites White Book. Tahoka Press.

Vargas, A., Shan, H., 2016. A Numerical Approach for Modeling Roughness for Marine Applications, in: Fluids Engineering Division Summer Meeting. American Society of Mechanical Engineers.

Vargas, A., Shan, H., Holm, E., 2019. Using CFD to Predict Ship Resistance due to Biofouling, and Plan Hull Maintenance, in: 4th Hull Performance & Insight Conference (HullPIC'19). Gubbio, Italy, pp. 242–254.

Videla, H.A., 1996. Manual of Biocorrosion, Prevention, Control and Mitigation.

Wahl, M., 1989. Marine epibiosis. I. Fouling and antifouling: some basic aspects. Marine ecology progress series 58, 175–189.

Walker, J.M., Schultz, M.P., Flack, K.A., Steppe, C.N., Academy, U.S.N., 2014. Skin-friction drag measurements on ship hull coating systems, in: 30th Symposium on Naval Hydrodynamics. Hobart, Tasmania, Australia, pp. 1–10.

Watanabe, S., Nagamatsu, N., Yokoo, K., Kawakami, Y., 1969. The augmentation in frictional resistance due to slime. Journa of the Kansai Society of Naval Architects 131, 45–51.

White, F.M., 2011. Fluid Mechanics. McGraw Hill.

Yeginbayeva, I., Brink, A., Emilie, V., 2021. New Measurement Facility: Enhanced Skin-Friction Measurement over Large-Scale Plates in a Channel Flow, in: 6th Hull Performance & Insight Conference. Pontignano, Italy, pp. 149–160.

Yeginbayeva, I.A., Atlar, M., 2018. An experimental investigation into the surface and hydrodynamic characteristics of marine coatings with mimicked hull roughness ranges. Biofouling 34, 1001–1019.

Yeginbayeva, I.A., Atlar, M., Turkmen, S., Chen, H., 2020. Effects of 'in-service' conditions–mimicked hull roughness ranges and biofilms–on the surface and the hydrodynamic characteristics of foul-release type coatings. Biofouling 36, 1074–1089. https://doi.org/10.1080/08927014.2020.1855330

Yeginbayeva, I.A., Granhag, L., Chernoray, V., 2018. Review and historical overview of experimental facilities used in hull coating hydrodynamic tests: Journal of Engineering for the Maritime Environment 233, 1240–1259.

Zanoun, E.S., Nagib, H., Durst, F., 2009. Refined cf relation for turbulent channels and consequences for high-Re experiments. Fluid Dynamics Research 41.

Zhang, Y., Yeginbayeva, I., Brink, A., 2021. Modelling and Simulation of the Effect of Antifouling Coating on Ship Resistance, in: 6th Hull Performance & Insight Conference HullPIC'21. Pontignano, Italy, pp. 41–47.